Boder, Philipp Simon (2024) *Characterising the mechanisms of uromodulin secretion and trafficking with salt loading from the thick ascending limb in hypertension.* PhD thesis.

https://theses.gla.ac.uk/84163/

Copyright and moral rights for this work are retained by the author

A copy can be downloaded for personal non-commercial research or study, without prior permission or charge

This work cannot be reproduced or quoted extensively from without first obtaining permission from the author

The content must not be changed in any way or sold commercially in any format or medium without the formal permission of the author

When referring to this work, full bibliographic details including the author, title, awarding institution and date of the thesis must be given

Enlighten: Theses
https://theses.gla.ac.uk/
research-enlighten@glasgow.ac.uk

Characterising the mechanisms of uromodulin secretion and trafficking with salt loading from the thick ascending limb in hypertension

Philipp Simon Boder

BSc (Hon), MRes

Thesis submitted in fulfilment of the requirements for the Degree of Doctor of Philosophy (PhD)

School of Cardiovascular and Metabolic Health

College of Medical, Veterinary & Life Sciences

University of Glasgow

October 2023

© P S Boder

Summary

Uromodulin (UMOD) is a complex glycoprotein that is to a large extent secreted by renal epithelial cells lining the thick ascending limb (TAL) and is the most abundant protein found in the urine of healthy individuals. A number of functions have been associated with urinary UMOD, including regulation of salt transport and ion homeostasis, protection against urinary tract infections and kidney stones, kidney injury, and innate immunity. UMOD undergoes a number of conformational changes and post-translational modifications, including glycosylation, during its maturation and intracellular trafficking. UMOD secretion is polar by the fact that it can be secreted apically into the urine, or basolaterally into the serum. Importantly, altered urinary UMOD excretion and intracellular retention of UMOD have been linked to various kidney-related pathologies, including chronic kidney disease (CKD). Variants in the UMOD promoter have been associated with hypertension by genome-wide association studies. Hypertension is one of the main drivers of cardiovascular disease risk and is intricately linked to kidney function, with the kidneys playing a major role in blood pressure regulation. Increased salt intake is strongly linked to a number of detrimental cardiovascular outcomes, including renal end-organ damage and hypertension. Previously, studies have focused on the role of UMOD in salt reabsorption. However, the reverse (i.e., the effect of salt on UMOD) remained unexplored. In this thesis, the main aim was to investigate the influence of salt on UMOD excretion in order to gain a better understanding of the relationship between salt handling, blood pressure/hypertension, and kidney physiology. To model normotensive and chronic hypertensive conditions, Wistar-Kyoto (WKY) and Stroke-Prone Spontaneously Hypertensive (SHRSP) rats were utilised, respectively. These rats were administered 1% NaCl/salt in their drinking fluid, which is at a physiological concentration, thereby more closely replicating human conditions.

Initial dissection of the role of dietary salt in renal UMOD excretion rate was achieved by exposing WKY and SHRSP rats to a 3-week continuous 1% salt loading phase. Salt loading in the chronic hypertensive SHRSP led to increased blood pressure and expression of kidney injury markers kidney injury marker-1 (KIM-1) and neutrophil gelatinase-associated lipocalin (NGAL). Excretion of urinary UMOD was decreased by 26 % in WKY rats and 55% in SHRSP rats. It was hypothesized that the addition of anti-hypertensive drug nifedipine (calcium channel blocker) would assist in separating the blood pressure component from salt-induced effects on UMOD urinary excretion rate. Nifedipine treatment of salt-loaded rats did not inhibit the reduction in urinary UMOD

excretion rate in SHRSP, even with reduced blood pressure. Following this, the aim was to gain insights into the kidney physiology and intracellular mechanisms that may occur with salt loading. Examination of total kidney lysates from salt loaded WKY and SHRSP revealed a lack of UMOD protein and mRNA levels. Immunofluorescence and co-localization studies revealed increased intracellular UMOD retention in both WKY and SHRSP, specifically in the endoplasmic reticulum (ER). This was further corroborated by *ex-vivo* incubations with isolated medullary TAL (mTAL) tubules, the region with a high UMOD content in rats, incubated with mannitol (an osmotic control) and salt, whereby salt-incubated TAL showed greater UMOD retention, especially in the SHRSP. This highlighted the importance of salt in regulating urinary UMOD excretion and trafficking, and potential exacerbations in chronic hypertension and kidney injury. However, the dynamics and exact mechanisms behind the influence of salt on UMOD excretion and trafficking were not clear.

To explore the dynamics of salt loading on UMOD excretion rate, WKY rats were exposed to an intermittent salt loading regime whereby they received 1% salt in an on-off-on pattern over 3 weeks (1 week of salt loading, 1 week of normal water, 1 week of salt loading). The normotensive model was chosen to remove hypertension as a confounding factor and therefore provide mechanistic insight into a normal physiological setting. It was hypothesized that the salt-induced lowering of UMOD excretion rate would be reversible, and this would be apparent in UMOD trafficking. Intermittent salt loading resulted in an acute lowering of UMOD urinary excretion rate and a reversal to almost normal levels upon salt removal. Although there were differences in electrolyte levels, especially sodium and chloride levels, there was no change in intracellular UMOD accumulation in the normotensive background. This provided further proof of the acute influence of salt on UMOD excretion and suggested that UMOD accumulation occurs over a longer timescale.

Given that salt loading lowers UMOD excretion acutely and results in significant intracellular accumulation in the chronic hypertensive model, the next aim was to characterize the effects of long-term salt loading on UMOD excretion and trafficking. It was hypothesized that long-term salt loading would result in a “chronic hypertensive-like” phenotype in the normotensive models, with intracellular accumulation of UMOD and a change in renal physiology. Salt loading over a period of 3 months showed increased intracellular accumulation of UMOD in the ER of the epithelial cells in the TAL region. Moreover, this was paralleled by the upregulation of ER stress marker Binding Immunoglobulin Protein (BiP). This novel finding suggests a mechanism whereby long-term salt loading may trigger early deleterious processes in the kidneys of normotensive

WKY. These lead to accumulation of UMOD, which may contribute to renal injury as seen in the chronic hypertensive SHRSP. Only after continued salt exposure over a longer period of time, in combination with ER accumulation, is an ER stress response triggered. Whether this is related to increased UMOD processing times in the ER and the exact mechanistic contributions of UMOD to blood pressure, and ultimately the chronic hypertensive phenotype, remains to be characterized.

Given the evidence presented of the profound effect of salt on UMOD urinary excretion and trafficking, a suitable model was required to untangle the molecular mechanisms involved in the process. This would also assist in the discovery of novel therapeutic targets for the treatment of hypertension, as well as other UMOD-related diseases such as CKD, especially with regard to UMOD retention and ER stress. Previous models include primary mTAL cells. However, these lose UMOD expression during subculturing and undergo significant changes in morphology with salt incubation. To overcome this, a transgenic cell model is presented in this thesis expressing UMOD with a Yellow Fluorescent Protein tag (UMOD-YFP 293 FT cells). This model offers the advantage of inducible UMOD expression via a tetracycline promoter at a user-defined time point. Moreover, the YFP-tag would enable live cell imaging, which would help with understanding the kinetics of UMOD trafficking, to immunoprecipitation assays, which would greatly assist in identifying the interactors of UMOD and by extension the signalling pathways involved with salt loading. This thesis also therefore offers a novel resource for future molecular studies of UMOD.

Taken together, this thesis provides novel evidence for the salt-driven lowering of UMOD urinary excretion in both normotensive and chronic hypertensive models. In the chronic hypertensive model particularly, there is an increase in intracellular retention of UMOD and ER stress, paralleled by kidney injury. In the normotensive model, this accumulation and retention of UMOD in the medullary TAL only occurs after long-term salt loading, which provides a novel avenue of investigation: does salt induce ER stress which leads to retention of UMOD, or does the retention of UMOD induce ER stress? And importantly, how does this tie in with renal end-organ damage and the progression of hypertension? Further molecular characterisation is required in this regard and may eventually inform new therapies for the treatment of hypertension.

Table of Contents

Summary ii

Table of Contents v

List of Tables x

List of Figures xi

Acknowledgements xvi

Author's Declaration xviii

Abbreviations xix

Publications, Presentations and Awards xxii

Publications: xxii

Oral and Poster Presentations: xxii

Awards: xxiii

Chapter 1: Introduction 1

1.1 The Cardiovascular System 1

1.1.1 The Circulatory System 1

1.1.2 Blood Vessels 3

1.1.3 Blood Pressure Control Mechanisms 5

1.2 Hypertension 10

1.2.1 The Role of Genetics in High Blood Pressure 11

1.2.2 Immune System 13

1.2.3 Environmental Influences and Salt 17

1.3 Kidney Physiology 19

1.3.1 Kidney Function 19

1.3.2 Kidney Structure 20

1.3.3 Kidneys and Blood Pressure Regulation 22

1.4 Kidney Disease and Hypertension 23

1.4.1 Diabetes 24

1.4.2 Chronic Kidney Disease 24

1.4.3 Other important factors 24
1.5 The Study of Hypertension: Animal Models 24
1.5.1 Animal Models.....24
1.5.2 Rodent Models of Hypertension 25
1.6 Uromodulin: Physiology and Disease.....27
1.6.1 Gene 28
1.6.2 Protein and Structure.....29
1.6.3 Molecular Trafficking/Secretory Pathway 30
1.6.4 Function and Role in Diseases 32
1.6.5 Measuring UMOD and Clinical Relevance 32
1.6.6 UMOD and Hypertension 34
1.7 Uromodulin Interactions with the Major Components of the Thick Ascending Limb 40
1.7.1 Direct interactions 40
1.7.2 Indirect Interactions 47
1.8 Hypothesis and Aims 49
1.8.1 Hypothesis.....49
1.8.2 Aims 49
Chapter 2: General Materials and Methods 50
2.1 General Laboratory Practices.....50
2.2 Animals 50
2.2.1 Ethical Statement 50
2.2.2 Animal Strains.....51
2.2.3 Animal House 51
2.3 Animal Procedures.....51
2.3.1 Metabolic Cage 51
2.3.2 Blood Pressure Measurement.....51
2.3.3 Blood Collection 52
2.3.4 Tissue Collection and Processing Protocols 52

2.4 Gene expression 53
2.4.1 Ribonucleic Acid (RNA) extraction.....53
2.4.2 RNA quantification 53
2.4.3 Reverse Transcription Polymerase Chain Reaction (RT-PCR) 53
2.4.4 Quantitative Polymerase Chain Reaction (qPCR) 54
2.5 Western blots.....57
2.5.1 Protein Extraction.....57
2.5.2 Electrophoresis.....60
2.5.3 Blotting.....60
2.5.4 Blocking and Antibody Incubation 61
2.5.5 Detection and Analysis 61
2.5.6 Stripping Protocol 62
2.6 Histology.....62
2.6.1 Tissue Preparation for Histology 62
2.6.2 Immunofluorescence Staining.....63
2.6.3 Immunofluorescence Imaging and Analysis.....64
2.7 Enzyme-linked Immunosorbent Assay 64
2.8 Statistical analysis.....65
2.9 Antibodies 65
Chapter 3: Salt loading decreases urinary excretion and increases intracellular accumulation of uromodulin in stroke-prone spontaneously hypertensive rats.....69
3.1 Introduction.....70
3.2 Materials and Methods.....71
3.2.1 Animals and acute salt loading 71
3.2.2 N-Deglycosylation assay.....72
3.2.3 Histology.....72
3.2.4 Immunofluorescence Imaging and Analysis.....72
3.2.5 Ex vivo incubations of mTAL tubules.....73
3.3 Results.....73

3.3.1 Blood pressure and kidney structure changes with salt loading 73

3.3.2 Variations in adjustment to salt stress between WKY and SHRSP 78

3.3.3 Urinary UMOD excretion is decreased in WKY and SHRSP after 24 hours of salt loading 81

3.3.4 UMOD mRNA and total kidney proteins levels do not match changes in urinary UMOD excretion.....85

3.3.5 Salt loading increases the renal intracellular accumulation of UMOD in SHRSP 89

3.4 Discussion 93

Chapter 4: Effects of Intermittent Salt Loading on UMOD Trafficking 97

4.1 Introduction 97

4.2 Materials and Methods 97

4.2.1 Animals and intermittent salt loading 98

4.3 Results 99

4.3.1 Blood pressure and overall physiology of salt-loaded animals is unaffected 99

4.3.2 Intermittent salt loading does not significantly alter electrolyte homeostasis or renal parameters 101

4.3.3 Intermittent salt loading lowers urinary UMOD excretion rate 105

4.3.4 Trafficking of UMOD is not altered with intermittent salt loading 106

4.4 Discussion 109

Chapter 5: Long-term Effects of Salt Loading on UMOD trafficking.....113

5.1 Introduction 113

5.2 Materials and Methods 114

5.2.1 Animals and long-term salt loading 114

5.2.2 UMOD GFP MDCK Cells 114

5.2.3 Immunofluorescence analysis of UMOD-GFP MDCK cells.....115

5.3 Results 115

5.3.1 Long-term salt loading results in only minor blood pressure and systemic physiological changes in the WKY rats 115

5.3.2 There is a considerable impact on electrolyte balances in long-term salt loaded WKY rats 118

5.3.3 Long-term salt loading does not induce kidney damage in the normotensive WKY rats 123

5.3.4 Long-term salt loading directly and consistently lowers the urinary UMOD excretion rate 124

5.3.5 UMOD accumulates in the ER of long-term salt loaded WKY rats 126

5.3.6 The reduction in UMOD secretion is a result of salt-induced effects rather than changes in osmotic pressure 131

5.3.7 Long-term salt exposure induces a medulla-specific ER stress response 134

5.4 Discussion 139

Chapter 6: Cell Culture Models for Studying UMOD Expression 144

6.1 Introduction 144

6.2 Materials and Methods 145

6.2.1 Medullary Thick Ascending Limb Tubules 145

6.2.2 Transgenic UMOD expressing FT-293 Cells 145

6.3 Results 153

6.3.1 Characterisation of primary TAL cell lines 153

6.3.2 Effect of salt stress on UMOD secretion from primary TAL cells 155

6.3.3 Characterisation of HEK UMOD-YFP cell line 158

6.4 Discussion 162

Chapter 7: General Discussion 165

7.1 Final Conclusions 169

Chapter 8: Appendix 171

8.1 Materials 171

8.1.1 Laboratory-Prepared solutions 171

8.2 Tissue Harvest Protocol 173

References 175

List of Tables

Table 1.1. Structure and function of vessels in the circulatory system. 4
Table 1.2. Summary of Rodent Models of Hypertension and their Clinical Relevance 26
Table 1.3. Risk variants of the *UMOD* and allele frequency. 36
Table 1.4. Clinical factors influencing urinary UMOD secretion. 39
Table 2.1 Reaction set-up for the RT-PCR reactions to produce cDNA from RNA. 54
Table 2.2 Optimum temperatures and times for each reaction step in the High-Capacity RNA to cDNA Kit. 54
Table 2.3 Reagent volumes for TaqMan^{TM} qPCR reactions 55
Table 2.4 List of TaqMan^{TM} probes and their designation 56
Table 2.5 List of primary and secondary antibodies used in the thesis. 65
Table 3.1. Histological scoring of kidney sections. 76
Table 3.2. Renal parameters of WKY and SHRSP rats prior to salt loading (at 11 weeks, baseline). 78
Table 3.3. Renal parameters of WKY and SHRSP rats after 3 weeks of salt loading. 79
Table 4.1. Plasma and urine electrolyte levels before and after intermittent salt loading. 103
Table 5.1. Plasma and urinary electrolyte levels before and after long-term salt loading. 122
Table 6.1 Primers for production of the UMOD-YFP plasmid. 147
Table 6.2 Thermal Cycler Programme for DNA amplification of UMOD-YFP products. 148
Table 8.1 Tissue harvest protocol sheet for rat culls. 173

List of Figures

Figure 1.1. Design of the cardiovascular system (CVS). 3
Figure 1.2 Short-term blood pressure regulatory mechanisms of the autonomic nervous system. 7
Figure 1.3. Illustration of the components and function of the renin-angiotensin aldosterone system (RAAS). 9
Figure 1.4. A summary of the two branches of the immune system and their role in hypertension. 13
Figure 1.5. Illustration of pathways involved in pathogenesis of various diseases as a result of excessive salt intake. 19
Figure 1.6. Basic Structure of the Kidney Nephron. 21
Figure 1.7. The structure and domains of Uromodulin (UMOD). 29
Figure 1.8. The physiology of the thick ascending limb and its involvement in ion homeostasis. 31
Figure 1.9. Links between different phenotypes and the genomic *UMOD* locus. 34
Figure 1.10. The network of interactions occurring between UMOD and various signalling components within the thick ascending limb (TAL). 41
Figure 2.1. Diagrammatic representation of the Mem-PER™ Plus Membrane Protein Extraction Kit (ThermoFisher Scientific, UK). 59
Figure 2.2. Example of non-specific bands on a Western blot using the UMOD primary antibody provided by Abcam (Ab207170) on kidney medulla samples. 68
Figure 2.3. Example of non-specific bands on a Western blot using the NKCC2 primary antibody provided by ThermoFisher Scientific (PA5-88905) on total kidney samples. 68
Figure 3.1. SHRSP at baseline have higher systolic blood pressure (SBP) compared to WKY. 74
Figure 3.2. Salt loading for 3 weeks increases SBP in SHRSP rats. 75
Figure 3.3. SHRSP rats after salt loading demonstrate arteriolar hyalinosis. 76
Figure 3.4. Scoring criteria for glomeruli of kidney sections. 77
Figure 3.5. SHRSP rats after salt loading demonstrate mild distal tubule injury. 77
Figure 3.6. Salt loading increased kidney weight in both WKY and SHRSP rats after salt loading. 80
Figure 3.7 Salt loading increased the albumin-to-creatine ratio (ACR) in salt-loaded SHRSP rats. 80

Figure 3.8. Expression of early tubule injury markers are increased in SHRSP after salt loading. 81
Figure 3.9. Increased Urinary UMOD Excretion Rate in SHRSP rats at baseline. 81
Figure 3.10. Timeline of gradual decrease in urinary UMOD (uUMOD) excretion with salt loading in WKY and SRHSP. 82
Figure 3.11. Salt loading of 3 weeks significantly lowers urinary UMOD excretion rate in SHRSP rats. 83
Figure 3.12. A percentage decrease in urinary UMOD excretion rate occurs in WKY and especially in SHRSP. 84
Figure 3.13. Sodium and urinary UMOD excretion show an inverse relationship after salt loading. 84
Figure 3.14. NKCC2 abundance do not change with salt loading in WKY or SHRSP. 85
Figure 3.15. Total kidney intracellular UMOD levels are unchanged with salt loading in WKY and SHRSP. 86
Figure 3.16. The total kidney UMOD mRNA levels slightly decrease in salt loaded SHRSP. 86
Figure 3.17. The total kidney UMOD mRNA fold-change remained unchanged in both WKY and SHRSP with salt loading. 87
Figure 3.18. Nifedipine has no direct effect on UMOD secretion from isolated medullary TAL tubules in WKY and SHRSP. 88
Figure 3.19. Nifedipine does not directly affect UMOD intracellular protein levels in isolated medullary TAL tubules from WKY and SHRSP. 88
Figure 3.20. Salt loading does not significantly alter hepsin expression in kidneys isolated from WKY and SHRSP rats. 89
Figure 3.21. Salt loading increases intracellular accumulation of UMOD in both WKY and SHRSP. 90
Figure 3.22. SHRSP have higher UMOD in the ER compared to WKY rats. 90
Figure 3.23. Salt loading altered membrane and cytosolic levels of UMOD in WKY and SHRSP medullary TAL tubules. 91
Figure 3.24. Calnexin expression is increased in medullary TAL tubules expressing UMOD after salt loading. 92
Figure 3.25. Calnexin protein expression is increased in kidneys of salt loaded WKY and SHRSP. 92
Figure 3.26. Calreticulin protein expression remains unchanged with salt loading in WKY and SHRSP. 93

Figure 3.27. Salt loading increases the polymerisation incompetent form of UMOD in both WKY and SHRSP. 93
Figure 4.1. Systolic blood pressure was not significantly altered with intermittent salt loading. 99
Figure 4.2. Body weight of WKY rats gradually increases but is unaffected by intermittent salt loading. 100
Figure 4.3. Kidney weight is unchanged with intermittent salt loading in WKY rats. 100
Figure 4.4. The percentage of red blood cells is unaffected after intermittent salt loading period. 101
Figure 4.5. Urinary output increases during salt loading week in WKY. 102
Figure 4.6. Water intake increases during salt loading week in WKY. 102
Figure 4.7. Intermittent salt loading does not significantly influence KIM-1 expression. 105
Figure 4.8. Intermittent salt loading does not significantly influence NGAL expression.105
Figure 4.9. Intermittent salt loading-acutely decreases urinary UMOD excretion rate. 106
Figure 4.10. Total Kidney UMOD mRNA levels did not change with intermittent salt loading. 107
Figure 4.11. Total kidney UMOD protein levels were not altered with intermittent salt loading. 107
Figure 4.12. The medullary UMOD levels were not significantly different compared to controls after intermittent salt loading. 108
Figure 4.13. Membrane UMOD protein levels in the medullary region were not changed with intermittent salt loading. 109
Figure 4.14. There was a trend towards decreased cytosolic UMOD levels in intermittent salt loaded WKY rats. 109
Figure 5.1. Systolic Blood Pressure was not significantly different after 3 months of salt loading compared to controls. 116
Figure 5.2. Body weight increased with age in WKY rats in both control and salt-loaded groups. 116
Figure 5.3. Kidney weight remained unchanged in WKY rats after 3 months of salt loading. 117
Figure 5.4. The percentage of red blood cells is unchanged during long-term salt loading 117
Figure 5.5. There is no statistically significant difference in percentage of red blood cells in WKY after 3 months of salt loading. 118
Figure 5.6. Urinary output is significantly increased after 3 months of salt loading both between control groups and compared to week 1. 119

Figure 5.7. Water intake increased significantly in WKY after 3 months of salt loading. 119
Figure 5.8. Urinary sodium excretion was significantly increased in the salt-loaded group after long-term salt loading. 120
Figure 5.9. Long-term salt loading does not significantly influence kidney KIM-1 expression.....123
Figure 5.10. Long-term salt loading does not significantly influence kidney NGAL expression.....123
Figure 5.11. Long-term salt loading consistently lowers urinary UMOD excretion rate. .124
Figure 5.12. Serum UMOD levels were unaltered after 3 months of salt loading compared to controls.....125
Figure 5.13. The urinary excretion of epidermal growth factor (EGF) after long-term salt loading were unchanged.....126
Figure 5.14. The intracellular levels of epidermal growth factor (EGF) in TAL region of kidneys from WKY rats after long-term salt loading were unchanged. 126
Figure 5.15. Total kidney UMOD mRNA levels did not change significantly after 3 months of salt loading. 127
Figure 5.16. Total kidney UMOD protein levels significantly increased in the long-term salt loading group. 127
Figure 5.17. Long-term salt loading significantly increased UMOD protein levels in the kidney medullary region. 128
Figure 5.18. Membrane and Cytosolic UMOD protein levels in the medullary region were not changed with long-term salt loading. 129
Figure 5.19. Long-term salt loading leads to increased co-localization of UMOD with the ER marker calnexin in the medullary TAL of WKY rats. 130
Figure 5.20. There is an accumulation of immature UMOD in the ER of medullary TAL of WKY rats. 131
Figure 5.21. MDCK cells have decreased secretion of UMOD into the media with salt incubation for 18 hours. 132
Figure 5.22 Intracellular levels of UMOD remain unchanged in MDCK cells after salt incubation for 18 hours. 132
Figure 5.23 The expression of UMOD mRNA levels remains unchanged in MDCK cells after salt incubation for 18 hours. 133
Figure 5.24. There is a reduction in UMOD on the membrane surface of MDCK cells after 18 hours of salt loading. 134
Figure 5.25. BiP protein levels in total kidneys were unchanged after long-term salt loading in WKY rats. 135

Figure 5.26. PDI protein levels in total kidneys were unchanged after long-term salt loading in WKY rats. 136
Figure 5.27. BiP protein levels in the medullary region of the kidneys were increased after long-term salt loading in WKY rats. 137
Figure 5.28. PDI protein levels in the medullary region of the kidneys were increased after long-term salt loading in WKY rats. 138
Figure 5.29. Acute salt loading did not significantly alter BiP protein expression in chronic hypertensive SHRSP rats. 139
Figure 6.1 The UMOD-YFP insert in the pcDNA5-FRT/TO backbone vector. 149
Figure 6.2 Diagrammatic Representation of The Flp-In System 152
Figure 6.3. Characterisation of the growth of primary mTAL epithelial cell cultures over 5 days. 153
Figure 6.4. Calcium at varying concentrations does not influence the morphology of primary mTAL epithelial cell cultures. 154
Figure 6.5. Salt stress alters the morphology of primary mTAL epithelial cells. 155
Figure 6.6. Salt incubation does not alter UMOD protein levels in the plasma membrane of primary mTAL epithelial cells. 156
Figure 6.7. Salt incubation lowers UMOD protein levels in the cytosol of primary mTAL epithelial cells.....157
Figure 6.8. Primary mTAL epithelial cells have reduced UMOD mRNA expression with increasing passage number.....158
Figure 6.9. Agarose gel confirming PCR products of YFP, UMOD, and pcDNA5 FRT/TO expression vectors. 159
Figure 6.10. Confirmation of expression of UMOD-YFP fusion protein in 293FT lysate after induction with tetracycline.....160
Figure 6.11. Immunofluorescence analysis confirms UMOD expression in tetracycline-induced UMOD-YFP 293FT cells after transient transfection. 161
Figure 6.12. Stable expression of UMOD in 293FT cells after Flp-In^{TM} recombination of the UMOD-YFP vector. 162

Acknowledgements

I would like to extend my sincerest thanks to the British Heart Foundation for supporting my studies and work presented here. They have helped finance most of my PhD and allowed me to focus primarily on my studies. This highlights the importance of charities in enabling research in the UK and in fostering the next generation of scientists.

A project of this magnitude requires excellent supervision, and luckily, I had the most amazing supervisors to guide and assist me through my various studies. I would like to thank all my supervisors – Paddy, Christian, and James. I'd also like to thank Sheon for all her help behind the scenes and for her day-to-day support. A special shoutout goes to Christian, who originally fought for me to work under his supervision and join the wonderful Delles lab team. He has been a source of constant support, kindness, understanding, and know-how, both academically and in my personal life, despite his very busy schedule. All in all, I could not have asked for a better boss!

I would also like to thank the support I received from all my friends and colleagues in the School of Cardiovascular and Metabolic Health. There was always a helping hand or someone to talk to, and for that, I am eternally grateful.

I am very fortunate to have collaborated with multiple scientists throughout my studies, all of whom have shared their expertise and incredible knowledge to help expand and build upon my work. Specifically, I would like to thank Luca for his years of experience in uromodulin, kidneys, renal physiology, and disease. Your insights and ideas were always greatly appreciated. Also, I am very grateful to Nuria, who very graciously allowed me to visit her lab in Barcelona and learn about 3D kidney organoids. The whole Montserrat lab team were very kind and patient and made me feel very welcome. With this in my, I could not have funded this trip without assistance from the Royal Society of Edinburgh. A big thank you to them for believing in my project and helping me learn new techniques that would otherwise have been impossible. Barcelona was a life-changing experience for me and helped me understand my core values as a person. I highly encourage all PhD students to undertake a placement project during their studies.

A huge thank you also goes out to my ever-supportive friends and family. Mum, Dad, and Patty – you all kept me alive and sane throughout these years, I couldn't have done it without you. From my little scientist stage, playing with frogs in the back garden, to the slightly larger scientist I am today working at a cutting-edge university. Mum, I can always count on your support and thank you for believing in me (and pushing me constantly to

finish this thing!). Dad, you did not need to support my studies, and yet you were always there to help me – no questions asked. Patty, no one could have asked for a better sister – you are the best and I am so grateful for your love and support. Although you cannot read or comprehend human constructs, much love to my three dogs (Balloo, Pedro, and Luna) for distracting me and putting a smile on my face when times were tough. Also, I owe a big thank you to my new Scottish family (Nancy, Hugh, Matt, and Bee)– the Rooneys – your support, love, acceptance, and kindness is so amazing! Jithin, thanks for all our crazy lab talks and friendship since day one of the PhD programme. Daniel, you came to visit me in Barcelona and in Glasgow, and we have known each other since high school, always there for a good chat and a laugh, thank you old friend. Michael, you are one of my closest friends and thanks for all the good times, big cat.

On that note, I cannot forget the one person that means everything to me. The one person who was always been there for me, through the good times and the bad. The person who makes me laugh, who looks after me when I am down, my best friend and the one I will spend the rest of my life with. Becca, or just simply “my B”, I love you so much and thank you for your unwavering support. I definitely would not have come this far without you; you make this whole “life” thing worth it. My heart belongs to you.

Author's Declaration

I declare that the work presented in this thesis has been carried out by myself except where otherwise cited or acknowledged. It is entirely of my own composition and has not, in whole or part, been submitted for any other higher degree. Figure 1.9 in Chapter 1 was generated in collaboration with Professor Sandosh Padmanabhan. It should be noted that Chapter 3 is being presented as an "Alternative Thesis Format" chapter and has previously been published in the *Clinical Science* journal. In Chapter 3, Dr David Kipgen helped with the formal analysis and validation of the histology of the kidney tissues. Also, Arun Flynn and Nicola Britton assisted with the preparing of kidney sections for histological and immunofluorescence analysis. Nicola Britton provided further help in this regard in Chapters 4 and 5. This work was supervised by Professor Patrick Mark, Professor Christian Delles, and Professor James Leiper.

Abbreviations

293FT .....Flp-In™ T-REx™ 293 cells
ACE .....Angiotensin-Converting Enzyme
ADTKD-UMOD .....Autosomal Dominant Tubulointerstitial Kidney Disease Related to UMOD
AngII ..... Angiotensin II
APC ..... Antigen-Presenting Cells
ARBs ..... Angiotensin-Receptor Blockers
AVP ..... Vasopressin
BiP ..... Binding Immunoglobulin Protein
BP ..... Blood Pressure
CaSR .....Calcium-Sensing Receptor
CKD ..... Chronic Kidney Disease
CLC – Kb ..... Chloride Channel Kb
CLDNs ..... Claudins
CO ..... Cardiac Output
DBP .....Diastolic Blood Pressure
DCT ..... Distal Convoluted Tubule
dDVAP ..... 1-Desamino-8-D-Arginine Vasopressin
DOCA ..... Deoxycorticosterone Acetate
EGF .....Epidermal Growth Factor
EHP ..... External Hydrophobic Patch
ENaC ..... Epithelial Sodium Channel
eNOS .....Endothelial Nitric Oxide Synthase
ER ..... Endoplasmic Reticulum
ERAD .....ER-Associated Degradation
GFP .....Green Fluorescent Protein
GFR ..... Glomerular Filtration Rate
GWAS .....Genome-Wide Association Study
HNF1 ..... Hepatocyte Nuclear Factor 1-β
HPLC ..... High Pressure Liquid Chromatography
HSP70 ..... Heat Shock Protein 70
IFN-γ ..... Interferon Gamma
IHP ..... Internal Hydrophobic Patch

IL ..... Interleukin
KIM-1 ..... Kidney Injury Marker-1
LD ..... Linkage Disequilibrium
MAP ..... Mean Arterial Pressure
MDCK ..... Madin-Darby Canine Kidney
MS ..... Mass Spectrometry
mTAL ..... medullary Thick Ascending Limb
NaCl ..... Sodium Chloride/Salt
NADPH ..... Nicotinamide Adenine Dinucleotide Phosphate
NCC ..... NaCl Cotransporter
NFAT ..... Nuclear Factor of Activated T Cell
NGAL ..... Neutrophil Gelatinase-Associated Lipocalin
NHE ..... Na+/H+ exchanger type 3
NK ..... Natural Killer Cells
NKCC2 ..... Na+-K+-2Cl- cotransporter
NM2 ..... Non-Muscle Myosin II
Nox ..... NADPH Oxidase
OSR1 ..... Oxidative Stress Response 1
PAMPs ..... Pathogen-Associated Molecular Patterns
PAS ..... Periodic Acid-Schiff
PBS ..... Phosphate Buffered Saline
PCV ..... Packed Cell Volume
PDI ..... Protein Disulphide Isomerase
PGE2 ..... Prostaglandin E2
PRRs ..... Pattern Recognition Receptors
qPCR ..... quantitative Polymerase Chain Reaction
QTL ..... Quantitative Trait Loci
RAAS ..... Renin-Angiotensin-Aldosterone System
ROMK ..... Renal Outer Medullary Potassium Channel
ROS ..... Reactive Oxygen Species
SBP ..... Systolic Blood Pressure
SHR ..... Spontaneously Hypertensive Rat
SHRSP ..... Stroke-Prone Spontaneously Hypertensive Rat
SNP ..... Single Nucleotide Polymorphism
SPAK ..... SPS1-Related Proline-Alanine-Rich Kinase
SV ..... Stroke Volume

TAL ..... Thick Ascending Limb
TCR ..... T-Cell Receptor
TGFβ ..... Transforming Growth Factor Beta
TLRs ..... Toll-Like Receptors
TNFα ..... Tumour Necrosis Factor-α
TPR ..... Total Peripheral Resistance
TRPM ..... Transient Receptor Potential Melastin
UAKD ..... Uromodulin-Associated Kidney Disease
UMOD ..... Uromodulin
WKY ..... Wistar-Kyoto Rat
WNK ..... With No Lysine Kinases
WT ..... Wild-Type
YFP ..... Yellow Fluorescent Protein
ZP ..... Zona Pellucida

Publications, Presentations and Awards

Publications:

- Chen, J., Khai Syuen Chew, Mary, S., **Boder, P.**, Domenico Bagordo, Gian Paolo Rossi, Touyz, R.M., Delles, C. and Rossitto, G. (2023). Skin-specific mechanisms of body fluid regulation in hypertension. 137(3), pp.239–250. doi: https://doi.org/10.1042/cs20220609.
- Mary, S., **Boder, P.**, Padmanabhan, S., McBride, M.W., Graham, D., Delles, C. and Dominiczak, A.F. (2022). Role of Uromodulin in Salt-Sensitive Hypertension. Hypertension, 79(11), pp.2419–2429. doi: https://doi.org/10.1161/hypertensionaha.122.19888.
- Mary, S., **Boder, P**., Rossitto, G., Graham, L., Scott, K., Flynn, A., Kipgen, D., Graham, D. and Delles, C. (2021). Salt loading decreases urinary excretion and increases intracellular accumulation of uromodulin in stroke-prone spontaneously hypertensive rats. Clinical science (London, England: 1979), [online] 135(24), pp.2749–2761. doi: https://doi.org/10.1042/CS20211017.
- **Boder, P**., Mary, S., Mark, P.B., Leiper, J., Dominiczak, A.F., Padmanabhan, S., Rampoldi, L. and Delles, C. (2021). Mechanistic interactions of uromodulin with the thick ascending limb: perspectives in physiology and hypertension. Journal of Hypertension, [online] 39(8), pp.1490–1504. doi: https://doi.org/10.1097/HJH.0000000000002861.
- Rossitto, G., Mary, S., Chen, J.Y., **Boder, P**., Chew, K.S., Neves, K.B., Alves, R.L., Montezano, A.C., Welsh, P., Petrie, M.C., Graham, D., Touyz, R.M. and Delles, C. (2020). Tissue sodium excess is not hypertonic and reflects extracellular volume expansion. Nature Communications, [online] 11(1), p.4222. doi: https://doi.org/10.1038/s41467-020-17820-2.

Oral and Poster Presentations:

- Scottish Cardiovascular Forum (SCF)
    - 2020, Glasgow, UK. Poster. Title: The Role of Calcium in Uromodulin Expression and Secretion from Renal Medullary Epithelial Cells of Hypertensive and Normotensive Rats.
    - 2023, Aberdeen, UK. Oral Presentation. Rodger-Wadsworth Prize Nominee. Title: Deciphering the Molecular Mechanisms of Uromodulin

Secretion by the Thick Ascending Limb and its Functional Relevance in Hypertension.

- The 29th Scientific Meeting of the International Society of Hypertension (ISH 2022)
    - 2022, Kyoto, Japan. Poster. Title: Salt directly regulates UMOD trafficking in a normotensive background.
- British and Irish Hypertension Society Meeting (BIHS)
    - 2021, Brighton, UK. Poster Presentation. Title: The Role of Calcium in Uromodulin Expression And Secretion From Renal Medullary Epithelial Cells Of Normotensive and Hypertensive Rats.
- 58th European Renal Association – European Dialysis and Transplant Association (ERA-EDTA) Congress
    - 2021, Virtual. Mini-Oral Presentation. Title: The Role of Calcium in Uromodulin Expression and Secretion from Renal Medullary Epithelial Cells of Normotensive and Hypertensive Rats.
- British Heart Foundation Student Conference
    - 2021, Virtual. Poster Presentation. Title: Salt Directly Influences Uromodulin Secretion from Renal Thick Ascending Limb Cells Independent of Blood Pressure Changes. 2019, London, UK. Attendee.
- European Society of Hypertension-International Society of Hypertension (ESH-ISH) Joint Meeting
    - 2021, Virtual. E-Poster. Title: The Role of Calcium in Uromodulin Expression and Secretion from Renal Medullary Epithelial Cells of Normotensive and Hypertensive Rats.
- European Council for Cardiovascular Research (ECCR) 23rd Annual Meeting
    - 2021, Virtual. Oral Presentation. Title: The Role of Calcium in Uromodulin Expression and Secretion from Renal Medullary Epithelial Cells of Hypertensive and Normotensive Rats.

Awards:

- Short-listed: Scottish Cardiovascular Forum Roger Wadsworth Prize (2023).
- College of Medical Veterinary and Life Science Conference Support Award (The 29th Scientific Meeting of the International Society of Hypertension). 750 GBP.
- The 29th Scientific Meeting of the International Society of Hypertension Travel Grant. 600 USD.

- Royal Society of Edinburgh Saltire Early Career Fellowship Award for a 3-month Project Placement (2022). Title: Kidney Organoids as a Model System for Studying the Molecular Mechanisms of Uromodulin Trafficking with Salt Stress in Hypertension. Institute for Bioengineering of Catalonia (IBEC). Barcelona, Spain. Under the Supervision of Professor Nuria Montserrat. 6,268 GBP.

Chapter 1: Introduction

1.1 The Cardiovascular System

1.1.1 The Circulatory System

The cardiovascular system is a complex network of interactions between different organ systems that work together to ensure the proper functioning of the circulatory system. It involves the heart, blood vessels, and blood, as well as interactions with the respiratory, brain, and other organ systems (Chaudhry et al., 2023). It plays a key role in maintaining homeostasis and delivering oxygen, nutrients, and hormones to various tissues and organs throughout the body. The system consists of the heart, which acts as a pump, and a network of blood vessels, including arteries, veins, and capillaries. The heart pumps oxygenated blood from the lungs to the rest of the body through systemic circulation, while deoxygenated blood is returned to the heart through pulmonary circulation to be reoxygenated (Pollock et al., 2023). The blood vessels serve as conduits for transporting blood and nutrients to the tissues and organs, as well as removing waste products (Pollock et al., 2023) (Figure 1.1).

A key aspect of the cardiovascular system is its interaction with the respiratory system, which includes the lungs and airways. This is responsible for the exchange of oxygen and carbon dioxide between the body and the environment. The cardiovascular system delivers oxygenated blood to the tissues, while the respiratory system removes carbon dioxide, a waste product of cellular metabolism, from the body (Moore et al., 2003). The cardiovascular system also interacts with the brain and the nervous system. This mediates cardiovascular function through the autonomic nervous system, which controls heart rate, blood pressure, and blood vessel constriction or dilation (Moore et al., 2003). The brain receives information from the cardiovascular system and sends signals to regulate its activity, ensuring that the body's needs are met (Moore et al., 2003). Additionally, the cardiovascular system has multiple interactions with other organ systems, such as the musculoskeletal system, which includes the muscles and bones, and the immune system. For instance, the musculoskeletal system is involved in physical activity and exercise, which can have a significant impact on cardiovascular health (Slater et al., 2011). Similarly, the immune system has long-term impacts on the cardiovascular system, with inflammation and immune responses influencing blood vessel integrity and the development of cardiovascular conditions (Lazzerini et al., 2019).

The interactions between these different organ systems within the cardiovascular system are complex and involve both linear and nonlinear interactions (Parati et al., 2019). These interactions can be described as closed loops with feed-forward and feedback mechanisms (Parati et al., 2019). The cardiovascular system exhibits multiscale, multiorgan, and multivariate complexity, emphasizing the interconnectedness and interdependence of its components (Pittman, 2011). Understanding the complex network of interactions within the cardiovascular system is crucial for studying its function, as well as for diagnosing and treating cardiovascular diseases. Advances in technology, such as mathematical modelling, network analysis, and imaging techniques, have provided insights into the dynamics and interactions of the cardiovascular system (MacLellan et al., 2012) (Niederer et al., 2019).

Cardiac output (CO) is a fundamental parameter that represents the volume of blood ejected by one ventricle in one minute (King and Lowery, 2023). It is calculated by multiplying the stroke volume (SV), which is the volume of blood ejected per heartbeat, by the heart rate (HR), the number of heart beats per minute (King and Lowery, 2023). The cardiac output is a dynamic measure that varies based on the oxygen demand of the body (King and Lowery, 2023). This means that during periods of increased physical activity or stress, the cardiac output increases to meet the higher oxygen requirements of the tissues. Conversely, during periods of rest or relaxation, the cardiac output decreases.

The movement of blood through the cardiovascular system is driven by a pressure gradient (Grassi et al., 1998). Blood pressure, which is measured in millimetres of mercury (mmHg) above atmospheric pressure, plays a crucial role in maintaining blood flow (Huang et al., 2013). Blood pressure is influenced by various factors, including cardiac output, peripheral resistance, and blood volume. During systole, when the left ventricle contracts, the pressure in the systemic arterial circulation is approximately 120 mmHg above atmospheric pressure. This pressure decreases to approximately 80 mmHg during diastole (Huang et al., 2013). The standard measurement of blood pressure is expressed as systolic

pressure over diastolic pressure, such as 120/80 mmHg (Huang et al., 2013). This is considered within the normal range of blood pressure (Charkoudian and Rabbitts, 2009).

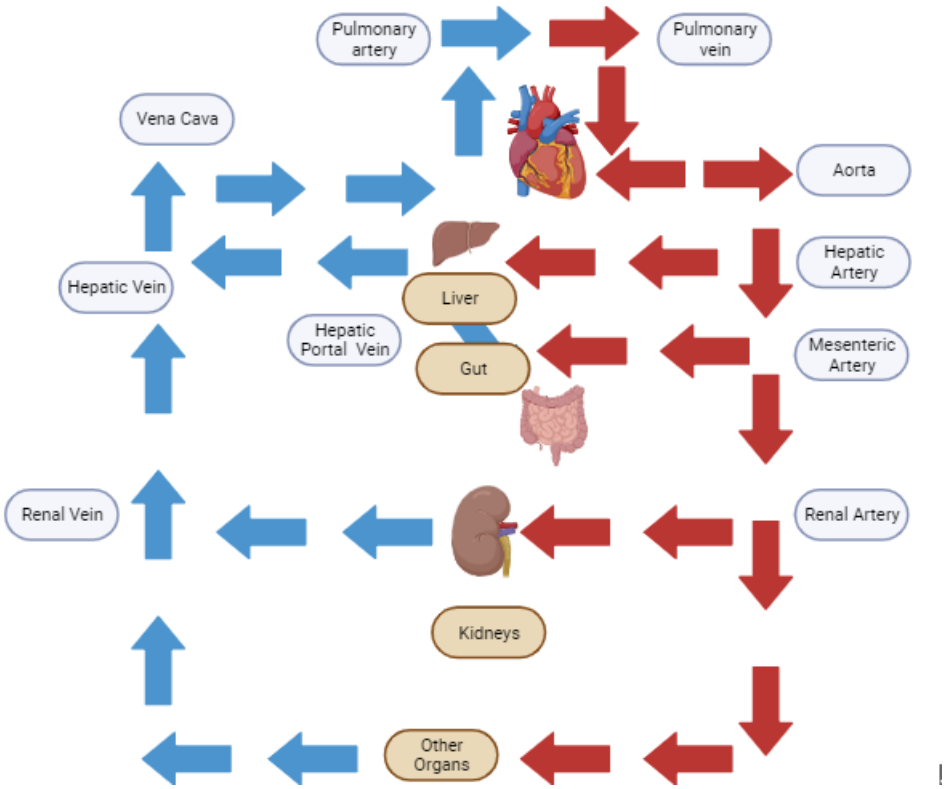

Figure 1.1. Design of the cardiovascular system (CVS).
The CVS consists of two main loops, systemic circulation (represented in red) and pulmonary circulation (in blue). The systemic circulation provides oxygenated blood and nutrients to the body, whereas the pulmonary circulation ensures the oxygenation of the blood. The two systems are connected in series through four chambers of the heart, pumping blood from the left ventricle into systemic organs and then back to the right ventricle and into the lungs. The consequences of this system are as follows, 1) the stroke volume ejected from the left ventricle is split among various organs before entering the venous outflow of the specific organ, 2) the blood in the systemic circulation provides the same composition to each organ, 3) the blood pressure entering each organ is identical, and 4) blood flow to each organ can be controlled locally and independent of one another. The illustration was made in BioRender. Adapted from (Chaudhry et al., 2023).

1.1.2 Blood Vessels

The cardiovascular system, which includes the heart and blood vessels, is responsible for pumping blood throughout the body. The heart pumps blood into the arteries, which carry oxygenated blood to the tissues. The blood vessels, particularly the arteries, play a crucial role in blood pressure regulation. The constriction and dilation of blood vessels, known as vasoconstriction and vasodilation, respectively, can significantly affect blood pressure. Vasoconstriction increases blood pressure, while vasodilation decreases it (Boedtkjer et al., 2011, Nyberg et al., 2012).

Both arteries and veins have the same three distinct tissue layers, the tunica intima, the tunica media, and the adventitia. Arteries and arterioles have thick walls that help them withstand and maintain large pressures. The functions and composition of each artery and vein type are described in Table 1.1. Blood flow through a vessel is determined by two main factors, (1) the pressure difference between the two ends of the vessel (ΔP) and (2)

the resistance to blood flow through the vessel (R). The Poiseuille equation can be used to describe blood flow (Mayet and Hughes, 2003):

$$F = \Delta P/R$$

Radius is the main factor for control of the resistance by the cardiovascular system as it controls the conductance of blood flow, with resistance mainly being located in the arterioles. Smaller arterioles need a larger difference in pressure to drive blood flow. This can be expressed as the resistance index, which measures the difference in pressure required to drive blood flow. The main resistance vessels in humans, i.e. precapillary sphincters, arterioles, and small arteries regulate up to 90% of peripheral vascular resistance (Lee et al., 2017).

Table 1.1. Structure and function of vessels in the circulatory system.

Feature	Arteries	Arterioles	Capillaries	Veins
Number	Several hundred	500,000	10 billion	Several hundred
Special Features	Thick, highly elastic walls, large radius	Highly muscular, well-innervated walls, small radius	Very thin-walled, large total cross-sectional area	Thin walled compared to arteries, highly distensible, large radius
Functions	The passageway from the heart to organs, pressure reservoir	Primary resistance vessels, determine the distribution of cardiac output	Site of exchange, determine the distribution of extracellular fluid between plasma and interstitial fluid	The passageway to the heart from the organs, blood reservoir
Structure	Endothelium, Elastin fibres, Smooth muscles, Connective tissue coat (mostly collagen fibres)	Endothelium, Smooth Muscle, Connective Tissue Coat (mostly collagen fibres)	Endothelium	Venous Valves, Endothelium, Smooth muscle/elastin fibres, connective tissue (mostly collagen fibres)
Relative thickness of layers	Smooth muscle is the thickest, followed by elastin fibres, collagen fibres, and endothelium	Smooth muscle is the thickest, followed by collagen fibres and endothelium	The endothelium is the thickest	Smooth muscle is the thickest, followed by collagen fibres, endothelium, and elastin fibres.

The table summarises the features and structure of the blood vessels in the cardiovascular system. The thickness of each layer comprising each layer is also included, which is important in determining resistance and ultimately blood pressure. The table was adapted from (Tucker et al., 2023).

1.1.3 Blood Pressure Control Mechanisms

Blood pressure regulation is a complex physiological process that involves the coordination of various systems in the body. The maintenance of blood pressure within a normal range is crucial for the proper functioning of organs and tissues. Several systems, including the nervous system, the renin-angiotensin-aldosterone system (RAAS), and the cardiovascular system, work together to regulate blood pressure (Armando et al., 2011, Crowley et al., 2005, Gangel et al., 2017, Beard et al., 2013). For the purposes of this thesis, the term “blood pressure” will be used as an umbrella term for systemic arterial blood pressure. There are both short- and long-term mechanisms of blood pressure regulation, which are often dynamic and vary with age, race, gender, circadian rhythm, and transient environmental factors. Blood pressure is calculated by multiplying CO by total peripheral resistance (TPR), which is the amount of force exerted on circulating blood by the vasculature of the body ($BP = CO \times TPR$). The Poiseuille equation as described in section 1.1.2 applies here, whereby F is CO, ΔP is the mean arterial pressure (MAP) minus the right atrial pressure (RAP), and R is the TPR. As the RAP is close to zero and negligible in comparison to MA, the equation approximates to $MAP = CO \times TPR$. Short-term mechanisms of blood pressure regulation are mainly geared towards controlling TPR, whereas longer-term mechanisms involve adjusting CO.

1.1.3.1 The Nervous System

The nervous system plays a vital role in blood pressure regulation (Figure 1.2). The autonomic nervous system, which consists of the sympathetic and parasympathetic branches, controls the constriction and dilation of blood vessels and the heart rate. The sympathetic nervous system increases blood pressure by constricting blood vessels and increasing heart rate, while the parasympathetic nervous system has the opposite effect (Ewing, 2010, Gangel et al., 2017). Cardioaccelerator (sympathetic) and cardioinhibitory areas (parasympathetic) are components of the paired cardiac centres located in the medulla oblongata of the brain Both centres provide slight stimulation to the heart during rest, thereby contributing to autonomic tone.

The cardiovascular centre receives input from a series of visceral receptors, the chief of which are baroreceptors. Baroreceptors control short-term fluctuations in blood pressure and are located in the carotid sinuses proximal to the glossopharyngeal nerve, (sympathetic, increases heart and force of contraction) as well as the aortic arch which

joins to the vagus nerve (parasympathetic, decreases hear rate) (Levick, 2010). They control blood pressure as a negative feedback loop, whereby increases in arterial blood pressure will result in an increased rate of impulse firing. The resulting increased stimulation of the nucleus tractus solitarius by the arterial baroreceptors leads to inhibition of sympathetic outflow to peripheral vasculature, ultimately leading to vasodilation and decreased TPR. The opposite occurs in decreases in blood pressure, whereby vasoconstriction and increases in TPR occur (Armstrong et al., 2023). Cardiopulmonary baroreceptors on the other hand will increase their rate of firing as a response to increased blood volume and blood pressure, which triggers sympathetic outflow to the sinoatrial node and decreased HR and CO. Sympathetic outflow to the kidneys increases, thereby increasing renal blood flow and urine production, resulting in lower fluid volume of the body (Armstrong et al., 2023).

Carotid and aortic bodies, the key peripheral chemoreceptors, are located at the bifurcation of the common carotid arteries and aortic arch, respectively. They detect changes in arterial blood oxygen (O_2), carbon dioxide (CO_2), and pH and hyperkalaemia, and are as such potent regulators of blood pressure (Prabhakar et al., 2015). These increase blood pressure through tachycardia and vasoconstriction, increasing stroke volume and TPR.

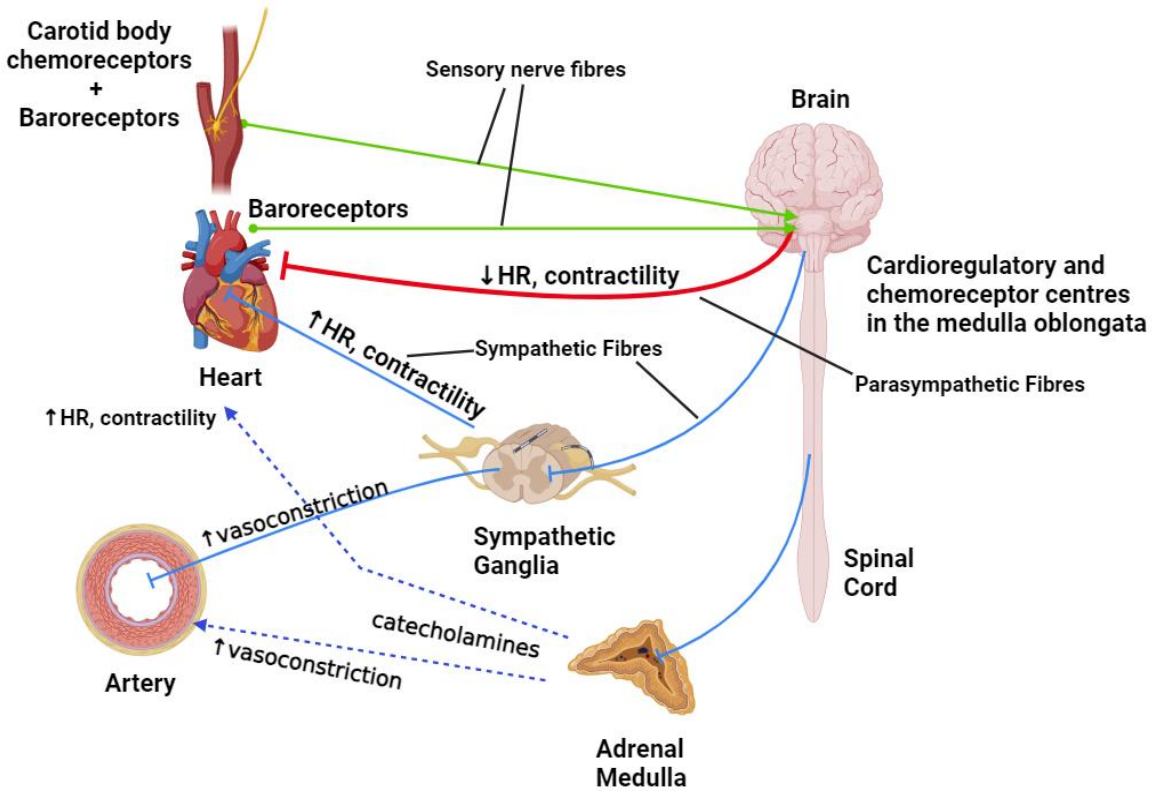

Figure 1.2 Short-term blood pressure regulatory mechanisms of the autonomic nervous system.
The arterial baroreceptors are found in the aortic arch and the carotid sinuses. The cardiopulmonary baroreceptors are located in the atria, ventricles, vena cava, and pulmonary vessels. On the other hand, chemoreceptors are found peripherally (carotid bodies and aortic arch) and centrally. The medulla oblongata in the brainstem contains the vasomotor centre, which regulates circulation. It receives signals from the sensory nerves known as the glossopharyngeal and the vagus nerve (represented by green lines). The sympathetic nerves (represented as blue lines) originate from the medulla oblongata and emerge from the upper spinal cord and end up in the sympathetic ganglia in the direction of their target organs, including the heart, the vessels, and the adrenal glands. A portion of sympathetic nerves also activate the adrenal medulla, which induces adrenaline and noradrenaline secretion (dashed blue lines) into the bloodstream. In contrast, the parasympathetic nerves also originate from the brainstem as neurones in the vagal nerve and terminate on the parasympathetic cardiac ganglia. During hypotension, vagal centres are inhibited, and the sympathetic pathway is stimulated. Figure generated in BioRender. Adapted from (Carrara et al., 2021).

1.1.3.2 The Renin Angiotensin Aldosterone System and other peptide/hormonal systems

The RAAS is another important system involved in blood pressure regulation (Figure 1.3). It is responsible for maintaining fluid and electrolyte balance in the body. The renin enzyme is released by the kidneys in response to low blood pressure or low blood volume. Renin then converts angiotensinogen, a protein produced by the liver, into angiotensin I. Angiotensin I is further converted into angiotensin II by the action of the angiotensin-converting enzyme (ACE). Angiotensin II is a potent vasoconstrictor that increases blood pressure by constricting blood vessels. It also stimulates the release of aldosterone, which promotes sodium and water retention, further increasing blood pressure via systemic vasoconstriction and stimulation of the hypothalamus (Crowley et al., 2005, Beard et al., 2013). Aldosterone is synthesized primarily in the zona glomerulosa of the adrenal cortex. It mediates its effects by binding to renal mineralocorticoid receptors on principal

epithelial cells in the cortical collecting duct (Fountain et al., 2023). Sodium is reabsorbed via the epithelial sodium channel (ENaC) on the apical membranes of principal cells in the collecting tubules. Moreover, aldosterone triggers Na-K ATPase activation at the basolateral membrane of the apical cells, resulting in sodium transport into the extracellular space and increased potassium uptake into apical cells.

Vasopressin is a nonapeptide, produced primarily in the supraoptic nucleus and paraventricular nucleus of the hypothalamus (Lozic et al., 2018). It is a key contributor to hydromineral homeostasis and induces vasoconstriction via three distinct subtypes of receptors: V1a, V1b, and V2 receptors. The V1a receptors are located in the periphery, specifically the blood vessels, kidneys, and adrenal glands, where they induce the production of aldosterone and glucocorticoids and renin production. They also work to regulate sympathetic outflow and baroreflex function. On the other hand, V1n receptors and corticotrophin-releasing factor (CRF) mediate the secretion of adrenocorticotropic hormone (ACTH) and catecholamines from the adrenal gland. The V2 receptors are highly expressed in the kidneys and act to control water retention, thereby maintaining plasma volume and osmolality (Lozic et al., 2018). At lower blood pressure, vasopressin acts to induce systemic vasoconstriction and lowering urine output from the kidney.

Another form of blood pressure regulator are the natriuretic peptides, specifically atrial natriuretic peptide (ANP) and B-type natriuretic peptide (BNP). Both ANP and BNP are expressed and stored as prohormones in granules of the atrial myocytes a in mammalian hears and released into the bloodstream upon distension of atrial or ventricular cardiomyocytes (Zois et al., 2014). They have various functions, one of the most important being blood pressure regulation. Increasing circulating concentrations of ANP and BNP are associate with lower blood pressure and reduced risk of hypertension (Zois et al., 2014). ANP has the highest levels physiologically compared to BNP, although increased circulating concentration of the latter is found in patients with advanced essential hypertension (Macheret et al., 2012). These peptides reduce plasma volume by vasodilation and increasing salt and fluid excretion in the kidneys (Harris et al., 1987). They also act as physiological antagonists of the RAAS (Kuhn, 2016). Furthermore, natriuretic peptides also attenuate sympathetic nervous system activity in part through interaction with central vasopressin pathways.

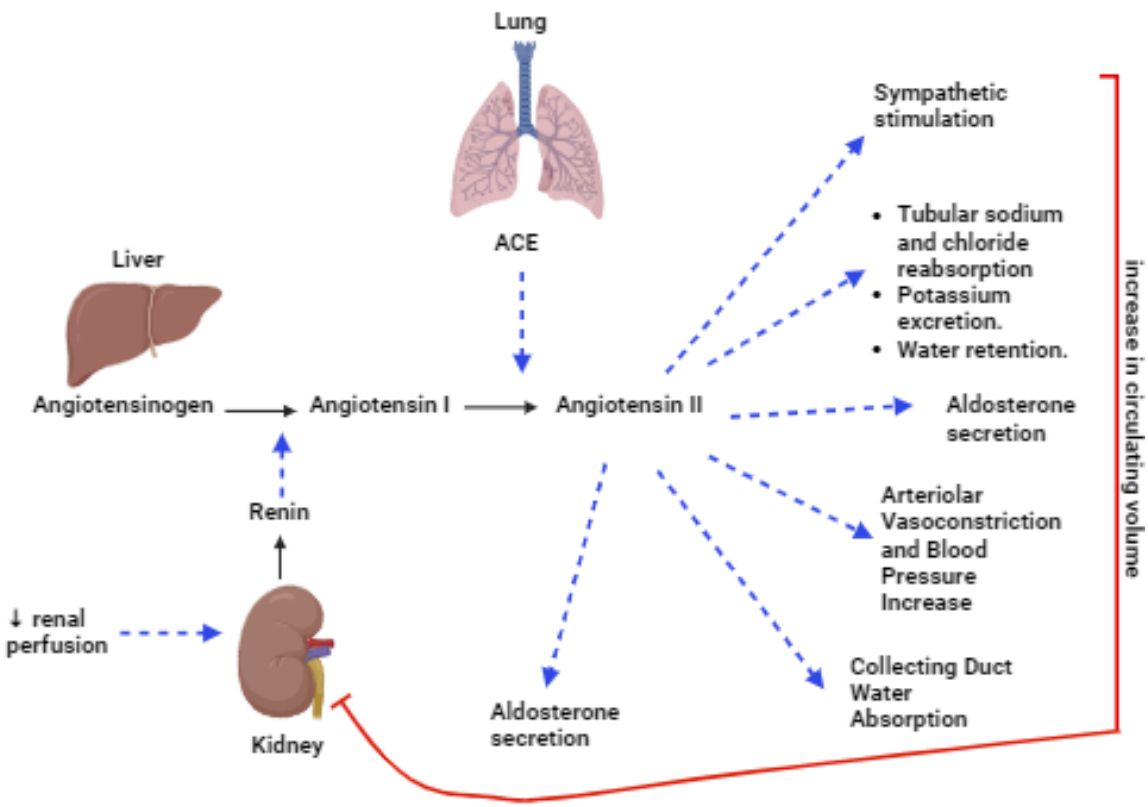

Figure 1.3. Illustration of the components and function of the renin-angiotensin aldosterone system (RAAS). The RAAS is chiefly involved in regulating salt and water balance, and by extension blood pressure. Renin catalyses the conversion of angiotensinogen into angiotensin I, which is in turn converted to angiotensin II by the angiotensin-converting enzyme (ACE). Angiotensin II has been associated with a host of different functions, including sodium retention and water retention by inducing secretion of antidiuretic hormones. High sodium intake and plasma volume/osmolality increases trigger negative feedback on renin secretion. Also, high sodium decreases aldosterone concentration, therefore lowering sodium reabsorption and promoting sodium excretion. More "novel" components of the RAS and particularly those deriving from ACE2 are not depicted here. Image generated in BioRender. Adapted from (de Almeida and Coimbra, 2019).

1.1.3.3 Reactive Oxygen Species

Reactive oxygen species, including superoxide ($O_2^{\bullet-}$) and hydrogen peroxide (H_2O_2), are signalling molecules that are important in a variety of physiological processes, including blood pressure control. Reactive Oxygen Species (ROS) are produced from cellular respiration and metabolic processes as byproducts via the activation of enzymes such as xanthine oxidoreductase, uncoupled NO synthase (NOS), mitochondrial respiratory enzymes, as well as nicotinamide adenine dinucleotide phosphate (NADPH) oxidases (Nox). The Noxs are one of the most important sources of $O_2^{\bullet-}$ and H_2O_2 in the cardiovascular system. The association of ROS and blood pressure was proven initially in a rat model, whereby Angiotensin II induced hypertension in rats increased vascular ROS production via non-phagocytic NADPH oxidase activation (Rajagopalan et al., 1996). Since then, it has been demonstrated that most experimental models of hypertension exhibit some degree of oxidative stress (Montezano and Touyz, 2014). Mice models with reduced antioxidant enzyme systems and those with deficient NADPH oxidase exhibit higher blood pressures than the respective wild-type animals. ROS have been directly

implicated in blood pressure increases via the kidney, wherein they induce sodium retention (Sedeek et al., 2013). The exact mechanisms by which ROS influence blood pressure remain unclear. Excess or unmitigated ROS production promotes oxidative stress, which can cause damage to DNA, proteins, and lipids, leading to cell injury and cytotoxicity (Montezano and Touyz, 2014). In the vascular system, since ROS control endothelial function and vascular tone, oxidative stress leads to endothelial dysfunction, inflammation, and vascular remodelling, all of which are hallmarks of hypertension (Al Ghouleh et al., 2011, Bir et al., 2012, Tabet et al., 2008, Ushio-Fukai et al., 1998)

1.1.3.4 Environmental Factors

In addition to these systems, environmental stressors can also influence blood pressure. One such stressor is NaCl (referred to as “salt” hereafter). High salt intake has been associated with increased blood pressure in individuals with essential hypertension (Nyberg et al., 2012). The World Health Organization defines over 5 grams of sodium per day as excessive sodium consumption (Mente et al., 2021). In contrast, a reduction in sodium intake has been demonstrated to decrease blood pressure and hypertension incidence (Whelton and He, 2014). The mechanisms by which salt affects blood pressure are not fully understood, but it is believed to involve the regulation of fluid balance and the renin-angiotensin system (Van Vliet and Montani, 2008). One proposed mechanism postulates that increased salt intake induces water retention, thus leading to a condition of higher flow in arterial vessels. This can also influence vascular resistances. Salt sensitivity, which refers to an individual’s blood pressure response to changes in salt intake, varies among individuals. Some individuals are more sensitive to the blood pressure-raising effects of salt than others (Tomiyama et al., 1992, Yamasue et al., 2006), known as salt-sensitive individuals.

1.2 Hypertension

Hypertension is a prevalent and significant health condition that affects a large proportion of the global population. It is a major risk factor for cardiovascular diseases, including stroke, coronary artery disease, and heart failure. Hypertension is characterized by persistently elevated blood pressure levels, typically defined as systolic blood pressure (SBP) of 140 mmHg or higher and/or diastolic blood pressure (DBP) of 90 mmHg or higher (Flack and Adekola, 2020), but values below this can be called “high normal”. Approximately 95% of hypertensive cases are known as essential hypertension, which is defined as having an unknown cause resulting from mixed interactions of genetic and

environmental factors. The remaining 5% of cases are classed as secondary hypertension, of which 1% are monogenic disorders (Cowley, 2006).

Statistics indicate that hypertension is a global public health concern. According to the World Health Organization (WHO), approximately 1.13 billion people worldwide have hypertension, and this number is projected to increase to 1.56 billion by 2025 (Anthony, 2019). In Scotland, around a quarter of the population aged 16 years and over had raised blood pressure in 2019 (Observatory, 2022). Furthermore, hypertension is responsible for a significant burden of disease, contributing to approximately 7.6 million deaths annually). Rather surprisingly, over a third of hypertensive patients remain undiagnosed (Arima et al., 2011).

The development and progression of hypertension involve a complex interplay of various factors. Lifestyle factors, such as unhealthy diet, physical inactivity, tobacco use, and excessive alcohol consumption, contribute to the development of hypertension (Flack and Adekola, 2020). Genetic factors also play a role, as there is evidence of a hereditary component to hypertension (Natekar et al., 2014). Additionally, other medical conditions, such as obesity, diabetes, and CKD, are closely associated with hypertension (Choi et al., 2005, Hall et al., 2014).

1.2.1 The Role of Genetics in High Blood Pressure

Genetic factors are a key challenge for causal studies of hypertension. Twin and family-based studies have demonstrated that 30-50% of the variance in blood pressure readings may be heritable. Blood pressure data acquired across three generations in the Framingham Heart Study indicated that higher blood pressure in grandparents is `associated with a higher risk of reoccurrence in third-generation offspring (Niiranen et al., 2017). Genetics as a contribution to hypertension was recognized in Page's "Mosaic Theory of Hypertension" (Olczak et al., 2021), which contained evidence from multiple familial studies and rare disorders that have contributed to the discovery of causal Mendelian mutations (Ehret and Caulfield, 2013). The polygenic nature of hypertension was first argued by Pickering, who theorised that Gaussian distribution of blood pressure throughout the population is determined by a collection of genes (Brown, 2012). In this regard, hypertension is a quantitative trait with a normal distribution. In fact, later studies estimating the heritability of hypertension supported this, with clinical SBP and DBP at 15-40% and 15-30%, respectively (Havlik et al., 1979).

Gene mapping techniques enabled by The Human Genome Project hugely assisted in linkage analysis, which helped provide chromosomal locations of genes for traits. Studies of monogenic disorders of hypertension allowed identification of blood pressure associated genes and highlighted the importance of the kidneys and adrenal glands in blood pressure control (Raina et al., 2019). For instance, research on patients with Liddle syndrome uncovered gain-of-function mutations in *SCNN1B* and *SCNN1G* genes that encode subunits of ENaC. This underlined the role of sodium reabsorption in the regulation of blood pressure. However, monogenic disorders only account for a small percentage of hypertensive patients.

Polygenic forms of hypertension were analysed using candidate linkage studies in cohorts including large families (Olczak et al., 2021). A linkage analysis of 63 White European families identified variants of the *AGT* gene encoding angiotensinogen, which showed variation between different ethnic populations in subsequent studies (Gurdasani et al., 2019). However, the nature of these studies was inherently underpowered and lacked reproducibility. To this extent, the advent of genome-wide association studies (GWAS) helped identify loci across the entire genome without bias. These studies helped discover numerous quantitative trait loci (QTLs), which are regions of DNA linked to variations in a phenotype, linked with hypertension (Ehret et al., 2009, Munroe et al., 2006, Chang et al., 2007). However, the interpretation of such data is limited as QTLs span broad regions of DNA and thus identification of variants with smaller effect sizes or single genes difficult (Cowley, 2006). Functional studies in animal models and bioinformatic analysis can assist greatly in this matter (Ehret et al., 2011, Bai et al., 2013).

1.2.2 Immune System

The role of the immune system in the pathogenesis of hypertension has been firmly established by numerous studies (Figure 1.4). The immune system contributes significantly to hypertension development by inducing inflammation in the nervous system, the cardiovascular and the renal systems, all of which are pivotal to blood pressure regulation (Singh et al., 2014). There are various experimental models of hypertension that have linked specific cytokines and lymphocytes to the development of hypertension and hypertensive organ injury, such as the spontaneously hypertensive rat (SHR), deoxycorticosterone acetate (DOCA)-salt, and angiotensin II and renal damage, to name a few (Singh et al., 2014).

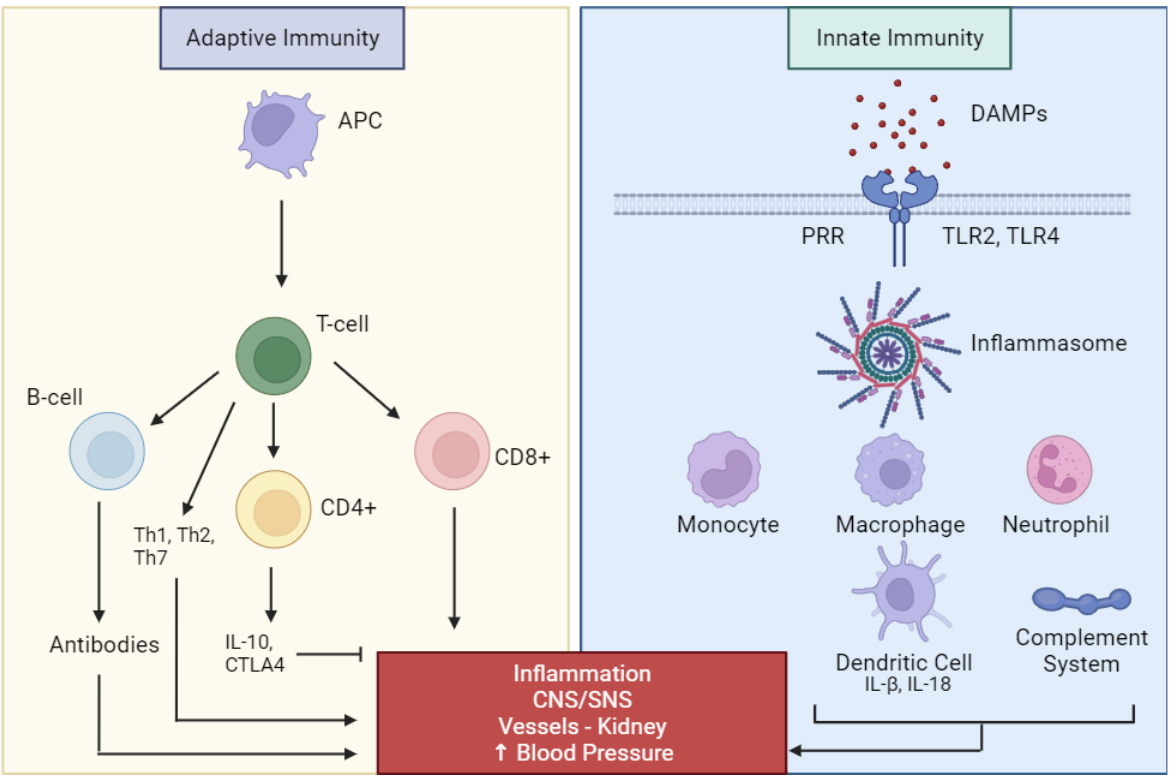

Figure 1.4. A summary of the two branches of the immune system and their role in hypertension.
The two main branches of the immune system are the adaptive and innate immune system. They both contribute to establishing inflammation in the kidney, arteries, and the autonomic nervous system. In the adaptive immune system, antigens are recognised and presented by antigen-presenting cells (APC) to naïve T lymphocytes (specifically, the T-cell receptor) via the major histocompatibility complex (MHC). This induces stimulation of the antibody producing B cells and helper (CD4+) and cytotoxic (Cd8+) T cells. The CD4+ T-cells produce a proinflammatory cytokine response via Th1, Th2, and IL-17, as well as T regulatory cells (Tregs) to modulate the inflammation. In contrast, the innate immune system is triggered by danger-associated molecular patterns (DAMPs) which are identified by pattern recognition receptors (PRR), mainly via the toll-like receptors (TLR). The TLR stimulate the inflammasome complex, which is the main driver of the innate immune response. The most important innate immune cells involved in this process are monocytes, macrophages, neutrophils, dendritic cells, as well as natural killer cells and the complement system. The black arrows represent stimulation, whereas an arrow with a solid dash at the end symbolises inhibition. This illustration was generated in BioRender. Adapted from (Rodriguez-Iturbe et al., 2017).

1.2.2.1 An Overview of the Types of Immune Responses

There are two main components of the immune system, innate immunity, and adaptive immunity. The innate immune system is responsible for the acute response to antigens and is often referred to as the “first line of defence”. The two main pattern of antigens

recognised by the innate immune system are those generated by pathogenic microorganisms, known as pathogen-associated molecular patterns (PAMPs), or produced by endogenously expressed cellular stress signals, or danger-associated molecular patterns (DAMPs). These signals are recognised by pattern recognitions receptors (PRRs) that induce caspase-1acgtivating complexes referred to as inflammasomes. The inflammasomes initiate signalling that leads to the processing and secretion of proinflammatory cytokines, which ultimately induce cell death via pyroptosis (Schroder and Tschopp, 2010). There are four main inflammasome complex (NLRP1, NLRC4, NLRP3, and AIM2), of which the most interesting is NLRP3 which has been shown to be activated during hypertension. Toll-like receptors (TLRs) are a group of PRR that are expressed by T and B lymphocytes, monocytes, dendritic cells, as well as somatic cells. They also activate the inflammasome pathways, which leads to the upregulation of a variety of inflammatory factors such as NF-κB, AP-1, and interferon-regulatory factors, as well as Il-1β and IL-18. Furthermore, the inflammasome plays an important role in activating the acquired immune response (or adaptive immunity) by presenting antigens to T-cells (Martinon and Tschopp, 2004).

The adaptive immune response is characterized by its specificity towards exogenous and endogenous antigens. The system functions primarily through effectors cells known as T and B lymphocytes. The activation of T-cells typically requires presentation of antigens by antigen-presenting cells (APC) via a major histocompatibility complex (MHC). This interaction involves interactions of the antigen with a specific T-cell receptor (TCR), co-stimulation with CD80 or CD86 which link to CD28 on the T-cell. Depending on proper activation, this may then lead to clonal expansion (Curtsinger and Mescher, 2010). Also, the adaptive immunity has the capability of memory, or more specifically an accelerated response to subsequent to a repeat antigen, which is provided by memory T-cells. Finally, cytokines generated by CD4+ T cells generate and maintain B-cell humoral immune responses, which are responsible for antibody production.

1.2.2.2 Cytokines and Hypertension

The key cytokines relevant to hypertension are generated by T-cells, B cells, mast cells, macrophages, and dendritic cells. Importantly, the balance of cytokines will determine the impact on hypertension. For example, angiotensin-induced hypertensive renal damage is associated with upregulation of Th1 cytokine interferon gamma (IFN-γ) and a decrease in Th2 cytokine IL-4 (Shao et al., 2003). However, it should be noted that cytokines often have overlapping functions, which needs to be considered when evaluating the effects of individual cytokines on hypertension progression (Crowley and Jeffs, 2016).

One of the most important cytokines involved in hypertension development is Tumour Necrosis Factor-α (TNFα). It is produced by macrophages, natural killer (NK) cells, and T-cells and has been proven to activate endothelial cells and neutrophils, as well as causing catabolism of fat and muscle. TNFα$^{-/-}$mice were shown to have increased endothelial nitric oxide synthase (eNOS) production and were guarded from hypertension progression, as well as sodium and water retention, induced by Angiotensin II infusions (Sriramula et al., 2008, Zhang et al., 2014a). Interestingly, since TNFα reduces renal blood flow and inhibits NKCC2 activity, it has been postulated that blood pressure effects of TNFα are most likely dependent on the balance between vasoconstriction and renal sodium balance (Rodriguez-Iturbe et al., 2017). Another critical example of cytokines involved in hypertension is Transforming Growth Factor Beta (TGFβ), which is primary produced by regulatory T-cells and macrophages. It has roles in fibrosis, stimulating collagen production by fibroblasts, and inhibits activation and proliferation of several immune cells, such as T and B-cells. In the Dahl salt-sensitive rat model, administration of anti-TGFβ (effectively neutralising its effects) was associated with reduced renal and cardiac fibrosis (Dahly et al., 2002, Murphy et al., 2012). Cytokines do not only induce hypertension but play a key protective role as well. For instance, Interleukin (IL)-10 has anti-inflammatory properties and is produced by monocytes, Th2 lymphocytes, mast cells, B cells, and regulatory T-cells. In experimental models of preeclampsia, IL-10 administration was shown to attenuate hypertension and albuminuria (Tinsley et al., 2010). Alternatively, a deficiency in IL-10 promotes endothelial dysfunction and ROS production, highlighting its immunosuppressive role (Didion et al., 2009).

1.2.2.3 Innate Immunity and Hypertension

As mentioned earlier, the key complex involved in the innate immune response in hypertension is NLRP3 inflammasome. Lowering of TLR4 levels ameliorates or entirely prevent hypertension (Bomfim et al., 2012, Dange et al., 2015, Sollinger et al., 2014). Several components have been linked to the activation of inflammasome in hypertension, such as soluble and crystalline urate, reactive oxygen species, and ATP-induced activation of the P2X7 receptor (Rodriguez-Iturbe et al., 2017). The latter is an ion-gated channel that generates potassium efflux, which is key to inflammasome activation. Angiotensin II infusion in Dahl salt-sensitive rats leads to overexpression of P2X7 and hypertension, which can be ameliorated by its inactivation (Vonend et al., 2004, Ji et al., 2012). The binding of inflammasome end products, IL-1β and Il-18, to their specific receptors is critical for regulating activity of lymphocytes, monocytes, vascular endothelial cells, vascular smooth muscle cells, and renal epithelial tubular cells. Their activation triggers

downstream signalling of transcription factors such as NF-κB. Rat resistance arteries stimulated with IL-1β and IL-18 have increased ROS and impaired vasodilation (Jiménez-Altayó et al., 2006). Moreover, administration of IL-1β via osmotic pump to SHRSP animals led to increased hypertension and incidence of stroke (Chiba et al., 2012). Another significant aspect to consider in the innate immune system is the complement system, which is a network of proteins involved in inflammatory and cytolytic responses. Although, it remains poorly studied in the context of hypertension, one study showed that that deficiency of C3, a key complement factor, prevented hypertension and renal injury by preventing activation of RAAS and renal fibrosis (Zhou et al., 2013).

1.2.2.4 Adaptive Immunity in Hypertension

There are a plethora of studies highlighting the role of adaptive immunity in hypertension. As discussed earlier, antigen presentation is a key aspect to priming the adaptive immune system and in hypertension, this process is exacerbated. For example, it has been demonstrated that isoketal-modified proteins and overexpression of Heat Shock Protein 70 (HSP70) are antigens involved in hypertension activated immune reactivity (Kirabo et al., 2014, Ishizaka et al., 2002). B-cell activation has been shown to be critical to development of Angiotensin II-induced hypertension (Chan et al., 2015). Furthermore, the central nervous system and sympathetic nervous system are triggered by oxidative stress when induced by angiotensin I, thus triggering the release of activated T cells from the spleen and infiltration of immune cells into target (Carnevale et al., 2014, Xiao et al., 2015). Co-stimulation is another important factor in antigen presentation, which is underlined by the studies with DOCA-salt and angiotensin II-induced hypertensive models that demonstrated amelioration of hypertensive phenotype following blockade of the B7 costimulatory pathway or genetic deletion of CD80 and CD86 ligands (Vinh et al., 2010).

1.2.2.5 Pathophysiology of Inflammation and Renal Hypertension

The outcome of elevated blood pressure is a consequence of many factors, including activated immune cells, oxidative stress, angiotensin II induced inflammation of the kidney, arteries, and nervous system. Oxidative stress induced pro-inflammatory transduction pathways (JNK, p38 MAPL) and transcription factors such as NFκB, whereas inflammation is a strong amplificatory of oxidative stress by inducing increased ROS generation (Los et al., 1995). Angiotensin II interacts with both oxidative stress and inflammatory components, with increased circulating RAAS and intrarenal RAS activation contributing significantly to hypertension (Navar, 2004, Navar et al., 2002). Further experiments involving expression of the angiotensin-type I receptor have a supressed Th1

inflammatory response and protect kidneys from angiotensin-II induced injury (Navar et al., 2002, Szabo et al., 2000). On different immune cells, specifically LysM macrophages, supressing the angiotensin-type I receptor led to increased tubulointerstitial fibrosis, suggesting activation of the receptor normally attenuates the expression of proinflammatory macrophages (Zhang et al., 2014b).

Renal inflammation impacts the pressure-natriuresis response, i.e. maintenance of sodium balance, and elevation of blood pressure, indicating a key role in pathogenesis of hypertension (Guyton et al., 1972). In the kidney, renal infiltration of immune cells in spontaneous hypertensive rats (SHRs) occurs prior to development of hypertension (Rodríguez-Iturbe et al., 2004). Moreover, there is a direct correlation of intensity of immune cell infiltration in the kidneys with severity of hypertension in this model (Rodríguez-Iturbe et al., 2002). Interestingly, in salt-sensitive hypertension, the accumulation of immune cells in tubulointerstitial areas is inversely correlated with fractional sodium excretion (Franco et al., 2013). With regards to RAAS activity, renal inflammation has been linked to increased angiotensin II activity which impairs pressure-natriuresis. Also, chronic hypertension requires persistent renal RAAS activation and studies with inbred mice deficient renal ACE showed that renal ACE is key to salt sensitive hypertension development as a result of inflammatory injury (Franco et al., 2007, Franco et al., 2013).

1.2.3 Environmental Influences and Salt

Factors that determine an individual's risk of developing hypertension often involve a complex set of interactions between multiple genes as well as environmental factors (Kunes and Zicha, 2009). There is significant evidence for the involvement of the "modern" diet and lifestyle in driving the continued epidemics in obesity, hypertension, diabetes, atherosclerosis, and other symptoms of metabolic syndrome (Eaton and Eaton, 2003). This process is mostly exacerbated by a shift in diet from unprocessed food to one high in fat, sugar, and salt. Moreover, sedentary lifestyle and the resulting excess weight have been linked to subsequent increased cardiovascular event risks, such as non-fatal arrhythmia, myocardial infarction, spontaneous cardiac death (Myers et al., 2002). These are all modifiable risk factors that can prevent and treat cardiovascular disease progression. For instance, moderate physical activity (aerobic exercise) has been associated with significant blood pressure reductions (Kunes and Zicha, 2009). Additionally, there is an increased understanding that some environmental factors, such as stress, diet (e.g. salt), and temperature can be causal of certain diseases, including hypertension, if present in

critical development windows of an organism (Kunes and Zicha, 2006). For example, the association of low birth weight and onset of raised blood pressure later in life has led to the "programming hypothesis", which states that impairment of the intrauterine environment leads to greater risk of cardiovascular disease later in life, including hypertension (Eriksson et al., 2007). Although, controversy exists as to the underlying mechanisms involved in this process.

One important environmental factor that has been extensively studied in relation to hypertension, and is of particular interest in this thesis, is salt intake (Figure 1.5). Salt is an ionic compound consisting of 40% sodium and 60% chloride. The recommended daily salt intake for adults is less than 5 grams of salt per day (Grillo et al., 2019). Excess dietary salt has been identified as a major contributor to the development and severity of hypertension (Elijovich et al., 2016). High salt intake can lead to an increase in blood volume, resulting in elevated blood pressure (Graudal et al., 2011). In numerous epidemiologic, clinical, and experimental studies, dietary sodium has been linked to hypertension, with some patients being particularly salt-sensitive (He and MacGregor, 2010, Freis, 1992, Whelton et al., 1998, He et al., 1999, Sacks et al., 2001a, O'Donnell et al., 2014a). These patients exhibit a difference in mean arterial pressure that is 10mmHg greater when salt balance is altered by a combination of diet and loop diuretics (Elijovich et al., 2016). However, there are also studies suggesting a less prominent role for salt in hypertension (Stolarz-Skrzypek et al., 2011), with persons able to consume large amounts of salt without substantial rises in arterial pressure. A Cochrane review showed that dietary salt restriction attenuates blood pressure by 0.5mmHg in normotensive individuals, and by 4mmHg in hypertensive patients (Graudal et al., 2011). Therefore, reducing salt intake is often recommended as a lifestyle modification to manage and prevent hypertension (Graudal et al., 2011). However, dissecting the individual effects of salt intake on blood pressure is challenging due to high variability.

The kidneys play a crucial role in regulating sodium balance, and any dysfunction in this process can contribute to the development of hypertension (Grillo et al., 2019). Nearly known monogenic disorders of blood pressure affect kidney salt metabolism (Lifton et al., 2001). For instance, loss of function of the thiazide-sensitive NaCl cotransporter (NCC) expressed predominantly in the distal convoluted tubule, known as Gitelman's syndrome, leads to salt wasting and hypotension despite RAAS activation (Lifton et al., 2001). Moreover, excess salt and water retention are characteristic of certain forms of salt sensitivity, such as CKD (Vidal-Petiot et al., 2018). It is therefore prudent to consider

kidney physiology when analysing the mechanisms responsible for salt-sensitive hypertension.

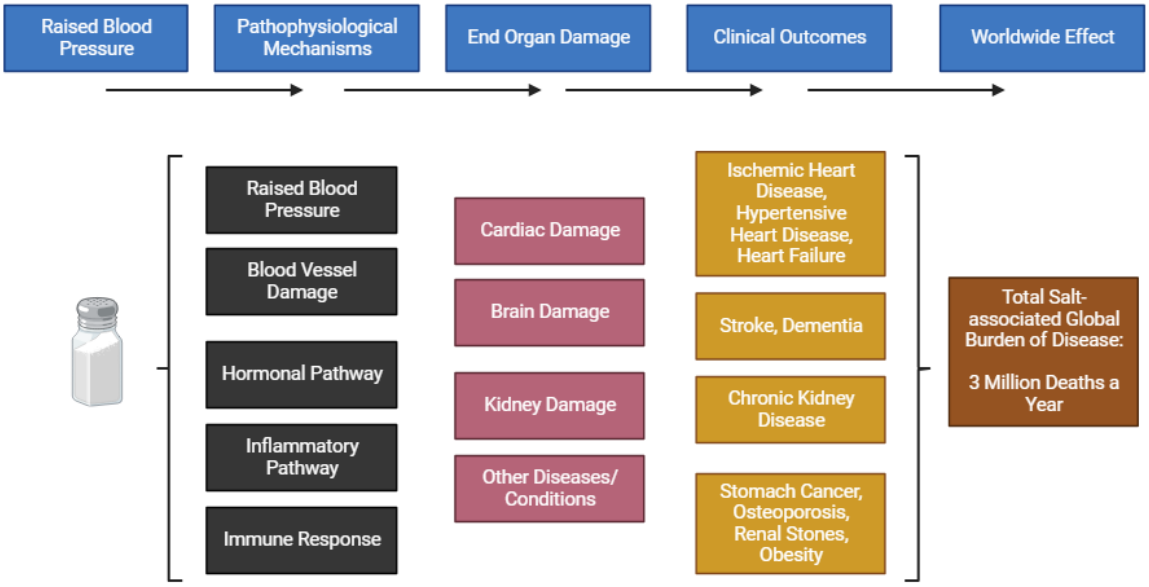

Figure 1.5. Illustration of pathways involved in pathogenesis of various diseases as a result of excessive salt intake. Excess salt diet induces multiple pathophysiological mechanisms that over time lead to end organ damage and chronic diseases. Together, this accounts for 3 million deaths a year worldwide. Figure made in BioRender. Adapted from (He et al., 2020). l

1.3 Kidney Physiology

1.3.1 Kidney Function

The kidneys are vital organs responsible for maintaining fluid and electrolyte balance, regulating blood pressure, and filtering waste products from the blood. They play a crucial role in maintaining homeostasis in the body. The structure and function of the kidneys are intricately linked, allowing them to perform their essential tasks efficiently (Denic et al., 2016, Ogobuiro and Tuma, 2023). They have a rich blood supply, whereby the renal artery brings oxygenated blood to the kidneys, which is then filtered by the nephrons. The filtered blood is collected by the renal veins and returned to the systemic circulation. The kidneys receive approximately 20% of the cardiac output, highlighting their importance in maintaining overall cardiovascular health (Dalal et al., 2023). In addition to their filtration and excretory functions, they produce hormones and bioactive molecules such as erythropoietin, a hormone that stimulates the production of red blood cells, and renin (Kurt and Kurtz, 2015).

The structure and function of the kidneys can be influenced by various factors. Ageing, for example, can lead to structural and functional changes in the kidneys, including a decline in GFR and changes in tubular reabsorption and secretion capacities (Denic et al., 2016). Environmental stressors, such as heat stress, can also affect kidney structure and function

(Chang et al., 2023). Additionally, certain diseases and conditions, such as CKD and diabetes, can cause detrimental alterations that ultimately result in loss of function (Nordheim and Geir Jenssen, 2021).

1.3.2 Kidney Structure

The basic structural unit of the kidney is the nephron (Figure 1.6). Each kidney contains millions of nephrons, which are responsible for filtering the blood and producing urine. The nephron consists of a renal corpuscle, which includes the glomerulus and Bowman's capsule, and a tubule system, which includes the proximal tubule, loop of Henle, distal tubule, and collecting duct (Preuss, 1993). The glomerulus is a network of capillaries surrounded by Bowman's capsule. It is responsible for the filtration of blood and the formation of the primary urine. The glomerular filtration rate (GFR) is a measure of the amount of blood filtered by the glomerulus per unit of time and is an important indicator of kidney function (Kaufman et al., 2023). The tubule system of the nephron is involved in the reabsorption and secretion of various substances. The proximal tubule is responsible for the reabsorption of water, electrolytes, and nutrients from the filtrate back into the bloodstream. The loop of Henle plays a crucial role in the concentration of urine by creating a concentration gradient in the medulla of the kidney. The distal tubule and collecting duct are involved in the final adjustment of urine composition and volume (Madsen et al., 1988).

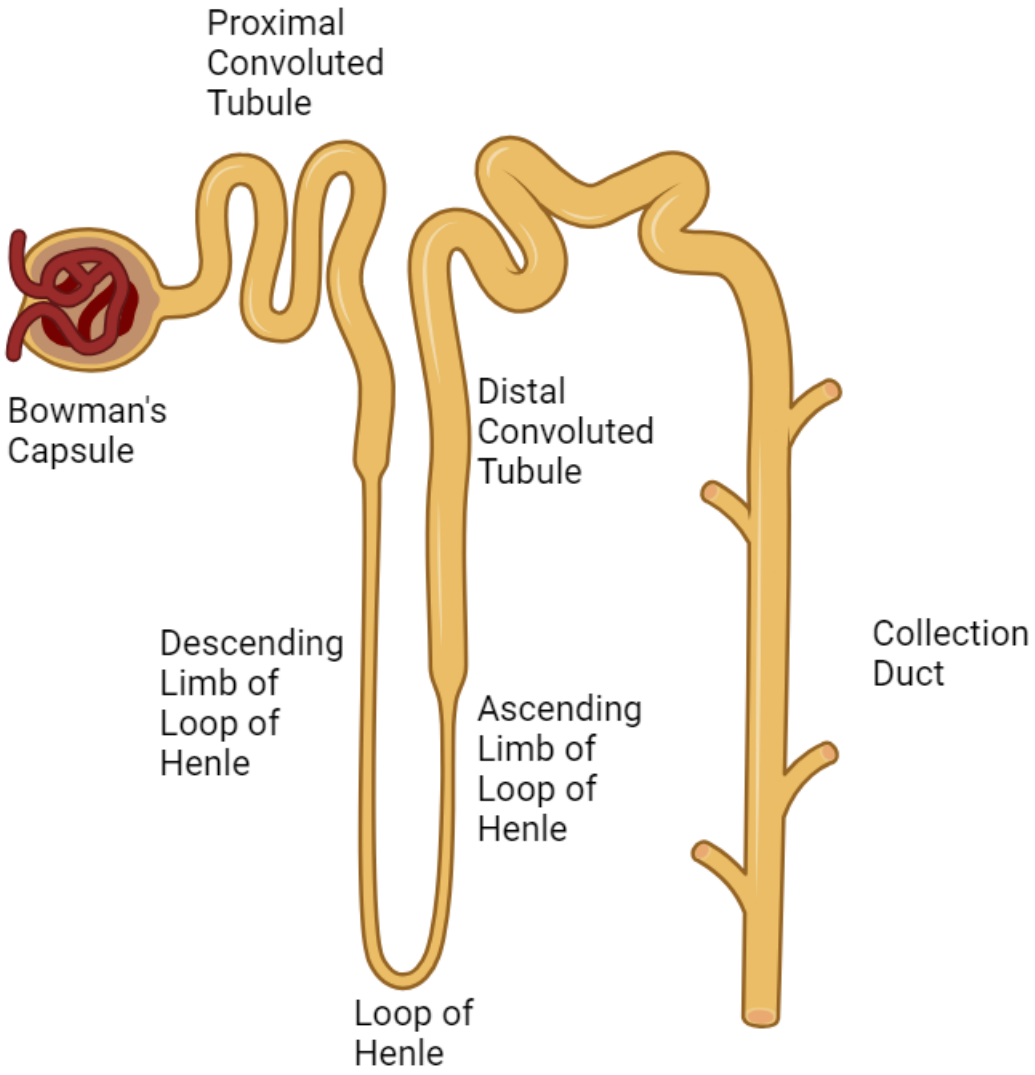

Figure 1.6. Basic Structure of the Kidney Nephron.
The nephron is the basic structural and functional unit of the kidney. In humans, there are approximately 1,200,000 nephrons (Feher, 2017). The nephron comprises of the glomerulus, Bowman's capsule, the proximal convoluted tubule, the loop of Henle, the distal convoluted tubule, and the collecting duct. The nephron can be classified into two main types: cortical nephrons and juxtamedullary nephrons. The former has a glomerulus located near the outer parts of the cortex and have relatively short loops of Henle. In contrast, the juxtamedullary nephrons have a glomerulus near the junction of the cortex and medulla, and their loops of Henle are longer, thus penetrating deeper into the medulla. In humans, 85% of nephrons are cortical nephrons, whereas 15% are juxtamedullary nephrons (Feher, 2017). In rats, this is 72% and 28%, respectively (Ichii et al., 2006). Urine formation begins in the Bowman's capsule inside the Bowman's space, whereby an ultrafiltrate of plasma is formed together with the glomerulus. The ultrafiltrate then flows along the tube of the nephron, firstly in the proximal convoluted tubule, wherein absorption of water, salt, amino acids, glucose, and bicarbonate. From here, the urine travels to the loop of Henle which acts as a countercurrent multiplier, establishing an osmotic gradient that runs from 300 mOsm in the cortex to as high as 1200 mOsm in the inner medullary interstitium. The point of interaction between thick ascending limb, afferent arteriole, and efferent arteriole is the juxtaglomerular apparatus. This is where the distal convoluted tubule starts, which is responsible for further reabsorption of water and salt. The distal convoluted tubule connects to the collecting duct where the final concentration of urine occurs. This greatly contributes to the concentration of the urine. Structures are not drawn to scale. Figure produced in BioRender.

1.3.2.1 The Thick Ascending Limb

The thick ascending limb (TAL) of the loop of Henle is a crucial segment of the nephron in the kidney. It plays a vital role in the reabsorption of sodium, potassium, and chloride ions, as well as the regulation of urine dilution. The epithelial cells that line the TAL are specialized for these functions and express specific transport proteins (Zacchia et al., 2018).

The TAL is responsible for the reabsorption of approximately 25% of filtered sodium and chloride ions. This reabsorption occurs through the activity of the Na^+-K^+-$2Cl^-$ cotransporter (NKCC2), which is highly expressed on the luminal membrane of the renal tubular epithelial cells in the TAL (Mount, 2014). NKCC2 is essential for the normal reabsorption of sodium, potassium, chloride, calcium, and magnesium ions (Castrop and Schießl, 2014). The transport of ions in the TAL is driven by the electrochemical gradient established by the basolateral Na-K ATPase, which pumps sodium out of the cell and potassium into the cell. The NKCC2 cotransporter uses the energy from this sodium gradient to transport sodium, potassium, and chloride ions into the cell (Castrop and Schießl, 2014). The reabsorption of sodium, potassium, and chloride ions in the TAL is critical for the generation of a concentration gradient in the medulla of the kidney. This gradient is essential for the reabsorption of water in the collecting ducts and the production of concentrated urine (Sands and Layton, 2009). In addition to ion transport, the TAL is also involved in the regulation of acid-base balance by reabsorbing bicarbonate ions and secreting hydrogen ions (Kim et al., 1999). Furthermore, TAL can contribute to the regulation of blood pressure through the production of vasoactive substances, such as prostaglandins (Gonzalez-Vicente et al., 2019).

The epithelial cells that line the TAL have unique characteristics that enable them to perform their specialized functions. These cells have a high density of mitochondria, which provide the energy required for active ion transport (Ohsaki et al., 2012). They also express specific transport proteins, such as NKCC2, that are essential for ion reabsorption (Ares et al., 2011). Additionally, the cells of the TAL express specific markers, such as uromodulin (also known as Tamm-Horsfall protein, abbreviated to UMOD hereafter), which is the most abundant urinary protein in healthy humans (Boder et al., 2021).

1.3.3 Kidneys and Blood Pressure Regulation

As mentioned earlier, the kidneys play a crucial role in the regulation of blood pressure, ensuring that it remains within a normal range to maintain proper organ and tissue function. The intricate interplay between the kidneys and various physiological systems allows for the fine-tuning of blood pressure control. The kidneys contribute to blood pressure regulation through several mechanisms, including RAAS, sodium and water balance, and the regulation of renal blood flow (Wadei and Textor, 2012).

The kidneys are pivotal to the maintenance of sodium and water homeostasis, which is essential for blood pressure regulation (Graham et al., 2017, Graham et al., 2018, Ares et al., 2011). The reabsorption of sodium and water from the renal tubules back into the

bloodstream helps to maintain blood volume and, consequently, blood pressure. The transport of sodium and water is tightly regulated by various transporters and channels in the renal tubules, such as NKCC2 in the TAL of the loop of Henle (Stanton and Kaissling, 1989).

Renal blood flow is another important factor in blood pressure regulation. The kidneys receive approximately 20% of the cardiac output, highlighting their significance in maintaining overall cardiovascular health (Ljungman et al., 1980, Dalal et al., 2023). Changes in renal blood flow can affect blood pressure through the regulation of sodium and water reabsorption and the release of vasoactive substances (Anderson et al., 1976, Van Beusecum and Inscho, 2015). Furthermore, the kidneys are involved in the regulation of blood pressure through the excretion of waste products and the control of fluid and electrolyte balance. The filtration of waste products, such as urea and creatinine, from the blood helps to maintain the composition of body fluids. This is linked to the balance of electrolytes, such as sodium, potassium, and calcium, which are essential for proper cellular function and fluid balance (Shrimanker and Bhattarai, 2023).

Several studies have provided molecular evidence supporting the role of the kidneys in blood pressure regulation. For example, the inhibition of soluble epoxide hydrolase (sEH), an enzyme involved in the metabolism of epoxyeicosatrienoic acids (EETs), has been shown to lower arterial blood pressure in animal models (Imig et al., 2002). Mutations in genes involved in renal sodium transport, such as WNK kinases, have been associated with hypertension (Wilson et al., 2003). Additionally, studies have demonstrated the impact of renal dysfunction on blood pressure control and the development of hypertension (Zbroch et al., 2012, Pugh et al., 2019).

1.4 Kidney Disease and Hypertension

Kidney disease and hypertension are closely intertwined, with hypertension being a major risk factor for the development and progression of kidney disease. Kidney disease encompasses a range of conditions that affect the structure and function of the kidneys, leading to impaired renal function and potential complications. Understanding the relationship between kidney disease and hypertension is crucial for effective management and prevention strategies (Jankowski et al., 2021). Prolonged elevation of blood pressure can damage the blood vessels in the kidneys and impair their ability to filter waste products and excess fluid from the body (Luyckx et al., 2013). This can lead to the development of CKD and increase the risk of cardiovascular events Dysregulation of the RAAS can contribute to the pathophysiology of hypertension and kidney disease (Ma et al., 2022,

Siragy and Carey, 2010). Medications that target the RAAS, such as ACE inhibitors and angiotensin receptor blockers (ARBs), are commonly used to manage hypertension and slow the progression of kidney disease (Zhang et al., 2020, Momoniat et al., 2019).

1.4.1 Diabetes

Diabetes is another profound risk factor for kidney disease, and hypertension often coexists with diabetes (Pyram et al., 2012, Long and Dagogo-Jack, 2011). Diabetic kidney disease, also known as diabetic nephropathy, is a common complication of both type 1 and type 2 diabetes. The combination of diabetes and hypertension can have a synergistic effect on kidney damage, leading to accelerated progression of kidney disease (Wang et al., 2017). Strict glycaemic control and blood pressure management are essential in managing diabetic kidney disease and reducing the risk of further renal damage.

1.4.2 Chronic Kidney Disease

CKD is a progressive condition characterized by a gradual loss of kidney function over time. It can result from various causes, including hypertension, diabetes, glomerulonephritis, and other systemic diseases (Webster et al., 2017). Hypertension is a common comorbidity in individuals with CKD and can contribute to the progression of kidney damage (MacRae et al., 2021). Effective management of hypertension is crucial in slowing the progression of CKD as well as preventing cardiovascular complications (Pugh et al., 2019).

1.4.3 Other important factors

Other important diseases, such as HIV infection, can also impact kidney health. HIV-infected individuals are at an increased risk of kidney disease, including HIV-associated nephropathy and immune-complex kidney disease (Peck et al., 2014). The management of kidney disease in HIV-positive individuals requires a comprehensive understanding of the unique factors associated with HIV infection (Peck et al., 2014). Further research is needed to explore novel treatment approaches and interventions that can effectively mitigate the impact of kidney disease and hypertension on global health.

1.5 The Study of Hypertension: Animal Models

1.5.1 Animal Models

One of the main challenges of establishing the mechanisms underlying the pathogenesis of hypertension is the lack of a model that appropriately emulates the complexity of the phenotype of hypertension (Lin et al., 2016). Animal models have enabled researchers to

elucidate multiple factors that regulate blood pressure, including environmental, genetic, physiological, and microbial factors (Lin et al., 2016). These animals often have varying mechanisms of blood pressure control. A key question is therefore, how do you capture the multifactorial nature of hypertension in a single model to study disease mechanisms?

Given the rise in gene-editing tools, such as CRISPR/Cas9, knockout rodent models have become key to decipher gene functions in hypertension (Jama et al., 2022). The application of this technology to larger animals is still limited, therefore rodent models still offer a significant advantage in hypertension modelling. Global or cell-specific knockout models of single or multiple genes can be generated, thereby enabling the investigation of specific genes and molecular pathways. Another advantage of using rodent models is the range of availability of assay and reagent tools for molecular techniques, including flow cytometry and immunohistochemistry, which are lacking in large animal models (Jama et al., 2022). Furthermore, rodent models offer reliable and accurate blood pressure measurements, such as via non-invasive tail-cuff plethysmography (Jama et al., 2022). These closely resemble intra-arterial blood pressure and are highly reproducible. Additionally, rodent models are advantageous in respect to their short life span and fast breeding capabilities, producing relatively large litters, which allows for intergenerational studies. As a result, these models are inbred and often have the same genetic background, which can be advantageous with regards to consistency of results but a disadvantageous when comparing to human populations which stem from diverse genetic backgrounds (Jama et al., 2022).

1.5.2 Rodent Models of Hypertension

There is a plethora of rodent models of hypertension, with different applications depending on the type of research being conducted. There are genetic models, which can be further subdivided into monogenic, transgenic models, and polygenic models. There also induced models. A summary of these models is provided in Table 1.2.

Table 1.2. Summary of Rodent Models of Hypertension and their Clinical Relevance

Model	Species	Organ Contribution	Relevance to clinical hypertension
Ang II	Rats or Mice	Renal, Vascular, Immune and Neurogenic	RAAS-dependent hypertension, respond to ACEi and ARBs
DOCA-salt	Mice or Rats	Renal, Vascular, and Immune	Low-renin hypertension, resistant to ACEi and ARBs
Dahl Salt-Sensitive	Rats	Renal, Vascular, and Immune	Genetically salt-sensitive, low-renin hypertension, resistant to ACEi and ARBs
L-NAME	Rats or Mice	Renal, Vascular, and Immune	NOS-deficient hypertension, respond to ACEi and ARBs
SHR	Rats	Renal, Vascular, Immune, and Neurogenic	Genetic model of hypertension, respond to ACEi and ARBs
SHRSP	Rats	Renal, Vascular, Immune, and Neurogenic	Genetic model of chronic hypertension, respond to ACEi and ARBs
Schlager BPH	Mice	Kidney and Neurogenic	Genetic white-coat hypertension, respond to ACEi

The most significant organ systems contributing to hypertension in these models are summarised under the "Organ Contribution" column. The clinical significance of this model and translatability to humans is summarised in the final column. (AngII, angiotensin II; DOCA, deoxycorticosterone acetate; RAAS, renin angiotensin aldosterone system; SHR, spontaneously hypertensive; SHRSP, stroke-prone spontaneously hypertensive rats; L-NAME, N^G-nitro-L-arginine methyl ester; ACEi, angiotensin-converting-enzyme inhibitor; ARBs, angiotensin II receptor blockers). The table was adapted from (Jama et al., 2022).

1.5.2.1 Stroke Prone Spontaneously Hypertensive Rat Model

Of particular interest for this thesis is the stroke-prone spontaneously hypertensive rat (SHRSP), which is a unique genetic model of severe hypertension and cerebral stroke (Nabika et al., 2012). The SHRSP model was established from a substrain of spontaneously hypertensive rats (SHR), which was obtained by selective inbreeding of Wistar-Kyoto (WKY) rats in 1974 by Okamoto *et al* (Okamoto et al., 1986). The SHRSP were generated under the following conditions: 1) the selection started using a 24th generation SHR, 2) a high risk of stroke was fixed after 3 generations of selective breeding, 3) which was co-existent with severe hypertension. This strain exhibited high incidence of stroke (80%) and severe hypertension (220-240mmHg) in adults, in contrast to SHR (10% and 180-120mmHg, respectively). In fact, SHRSP exhibit a rapid onset of hypertension over the first 5 weeks (Yamori et al., 1974). It should be noted that there is a large strain difference in the genome of WKY and SHR/SHRSP which does not contribute to hypertension. This is because WKY were established independently from another pair of ancestral rats in the same closed colony (Nabika et al., 2012). Before being established as fully inbred strains, the SHR, SHRSP, and WKY were distributed to multiple laboratories which has contributed to further genetic variation between strains. Thus, the SBP varies for the Glasgow sub strain of SHRSP used in this thesis compared to the general sub-strain, whereby values are around 190-200mmHg (Graham et al., 2007).

The SHRSP, unlike the WKY, are salt-sensitive, whereby administering 1%NaCl (or hereafter “1% salt”, also known as salt loading) solution produces a 30mmHg rise in blood pressure and increases risk of stroke (Yamori et al., 1981). The male SHRSP have a shorter lifespan (52-64 weeks) or 14-20 weeks with salt loading relative to the WKY, which live approximately 3 years (Nagura et al., 1995) (Doggrell and Brown, 1998). Due to its salt-sensitivity and well-defined cardiovascular phenotype, the SHRSP are an ideal model for studying human hypertension. The pathology of hypertension in SHRSP aligns with that found clinically in humans, including increased blood pressure rises with age, endothelial dysfunction, left ventricular hypertrophy, renal dysfunction, and sex differences in blood pressure (Clark et al., 1996, Kerr et al., 1999, Jeffs et al., 2000).

1.6 Uromodulin: Physiology and Disease

Uromodulin (UMOD), often referred to as Tamm-Horsfall protein, is a protein that is mostly produced by thick ascending limb (TAL) epithelial cells of the loop of Henle in the kidney (Rampoldi et al., 2011, Chabardes-Garonne et al., 2003) and, to a lesser extent, by the early part of the distal convoluted tubule (DCT1) (Tokonami et al., 2018b). It is the

protein that is secreted into the urine of healthy people in the greatest amounts (Kumar and Muchmore, 1990). The TAL is made up of an intricate system of parts that cooperate to control ion homeostasis. Due to the interdependence of this system, none of its functions are solely performed by UMOD; rather, UMOD works in concert with these other elements. The UMOD protein's expected functions in ion transport physiology and its participation in the development of the hypertension condition are the main focus of this thesis.

1.6.1 Gene

The UMOD gene consists of around 20kb and is located on chromosome 16p12.3-16p13.11 (Pennica et al., 1987, Pook et al., 1993). The primary mature structure of human uromodulin, a 616-amino acid, 85-kilodalton glycoprotein with in vitro immunosuppressive properties, was determined through isolation and characterization of complementary DNA and genomic clones. The amino acid sequence encoded by one of the exons of the uromodulin gene has homology to the low-density-lipoprotein receptor and the epidermal growth factor. It comprises 11 exons, of which exons 2-11 are coding, and is highly conserved across multiple species (Pennica et al., 1987, Devuyst et al., 2017). UMOD expression has been found in kidneys of all placental mammals, specifically the TAL, distal tubule of amphibians, but not in birds and reptile (Badgett and Kumar, 1998). UMOD expression is considered a marker of differentiation for TAL, appearing at 8 weeks of gestation in human foetal kidneys (Wallace and Nairn, 1971). It is most abundant transcript found in the rat kidney, accounting for 0.8% of the total transcriptome (Lee et al., 2015). Segmentation analysis of the rat nephron demonstrated that *Umod* expression was 10-fold higher in the cortical region compared to medullary TAL (Lee et al., 2015).

The factors involved in controlling and mediating *UMOD* expression are not well explored. Both *in vivo* chromatin immunoprecipitation and *in silico* prediction analysis have identified two binding sites for hepatocyte nuclear factor 1-β (HNF1), which a master regulator of transcriptional activity in the kidneys (Gresh et al., 2004). Transgenic kidney specific *Hnf1b* knockout mice showed a significant reduction in *Umod* mRNA levels, highlighting the importance of this transcription factor in UMOD expression. Further in silico phylogenetic footprinting analyses and protein-protein interactions studies indicate a large network of transcription factors that could regulate uromodulin expression, however, further validation is needed (Srivastava et al., 2014). Interestingly, common single nucleotide polymorphisms in a linkage disequilibrium (LD) covering the human *UMOD* promoter are associated with varying gene expression levels. For example, homozygous

subjects for major alleles exhibit a 2-fold higher renal *UMOD* transcript level compared to homozygotes for a minor allele combination (Trudu et al., 2013a). This is of particular importance in the context of disease, as will be discussed in section 1.6.6. Furthermore, more recent evidence suggests that *UMOD* expression may depend on the entire locus, with a genotype at a variant in the flanking region of *PDILT* showing association with varying urinary UMOD levels (Troyanov et al., 2016).

1.6.2 Protein and Structure

UMOD pre-cursor protein consists of a 640 amino acid composed of an N-terminal signal sequence (SP); 4 epidermal growth factor (EGF)-like domains (2 of which are calcium binding) which function in adhesion and receptor-ligand interactions; a cysteine-rich domain (D8C); a zona pellucida (ZP) domain; a C-terminal glycosylphosphatidylinositol (GPI) anchoring site (S614); and 8 potential N-linked glycosylation sites (Figure 1.7) (Micanovic et al., 2020). Endoplasmic reticulum (ER)-based SP cleavage results in substantial glycosylation of UMOD, which contributes to around 30% of its molecular weight, which ranges from 80 to 105 kDa (Serafini-Cessi et al., 2003). Before being sorted to the apical membrane of the TAL cells, facing the lumen of the tubule, UMOD continues to mature within the Golgi apparatus. Unknown trafficking proteins are involved in the movement of UMOD via different cellular compartments. Different isoforms of the non-muscle myosin II (NM2) motor proteins exhibit distinct distribution in the tubules and have been linked to vesicle formation at the Golgi (Miserey-Lenkei et al., 2010). In a preliminary investigation using conditional genetic knockout mice for the NM2 isoforms Myh9 and Myh10 in the TAL, the UMOD protein initially localised abnormally before steadily declining in quantities (Otterpohl et al., 2019).

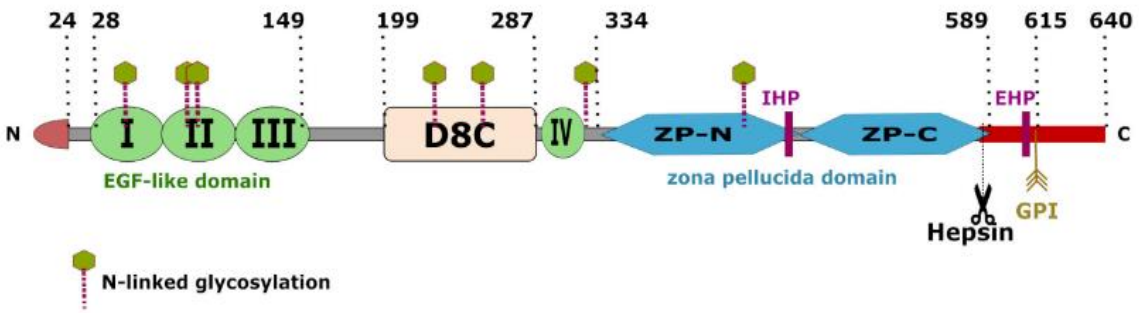

Figure 1.7. The structure and domains of Uromodulin (UMOD).
The structure of UMOD contains four N-terminal epidermal growth factor (EGF)-like domains, a cysteine rich region (D8C), a C-terminal Zona Pellucida (ZP) module containing ZP-N and ZP-C domains, an internal hydrophobic patch (IHP) within the ZP linker region, an external hydrophobic patch (EHP), and a glycosylphosphatidylinositol (GPI) anchoring site. The hexagon shapes sticking out from the main sequence symbolise N-glycosylation sites. The serine protease hepsin cleaves UMOD at residues 586-589 at the C-terminal for release into the urine. This results in a membrane-attached peptide coloured in red. The numbers in bold indicate location in the structure with regards to amino acid number. Figure taken from (Boder et al., 2021).

1.6.3 Molecular Trafficking/Secretory Pathway

A polymerization-inhibitory motif that is created by hydrophobic interactions between the external hydrophobic patch (EHP) at the C-terminal of UMOD and the internal hydrophobic patch (IHP) within the ZP linker region keeps UMOD in a polymerization-incompetent state during its maturation and intracellular trafficking (Schaeffer et al., 2009, Bokhove et al., 2016). The active, polymerization-competent UMOD is released into the urine after proteolytic cleavage between the ZP domain and EHP, but the fragment containing the EHP most likely stays anchored to the membrane via the GPI anchor. The transmembrane type II serine protease hepsin (Brunati et al., 2015), which cleaves at a conserved location located within residues 586-589 at the C-terminal, is thought to be the enzyme responsible for the proteolytic cleavage of UMOD (Figure 1.8). Cryo-electron microscopy research has more recently provided in-depth understanding of this process, in which the UMOD develops a one-start helix with 180-degree twists between subunits (Stsiapanava et al., 2020, Weiss et al., 2020). The filament core is made up of zigzag modules with a length of 8.5 nm (Weiss et al., 2020). The activation of the ZP-C end and the ZP-N domain of the succeeding subunit interact with each other in a head-to-tail method during polymerization, resulting in significant conformational changes in the interdomain linker region of the ZP module (Stanisich et al., 2020, Stsiapanava et al., 2020).

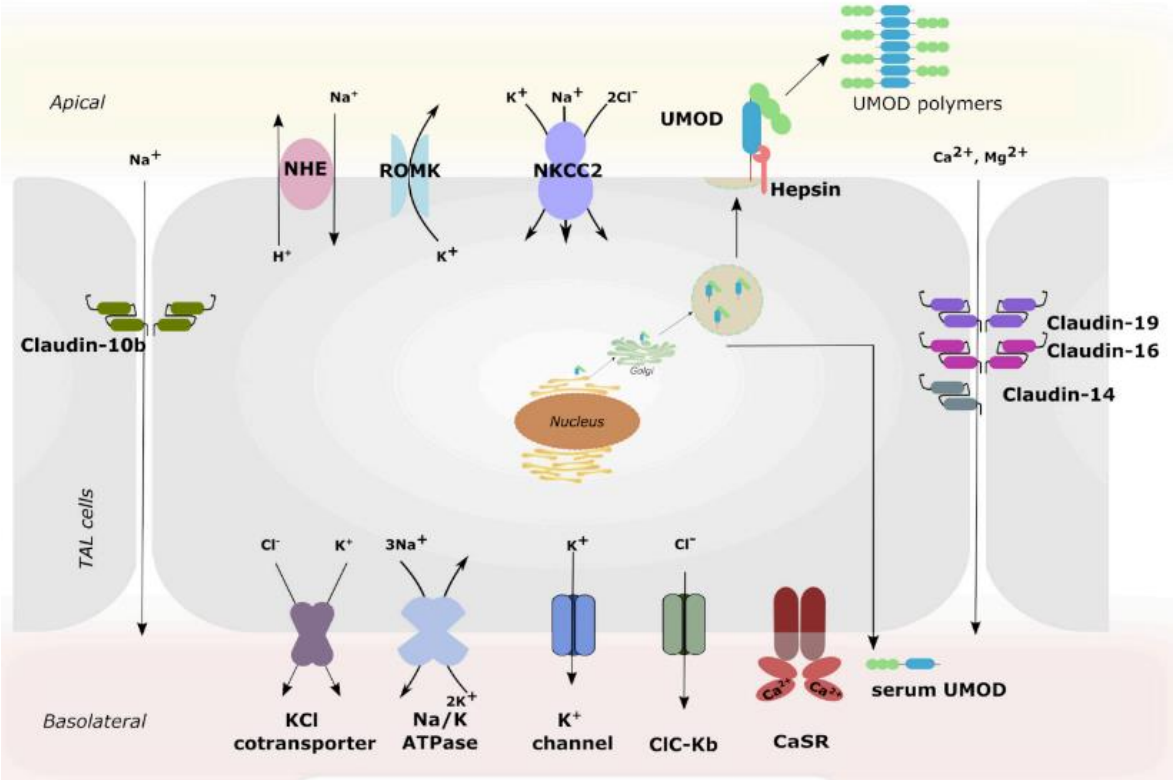

Figure 1.8. The physiology of the thick ascending limb and its involvement in ion homeostasis.
The TAL is bipolar in the sense that it has basolateral (blood) and apical (urine) compartments, which is key to ion homeostasis. The apical transporters are Na^+/H^+ exchanger type 3 (NHE), renal outer medullary K^+ channel (ROMK), and Na^+-K^+-2Cl− cotransporter type 2 (NKCC2). The basolateral transporters include KCl cotransporter, Na^+-K^+-ATPase, K^+ channels, and the Chloride Channel Kb (CLC – Kb). Together these transporters drive the paracellular reabsorption of divalent cations by producing a lumen-positive transepithelial potential. This occurs through the Claudin 16/19 complex (in the outer stripe of the outer medulla) and Na^+ via Claudin-10b (in the inner stripe of the outer medulla). The arrows symbolise the direction of ion movement. The secretory pathway of UMOD is also illustrated here. UMOD is co-translationally inserted into the endoplasmic reticulum (ER), before extensive modification of glycan changes in the Golgi, and final cleavage of the polymerisation-incompetent form of UMOD by hepsin. The UMOD monomer is released into the urine in a polymerisation-competent form. Here it polymerises into macromolecules. UMOD is also secreted via the basolateral membrane, in the form of serum/circulating UMOD. CaSR, calcium-sensing receptor. Figure taken from (Boder et al., 2021)

Through the TAL's basolateral membrane, UMOD is also released into the serum (El-Achkar et al., 2013). The relationship between serum UMOD and cardiovascular disease and CKD has recently attracted more attention (Steubl et al., 2020b). Through inactivating the transient receptor potential melastin 2 (TRPM2) channel, which is expressed in the brain, bone marrow, spleen, heart, liver, pancreas, lung, stomach, intestine, skeletal muscle, adipose, blood vessel, and placenta, serum UMOD functions as a renal and systemic oxidative stress inhibitor (LaFavers et al., 2019, Ru and Yao, 2014). In type 1 diabetic teenagers, it was discovered to be inversely correlated with aortic stiffness (Wiromrat et al., 2019b). We concentrate on how serum UMOD interacts with other TAL components in this article because the significance of serum UMOD in hypertension is largely unexplored. It should be emphasised that the concentrations of monomeric UMOD in the blood are 100–1000 times lower than those in the urine, and as a result, nothing is known about the biochemical characteristics of circulating UMOD (Scherberich et al., 2018). Serum UMOD is especially intriguing as a biomarker and has been the focus of in-

depth research elsewhere (Scherberich et al., 2018, Delgado et al., 2017, Lv et al., 2018, Wiromrat et al., 2019b).

1.6.4 Function and Role in Diseases

The urinary UMOD protein has been the subject of a huge number of biochemical research, although its specific physiological role is still unclear. It is known that urinary UMOD secretion varies greatly across and between persons (Delgado et al., 2017, Pruijm et al., 2016b). The involvement of UMOD in water homeostasis and urine concentration has been shown by research using conventional knockout mice (*Umod*$^{-/-}$) (Bachmann et al., 2005). It creates a 3D gel-like network and is thus thought to serve as a seal, preserving counter-current gradients in the interstitium, thereby preventing water leakage into the TAL (Devuyst et al., 2017). The apical NKCC2 is principally involved in the reabsorption of 30% of the filtered Na^+ by the TAL, which dilutes the urine and consequently creates a sufficient osmolality gradient for the vasopressin-dependent absorption of water in the collecting duct (Devuyst et al., 2017). The negative charge of UMOD in urine may prevent calcium oxalate and calcium phosphate from aggregating, hence preventing kidney stone formation (Mo et al., 2004). In addition to exhibiting immunomodulatory effects by preventing viral hemagglutination (Tamm and Horsfall, 1950) and suppressing in-vitro T-cell proliferation by interacting with tumour necrosis factor (TNF) and IL-1 (Devuyst et al., 2017), UMOD has also been linked to the prevention of urinary tract infections (Weiss et al., 2020, Bates et al., 2004).

1.6.5 Measuring UMOD and Clinical Relevance

It is important to take into account the different historical approaches used to assess UMOD in biological tissues or fluids when interpreting results. Early studies (Brunisholz et al., 1986) defined specific antibodies for human urine UMOD, and these antibodies have since been employed in other research (Akesson et al., 1978, Kobayashi and Fukuoka, 2001, Uto et al., 1991).Although, as discussed in more detail by Youhanna et al.(Youhanna et al., 2014), who have established a gold standard for UMOD ELISA, the concentration of UMOD reported varied due to differences in storage and processing of the urine prior to analysis, such as centrifugation, vortexing, choice of diluent, and freezing-thawing. Additionally, current research normalises UMOD levels from spot urine samples to creatinine in order to correct for variations in urine collection time, concentration, and flow rate (Tang et al., 2015). Utilising high pressure liquid chromatography (HPLC) and mass spectrometry (MS) is another way to quantify UMOD in urine. UMOD is typically enriched (e.g. with molecular weight cut-off columns (Matafora et al., 2014), salt

precipitation (Argade et al., 2009), diatomaceous earth (Argade et al., 2015), before analysis by mass spectrometry (MS) techniques, such as capillary electrophoresis-MS (CE-MS) (Carty et al., 2011, Mary et al., 2017, Krochmal et al., 2017b), liquid chromatography-mass spectrometry (LC-MS) (LaFavers et al., 2019, Matafora et al., 2014, Van et al., 2020), and matrix-assisted laser desorption/ionization time-of-flight mass spectrometry (MALDI-TOF) (Wu et al., 2010, Banach et al., 2019). The UMOD peptides discovered by these MS analyses will vary based on the type of disease and are helpful in identifying specific cohorts. The differential expression of UMOD peptides between cases and normotensive controls was discovered by peptidomics in the urine of preeclamptic women (Carty et al., 2011), and this finding was confirmed in studies in animals (Mary et al., 2017) and patients with moderate and severe preeclampsia (Kononikhin et al., 2016).

In clinical research, urine UMOD measurement is important for understanding renal pathophysiology. Numerous common and uncommon renal disorders have been linked to UMOD (Devuyst et al., 2017). Autosomal Dominant Tubulointerstitial Kidney Disease Related to UMOD (ADTKD-UMOD), a Mendelian condition brought on by uncommon UMOD mutations, results in CKD (Hart et al., 2002, Dahan et al., 2003). Glomerulocystic kidney disease (GCKD), medullary cystic kidney disease type 2 (MCKD2), familial juvenile hyperuricemia nephropathy (FJHN), and uromodulin-associated kidney disease (UAKD) are all included in the ADTKD-UMOD (Eckardt et al., 2015). Common UMOD mutations have been associated to renal function and CKD susceptibility in the general population by genome-wide association studies (GWAS) (Köttgen et al., 2009, Pattaro et al., 2016). These variations have an impact on gene expression and correspond to the UMOD promoter region (Trudu et al., 2013a). Any protein-coding mutation has no linkage disequilibrium (Köttgen et al., 2010). Figure 1.9 provides an overview of all the phenotypic connections of variations in and near the UMOD genomic region. Furthermore, independent of renal excretory function, UMOD promoter variations have been associated to hypertension (Trudu et al., 2013a). More thorough analysis of this was done in the past by Padmanabhan et al. (Padmanabhan et al., 2010).

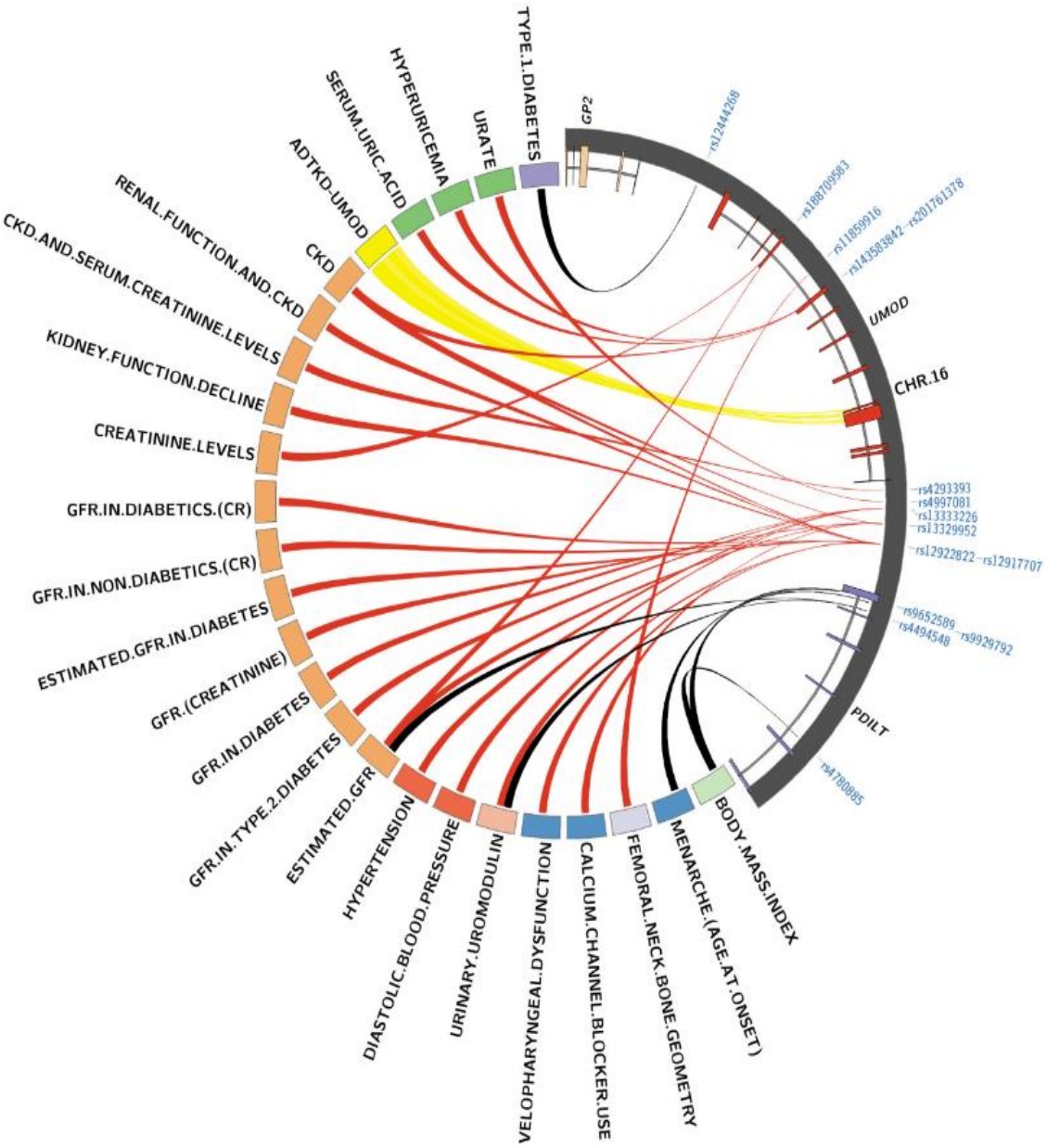

Figure 1.9. Links between different phenotypes and the genomic *UMOD* locus.
This figure illustrates the SNPs within *UMOD* and associated loci and their associations as uncovered by genome-wide association studies (GWAS). The threshold for inclusion was $p<10^{-6}$. The GWAS data was obtained from GWAScatalog (PMID: 30445434) and monogenic syndromes from OMIM (https://omim.org/). The figure demonstrates the multitude of functions and pathologies related to UMOD, some of which still require functional testing. ADTKD-UMOD, Autosomal dominant tubulointerstitial kidney disease caused by UMOD mutations; CKD, chronic kidney disease; GFR, glomerular filtration rate; PDILT gene (Protein Disulfide Isomerase Like, Testis Expressed); GP2 gene (Glycoprotein 2); CHR, chromosome. This figure was generated with the help of Prof Sandosh Padmanabhan. Figure taken from (Boder et al., 2021).

1.6.6 UMOD and Hypertension

It is generally well known that the TAL regulates blood pressure and has a role in the pathophysiology of hypertension; more recent reviews have gone into deeper detail on this (Gonzalez-Vicente et al., 2019). The part played by UMOD in hypertension, however, is less well understood. GWAS have been and remain crucial resources for identifying links between the UMOD gene and the risk of hypertension (Table 1.3). The minor G allele of a particular single nucleotide polymorphism (SNP) (rs13333226) in the 5' region of UMOD

was found to be associated with a lower risk of hypertension, decreased urinary UMOD secretion, and a higher estimated glomerular filtration rate (eGFR) in a GWAS based on data from hypertensive patients (Padmanabhan et al., 2010). This signal, which was still present after adjusting for eGFR (Padmanabhan et al., 2010), implies that UMOD may control renal excretion to affect hypertension. Carriers of the minor T-allele related with GFR but not blood pressure regulation were revealed by GWAS analysis of the rs12917707 variant-G>T, which is in linkage disequilibrium with rs13333226 (Algharably et al., 2017). Analysis of nephrectomy samples from patients homozygous for either the risk or protective alleles at variants rs12917707 (G and T, respectively) and rs4293393 (T and C, respectively) revealed that expression of UMOD was two times higher in patients with risk variants in the UMOD promoter. This information helped to clarify the biological effect of these variants (Trudu et al., 2013a). The rs12917707 risk allele (G) is strongly associated with renal function, and carriers of this variant had higher urinary UMOD levels than non-carriers, according to a meta-analysis of urinary UMOD levels in the general population (Olden et al., 2014). In addition, KCNJ1, SORSL1, and CAB3 gene variations that are expressed in the TAL are strongly correlated with urine UMOD (Olden et al., 2014). All things considered, this shows that UMOD's genetic and biochemical impacts on blood pressure are intricate.

It should be noted that due to variations in cohort composition, they are distinct GWASs and cannot be directly compared. GWAS are helpful, but they cannot identify the underlying molecular pathways at play. Given that UMOD is the most abundant protein generated in the TAL and that numerous studies have linked its expression and secretion levels to renal function and illnesses, indicating that it serves a crucial function in the kidney, more research into those mechanisms is necessary. Preclinical and clinical research support the hypothesis that salt, UMOD, and hypertension are related due to the intricate interactions in the TAL.

Table 1.3. Risk variants of the *UMOD* and allele frequency.

UMOD variant	Allele	GWAS Risk	Disease Association	Urinary UMOD levels	Frequency (%)[$]			References
					Africans	Europeans	East-Asians	
rs13333226	A	Risk	Hypertension	High	67	82	93	(Padmanabhan et al., 2010)
	G	Protective		Low	33	18	7	
rs12917707	G	Risk	CKD	High	96	83	99	(Köttgen et al., 2009), (Olden et al., 2014)
	T	Protective		Low	4	17	1	
rs4293393	T	Risk	CKD, Hypertension	High	70-80	70-80	90	(Trudu et al., 2013a), (Devuyst and Pattaro, 2018), (Gudbjartsson et al., 2010)
	C	Protective		Low	20-30	20-30	10	

[$]Data for allele frequency sourced from the National Library of Medicine dbSNP database. UMOD, uromodulin. CKD, chronic kidney disease. Table taken from (Boder et al., 2021).

1.6.6.1 Clinical Studies

Based on risk alleles discovered by GWAS, UMOD has been linked to hypertension. To find variations in 24h urine UMOD concentrations (mg/g of creatinine), a genotyping study of the Swiss Kidney Project on Genes and Hypertension (SKIPOGH) cohort was conducted (Trudu et al., 2013a). Comparing the protective variants (CT and CC) to the homozygous risk variation (TT), urine UMOD secretion was highest in the latter group (Trudu et al., 2013a). This coincided with the kidney samples with the risk haplotype showing a two-fold rise in UMOD transcript levels (Trudu et al., 2013a). In fact, patients homozygous for the risk allele had heightened natriuresis and blood pressure responses to the loop diuretic furosemide (Trudu et al., 2013a) Direct associations between blood pressure and urine UMOD secretion have also been found in clinical investigations that do not take genetic risk factors for hypertension into account. An increase in diastolic blood pressure was linked to a decrease in UMOD secretion, according to a cross-sectional investigation on random spot urine samples taken from 943 adults in a Canadian cohort (CARTaGENE) (Troyanov et al., 2016). A case-control study of incident CKD cases and matched controls was conducted on the Systolic Blood Pressure Intervention Trial (SPRINT) trial, a randomized controlled trial undertaken in non-diabetic patients with a high cardiovascular risk and a SBP of ≥130 mmHg that demonstrated a reduction in major cardiovascular events and death from any cause in patients receiving in the intensive SBP therapy arm (targeting a SBP of <120 mmHg) compared to those that received standard therapy (target SBP of < 140 mmHg) (Zhang et al., 2018, Wright et al., 2015). Patients in the intensive arm had a reduced incidence of new CKD during the study and had lower

UMOD in spot urine samples than those in the conventional arm after a year of therapy (Zhang et al., 2018). This would indicate that a higher SBP causes a rise in UMOD secretion. There was no discernible change in UMOD levels in 24-hour urine samples in a small investigation of non-diabetic normotensive and hypertensive subjects (Torffvit et al., 1999). In 24-hour, urine samples, it has been demonstrated in the past that urinary UMOD production declines with age (Pruijm et al., 2016b). However, it has also been noted that in healthy normotensive participants, but not in hypertension patients, the 24-hour urine UMOD secretion declines with age (Duława et al., 1998). Compared to old normotensive patients, elderly hypertension patients were shown to have a higher urine UMOD that was favourably linked with mean arterial blood pressure (Duława et al., 1998).

According to a study, there is no difference between baseline 24-hour urinary UMOD levels in hypertensive and control patients (Duława et al., 1992). The loop diuretic furosemide, nifedipine, or propranolol was given to these hypertensive patients for a 10-day treatment period, and only the furosemide group showed a significant rise in urine UMOD (Duława et al., 1992). A connection between UMOD and dietary salt intake has already been noted by a small population research (Torffvit et al., 2004). In this study, hypertension individuals were given a low-salt diet (10 mmol of sodium per day) for one week before switching to a high-salt diet (240 mmol of sodium per day), and urine samples were taken at 12 hours (overnight) and 24 hours (Torffvit et al., 2004). In comparison to the change from a low salt diet to a high salt diet, when UMOD levels increased, UMOD levels declined in 12-hour urine samples of low salt diet patients. In contrast, the 24-hour urine samples revealed no statistically significant difference between the baseline and low- or high-salt meals in urinary UMOD (Torffvit et al., 2004). As would be predicted in salt-sensitive hypertension, these patients' SBP dropped on a low-salt diet in comparison to baseline and the high-salt diet (Torffvit et al., 2004). Water intake is reduced overnight, which may impact urine concentration and volume, which may help explain the discrepancies between 12h and 24h urine samples (De Wardener and Herxheimer, 1957, Lynn et al., 1982). The SKIPOGH study's research of the effects of urinary UMOD levels on salt-induced blood pressure variations in 24-hour urine samples more recently revealed a tendency for greater SBP with higher sodium intake in people with high UMOD abundance (Ponte et al., 2021). When hypertensive patients were further separated into salt-sensitive and salt-resistant groups, a quantitative proteomics investigation indicated no difference in the levels of UMOD in the urine of hypertensive patients compared to healthy individuals (Matafora et al., 2014). However, those patients homozygous for the UMOD

risk variable PDILT_UMOD_rs4293393 emitted more urine UMOD, regardless of the presence of hypertension (Matafora et al., 2014).

Together, the clinical reports implicating UMOD in hypertension show significant disparities (Table 1.4 summarises these differences). The lack of a defined method for reporting urinary UMOD levels, which would take into account factors like whether to correct for creatinine levels, the kind of urine sample taken (spot, 12h, or 24h), and the applicability of risk alleles, may account for these discrepancies. There is little knowledge of the variables that control UMOD secretion in the general population. There is debate concerning the link between urinary UMOD secretion and eGFR, with some research finding a positive correlation and others not (O'Seaghdha et al., 2013). In SKIPOGH and Cohorte Lausannoise (CoLaus), two Swiss population cohorts, urine UMOD levels were examined in a cross-sectional investigation (Pruijm et al., 2016b). The SKIPOGH trial revealed a favourable connection between 24h urinary UMOD and eGFR. A positive connection between UMOD and eGFR was also observed in the CoLaus study, which examined spot morning urine UMOD concentrations adjusted for creatinine clearance (Pruijm et al., 2016b). More specifically, when eGFR is below 90 mL/min per 1.73m^2, there is a positive correlation between UMOD and eGFR (Pruijm et al., 2016b). The levels of urine UMOD, however, plateau and adopt Michaelis-Menten kinetics when eGFR is greater than 90 mL/min per 1.73m^2, as is the case in healthy individuals (Pruijm et al., 2016b). As a result, relationships at higher eGFRs might be less precise. Additionally, it emphasises how crucial a proper cohort structure is for population studies. It is noteworthy that processing and storage conditions for UMOD samples have a significant impact on UMOD concentrations and should be taken into account when interpreting results (Youhanna et al., 2014). This is particularly significant in light of the fact that it is not immediately obvious how UMOD was determined in these clinical investigations. Regarding urinary UMOD measurements, present and future studies should be open and adhere to a clear standard. Finally, little is known about how hypertension affects the alteration of the UMOD protein. When vitamin E was added, the level of oxidative modification of UMOD returned to normal in a study of 24-hour urine samples from hypertension patients compared to healthy controls (Sumitra et al., 2005). Further study is necessary since it is likely that UMOD experiences diverse post-translational changes in various illnesses.

Table 1.4. Clinical factors influencing urinary UMOD secretion.

Clinical Factors	Urine Sample	Urinary UMOD levels with respect to Controls	References
Age (SKIPOGH study 45±17 years and CoLaus study 53±11 years)	Spot and 24h	Lower	(Pruijm et al., 2016b)
Hypertension (>60 years)	24h	Higher	(Duława et al., 1998)
Salt-Sensitive Hypertension vs. Salt-Resistant Hypertension	Spot	No change (non-significant)	(Matafora et al., 2014)
High DBP	Spot	Lower	(Troyanov et al., 2016)
Intensive SBP therapy (<120 mmHg) vs. Standard SBP therapy (<140mmHg)	Spot	Lower	(Zhang et al., 2018)
Loop diuretic furosemide	24h	Lower	(Duława et al., 1992)
High Salt-Intake vs. Low Salt-intake	12h	Higher (high salt)	(Torffvit et al., 2004)
	24h	No change (non-significant)	(Torffvit et al., 2004)
High Salt-Intake vs. Low Salt-Intake	24h	Higher (high salt)	(Ponte et al., 2021)

UMOD, uromodulin; SBP, systolic blood pressure; DBP, diastolic blood pressure. Table adapted from (Boder et al., 2021).

1.6.6.2 Preclinical Studies

Animal studies have contributed significantly to our present understanding of the role of UMOD in hypertension. 129/sv, C57Bl/6, and Black Swiss mice were used in the breeding process to produce typical knockout *Umod*$^{-/-}$ mice, which do not exhibit any morphological abnormalities in their kidneys (Raffi et al., 2006). In healthy settings, these *Umod*$^{-/-}$ mice have lower SBP than wild-type (WT) mice (Graham et al., 2014). Similar to this, transgenic FVB mice's blood pressure was raised in a dose-dependent manner by tissue-specific *Umod* overexpression in TAL, and differences were noticeable as early as 2 months of age (Trudu et al., 2013a). At 16 months old, these mice display salt-sensitive hypertension and renal damage, mirroring the phenotypes seen in geriatric individuals homozygous for UMOD risk alleles (Trudu et al., 2013a). This may be explained by salt transport in the TAL via the NKCC2, which showed increased levels of activity in TAL cells from tissue-specific *Umod*-overexpressing animals compared to WT controls, despite NKCC2 transcript levels being unaltered (Trudu et al., 2013a). The latter suggests that rather than occurring at the genetic level, UMOD's functional impact on blood pressure happens at the level of protein interactions. As they recapitulate the effects observed in individuals with UMOD risk variations, these mice models remain useful for the investigation of UMOD (Trudu et al., 2013a, Köttgen et al., 2010).

Regarding the impact of salt, male Sprague-Dawley rats were fed a high-salt diet for 15 days, and the kidneys produced more UMOD mRNA and protein (Ying and Sanders, 1998). This was supported by a more recent investigation, in which WT C57/BL6 mice exposed to high salt levels for 2 months had increased urine UMOD secretion beginning on day 7; this increase continued at the 2-month timepoint (Olinger et al., 2019). Their SBP also rose in response to this. Urinary TNF levels were raised in ordinary *Umod*$^{-/-}$ knockout mice after salt loading (Graham et al., 2014). Additionally, it has been demonstrated that TNF can lower NKCC2 mRNA levels in primary TAL cells, which was made more effective by the absence of UMOD (Graham et al., 2014). According to a recent study, UMOD accumulation in the TAL at baseline, specifically in the ER, was increased in C57BL/6J mice with worldwide hepsin deficiency caused by ENU mutagenesis (Olinger et al., 2019). No increase in blood pressure or urine UMOD was seen in these hepsin-deficient mice when they were fed a high-salt diet for two months; instead, there was a rise in intracellular UMOD accumulation and more urinary salt waste than in the WT mice. Although poorly understood, abnormal UMOD secretion and increased ER stress brought on by its buildup in TAL cells may have a significant impact on how salt is handled, and blood pressure is controlled in hypertension.

Pregnancy-related hypertension is one condition that has not yet received much research. In the urine of normotensive WKY and SHRSP, my group have previously demonstrated that UMOD proteins exist in both polymerization-competent and incompetent forms, with levels of the latter rising during pregnancy in SHRSP (Mary et al., 2017). This would imply that UMOD and its polymerization play a part in pregnancies with high blood pressure. Given that cells lacking this protease only release UMOD that is incapable of polymerization, it is tempting to link this to the decreased or suppressed action of hepsin (Brunati et al., 2015).

1.7 Uromodulin Interactions with the Major Components of the Thick Ascending Limb

1.7.1 Direct interactions

1.7.1.1 Na^+-K^+-2Cl^-cotransporter type 2

The TAL area concentrates the urine by uptaking around 30% of the Na^+ burden in the kidney through NKCC2 while remaining impermeable to water (Figure 1.10) (Bennett et al., 1968). The apical surface of the TAL expresses both NKCC2A and NKCC2F isoforms, which regulate Na^+ influx accompanied by Cl^- and K^+ uptake and exhibit different Cl^-

affinities (high and low, respectively). As demonstrated by biochemical analyses of Dahl salt-sensitive rat models (Haque et al., 2011, Kirchner, 1992, Kirchner et al., 1995, Ares et al., 2012), genetic (Glorioso et al., 2001) and clinical (Jung et al., 2011) research in humans, NKCC2 is essential for blood pressure regulation and has been connected to salt-sensitive hypertension. Recently, this was thoroughly reviewed (Ares et al., 2011). Loop diuretics can increase Na^+ excretion by targeting NKCC2, which can help lower blood pressure (Shankar and Brater, 2003).

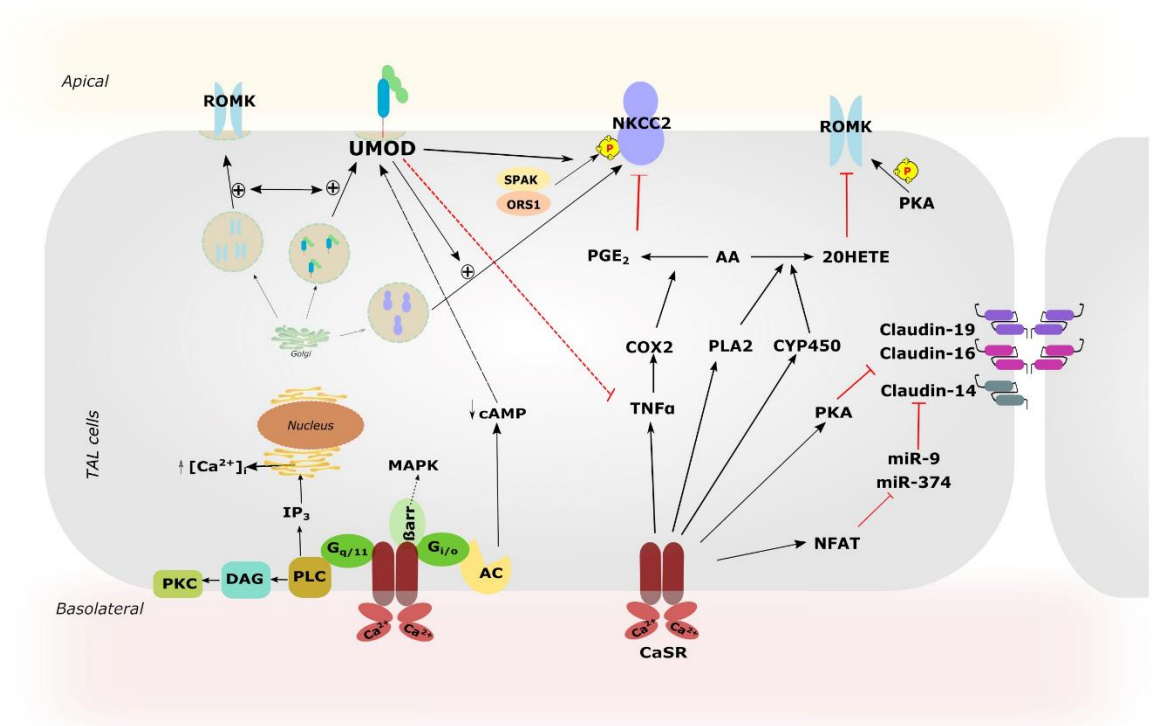

Figure 1.10. The network of interactions occurring between UMOD and various signalling components within the thick ascending limb (TAL).
Black arrows indicate stimulation and red T-lines indicate inhibition. Dashed lines indicate that the complete signalling cascade is unknown and are thus a prediction. Circular structures with a dashed circumference represent vesicles and the associated black arrows indicate exocytosis. The yellow circles with a red "P" in the centre indicate phosphorylation. AA, arachidonic acid; AC, adenylate cyclase; βarr, β-arrestin; cAMP, cyclic adenosine monophosphate; CaSR, calcium-sensing receptor; COX2, cyclooxygenase-2; CYP450, cytochrome P450; DAG, diacylglycerol; 20-HETE, 20-Hydroxyeicosatetraenoic acid; IP3, inositol triphosphate; MAPK, mitogen-activated protein kinase; NFAT, nuclear factor of activated T-cells (NFAT); miR, microRNA; NKCC2, Na+-K+-2Cl− cotransporter type 2; OSR1, oxidative stress response 1 kinase; PGE2, prostaglandin E2; PKA, protein kinase A; PKC, protein kinase C (PKC); PLA2, phospholipase A2; PLC, phospholipase C; ROMK, renal outer medullary K+ channel; SPAK, SPS1-related proline-alanine-rich kinase; TNFα, tumour-necrosis factor alpha; UMOD, uromodulin. Figure taken from (Boder et al., 2021).

The co-localization of UMOD and NKCC2 in studies suggests a possible biochemical interaction between the two proteins (Nielsen et al., 1998). Studies with standard *Umod*$^{-/-}$ knockout mice showed that these animals' urine concentration abilities were decreased and that NKCC2 expression was enhanced (Bachmann et al., 2005). This suggests that UMOD's direct impact on NKCC2 function is an adaptation to insufficient Na+ reabsorption. These mice specifically displayed an elevated level of subapical vesicular intracellular NKCC2 (Mutig et al., 2011b). This shows that UMOD influences the

intracellular trafficking of NKCC2 to enhance its activity in TAL. In response to the loop diuretic furosemide, which particularly targets NKCC2, transgenic FVB mice overexpressing HA-tagged Umod in a TAL-specific manner showed enhanced natriuresis and blood pressure decrease (Trudu et al., 2013a). This supports the link between UMOD and NKCC2 in terms of function.

The phosphorylation of threonine and serine residues on the protein's N-terminus controls the function of NKKC2 (Trudu et al., 2013a). SPS1-related proline-alanine-rich kinase (SPAK) and oxidative stress response 1 (OSR1) kinase are the enzymes that specifically target these phosphorylation sites (Richardson and Alessi, 2008). These become active in hypotonic and low Cl-environments. SPAK and ORS1 are activated by the upstream With No Lysine Kinases (WNK1 and WNK3) (Moriguchi et al., 2005, Ponce-Coria et al., 2008). NKCC2 phosphorylation has also been linked to PKA and AMPK in addition to this signalling cascade (Ares et al., 2011). Reductions in NKCC2 phosphorylation were found in immunodetection experiments performed on standard *Umod*$^{-/-}$ knockout mice (Mutig et al., 2011b). It is probable that UMOD's GPI anchor domain, which is frequently identified in membrane trafficking proteins, directs NKCC2 to the apical TAL membrane and serves as a scaffold to encourage the cotransporter's phosphorylation by SPAK and OSR1. In TAL-specific *Umod* over-expressing FVB mice, the levels of active SPAK and OSR1 are much higher, pointing to UMOD's potential promoter function in this kinase network (Trudu et al., 2013a). It is still unclear how exactly UMOD affects signalling pathways and NKCC2 regulation.

1.7.1.2 Renal outer medullary potassium channel

The apical membrane of the TAL contains the renal outer medullary potassium channel (ROMK), specifically the ROMK2 isoform, which is essential for maintaining K^+ homeostasis there (Boim et al., 1995). It creates two different types of K^+ channels in the TAL, 30pS and 70pS (Welling and Ho, 2009). K^+ ions are recycled by ROMK back into the tubular lumen after being taken up by NKCC2 or Na^+-K^+-ATPase at the apical or basolateral membrane, respectively. This causes the lumen-positive voltage that drives TAL's selective paracellular reabsorption of cations to be generated, as well as the K^+ conductance for NKCC2 activity. Type II Bartter's syndrome, marked by salt loss and dehydration, is brought on by ROMK channel mutations in humans and conditional ROMK knockout mice (Wang, 2012, Dong et al., 2016). Additionally, research has shown a link between polymorphisms in the ROMK gene and protection against hypertension at the age of 60 (Ji et al., 2008, Simon et al., 1996).

Factors affecting ROMK channel gating and molecular trafficking are the most notable regulators of ROMK channel activity. PKA phosphorylation and PIP2 binding enable ROMK to be activated and kept in a high open probability state, respectively (Xu et al., 1996, Huang, 2007). Cell surface expression of ROMK is dependent on phosphorylation of the N-terminal cytoplasmic residue S44, which suppresses an ER retention signal and encourages ROMK's apical migration (Yoo et al., 2005). The exact mediators are still unknown. However, yeast-2-hybrid, co-immunoprecipitation, and colocalization investigations have suggested a connection between ROMK2 and UMOD (Renigunta et al., 2011). The membrane trafficking machinery involved in this process has not yet been discovered. ROMK vesicular accumulation was enhanced in conventional *Umod*$^{-/-}$ knockout mice (Renigunta et al., 2011). Bartter-type 2 patients with KCNJ1 inactivating mutations and tissue-specific and global ROMK knockout (*Kcnj1*$^{-/-}$) mice both demonstrated impaired urine UMOD secretion (Schiano et al., 2019). Reduced trafficking to the apical membrane and increased intracellular accumulation of UMOD were the results of the in-vitro pharmacological inhibition and deletion of ROMK in TAL (Schiano et al., 2019). These two findings imply that UMOD and ROMK's interaction is necessary for their apical trafficking. Surprisingly, K^+ squandering is present in *Umod*$^{-/-}$ mice compared to wild-type (WT) mice (Graham et al., 2014).

1.7.1.3 The calcium-sensing receptor

The Calcium-Sensing Receptor (CaSR), a G-protein coupled receptor, is widely expressed along the nephron with TAL expressing it at the highest levels (Riccardi et al., 1995, Graca et al., 2016). It is situated on the TAL's basolateral surface. Contrary to the medullary TAL, the cortical TAL reabsorbs the majority of the calcium (Blaine et al., 2015). In hypertension models, it is well known that increasing dietary calcium decreases blood pressure (Hatton and McCarron, 1994). Calcimimetics, but not normotensive animals, have been demonstrated to lower blood pressure in spontaneously hypertensive rats (Ogata et al., 2003). Angiotensin II (AngII) levels are lowered and blood pressure is consequently reduced as a result of CaSR activation (Maillard et al., 2009). To pinpoint its precise function in TAL blood pressure regulation, more research is required.

The secretion of UMOD in TAL has been linked to CaSR signalling [121]. More particular, mice carrying global CaSR activating mutations (*Casr*$^{Nuf/Nuf}$) displayed reduced urinary UMOD secretion, whereas mice carrying global CaSR inactivating mutations (*Casr*$^{BCH002/+)}$ displayed increased UMOD secretion (Tokonami et al., 2018a). In CaSR agonist tests with TAL cells, calindol inhibited apical UMOD secretion, further supporting

these findings (Tokonami et al., 2018a). The cAMP levels dropped in calindol-treated cells, which is consistent with the CaSR-induced inhibition and active breakdown of cAMP, which reduced apical UMOD secretion (Tokonami et al., 2018a). Alternately, raising UMOD secretory levels by inducing 1-desamino-8-D-arginine vasopressin (dDVAP) elevated cAMP levels, which is blocked by concomitant calindol therapy (Tokonami et al., 2018a). This shows that by regulating cAMP signalling, the CaSR is essential for the control of UMOD trafficking in TAL. Since there are no alterations in total mRNA levels accompanying these changes in UMOD protein levels, this suggests that CaSR signalling predominantly affects UMOD trafficking (Tokonami et al., 2018a). Further research is needed to understand the signalling actions that follow cAMP inhibition, specifically with regard to how they affect UMOD trafficking. The study hypothesises that PKA may be involved (Tokonami et al., 2018a). To mediate its signalling actions, the CaSR uses a number of heterotrimeric G-proteins ($G_{i/o}$, $G_{q/11}$, and β-arrestin), which include promoting intracellular calcium release, activating mitogen-activated protein kinase (MAPK), ruffling membranes, and inhibiting cAMP (Gorvin, 2018). Expanding the study of biased CaSR G-protein signalling in response to different agonists to UMOD trafficking would be intriguing.

1.7.1.4 Direct interaction of uromodulin with distal convoluted tubule components: transient receptor potential melastatin 6, transient receptor potential cation channel subfamily V member 5 and transient receptor potential cation channel subfamily V member 6

A key location for controlled Mg^{2+} homeostasis is the kidney. The TAL reabsorbs around 70% of urine Mg^{2+} and the proximal tubule about 10% to 20% of it (Blaine et al., 2015). As previously mentioned, the paracellular pathway—where ROMK and NKCC2 help to create a positive lumen potential—is used by the TAL to reabsorb Mg^{2+}. It has been suggested that increasing dietary magnesium lowers blood pressure (Dyckner and Wester, 1983). Hypertension and elevated blood pressure have both been linked to hypomagnesemia, a low serum magnesium content (Guerrero-Romero et al., 2016, Hirschler et al., 2017).

The apical epithelial magnesium channel transient receptor potential melastin 6 (TRPM6), which is mostly expressed in DCT2, is used by the DCT to regulate the urinary magnesium absorption through an active transcellular route (Voets et al., 2004). Indicating the importance of renal Mg2+ homeostasis in blood pressure regulation and the pathophysiology of hypertension, a magnesium-deficient diet enhances TRMP6 expression

(Rondón et al., 2008). Recent research has shown that UMOD is critical for maintaining TRPM6 magnesium homeostasis [128]. Physically interacting with the receptor, secreted UMOD increases TRPM6 cell surface abundance and current density (Nie et al., 2018). Conventional *Umod*$^{-/-}$knockout animals exhibit decreased TRPM6 staining in the DCT. It was discovered using UMOD construct expression tests that TRPM6 up-regulation may not require membrane anchoring but may require all three UMOD domains (EGF-like domain, D8C cysteine-rich sequence, and ZP domain) (Nie et al., 2018). This is caused, in part, by UMOD inhibiting TRPM6's dynamin-2-dependent endocytosis in HEK293 cells (Nie et al., 2018). These findings were further supported by the observation of increased urine UMOD secretion in WT 129/SeEv mice fed low-Mg^{2+} (Nie et al., 2018).

The transient receptor potential cation channel subfamily V member 5 and 6 (TRPV5/6), Ca2+-selective channels expressed in the apical membrane of the second section of the DCT (DCT2) and connecting tubules (CNT) manage transcellular Ca2+ reuptake from the urine (Nijenhuis et al., 2003). TRPV5 apical expression on DCT2 was shown to rise in response to urinary UMOD synthesised in TAL and DCT1 (Wolf et al., 2013). Immunostaining studies revealed that TRPV5 labelling was significantly less in the DCT of conventional *Umod*$^{-/-}$ knockout mice than in WT mice (Wolf et al., 2013). Additionally, it has been demonstrated that extracellular UMOD increases TRPV5 surface abundance by reducing caveolin-mediated endocytosis (Wolf et al., 2013). It is intriguing to notice that UMOD seems to affect TRPM6 in the same cell it is synthesised in for DCT1, but in separate cells for TRPV5/6 (DCT2), indicating it may behave in a manner that is both autocrine and paracrine.

1.7.1.5 Tumour Necrosis Factor α

The proinflammatory and immunoregulatory effects of the TNF cytokine, as well as its modulation of ion and protein transport systems, are just a few of the many activities that the TNF cytokine performs in the renal system. TNF is expressed in TAL and has been linked to altered ion transport in the past (Ramseyer and Garvin, 2013). Through the activation of AT-1 receptors, AngII stimulation of TAL enhances TNF production (Ferreri et al., 1998). TNF seems to regulate blood pressure in a context-dependent manner. In some experimental models based on inflammation, it causes hypertension, whereas in other models, it might have protective effects (Graham et al., 2017).

More specifically, CaSR signalling via G_q and G_i proteins, which results in elevations in intracellular Ca^{2+}, activation of phospholipase C (PLC), and subsequent activation of nuclear factor of activated T cell (NFAT) by calcineurin, has been linked to TNF

generation in TAL (Abdullah et al., 2006, Abdullah et al., 2008). Nuclear factor-B (NF-B) and activator protein-1 (AP-1) are two transcription factors that are most likely involved in a PKC-dependent pathway that induces TNF production, according to studies on cardiac myocytes (Kalra et al., 2002).

In general, traditional $TNF^{-/-}$ knockout mice, TNF was demonstrated to reduce NKCC2 expression and function (Battula et al., 2011). On the other hand, protein tyrosine phosphatase signalling causes acute TNF addition to TAL cells to boost ROMK channel function (Wei et al., 2003). Though the molecular underpinnings of this relationship have not yet been clarified, it is known that UMOD directly interacts with TNF (Sherblom et al., 1988, Wu et al., 2012b). Increased urine TNF levels and higher NKC22 mRNA downregulation are seen in *Umod*$^{-/-}$ mice (Graham et al., 2014). According to studies, NFAT5 activation by NKCC2 is a component of a signalling pathway that causes the generation of TNF, which in turn inhibits NKCC2 activity through a negative feedback loop (Hao et al., 2013). This shows that TNF regulates NKCC2 function to maintain Na^+ homeostasis.

1.7.1.6 Hepatocyte Nuclear Factor 1β

Control of TAL function is governed by a sophisticated transcriptional network. A transcription factor called HNF1 that has a homeodomain interacts to DNA to trigger transcription. It has been established that the HNF1 transcription factor directly regulates the expression of the UMOD gene, and that kidney-specific conditional HNF1 inactivation in mice decreases Umod expression (Gresh et al., 2004). HNF1 is one of the most significant transcriptional regulators in TAL because of the several genes it interacts with that are involved in signalling pathways, receptors, and transporters.

In mice fed a low Mg^{2+} diet, renal HNF1 expression increased (Nie et al., 2018). Mg^{2+} reabsorption in TAL depends on the Na^+-K^+-ATPase-generated transepithelial electrical gradient. ATP1A1, which encodes the 1-subunit of Na^+-K^+-ATPase, was upregulated in patients with HNF1 mutations, although CLDN16 expression was unaffected (Faguer et al., 2012). A HNF1 knockdown immortalised mouse TAL cell line and kidney-specific conditional Ksp-cre HNF1 knockout mice have both shown that HNF1 regulates the expression of CaSR, Cldn14, Cldn19, Cldn10b, Cldn3 and Cldn14 genes (Kompatscher et al., 2018).

1.7.2 Indirect Interactions

1.7.2.1 Claudins and transcellular cation transport

The primary proteins that make up cellular tight junctions, claudins (CLDNs), are essential for maintaining paracellular permeability in the nephron. They are impermeable to water and primarily function as a selective barrier for tiny ions, such as Mg^{2+}, Ca^{2+}, and Na^{+} (Olinger et al., 2018). The two primary isoforms of CLDN that are present in TAL are CLDN16 and CLDN19, which work together to produce pores (Hou et al., 2008). Increased Ca^{2+} and Mg^{2+} urine waste was seen in studies using TAL-specific Cldn16 and Cldn19 siRNA knockdown mice, indicating the significance of this complex for ion reabsorption (Hou et al., 2009). Although CLDN16/19 have not been specifically examined in relation to blood pressure, their participation in cation handling and salt balance would indicate they may have a role in some aspect of blood pressure regulation.

TAL is known to express a different isoform, CLDN14 (Gong et al., 2012). By interacting with CLDN16, it has been demonstrated that this isoform lowers the CLDN16/CLDN19 complex's cation selectivity (Gong et al., 2012). lowering the permeability of the calcium and magnesium paracellular membrane. A high Ca^{2+} diet can initiate CaSR-calcineurin-NFAT signalling, which in turn increases the expression of the Cldn14 gene (Dimke et al., 2013) by suppressing microRNAs (miR-9 and miR-374) (Gong and Hou, 2014). It is significant that changes in dietary Ca^{2+} are related to changes in CLDN14 expression (Gong et al., 2012). Through PKA phosphorylation, the CaSR also inhibits CLDN16 (Ikari et al., 2008). The CaSR was demonstrated to diminish UMOD secretion (Tokonami et al., 2018a), which would be consistent with CLDN14's effects to lessen calcium reabsorption. The fact that conventional Umod-/-knockout mice secreted more urine calcium and magnesium demonstrates this even more (Nie et al., 2018). Uncertainty surrounds the specific mechanism behind this connection. It will take more investigation to support these hypothesised roles for UMOD in relation to claudins.

1.7.2.2 Angiotensin II receptor

As mentioned earlier, one of the most important regulatory systems for blood pressure and fluid balance is the RAAS (Sparks et al., 2014). Basolateral cell surface transmembrane receptors AT1 and AT2 support the biological effects of AngII in the TAL.

In vitro microperfusion flux studies using isolated rat TAL tubules, AngII reduces Cl- reabsorption, but when noradrenaline or cAMP are added, transport is stimulated (Bouby et al., 1997, Miyata et al., 1999). It has been demonstrated that 20-HETE and NO inhibit

NKCC2 via AngII signalling (Ramseyer et al., 2016). But AngII boosts PKC activity, which in turn promotes superoxide generation and ultimately stimulates NKCC2 (Herrera et al., 2010, Wu et al., 2013). Although AngII is crucial for TAL and hypertension physiology, it remains unclear how AngII affects the production of urine UMOD. Patients with essential hypertension have been shown to experience less UMOD secretion when taking ACE medications (Guidi et al., 1998). Two urine peptides of UMOD (VIDQSRVLNLGPITR and SVIDQSRVLNLGPITR), which were found at lower levels than those seen in individuals with normoalbuminuria, were discovered by CE-MS analysis in patients with macroalbuminuria (Rossing et al., 2005).

Additionally, it was discovered that one peptide (SVIDQSRVLNLGPITR) increased in a dose-dependent manner in response to the AngII receptor blocker candesartan (Rossing et al., 2005). Together, these findings imply that the effect of the AngII signalling arm on UMOD secretion is complex and calls for additional study.

1.7.2.3 Prostaglandins

Prostaglandins have a key role as lipid mediators in the kidney and regulate a variety of TAL processes. Prostaglandin E2 (PGE2) is the primary renal prostaglandin metabolite. The PGE2 production pathway's rate-limiting inducible enzyme, the COX-2 enzyme, is expressed in the TAL (Li et al., 2018). Prostaglandins are well known to play a significant part in controlling blood pressure (Hao and Breyer, 2008). According to clinical research, patients with hypertension who experience a COX-2-selective inhibition show Na^+ retention (Bresalier et al., 2005, Zhang et al., 2006). This suggests that prostaglandins play a function in preserving sodium homeostasis and normotension. Most research on PGE2 has focused on how it affects how vasopressin (AVP) works. Vasopressin 2 receptor (V2R)-mediated activation of the G-S protein results in an increase in cAMP synthesis, which in turn increases Na^+ absorption by TAL via NKCC2 (Li et al., 2018). However, CaSR-TNF pathway-induced intracellular PGE2 synthesis reduces NKCC2 activity (Abdullah et al., 2008).

About the interaction between PGE2 and UMOD, not much is known. Patients with hyperprostaglandin E-syndrome, a disease in which PGE2 synthesis is substantially increased, were reported to have lower levels of urine UMOD (Schröter et al., 1993). This would indicate that extracellular PGE2 typically inhibits the release of UMOD. On the other hand, mice lacking COX-2 globally exhibited reduced urine UMOD secretion and had lower intracellular PGE2 levels (Dou et al., 2005).

1.8 Hypothesis and Aims

1.8.1 Hypothesis

The overarching hypothesis of this thesis is that salt loading significantly alters UMOD urinary excretion and, by extension, trafficking. Specifically, it explores the axis of the influence of salt on UMOD, which remains largely unexplored. For UMOD specifically, it should be stated that "secretion" refers to secretion of UMOD from cells, whereas "excretion" refers to rate of secretion of UMOD in the urine. This will be applicable throughout the thesis. Given the association of UMOD and hypertension, it is postulated that salt loading will significantly impact UMOD secretion in kidneys from chronic hypertensive background, specifically the SHRSP. Analysing the differences in UMOD trafficking in normotensive WKY and chronic hypertensive SHRSP rat models will allow for discovery of novel mechanisms regulating these processes in the context of salt loading. Moreover, these will be of clinical relevance as they will help in understanding the pathogenesis of salt-induced hypertension and serve as novel research avenues for discovering therapeutic interventions.

1.8.2 Aims

The general aims that will be addressed in this thesis are:

- Characterise the effects of salt loading on UMOD urinary excretion and trafficking within the kidney in both normotensive WKY and chronic hypertensive SHRSP rodent models.
- Identify long-term impacts of salt loading on UMOD trafficking and renal physiology of normotensive models as an insight into potential pathophysiological changes that occur in hypertension.
- Establish and characterise animal and transgenic cell models for the study of molecular mechanisms of UMOD trafficking.

Chapter 2: General Materials and Methods

This Chapter outlines laboratory practices and methods common to more than one Chapter. Each subsequent results Chapter has a specific materials and methods section.

2.1 General Laboratory Practices

Laboratory equipment and reagents were of high-quality grade and commercially available. Reagents were assessed and dealt with appropriately if hazardous as described in the relevant control of substances hazardous to health regulations forms. Please see Appendix 8.1.1 for all laboratory reagents that were not obtained commercially. Reagents were weighed using a Mettler Toledo (0.001g) or Ohaus Adventurer Balance AR1530 (0.1g). Sterile disposable plastic ware or standard laboratory glassware was used to prepare reagents. Glassware was washed using Decon 75 detergent, rinsed with distilled H_2O (dH_2O) and placed in a drying cabinet (at 37°C). RNase free disposable plastic ware (ThermoFisher Scientific, UK) was used when appropriate. Volumes (1 µL – 1mL) were measured using Rainin pipettes and disposable tips or RNase free filter tips (ThermoFisher Scientific, UK) wherever appropriate. Water used for experiments was either dH_2O (milliQ-purified distilled water (Millipore, UK)) or High-Performance Liquid Chromatography (HPLC)-grade, unless specified otherwise. To dissolve solutions, a Jenway 1000 Hotplate and Stirrer was used. Solutions were mixed with Stuart Autovortex Mixer. Samples with a smaller volume (<2mL) were centrifuged using Eppendorf Centrifuge 5415R. Samples with larger volumes were centrifuged using a Mega Star 3.0R. A Fisherbrand Heating Water Bath Model FB60305 was used for experiments or samples requiring incubations from 37°C to 65°C, or an Eppendorf ThermoMixer was used for experiments requiring temperatures ranging from 4°C to 95°C, as appropriate. The pH of solutions was measured using a ThermoFisher Scientific Orion Star AIII pH meter calibrated with pH 4.0, 7.0 and 10.0 standards (ThermoFisher Scientific, UK).

2.2 Animals

2.2.1 Ethical Statement

All procedures were performed in accordance with Home Office regulation and with the United Kingdom Animals Scientific Procedures Act 1986 (PPL No. 70/9021, PPL No. PP0895181, PIL IBF0A9650) and ARRIVE guidelines and were approved by the institutional ethics review committee and performed at the CVRU unit at the University of Glasgow.

2.2.2 Animal Strains

The strains of animals used in this thesis are the chronic hypertensive stroke prone SHRSP and the normotensive WKY rat. These inbred strains have been maintained at the CVRU unit at the University of Glasgow since 1991 when 6 males and 7 females of each strain were gifted to Prof A.F. Dominiczak from Dr D.F. Bohr from the University of Michigan, USA. These animals were previously sourced from the National Institutes of Health, Bethesda, USA. The Glasgow strain of SHRSP (SHRSP/Gcrc) have slightly lower blood pressures than the original strain (16-week-old males: Glasgow 190-200 mmHg, original strain 230-250mmHg). The SHRSP are considered a chronic hypertensive model throughout this thesis.

2.2.3 Animal House

All animals were housed under controlled lighting (from 0700-1900 hours) and temperature (21±3°C) and received a normal diet (rat and mouse no. 1 maintenance diet; Special Diet Services, Grangemouth, United Kingdom).

2.3 Animal Procedures

2.3.1 Metabolic Cage

The metabolic cage allows individual housing of an animal to collect information on water intake and urine output over 24 hours. The metabolic cage has a gridded bottom to allow passage of urine and faeces. These are separated via a funnel to allow individual collection. A fixed amount of water (250mL) was given, and food was available *ad libitum* over the 24-hour period. Animals were acclimatized for 2 hours, 3 days before the first measurement. Urine samples were collected over 24 hours and then aliquoted and stored at -80°C until further use, no more than 4 occasion over any study period. Individual study collection details will be further elucidated under the appropriate corresponding chapter.

2.3.2 Blood Pressure Measurement

SBP was monitored weekly by tail-cuff plethysmography in an operator blinded fashion (Evans et al., 1994). The rats were warmed in a separate enclosure under lamps, which act as a heat source. During the measurement, animals are kept on preheated heating pads (at 33-35°C). The animals were restrained, before a cuff was attached on the tail and inflated/deflated via a computer to account for pressure differences. The sensor cuff detected changes in the tail volume as the blood returned to the tail during the occlusion cuff deflation. Piezoceramic transducers were then used to detect a pulse in the rat’s tail.

The occlusion cuff was inflated to 250mmHg and deflated over 20s. Each recording session consisted of 10 inflation and deflation cycles per set, of which the first cycle was considered “acclimation” cycle and was not used in the analysis. Rats were habituated at least 2 days prior to baseline blood pressure measurements. Recordings were taken on a weekly basis for all studies described in this thesis.

2.3.3 Blood Collection

Heparinized blood was collected by tail vein puncture under isoflurane anaesthesia (2.5% isoflurane in 1.5L/min oxygen). Timepoint collection details will be elucidated as part of the chapter-specific methods. At the end of a study, heparinized and EDTA blood samples were collected by cardiac puncture and rats were killed by exsanguination under terminal general anaesthesia. Haematocrit was determined using a A14 Jouan Centrifuge at 13,800xg for 5 minutes at room temperature. Biochemical plasma and urinary analyses for electrolyte, albumin and creatinine concentration were performed using Roche Cobas C311 Analyzer and commercially available rodent kits (Roche, Sussex, UK).

2.3.4 Tissue Collection and Processing Protocols

Animals were sacrificed under terminal general anaesthesia (2.5 % isoflurane). The thoracic cavity was cut open and blood collected via cardiac puncture of the left ventricle using a disposable 5mL syringe and 23-gauge needle. Blood was transferred into heparinised and EDTA Vacuette 5mL tubes (BD, UK). These were kept immediately on ice and then centrifuged at 3500xg for 15 minutes at 4°C to obtain plasma in the resulting supernatant. This was then aliquoted on ice and stored in -80°C before further use. Tissues from the animals were harvested and then fixed in 10% formalin for histological processing or snap frozen in liquid nitrogen. Specifically, the heart, liver, spleen, pancreas, aorta, kidney, and adrenal gland. Both kidneys were cut out and weighed separately. The renal capsule was manually removed, and the two kidneys divided into multiple sections; one of the kidneys was put away in Phosphate Buffered Saline (PBS) on ice (Appendix 8.1.1.1). This was later dissected separately into 3 fractions of the kidney, the papilla, the medulla and the cortex, before being snap frozen and stored for later usage at -80°C. The second kidney was cut in half along the sagittal plane. One half was immediately placed in fixative solution, whereas the other half was cut into half along the transverse plan. The resulting two sections of the kidney were allocation for RNA and protein extraction separately and snap frozen in liquid nitrogen. Snap frozen tissues were stored in -80°C until further use. In order to establish good laboratory practice, reproducibility, and record keeping, a tissue harvest protocol worksheet was generated (Appendix 8.2).

2.4 Gene expression

2.4.1 Ribonucleic Acid (RNA) extraction

All tissue was homogenised mechanically using the Qiagen 85210 TissueLyser Universal Laboratory Mixer-Mill Disruptor (Qiagen, UK) in 2mL Eppendorf tubes. Samples were homogenised in 500µL or 700µL of Qiazol (Qiagen, UK) depending on the size of the tissue. The lyser was set at a frequency of 30 Hertz for 20 seconds at a time in the presence of a stainless-steel bead to assist in breaking down the tissue. This was repeated twice or thrice until a homogenise solution is obtained. For kidney tissue, the tissue-Qiazol mix was snap frozen on dry ice prior to homogenisation to prevent excess foaming. Tissue homogenisation was continued until all the tissue had dissolved in Qiazol. RNA was extracted using the RNeasy Mini kit (Qiagen, UK). To summarise the protocol, 140µL of chloroform was added to tissue homogenate. This was then inverted by hand until the solution became opaque. Following this, the solution was incubated at room temperature for 2 minutes before undergoing centrifugation at 10,000xg for 15 minutes at 4°C. The RNA remains in the clear aqueous phase which was then collected into a new tube. These are precipitated with the addition of 1.5 volumes of ethanol. The resulting solution was then filtered through the RNeasy Mini Column, with the charged RNA sticking on the silica-membrane of the spin columns. The solution underwent a number of washing steps using ethanol-based wash buffer: RWT and RPE. The RNA was finally eluted using 30µL of nuclease free H_2O and centrifugation at 8000xg for 2 minutes at room temperature. An additional through-flow of the column was performed in certain cases to maximise RNA extraction (i.e., if RNA concentration readings were low). The resulting eluate was immediately placed on ice before reading concentrations, and stored in -80°C.

2.4.2 RNA quantification

Total RNA concentration (ng/µL) was determined by NanoDrop ND1000 (ThermoFisher, UK). A ratio of 2 for 260/280nm wavelengths and 2.0-2.2 for 260/230nm wavelengths was used to indicate purity of RNA (DNA/phenols and thiocyanate and protein contamination, respectively). RNA was stored in -80°C until use.

2.4.3 Reverse Transcription Polymerase Chain Reaction (RT-PCR)

RT-PCR allows conversion and amplification of RNA to produce complimentary DNA (cDNA). For this thesis, the High-Capacity RNA to cDNA kit (Applied Biosystems, UK) was used. In this one-step reaction, a master mix was generated containing a mix of random primers. These annealed to the template mRNA strand and provided RT enzymes a

starting point for synthesis. The RT enzyme offered high thermal stability to ensure cDNA synthesis at higher temperatures thereby ensuring higher yields. 1µg of RNA input diluted in RNase free water was used in a 20uL reaction volume (Table 2.1).

Table 2.1 Reaction set-up for the RT-PCR reactions to produce cDNA from RNA.

Component	**Volume (µL)**
10X RT Buffer Mix	2
25X dNTP Mix (100mM)	0.8
10X RT Random Primers	2
20mX RT Enzyme (MultiScribe)	1
RNase inhibitor	1
$MgCl_2$	1.4
Nuclease-free H_2O	1.8
Total per reaction	10

Reactions were set up in a 96 well skirted plate (Starlab, Germany) and sealed with an adhesive sealing sheet to prevent evaporation (ThermoFisher Scientific, UK). The reaction was run on a Multi block System Satellite 0.2 Thermo Cooler (ThermoFisher Scientific, UK) using the settings described in Table 2.2. The cDNA was stored in -20°C until further use, directly in the sealed plate.

Table 2.2 Optimum temperatures and times for each reaction step in the High-Capacity RNA to cDNA Kit.

Setting	**Step 1**	**Step 2**	**Step 3**	**Step 4**
Temperature (°C)	25	37	85	4
Time	10 min	120 min	5 sec	∞

2.4.4 Quantitative Polymerase Chain Reaction (qPCR)

qPCRs were performed in order to quantify the expression of genes of interest in a sample based on cDNA synthesised in section 2.4.3. Specifically, we utilised fluorescence-based qPCR which utilises a fluorescence reporter in a PCR reaction to quantify production of

DNA. In the log linear phase of the PCR reaction, fluorescence from the generated DNA was higher than the background, which could be expressed as a threshold cycle (Ct). The primary probes used in this thesis were bought from ThermoFisher Scientific (TaqMan™), which were based on a probe directly conjugated to a fluorophore. Due to the variety of fluorophores that can be attached to the probe of interest, TaqMan™ assays allow for multiplexing – i.e., allowing the expression of multiple genes to be measured in one reaction.

Housekeeping genes with a VIC labelled probe were run in duplex. These genes were selected from a series of validation experiments, whereby their Ct value was monitored across multiple different samples, specifically kidney lysate or ex vivo TAL tubule incubations from salt loading or salt-incubated groups, respectively, as well as controls. The gene with the least amount of Ct variation between sample within groups was chosen as the final housekeeping gene for analysis. The reaction set up with reagents can be seen in Table 2.3.

Table 2.3 Reagent volumes for TaqMan™ qPCR reactions

Reagent	**Volume (µL)**
2x TaqMan Mastermix	2.5
FAM-labelled probe	0.25
VIC labelled probe if duplex/appropriate volume of nuclease-free water if singleplex	0.25
cDNA (1µg)	2
Total	5

A 384 well plate (ThermoFisher Scientific, UK) was used as the reaction vessel and this was sealed with an optical adhesive sealing sheet (ThermoFisher Scientific, UK).Gene expression were run on a QuantStudio 12K Flex (version 1.3) (ThermoFisher Scientific, UK) with the following settings: 95°C for 15 minutes, 40 cycles of 95°C for 15s, and then 60°C for 1 minute. Ct values were analysed using the $2^{-\Delta\Delta Ct}$ method, whereby ΔCt pertains to normalisation to the housekeeper. Calculations of ΔCt and fold change (FC) were performed manually in Microsoft Excel (Microsoft, USA) and the graphs were created in GraphPad Prism version 9 (GraphPad Software, USA). All the probes and housekeeping genes used in this thesis are listed in Table 2.4.

Table 2.4 List of TaqMan™ probes and their designation

Gene	Full Name	Probe/Category number
Hprt1	Hypoxanthine phosphoribosyltransferase 1	C102626258
Ubc	Ubiquitin C	Rn01789812, Hs00824723
Tnf	Tumor necrosis factor	Rn99999017, Hs01113624
Gapdh	Glyceraldehyde-3-phosphate dehydrogenase	Rn01462661, Hs02786624, Rn01462661, Rn99999916
18S	18S Ribosomal RNA	Hs9999901
Havcr1	Kidney Injury Molecule-1	Rn00597703, Hs00930379
Adrb2	Beta-2-adrenergic receptor	Rn04219332
Umod	Uromodulin	Rn00567186, Rn01507237, Hs00358451, Hs00358451,

Aqp1	Aquaporin-1	Rn005652834
Lcn2	Neutrophil gelatinase-associated lipocalin	Rn00590612, Hs01008571
Casr	Calcium-sensing receptor	Rn01462661
Rplp0	60S acidic ribosomal protein P0	Rn03302271
Actb	B-actin	Rn00667869
Ednra	Endothelin Receptor Type A	Rn00581137
Nfat6	Nuclear Factor of Activated T cell 6	Rn01762487
Slc12a1	Sodium-potassium-chloride cotransporter	Rn00692576, Hs00165731
Kcnj1	Potassium Inwardly Rectifying Channel Subfamily J Member 1	Rn00566732, Hs04906030
Aqp2	Aquaporin-2	Rn00563755
Hspa5	Heat Shock Protein Family A Member 5	Hs00607129
Nfat5	Nuclear Factor of Activated T cell 5	Hs00232437

2.5 Western blots

2.5.1 Protein Extraction

2.5.1.1 Kidney/Tissue

Kidney tissues were lysed with Cell Extraction Buffer 5X at 1X (from Rat Uromodulin ELISA kit, Abcam, UK) or RIPA (Appendix 8.1.1.5) for total protein extraction and lysed

as explained in section 2.4.1. In other cases, a Qiagen user-developed protocol was used for extraction of proteins from the Qiazol Lysis Reagent (Qiagen, UK) after or without RNA extraction. Briefly, all traces of the aqueous phase after the chloroform phase separation step in the RNA extraction protocol are removed. After which, 0.3mL of 100% isopropanol was added to the remaining interphase and phenol phases. These are mixed by inversion and left at room temperature for 2 minutes. The solution was then centrifuged at 2000xg at 4°C for 2 minutes to precipitate the DNA. The phenol supernatant was then transferred to a new 1.5mL Eppendorf reaction tube and stored in guanidine-ethanol solution (0.3M guanidine-hydrochloride in 95% ethanol) for 20 minutes at room temperature or at 4°C (for at least 1 month). Following this, the samples were centrifuged at 7500xg for 5 minutes at room temperature and the supernatant removed. The remaining pellet was allowed to air dry for 5 minutes and dissolved in 500µL of urea/DTT solution (10M urea, 50mM DTT). The pellet was manually broken apart using a needle and then incubated at 95°C for 3 minutes to aid dissolving. The solution was then immediately placed on ice to avoid foaming and sonicated 10 times for short bursts (5 seconds). Finally, the sample was centrifuged at 10,000xg for 10 minutes at room temperature and the supernatant stored in a new 1.5mL Eppendorf tube.

2.5.1.2 Cells

For cells, RIPA lysis buffer pH 8.8 (Appendix 8.1.1.5) was used to extract protein. The cells were lysed by manual pipetting several times. Homogenates were centrifuged at 10,000xg for 10 minutes and the resulting supernatant collected and stored. In all cases, extraction buffers were supplemented with 2% Octyl β-D-1-thioglucopyranoside, cOmplete™ Mini EDTA-free Protease Inhibitor Cocktail (Merck, Germany), and PhosSTOP Inhibitor (Merck, Germany) according to the manufacturer's instructions as to inhibit protein degradation by proteases and loss of phosphorylation patterns by phosphatases, respectively. Protein lysates were stored in -80°C until further processing.

2.5.1.3 Urine

Urine samples were concentrated with the use of molecular weight cut-off (MWCO) columns prior to protein quantification. These allow concentration of proteins by separating components in biological and environmental samples by molecular weight, as well as desalt and dialyze proteins. In this work, 500µL or 2mL of urine volumes were used which were concentrated using 3kDa MWCO columns with Amicon Ultra 15-Centrigugal Unit and Amicon Ultra-0.5mL centrifugal filters (Sigma-Aldrich, UK), respectively, to final volumes of 100µL (5X or 20X concentration factor). For the Amicon

Ultra-0.5mL centrifugal filters, samples were centrifuged in a fixed angle rotor at 14,000xg at room 4°C. For the Amicon Ultra 15-Centrigugal Unit, samples were centrifuged in a swinging bucket rotor at 3000xg at room temperature.

2.5.1.4 Membrane and Cytosolic Fraction

Membrane and cytosolic protein fractions were extracted from kidney medulla sections or cells using Mem-PER™ Plus Membrane Protein Extraction Kit (ThemoFisher Scientific, UK) as per manufacturer's instructions. This kit enabled the extraction of integral membrane proteins and plasma membrane-associated proteins from cultured mammalian cells or tissues. Briefly, the kit utilized a mild detergent to selectively extract membrane proteins without phase separation (Figure 2.1). Initially, the cells were permeabilized to extract soluble cytosolic proteins. A secondary detergent was then applied to extract plasma membrane proteins.

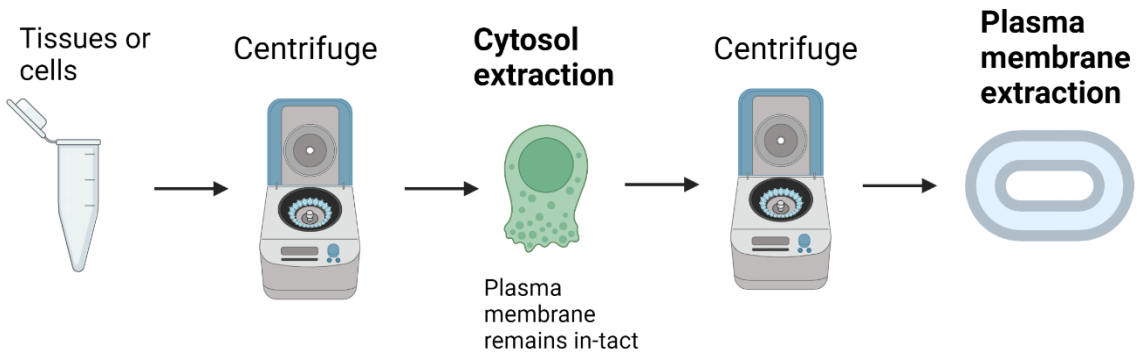

Figure 2.1. Diagrammatic representation of the Mem-PER™ Plus Membrane Protein Extraction Kit (ThermoFisher Scientific, UK)
The protocol involves lysing the cell in an initial centrifugation step that isolates only the cytosol (e.g., organelles, cytosolic proteins, etc.) in the supernatant while maintaining the cell's plasma membrane. The plasma membrane is maintained in the pellet and extracted with a membrane-specific buffer after another centrifugation step, whereafter the plasma membrane fraction can be obtained from the supernatant. Image generated in BioRender.

For the medulla, the frozen tissue was kept on dry ice throughout the procedure as to minimize protein degradation. Tissue pieces equivalent to half a kidney were kept in a 2mL Eppendorf tube and washed with Cell Wash Solution (component of Mem-PER Plus Membrane Protein Extraction Kit). The pieces were then transferred to a 1.5mL Eppendorf tube and cut into small 1-2mm^2 chunks using sterilised surgical scissors. These were then transferred to a fresh 2mL Eppendorf tube for another wash step with gentle vortexing for 5 seconds. The cell wash solution was then aspirated before adding 300µL of permeabilization buffer. A stainless-steel bead was then added to the tube before homogenisation with the 85210 TissueLyser Universal Laboratory Mixer-Mill Disruptor (Qiagen, UK) at 30 Hertz for 30s intervals until an even suspension was obtained. The remaining homogenate was transferred to a new 1.5mL Eppendorf tube for incubation at

4°C for 5 minutes at constant mixing (300 rpm). The tube was then centrifuged at 14,000xg for 15 minutes at 4°C to pellet the permeabilized cells. The supernatant was stored in a separate 1.5mL Eppendorf tube and contains the cytosolic proteins. The remaining pellet was then resuspended in 150µL of Solubilization buffer. This was then gently pipetted until a homogenous suspension is achieved. The tube was kept at 4°C with constant mixing at 300rpm. A final centrifugation step at 14,0000xg for 15 minutes at 4°C was performed and the resulting supernatant stored in a 1.5mL Eppendorf tube as the membrane protein fraction. To all buffers, proteinase and phosphatase inhibitors were added as described in section 1.5.1.2. Aliquots were stored in -80°C. This protocol was adapted for cells, whereby 200µL of Permeabilization Buffer and 50µL of Solubilization buffer were used instead. Also, all homogenisation was performed using pipetting.

2.5.2 Electrophoresis

Protein concentration was determined using QuickStart Bradford assay (Bio-Rad, UK), according to manufacturer's instructions. The following 7 concentrations of BSA standard were used to determine relative protein concentrations: 2, 1.5, 1, 0.75, 0.5, 0.25, 0.125 mg/mL (Bovine Serum Albumin Standard Set, Bio-Rad, UK). The concentration was determined at 595nm using a Viktor X3 Plate Reader (Perkin Elmer, USA). The standard curve was calculated using Microsoft Excel (Microsoft, USA) and fitted to an R^2 value of 0.99. Protein samples were diluted in SDS sample buffer (Appendix 8.1.1.8) to a final concentration of 1X and will be defined on a chapter-by-chapter basis. Samples were incubated at 85°C for 10 minutes. Proteins were resolved according to their molecular weight using pre-cast Bolt™ Bis-Tris Plus gels (4-12% or 10%, depending on the type of sample) (ThermoFisher Scientific, UK) for separation by electrophoresis in 1X Bolt MOPS SDS Running Buffer (ThermoFisher Scientific, UK) at 125V for 1 hour using a PowerEase Touch 350W Power Supply (ThermoFisher Scientific, UK). As a protein ladder, 2µL of PageRuler Plus Prestained Protein Ladder (10 to 250kDa) was loaded in the first lane (furthest left) to determine protein size.

2.5.3 Blotting

Following separating, proteins were transferred using semi-dry transfer technique whereby no buffer tanks or gel cassettes are required. For this, the semi-dry Thermo Scientific Pierce Power Blotter system was utilised (ThermoFisher Scientific, UK) in Pierce 1-step transfer buffer. If one blot was transferred, this was for 20 minutes at 1.3A using the high molecular weight setting. For 2 blots, 14 minutes at 2.5A using the high molecular weight setting was used. For 3 or more blots, 12 minutes at 2.5A using the high molecular weight

setting was used. Proteins were transferred to Immobilon-FL PVDF 0.45µm membranes with 9cm x 6cm dimensions. These had been activated in methanol (VWR International, UK) for 5 minutes at room temperature, as well as 1X Pierce 1-step transfer buffer for 5 minutes.

2.5.4 Blocking and Antibody Incubation

Membranes were blocked with 5% Bovine Serum Albumin (BSA) (Merck, UK) in Phosphate-Buffered Saline with 0.1% Tween-20 (PBST) for all non-phosphorylated proteins and Tris-Buffered Saline with Tween-20 (TBST) (Appendix 8.1.1.4) for all phosphorylated proteins. This was followed by incubation with the respective primary antibody (in 2% BSA/PBST) overnight at 4°C. Membranes were then washed in PBST or TBST, depending on the type of antibody, three times for 15 minutes at room temperature. The membranes were then incubated with the appropriate secondary fluorescence-conjugated antibody in 5% BSA in PBST or TBST at room temperature for 1 hour. Specific details for the type of antibody used, type of secondary antibody, and their dilutions can be found in Table 2.5. Validation work was conducted on primary antibodies used for detection of proteins of interest in this thesis with regards to loading to establish linearity and positive controls for detection. For UMOD, it was determined that loading of 1µg of urine sample provided optimum UMOD band detection (Abcam UMOD antibody). The validity of UMOD detection by the Abcam UMOD antibody was confirmed by running of a positive control alongside urine samples, mainly purified mouse or human recombinant UMOD protein. For kidney and cell lysate samples, a loading of 20µg of protein provided the optimum band signal on the Western blot for UMOD antibodies, and 40µg for the remaining antibodies provided in Table 2.5. The detection of UMOD in this context was again confirmed with purified mouse or human recombinant UMOD protein as a positive loading control. No positive controls were used for the remaining primary antibodies.

2.5.5 Detection and Analysis

Imaging of proteins was performed on the Odyssey Clx (at 700 and 800nm). For total protein detection, revert 700 Total Protein Stain (LI-COR Biotechnology, UK) protocol was performed. After transfer was completed, the PVDF membrane was rinsed in dH_2O for 5 mins at room temperature. The membrane was then incubated with 5mL of Revert 700 Total Protein Stain for 5 minutes at room temperature with gentle shaking, ensuring that blot itself was covered in the dark. The solution was then decanted, and the membrane briefly rinsed in dH_2O. After this, 5mL of Revert 700 Wash Solution (.7% (v/v) glacial

acetic acid, 30% (v/v) methanol) was added to membrane two times for 30 seconds at room temperature with gentle shaking. The Revert 700 Wash Solution was then decanted and briefly rinsed with dH_2O. The membrane was then immediately imaged with the Odyssey Clx (at 700nm). Following this, the membrane was washed in dH_2O briefly before 5 mL of Revert Destaining Solution (0.1 M sodium hydroxide, 30% (v/v) methanol) was added for 10 minutes while continuous shaking until the stain is no longer visible by eye. Finally, the membrane was briefly rinsed in dH_2O before proceeding to immediately blocking and immunodetection.

Analysis of the Western blots was performed on ImageStudio v5.0 (LI-COR Biotechnology, UK). The relative intensity of the bands was determined using Shapes tool, by drawing the rectangle around each of the bands (or in the case of Revert 700 Total Protein Stain, the total blot). Rectangle size was maintained constant for each of bands on the same blot. An additional rectangle was drawn outside the band region, as a background value, a subtracted from all protein bands. For normalization of bands, loading controls were used (see individual figures for details). A series of optimisation experiments were performed prior to individual experiments and analyses conducted in each chapter to determine the optimum loading control for each sample type. Samples from across different salt loading conditions were used for comparison. The primary antibody showing the least amount of variation in band signal intensity across these groups was chosen as the loading control. In case of comparison of signals between multiple blots, the sum of replicate methodology was utilised (Degasperi et al., 2014). In this method, each data point on a replicate is divided by the sum of the values of all data points in that replicate. This way the data in each replicate becomes relative to this sum.

2.5.6 Stripping Protocol

In some cases, blots underwent a stripping protocol to remove prior antibodies with 0.2M NaOH for 10 minutes at room temperature (under constant shaking). This was followed by blocking and re-incubation with another set of primary and secondary antibodies.

2.6 Histology

2.6.1 Tissue Preparation for Histology

Tissues were fixed in for 24 hours in 10% formalin/4 % paraformaldehyde (PFA) at room temperature. These were then washed three times in PBS with continuous shaking on a rotational platform shaker. Tissues were then placed in 4°C until further use. For histology purposes, tissues were placed in histology cassettes (ThermoFisher Scientific, UK) and

placed in a Citadel 1000 processor (Fisher Scientific, UK) at the following settings: 70% ethanol 30 minutes, 95 % ethanol 30 minutes, 100% ethanol 30 minutes, 100% ethanol 30 minutes, 100% ethanol 45 minutes, 100% ethanol 60 minutes, 100% ethanol/xylene 30 minutes, xylene 30 minutes, xylene 30 minutes, wax 30 minutes, wax 30 minutes, wax 45 minutes, wax 45 minutes. The total running time was 8 hours and 30 minutes. Tissues were embedded with the Shandon Histocentre 3 embedding centre (Fisher Scientific, UK) and Histoplast paraffin (ThermoFisher, UK). Kidneys were cut transversely and placed face down. Paraffin sections of 2, 3 or 5µm were cut using a Leica Finese 325 Microtome (Fisher Scientific, UK) and baked on silanised slides (Clarity Microscope Slides C360) at 65°C overnight. Slides were the stored at room temperature until use. Paraffin blocks were stored at 4°C. Prior to staining, the slides underwent a deparaffinisation and antigen retrieval protocol. This involved deparaffinisation in Xylene-substitute (Sigma-Aldrich, UK) 2 x 10 minutes and then rehydrated through an ethanol gradient (100%, 95%, and 70%, 10 minutes each) before a final distilled H_2O step for 10 minutes.

Deparaffinised slides initially underwent an antigen retrieval step (heat-induced epitope retrieval) to allow for binding of the various antibodies to allow for immunofluorescence imaging. This involved boiling the slides in a microwave (100% power) for 2 minutes in pre-heated (95°C) citrate buffer (Appendix 8.1.1.6). After this, a series of heating steps are performed (2 x 4 minutes at 80% power) ensuring the evaporated buffer is topped with citrate buffer when required. Finally, the slides are transferred to new citrate buffer and left to cool at room temperature for 30 minutes. After this, the slides were washed twice in distilled H_2O for 5 minutes and once in 1X TBS at room temperature.

2.6.2 Immunofluorescence Staining

The kidney section was circled with a hydrophobic pen (ThermoFisher Scientific, UK) and incubated with 200µL of 1X Carbo-Free Blocking Solution (1X, Vector Laboratories, USA) for 1 hour at room temperature in a humidified chamber.

For cells, the samples were fixed in neutral buffered formalin at room temperature for 1 hour after 3 x 5-minute washes in 1X PBS. Cells were then permeabilised with PBS containing 0.1% Triton X-100 for 10 minutes at room temperature. Blocking occurred as for tissues mentioned above, with 1X Carbo-Free Blocking Solution.

Following the blocking step, primary antibody and secondary antibodies were added in a sequential manner (1 hour at room temperature in a dark, humidified chamber) separated by 3 x 5-minute washes in 1X TBST. Primary antibodies are the same used in Western

blotting (see Table 2.5), secondary antibodies used for immunofluorescence analysis can be found in Table 2.5. All antibody solutions were made in 1X Carbo-Free Blocking Solution (Vector Laboratories, USA). After the final antibody incubation, the sections were incubated with Mounting Medium with DAPI – Aqueous, Fluoroshield (Abcam, UK) and covered with High precision Cover glasses (24x25mm No 1.5). The edges were sealed with transparent nail polish.

2.6.3 Immunofluorescence Imaging and Analysis

Images were acquired with the Zeiss LSM 900 Axio Observer.Z1/7 confocal microscope equipped with a Plan-Apochromat 63x/1.40 Oil DIC M27 objective or Plan-Apochromat 40x/0.95 DIC M/N2 operating with Zen Blue software version 3.3.89.0004 (Carl Zeiss, Germany). For Z-stack images, optimal interval slices were used according to the optimum calculated by the software. The analyst was blinded for imaging and analysis of sections.

2.7 Enzyme-linked Immunosorbent Assay

UMOD protein concentration levels in urine and total kidney lysate were quantified using the one-step Rat Uromodulin ELISA kit (ab274405) according to manufacturer's instructions. The range of detection for UMOD standards was 625-40000 pg/mL. The method used a 7-point standard curve. Validation work was performed for the primary antibodies used for the UMOD ELISAs. Signal linearity was established for both kidney lysates and urine samples over a range of different dilutions as recommended by the supplier. A range of 1:1000 to 1:8000 was chosen for urine samples and 12.5 to 200 ng/µl for kidney lysates. Urine samples and kidney lysate samples were diluted 1 in 4000 and 25µg/mL, respectively. For assessment of kidney UMOD protein, the kidney was chopped into smaller pieces and washed in PBS before homogenization in cell extraction buffer provided by the kit. Homogenisation was carried out as described in section 2.4.1. The relative concentration of total kidney protein per sample was determined by QuickStart Bradford assay (Bio-Rad, UK) to enable equal loading of protein in each well. This was not applicable for urine samples, due to the low protein concentrations in the undiluted urine which could not be detected by the Quick Start Bradford assay. Urine samples were diluted 1:4000 and volumes kept constant. Sample protein extraction and quantification was performed on the same day to minimize batch variation. The analyst was blinded to sample details during experiments and analysis.

2.8 Statistical analysis

Statistical analyses were performed on GraphPad Prism version 9 (GraphPad Software, USA). The sample numbers per group were determined on power calculations based on previous blood pressure studies in rats. By examining the mean systolic blood pressure, it may be estimated that 8 rats per group will allow 80% power at $\alpha = 0.05$ to detect differences in 15 mmHg. Student's t-test, Welch's t-test or Mixed-effects analysis were performed as appropriate. The effect of two factors was tested by two-way ANOVA (or mixed model). Figure legends denote the type of test used for all analyses. All statistical tests were two-tailed and P-value <0.05 was considered significant. Values are expressed as mean ± standard error of the mean (SEM). For ELISA analysis, four-parameter curve fit (4PL) without constraints was used to determine the curve fit for standard values in GraphPad Prism. For PCR, the Ct values obtained from QuantStudio 12K Flex software version 1.3 (ThermoFisher Scientific, UK) were used for calculation of ΔCt and fold change (FC) manually in Excel, and the graphs were created in GraphPad.

2.9 Antibodies

Table 2.5 List of primary and secondary antibodies used in the thesis.

Antibody	**Supplier/Catalogue Number**	**Dilution**
Vinculin	Sigma-Aldrich/SAB4200729	1:10,000
Calnexin	ThermoFisher Scientific/PA5-77839, Abcam/Ab192439, Abcam/Ab22595	1:1000
NKCC2	ThermoFisher Scientific/PA5-88905, Abcam/Ab171747	1:1000
Hepsin	Novus Biologicals/NBP1-86931, Abcam/Ab189246	1:5000
GAPDH	Abcam/Ab1811602	1:10,000

Flotillin-1	Abcam/Ab41927	1:2000
Flotillin-2	ThermoFisher Scientific/PA5-79268	1:1000
EGF	Abcam/Ab184265	1:1000
B-actin loading control 800	ThermoFisher Scientific/MA5-15739 D800	1:10,000
CHOP	Novus Biologics/NB600-1335	1:200
ERO1L	Novus Biologics/NB100-2525	1:500
eIF2	Novus Biologics/NB2-02669	1:500
IRE1a	Santa-Cruz/Sc390960	1:250
HSPA1B	ThermoFisher Scientific/PA5-28369	1:1000
PDI	Cell Signalling/3501S	1:1000
BiP	Cell Signalling/31835	1:1000
pIRE1	ThermoFisher Scientific/PA5-105424	1:500
eIF2a	Novus Biologics/NBP2-67353	1:1000
UMOD	Novus Biologics/NBP233393, R&D Systems/AF5144, Abcam/Ab207170.	1:1000
GFP	Cell Signalling/2955S	1:1000

Anti-mouse 680	ThermoFisher Scientific/A21057	1:10,000
Anti-mouse 700	ThermoFisher Scientific/A21036	1:10,000
Anti-mouse 800	ThermoFisher Scientific/A32735	1:10,000
Anti-sheep 680	ThermoFisher Scientific/A21102	1:10,000
Anti-goat 800	ThermoFisher Scientific/A232930	1:10,000
Anti-rabbit 800	ThermoFisher Scientific/A21109	1:10,000
Goat anti-rabbit 647	ThermoFisher Scientific/A21244	1:500
Donkey anti-goat 546	ThermoFisher Scientific/A11056	1:500
Donkey anti-goat 488	ThermoFisher Scientific/A11055	1:500

The primary antibodies used for UMOD detection varied depending on sample type and analysis. The UMOD antibody supplied by Novus Biologics was used for detecting UMOD bands in Western blots with kidney lysate samples. The UMOD antibody supplied by R&D Systems was utilised in the N-deglycosylation assays for UMOD for determining glycosylated and non-glycosylated bands in Westerns blots for urine samples. The UMOD antibody provided by Abcam had the widest application set, including Westerns blots for urine, cell, and kidney lysate, as well as immunofluorescence staining of kidney sections.

For Western blots, certain antibodies produced non-specific banding which were excluded from the final analysis. For transparency, this thesis will include example blots of these antibodies and highlight the bands which were chosen for relative quantification of protein expression. The main antibodies of concern are UMOD (Abcam/Ab207170) used on

kidney medulla protein lysates in Figure 2.2 and NKCC2/pNKCC2 in total kidney lysates shown in Figure 2.3.

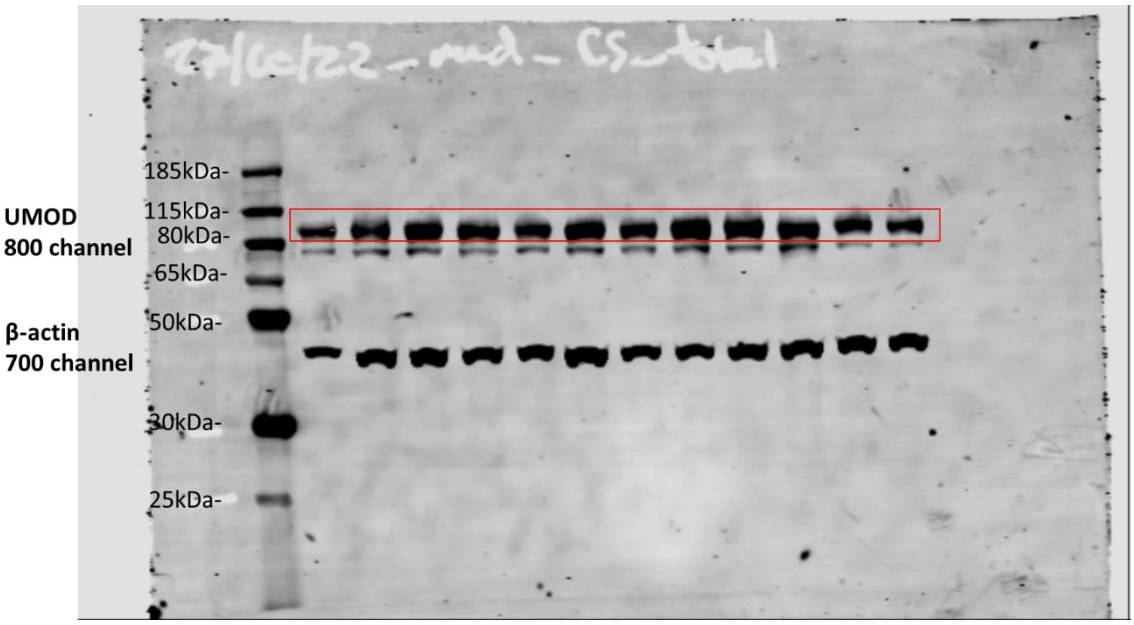

Figure 2.2. Example of non-specific bands on a Western blot using the UMOD primary antibody provided by Abcam (Ab207170) on kidney medulla samples.
A total of 20μg of kidney medulla lysate was loaded onto the gel. The top band (85kDa) highlighted in red is UMOD, whereas the bottom band (78kDa) is considered to be non-specific binding and excluded in the final analysis. Also shown on the same blot is the β-actin loading control (42kDa) which was used for normalising the UMOD signal.

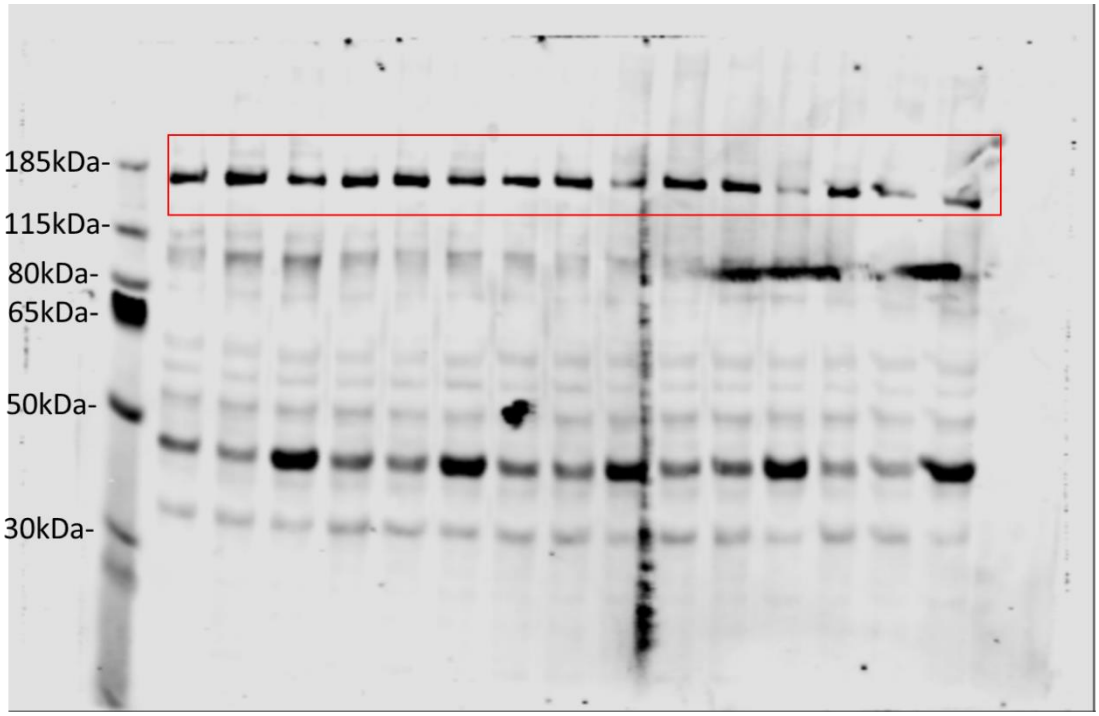

Figure 2.3. Example of non-specific bands on a Western blot using the NKCC2 primary antibody provided by ThermoFisher Scientific (PA5-88905) on total kidney samples.
A total of 40μg of total kidney lysate was loaded onto the gel. The top band (121kDa) highlighted in red is NKCC2, whereas the other bands are considered to be non-specific binding and therefore excluded in the final analysis.

Chapter 3: Salt loading decreases urinary excretion and increases intracellular accumulation of uromodulin in stroke-prone spontaneously hypertensive rats

Alternative Format Thesis Declaration:

Significant portions of this chapter have been published in *Clinical Science* (Mary et al., 2021). The following is a list of my specific contributions to this publication:

- Conceptualisation: Contributed to the formulation and evolution of the main research goals of the paper: 1) investigating the influence of salt on UMOD excretion and 2) the effect of salt on UMOD excretion in the context of blood pressure.
- Data Curation: A significant portion of the managing and maintaining data was carried out by me, including maintaining shared drives (i.e. on OneDrive and local J-drives) and appropriate labelling of data for initial use and later re-use.
- Formal Analysis: I was involved in and carried out most of the statistical and analytical techniques that generated the study data. This includes Western blot analyses, analysis of UMOD quantitation by ELISA, immunofluorescence analysis, qPCR analysis, and all the associated statistical evaluation using GraphPad Prism.
- Investigation: Most of the investigation and data/evidence collection was carried out by me, including the animal work, tissue collection and urine analysis, Western blots and ELISAs, immunofluorescence imaging, RNA extraction and qPCR analysis, and mTAL tubule isolation and incubations.
- Methodology: I contributed to the design and development of most of the methodology, including optimisation of Western blots for analysis of UMOD, optimisation of the immunofluorescence incubation and imaging, ELISA linearity determination and analysis with UMOD, and animal sample collection.
- Project Administration: I was responsible, in part, for the planning and coordination of the research activity and execution. Timelines for animal work, as well as experimental procedures such as Western blotting and ELISAs, were all planned and executed by me.
- Visualisation: I provided significant contributions to the preparation and presentation of the manuscript. This included figure generation of Western blots,

ELISA graphs, and immunofluorescence images. Panel layout was also facilitated by me.

- Writing – original draft: I contributed significantly to the writing of the original manuscript, including the introduction, results, methods, and discussion sections.
- Writing – review & editing: I contributed to additional experiments suggested by reviewers and contributed to a number of edits in the manuscript, including the addition of the clinical perspectives section.
- Validation: Verification of reproducibility of the results was carried out by me, whereby I ensured sample numbers were appropriate across experiments/animal studies.

3.1 Introduction

There is increasing consensus that UMOD is key to sodium homeostasis in the kidneys and by extension, blood pressure regulation (Graham et al., 2014, Trudu et al., 2013b). Transgenic mouse models overexpressing UMOD in an FVB/N background strain showed increased renal injury as well as hyperactivation of NKCC2 (Trudu et al., 2013b). This led to salt-sensitive hypertension in these models. In another study, a global UMOD knockout mouse model exhibited resistance to salt-sensitive blood pressure changes (Graham et al., 2014). With regards to the effects on UMOD secretion, a study with salt-sensitive and resistant hypertensive patients demonstrated greater UMOD secretion compared to healthy control individuals (Matafora et al., 2014). This is inversely associated with urinary sodium excretion in these individuals. More importantly, UMOD seems to be an important cardiovascular health marker, whereby both serum and urinary UMOD excretion are inversely associated with CVD as well as progressive kidney disease in humans (Steubl et al., 2020c, Garimella et al., 2019, Garimella et al., 2015). This would suggest that lowering urinary UMOD has cardiovascular protective effects, which makes the findings that it is overexpressed in salt-sensitive hypertension and kidney damage paradoxical (Graham et al., 2014, Matafora et al., 2014). Therefore, more research is warranted in deciphering the association between sodium and UMOD.

Multiple animal models have been utilised to study the role of UMOD in hypertension, including UMOD or hepsin knockouts, or via transgenic overexpression of UMOD (Graham et al., 2014, Matafora et al., 2014, Olinger et al., 2019). Of note, all of these models lack an underlying genetic predisposition to hypertension. A retrospective analysis of the DASH-sodium trial concluded that higher urinary UMOD levels were not associated with higher systemic blood pressure in the context of greater dietary salt intake (Bakhoum

et al., 2021). In another more recent interventional study involving a Chinese cohort, high dietary salt intake was significantly associated with increased plasma and urinary UMOD concentrations (Du et al., 2021). These human clinical studies pose interesting questions: to what extent does salt itself influence UMOD from expression to excretion? And if so, is there a difference between normotensive and chronic hypertensive settings?

This chapter aims to offer novel perspectives to these questions and a greater understanding of the effects of salt on UMOD, a previously not well explored axis. To do this, we used the SHRSP rat, a polygenic model of chronic hypertension. In fact, it has been rated to have the highest SBP when compared to 179 rat strains (Mashimo et al., 2005). This well-studied model has multiple aetiologies contributing to cardiovascular disease, including stroke (Yamori et al., 1977), chronic hypertension (Houston, 2011), vascular dysfunction (Harvey et al., 2017), and renal end-organ injury (Churchill et al., 2002). The SHRSP model is of particular interest for this study, in that it is genetically predisposed to develop renal damage, with salt supplementation accelerating this process and magnitude of hypertension (Churchill et al., 2002).

The main hypothesis of this chapter is that salt regulates UMOD expression and secretion in both normotension and hypertension. This chapter will address (i) how salt influences UMOD excretion in medullary TAL; (ii) potential differences in the effects of dietary salt loading on UMOD urinary excretion in normotensive WKY and chronic hypertensive SHRSP models; (iii) whether the influence of salt on UMOD excretion is blood pressure dependent. The final aim is specifically addressed through the use of calcium channel blocker nifedipine, an anti-hypertensive (blood pressure lowering) drug which has been shown to alleviate salt-induced hypertension in SHRSP (Nito et al., 1995, Kyselovic et al., 2001). This will therefore separate blood pressure and salt components. This work has been published in Clinical Science (Mary et al., 2021).

3.2 Materials and Methods

General Materials and Methods can be found in Chapter 2.

3.2.1 Animals and acute salt loading

In this chapter, we utilised male and female SHRSP (*n* =54) and WKY (*n* =32) at 11 weeks of age (referred to as “baseline”). At 12 weeks of age, littermates were randomized into groups of *n* = 8 per sex and per group. The following groups were assigned: normal drinking water (normal salt, NS) and 1 % NaCl (hereafter: 1% salt) in the drinking water (high salt, HS) for 3 weeks. A subset of SHRSP on HS (n=8/sex) was administered the

calcium channel blocker nifedipine (Sigma-Aldrich, UK), which was provided daily for 3 weeks at 10 mg/kg/day in 1mL of baby food (Heinz Custard, UK) as well as 15mg/kg/day in their drinking water, as previously reported (Small et al., 2016). To maintain consistency, all groups were fed baby food (with or without nifedipine). Urine and blood samples, as well as SBP readings, were collected every week, as detailed in the General Methods Section.

3.2.2 N-Deglycosylation assay

UMOD was N-deglycosylated with PNGase F (New England Biolabs, USA) under reducing conditions. 2µg of UMOD was denatured with the buffer provided by the manufacturer and then incubated with PNGase F at 37°C for 1 hour. The samples were then separated on 4-12% Bis-Tris NuPAGE gels and transferred on PVDF membranes prior to imaging, as described in General Methods Chapter.

3.2.3 Histology

Paraffin-embedded kidneys were sectioned (2µm) for histological staining and immunofluorescence (*n* =8 per group (4/sex) kidneys were evaluated and scored in a blinded fashion. Periodic acid-Schiff (PAS) staining was used to assess morphological differences. The PAS stain was based on oxidation of certain tissue elements to aldehydes by periodic acid. This allowed documentation of polysaccharides, neutral mucosubstances, and basement membranes. The tissues are initially deparaffinized and hydrated as mentioned in the General Materials and Methods chapter. Following this, sections were placed in 0.5% Periodic Acid solution (Sigma-Aldrich, UK) for 15 minutes at room temperature. These were then washed in distilled water prior to incubation with Schiff reagent (Sigma-Aldrich, UK) for 15 minutes. To develop the full colour, the sections were then washed under tepid water for 1-2 mins. The slides were then counterstained with Haematoxylin-Eosin staining solution (Sigma-Aldrich, UK). After further washing in distilled water, the sections were dehydrated in 95% ethanol for 5 minutes, followed by a 5-minute clearing step with xylene-substitute.

3.2.4 Immunofluorescence Imaging and Analysis

At least 5 images were taken per sample and processed and analysed using Zen Blue software. Co-localisation analysis was conducted by cutting out TAL regions where overlap of UMOD and calnexin were visible. All images underwent background subtraction and Gauss smoothening. For quantification of co-localization of UMOD and calnexin, the open source ImageJ plug-in EzColocalization was used (Stauffer et al., 2018).

3.2.5 Ex vivo incubations of mTAL tubules

Kidneys of WKY and SHRSP at age 15 ± 1 weeks were used for mTAL tubule isolation. The kidney was cut along the corticopapillary axis, to allow isolation of the inner stripe of the outer medulla. This dissected region was then cut in 0.1% collagenase solution prepared in HBSS and incubated at 37°C for 10 minutes. The cell suspension was sedimented on ice and mixed with HBSS containing 2% (w/v) to neutralise the collagenase enzyme activity. This crude suspension of tubules was then centrifuged at 1000rpm for 10 minutes and resuspended in basal HBSS. This solution was then filtered through a 52µm nylon mesh membrane (Fisher Scientific, UK). The nylon mesh would therefore trap tubules on the surface based on their size. These tubules were washed off with HBSS into a new 50mL collection tube, which was centrifuged at 500 rpm for 5 minutes at room temperature. The resulting supernatant was resuspended with DMEM (with sodium pyruvate and glutamine) and contained the free-floating tubules in suspension. These were then aliquoted into separate 2mL Eppendorf tubes for incubation with the following DMEM solutions: 1) with nifedipine (10mM) or 2) an additional 154mM of NaCl to the pre-existing NaCl present in the media (salt stress study). The tubule suspensions were incubated for 4 hours at 37°C in a rotating incubator. Following this, the tubule suspension was centrifuged to 1000rpm for 10 minutes at room temperature and the supernatant collected, before being stored at -80°C. The tubule pellet was lysed with either 1) Qiazol for RNA or 2) Mem-PER Plus membrane protein extraction kit (as described in General Methods). The yield of tubules isolated from each kidney was low and therefore tubules of several kidneys were pooled per strain and incubations performed in triplicate per experiment. The results are representative of two experiments (biological replicates) performed in each of WKY (n=4) and SHRSP (n=6).

3.3 Results

3.3.1 Blood pressure and kidney structure changes with salt loading

The 11-week-old control SHRSP had significantly higher SBP than aged-matched WKY (Figure 3.1), which matches with previous studies (Kim et al., 1992). Male SHRSP demonstrated a higher SBP than females, while WKY showed no significant difference (Figure 3.1).

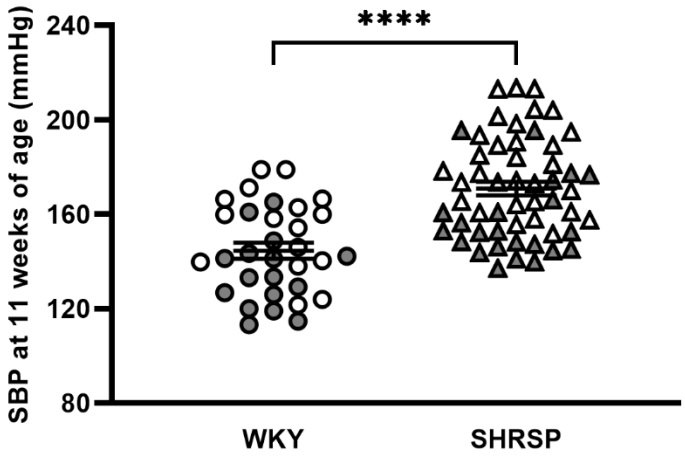

Figure 3.1. SHRSP at baseline have higher systolic blood pressure (SBP) compared to WKY.
SBP was measured using tail-cuff plethysmography in 11-week-old animals. Each single dot in the scatter plot represents the mean of 6-10 consecutive weekly SBP measurements. The graph shows the difference in SBP between WY (*n*=32) and SHRSP (*n*=54). ****p<0.0001 (Welch's t-test). Male rats are represented as circular dots for WKY and triangles for SHRSP with no fill. Female rats are represented as circular dots for WKY and triangles for SHRSP with a shaded grey fill. A sexual dimorphism in SBP was observed in SHRSP. Bars indicate mean ± S.E.M.

Salt loading resulted in a gradual increase in SBP in SHRSP, suggesting salt-induced hypertension (Figure 3.2). After 3 weeks of salt loading, SBP was significantly increased in SHRSP, unlike in WKY (Figure 3.2). To alleviate the rise in blood pressure, a group of salt loaded SHRSP were given anti-hypertensive nifedipine. This resulted in a significant reduction in SBP (Figure 3.2).

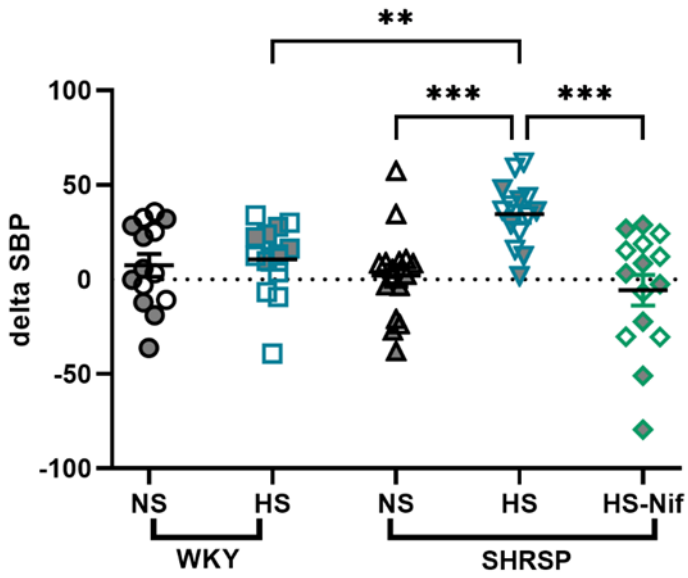

Figure 3.2. Salt loading for 3 weeks increases SBP in SHRSP rats.
SBP was measured using tail-cuff plethysmography. The scatter plot shows differences in SBP (ΔSBP) between baseline (11-week-old) and after 3 weeks of 1% salt loading. WKY were split into two groups (*n*=16/group): normal salt (NS; drinking water only) and high salt (HS; 1% salt in drinking water). SHRSP were split into 3 groups (*n*=16/group): NS, HS, and high salt with nifedipine (HS-Nif). Shaded grey fill indicates female rats, whereas no fill represents male rats. Nifedipine significantly lowered SBP in salt loaded SHRSP to control NS levels. ** $p<0.01$, *** $p<0.001$ (Brown-Forsythe Welch ANOVA test). Bars indicate mean ± S.E.M.

Analysis of the renal histology with PAS staining revealed little or very mild abnormalities in the WKY and SHRSP. A set of scoring criteria was used to assess for acute tubular injury in these strains, specifically for glomerular ischemia and arterial intimal thickening (Table 3.1, Figure 3.3, Figure 3.4). There was no significant difference between the groups. The male SHRSP salt-loaded group with increases in SBP exhibited arteriolar hyalinosis (Figure 3.3). Comparing proximal and distal tubule injury, the former showed no acute injury in any groups while the latter demonstrated mild flattening and loss of occasional tubular epithelial nuclei specifically in the SHRSP (Figure 3.5). Notably, salt loading at 1% (physiological salt concentration) for 3 weeks did not result in severe histological kidney damage in the chronic hypertensive SHRSP.

Sex	Animals	WKY-NS			WKY-HS			SHRSP-NS			SHRSP-HS			SHRSP-HS-CC		
		g	cv	ah	g	cv	ah	g	cv	ah	g	cv	ah	g	cv	ah
male	1	2	0	0	1	0	0	1	0	0	2	0	1	1	0	0
male	2	2	0	0	1	0	0	1	0	0	1	0	1	1	0	0
male	3	1	0	0	1	0	0	2	0	0	0	0	1	1	0	0
male	4	1	0	0	1	0	0	1	0	0	1	0	1	1	0	0
female	5	1	0	0	1	0	0	2	0	0	1	0	0	1	0	0
female	6	1	0	0	1	0	0	0	0	0	1	0	0	2	0	0
female	7	1	0	0	1	0	0	1	0	0	1	0	0	1	0	0
female	8	1	0	0	1	0	0	1	0	0	2	0	0	1	0	0
Median		1	0	0	1	0	0	1	0	0	1	0	0.5*	1	0	0

Table 3.1. Histological scoring of kidney sections.
The columns represent the scoring of kidney sections (2µm) (*n*=8 per group, 4 per sex) after Period Acid Schiff staining. This was used to assess morphological differences. g: Glomerular perfusion; 0 = glomeruli all normal, 1 = mild ischaemia (moderately shrunken outer glomeruli, mild or normal inner glomeruli), 2 = severe ischaemia (severely shrunken outer glomeruli, moderate or mild inner glomeruli). cv: Arterial fibrointimal thickening; 0=absent, 1=present. ah: Arteriolar Hyalinosis; 0=absent, 1=present. All scoring and evaluation were performed in a blinded fashion.

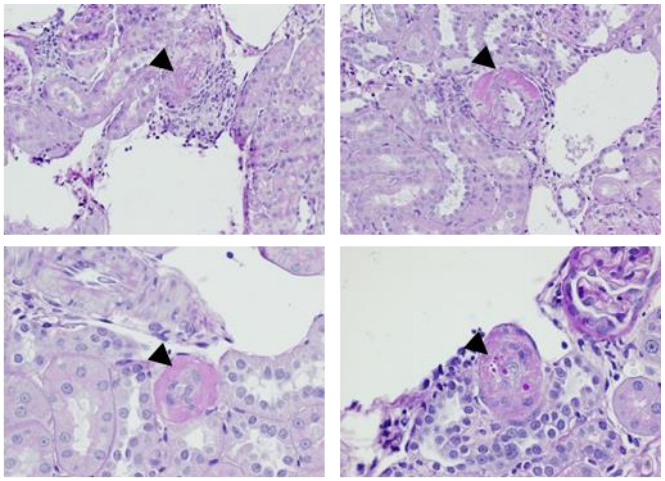

***abnormalities in arterioles (black arrow) in 4 male SHRSP-HS**

Figure 3.3. SHRSP rats after salt loading demonstrate arteriolar hyalinosis.
Representative images of kidney sections (2µm) after Period Acid Schiff stain images. These animals also exhibited increases in SBP after 3 weeks of salt loading (SHRSP-HS). Black arrows represent areas of focus.

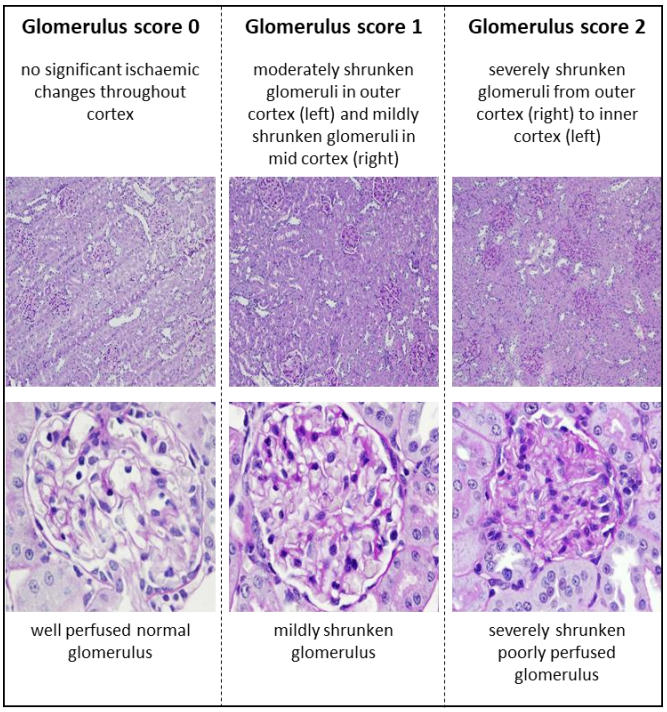

Figure 3.4. Scoring criteria for glomeruli of kidney sections.
The three-point scale was used to determine glomerular injury or abnormalities in kidney sections (2µm) of salt-loaded WKY and SHRSP animals. This was performed in a blinded fashion.

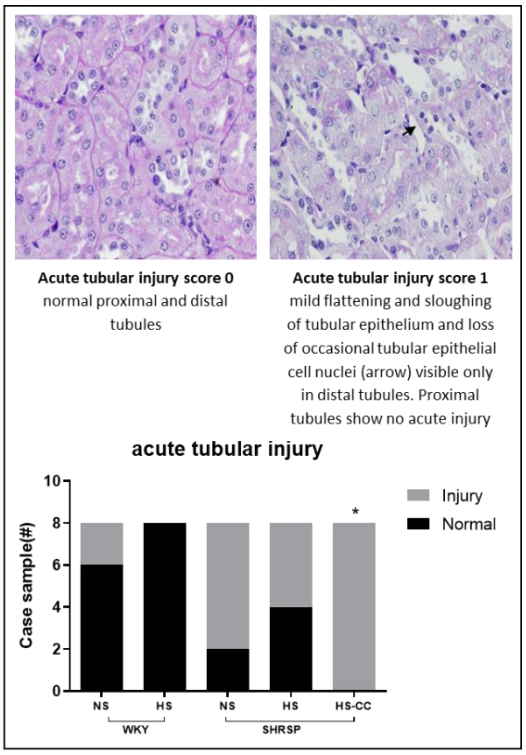

Figure 3.5. SHRSP rats after salt loading demonstrate mild distal tubule injury.
The top half of the figure demonstrates the scoring criteria used to assess the acute tubule injury. The kidney sections (2µm) were analysed in a blinded fashion. The lower half of the figure demonstrates the analysis of acute kidney injury. Kidney scoring was conducted for (*n*=8 per group, 4 per sex). SHRSP exhibit very mild flattening and occasional loss of tubular epithelial nuclei in distal tubules.

3.3.2 Variations in adjustment to salt stress between WKY and SHRSP

To determine differences in renal adaption to salt stress in WKY and SHRSP rats, sodium and water homeostasis were measured in kidneys harvested from these groups at baseline and after 3 weeks of 1% salt loading. At baseline, no discernible differences were noticed between groups (Table 3.2).

Table 3.2. Renal parameters of WKY and SHRSP rats prior to salt loading (at 11 weeks, baseline).

Strain	**WKY**		**SHRSP**		
Condition	NS	HS	NS	HS	HS-CC
n	16	16	16	16	16
Body weight (BW, g)	203.0 ± 13.6	202.5 ± 13.9	190.7 ± 8.7	186.4 ± 8.6	193.5 ± 10.5
Water intake (ml/h)	1.4 ± 0.1	1.4 ± 0.1	1.2 ± 0.1	1.2 ± 0.1	1.2 ± 0.1
Urine output (ml/h)	0.5 ± 0.1	0.7 ± 0.1	0.4 ± 0.1	0.4 ± 0.0	0.3 ± 0.0
u-Na^+ excretion (mmol/day)	0.7 ± 0.1	0.9 ± 0.1	0.9 ± 0.2	0.8 ± 0.1	0.7 ± 0.1

The table shows metabolic cage data collected from WKY and SHRSP at 11 weeks of age prior to 1% salt loading for 3 weeks. NS: normal salt (drinking water), HS: high salt (1% salt) and HS-CC: high salt with nifedipine. Data are expressed as mean ± SEM.

Salt-loaded rats of both strains exhibited significantly increased water intake, matched by increased 24-hour urine and sodium excretion (Table 3.3). Nifedipine treatment partially reversed these effects, with 24-hour urine and sodium excretion returning to control levels. Plasma levels of sodium remained unaffected in the different groups. Calculation of net balance demonstrated an increased retention of water ($p = 0.046$ vs. control SHRSP) and sodium ($p = 0.002$ vs the null hypothesis of even intake and output) in salt loaded SHRSP (Table 3.3). The unmeasurable water losses for absolute balance calculation could not be assessed. These were remedied by treatment with nifedipine ($p<0.001$ and $p=0.011$, respectively).

Table 3.3. Renal parameters of WKY and SHRSP rats after 3 weeks of salt loading.

Parameters	WKY		SHRSP			2-way ANOVA	
	NS	HS	NS	HS	HS-Nif	Strain	HS
n	16	16	16	16	16		
Body weight (BW, g)	261.6 ± 13.2	267.2 ± 13.6	222.5 ± 10.1$	223.3 ± 10.3	225.8 ± 11.0	***	ns
Water intake (ml/h)	1.28 ± 0.11	2.61 ± 0.30***	1.45 ± 0.12	2.78 ± 0.19***	1.63 ± 0.10###	ns	***
Urine output (ml/h)	0.56 ± 0.06	1.80 ± 0.22***	0.53 ± 0.06	1.57 ± 0.13***	1.01 ± 0.10***,##	ns	***
Water intake-urine output (ml/h)	0.72 ± 0.07	0.82 ± 0.13	0.91 ± 0.09	1.21 ± 0.11*	0.63 ± 0.08*,###	**	0.05
p-Na^+ (mmol/L)	135.1 ± 1.27	136.7 ± 0.90	136.3 ± 1.04	136.0 ± 1.59	137.5 ± 0.98	ns	ns
u-Na^+ excretion (mmol/day)	0.83 ± 0.13	10.86 ± 1.18***	0.71 ± 0.10	10.64 ± 0.79***	7.28 ± 0.54***,##	ns	***
Excess Na^+ balance (mmol/day)	-	0.27 (-0.65 to 2.51)	-	1.60 (0.74 to 2.50)†	0.13 (-1.04 to 0.31) #	-	-
p-creatinine (mmol/L)	26.44 ± 1.39	25.25 ± 1.59	18.47 ± 1.21 $$$	20.07 ± 1.26	20.13 ± 1.24	***	ns
u-creatinine (µmol/day)	73.39 ± 4.72	84.41 ± 3.89*	59.37 ± 3.54 $	67.65 ± 3.40	64.51 ± 2.42	**	*

The table shows metabolic cage data collected from WKY and SHRSP after 3 weeks of 1% salt loading. . NS: normal salt (drinking water), HS: high salt (1% salt) and HS-CC: high salt with nifedipine. Excess sodium (Na^+) balance was calculated for salt-loaded groups as follows: sodium from solid food (estimated by average 24-hour sodium urinary excretion from NS animals) + sodium in drinking water – urinary sodium excretion. The results were compared to 0 by Wilcoxon Signed Rank test, under the null hypothesis of a net sodium balance. * $p<0.05$ vs same strain NS; $ $p<0.05$ SHRSP-NS vs WKY-NS; # $p<0.05$ vs SHRSP-HS. * $p<0.05$, ** $p<0.01$, *** $p<0.001$ for group comparison and 2-way ANOVA results; same for $ and #. † ≠ 0, $p<0.05$. Data are expressed as mean ± SEM.

To determine any kidney injury, we examined total kidney weight in both strains which showed a greater weight of SHRSP kidneys compared to WKY (Figure 3.6). This implied a degree of functional hypertrophy in SHRSP. After salt loading, there was a mild but significant increase in kidney weight in both strains and was unaffected by treatment with nifedipine in salt loaded SHRSP.

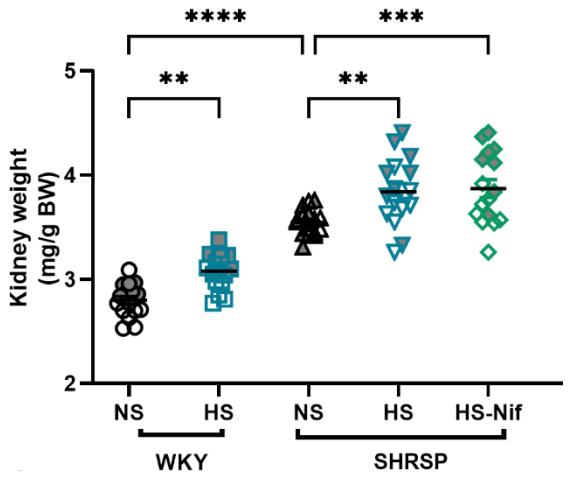

Figure 3.6. Salt loading increased kidney weight in both WKY and SHRSP rats after salt loading.
Data are shown as a scatter plot with the following groups: NS: normal salt, HS: high salt (1% salt) and HS-Nif: high salt with nifedipine, *n* = 16 per group. Symbols with grey fill symbolise female sex. The bars indicate mean and error bars mean ± SEM. **p<0.01, ***p<0.001, **** p<0.0001 (ANOVA with Bonferroni multiple comparison test).

To test for albuminuria, we measured the albumin-to-creatinine ratio (ACR) in WKY and SHRSP. There was no significant difference between the strains without salt loading, however salt loading led to a significant rise in ACR in SHRSP compared to baseline and all other groups (Figure 3.7). This was entirely ameliorated by nifedipine treatment (Figure 3.7).

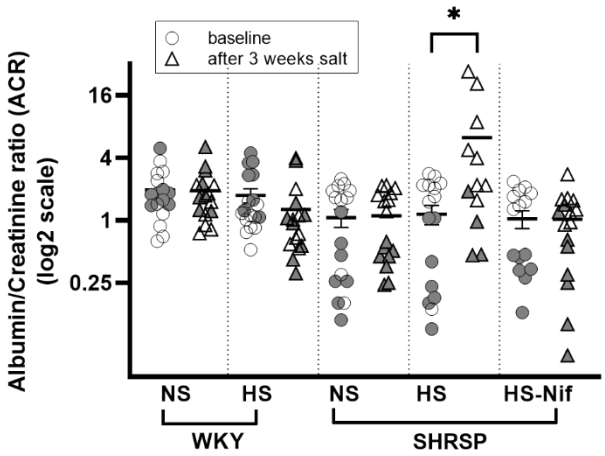

Figure 3.7 Salt loading increased the albumin-to-creatine ratio (ACR) in salt-loaded SHRSP rats.
Data are shown as a scatter plot with the following groups: NS: normal salt, HS: high salt (1% salt) and HS-Nif: high salt with nifedipine, *n* = 16 per group. Symbols with grey fill symbolise female sex. The increase in ACR ratio in the SHRSP rats is corrected by treatment with nifedipine. *p<0.05 (Students t-test). The bars indicate mean and error bars mean ± SEM.

We next investigated early molecular tubular injury markers to further understand renal damage occurring under salt stress. Specifically, we examined the expression of KIM-1 (proximal tubule injury marker) and NGAL (TAL and distal tubule marker). Both KIM-1 (fold change, 3.4; p = 0.003) and NGAL (fold change, 2.0; p -= 0.012) were significantly upregulated in salt-loaded SHRSP compared to the respective normal salt controls.

Nifedipine treatment significantly lowered the expression of KIM-1 in the salt-loaded SHRSP rats, whereas NGAL remained highly upregulated.

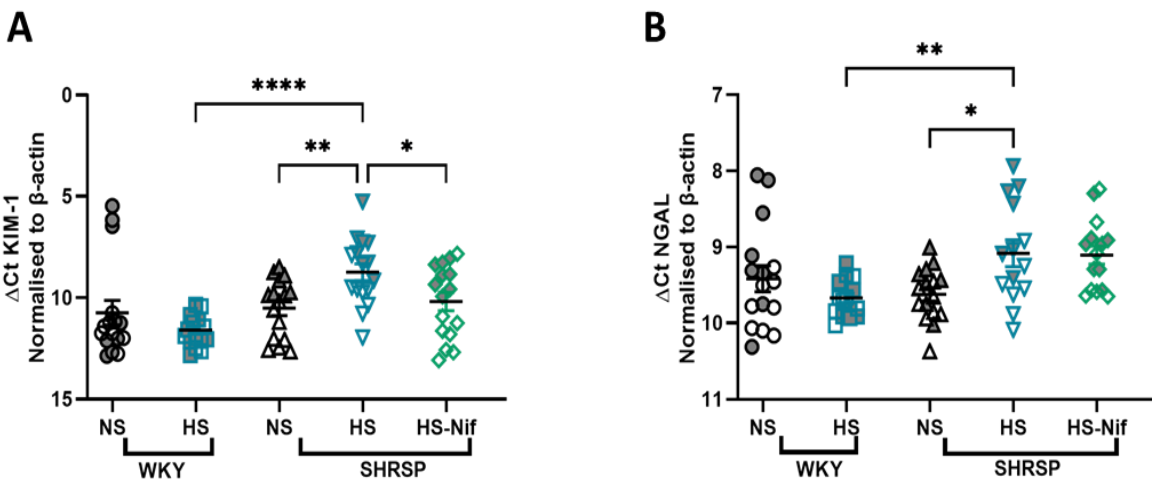

Figure 3.8. Expression of early tubule injury markers are increased in SHRSP after salt loading.
The panel represents the mRNA expression of (**A**) kidney injury marker-1 (KIM-1) and (**B**) neutrophil gelatinase-associated lipocalin (NGAL). Data are shown as a scatter plot with the following groups: NS: normal salt, HS: high salt (1% salt) and HS-Nif: high salt with nifedipine, *n* = 16 per group. Symbols with grey fill symbolise female sex. *p<0.05, ** p<0.01, **** p<0.0001 (Brown-Forsythe Welch ANOVA test). The bars indicate mean and error bars mean ± SEM.

3.3.3 Urinary UMOD excretion is decreased in WKY and SHRSP after 24 hours of salt loading

To examine the effects of salt loading on urinary UMOD excretion rate, the concentration of UMOD in 24-hour urine samples of WKY and SHRSP rats was analysed. At baseline, the urinary UMOD excretion rate in SHRSP was significantly higher than in WKY of the same age (Figure 3.9).

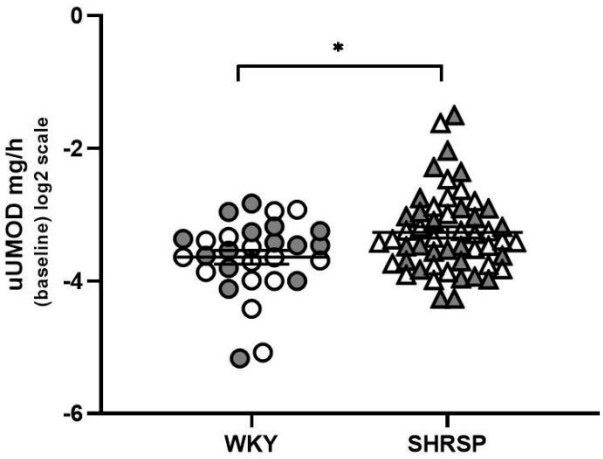

Figure 3.9. Increased Urinary UMOD Excretion Rate in SHRSP rats at baseline.
The scatter plot illustrates 24-hour urine samples collected from rats in metabolic cages at 11 weeks of age (baseline). The urinary UMOD (uUMOD) concentrations were determined using ELISAs. The values are normalised to the total urinary volume over 24 hours. WKY (n=32) and SHRSP (n=54). * p<0.05 (Mann Whitney test). Data are expressed as mean ± SEM. Symbols with grey fill symbolise female sex.

After 3 weeks of salt loading, there was a significant and gradual decrease in urinary UMOD excretion rate in both WKY and SHRSP, starting in week 1.

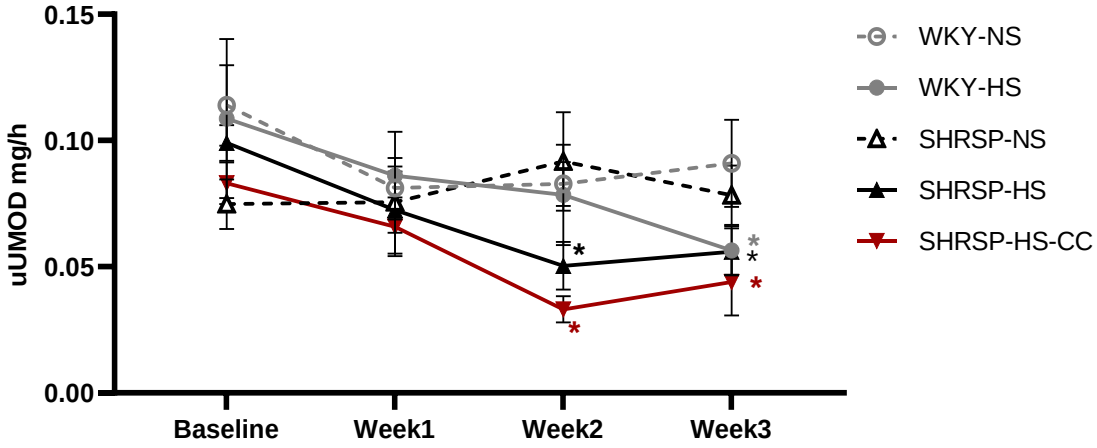

Figure 3.10. Timeline of gradual decrease in urinary UMOD (uUMOD) excretion with salt loading in WKY and SRHSP.
The graph represents urine samples collected from salt-loaded WKY and SHRSP rats in metabolic cages on weekly basis. The urinary UMOD (uUMOD) concentrations were determined using ELISAs. The values are normalised to the total urinary volume over 24 hours. Data are expressed as mean ± SEM. NS: normal salt, HS: high salt (1% salt) and HS-Nif: high salt with nifedipine, *n* = 16 per group. * p<0.05 (Mixed Model ANOVA with repeated measures, comparisons are with respective NS group of each strain).

At week 3, the urinary UMOD excretion rate was significantly lower than the respective normal salt controls for both WKY (fold change, 0.5; p=0.028) and SHRSP (fold change, 0.6; p=0.018) rats (Figure 3.11).

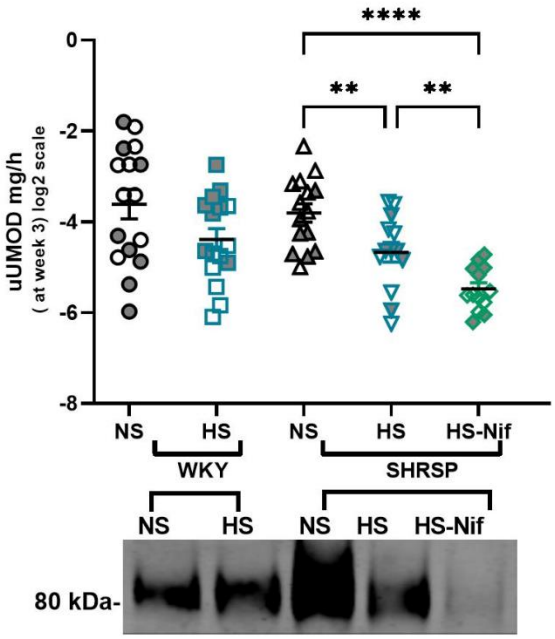

Figure 3.11. Salt loading of 3 weeks significantly lowers urinary UMOD excretion rate in SHRSP rats. The graph represents 24 hours urinary UMOD (uUMOD) samples collected from salt-loaded WKY and SHRSP after 3 weeks. The uUMOD concentrations were determined using ELISAs. The values are normalised to the total urinary volume over 24 hours. Data are expressed as mean ± SEM. NS: normal salt, HS: high salt (1% salt) and HS-Nif: high salt with nifedipine, n = 16 per group. $p<0.05$, ** $p<0.01$, *** $p<0.001$ (Brown-Forsythe Welch ANOVA test). A representative Western blot for UMOD is shown for pooled samples from each group. Symbols with grey fill symbolise female sex.

When analysed with regards to percentage change from baseline, after 3 weeks the WKY exhibited a 26% while SHRSP showed a 55% reduction in urinary UMOD excretion after salt loading (Figure 3.12). Given that even the WKY showed a decrease in urinary UMOD excretion with salt loading, without any structurally or functionally impacted tubules, it is unlikely that the structural tubule damage we demonstrated with renal histology in the SHRSP is the cause of this decrease in UMOD excretion.

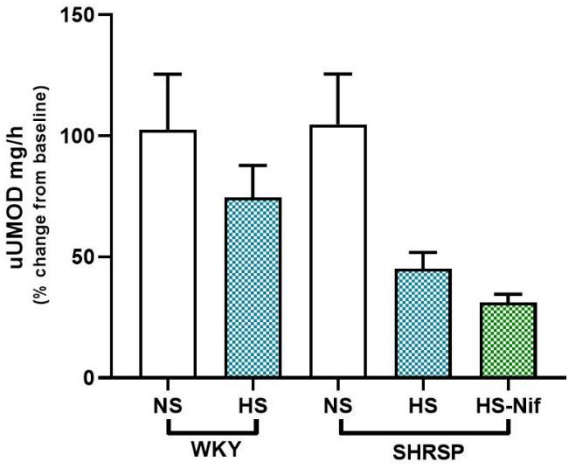

Figure 3.12. A percentage decrease in urinary UMOD excretion rate occurs in WKY and especially in SHRSP. The graph represents percentage change of urinary UMOD (uUMOD) after 3 weeks of salt loading compared to baseline values in samples collected from WKY and SHRSP. The uUMOD concentrations were determined using ELISAs. Data are expressed as mean ± SEM. NS: normal salt, HS: high salt (1% salt) and HS-Nif: high salt with nifedipine, *n* = 16 per group.

With regards to sodium excretion, upon salt loading and regardless of group or treatment, urinary UMOD excretion rate was inversely associated with absolute (Spearman ρ=-0.502, p=0.0005) and fractional (Spearman ρ=-0.368, p=0.016) excretion of sodium (Figure 3.13). To test whether sodium reabsorption was affected via NKCC2, we measured NKCC2 abundance (both protein and mRNA expression) as well as the abundance of phosphorylated NKCC2 as a surrogate of activity. There was no significant difference in total abundance or activity of NKCC2 (Figure 3.14).

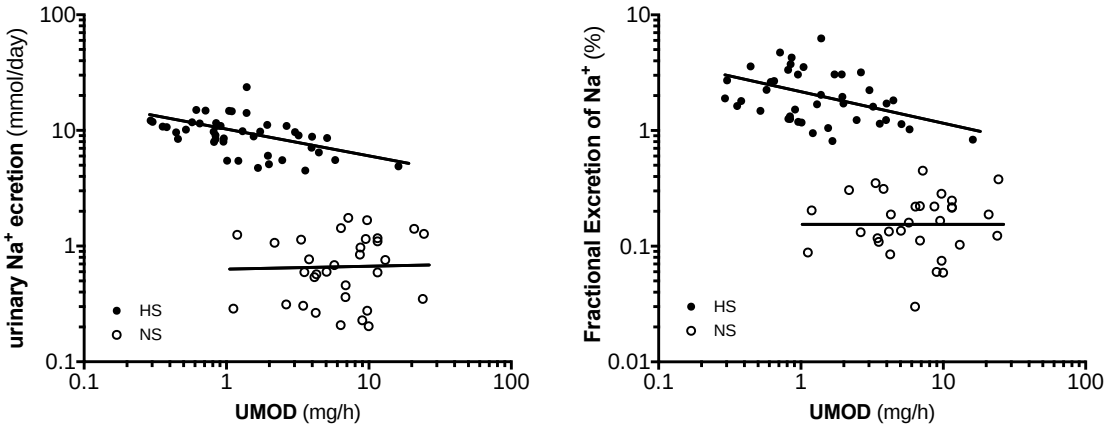

Figure 3.13. Sodium and urinary UMOD excretion show an inverse relationship after salt loading. Fractional excretion of sodium excretion is the percentage of sodium filtered by the kidney which is excreted in the urine and was calculated as follows: serum creatinine (µmol/L) × urinary sodium (mmol/L)/serum sodium (mmol/L) × urinary creatinine (µmol/L) × 100. Graphs showing Spearman correlation showing inverse association of urinary UMOD with urinary (left-hand side, r= 0.502, p=0.0005) and fractional (right-hand side, r=-0.368, p=0.016) excretion of sodium after salt loading (combined WKY and SHRSP, irrespective of group). NS; normal salt, HS: high salt (1% salt).

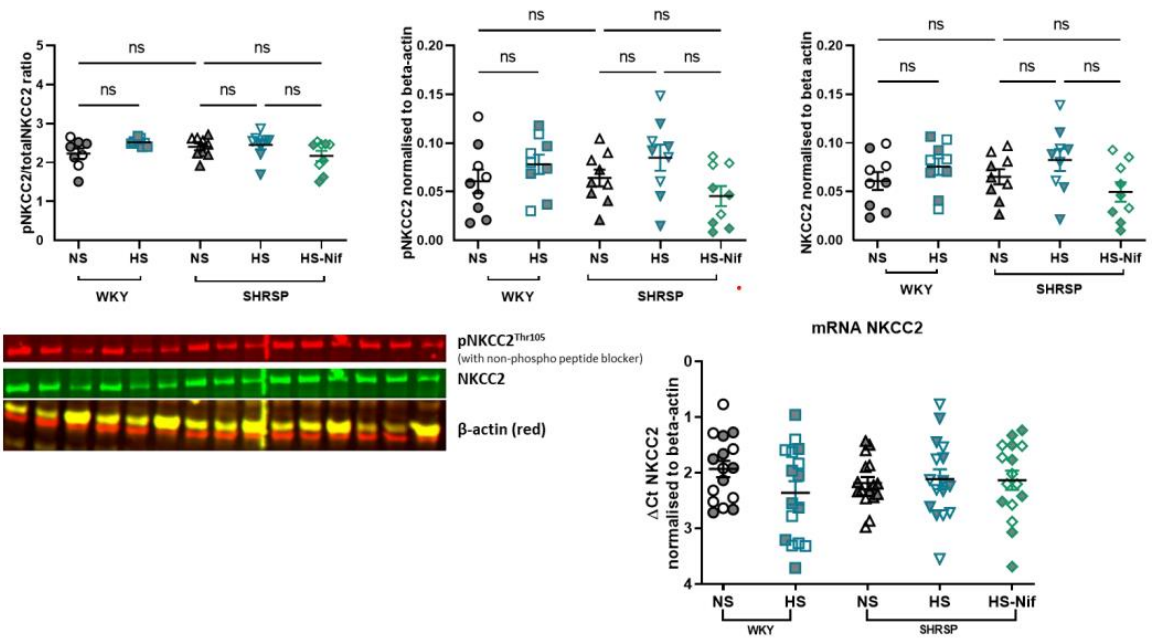

Figure 3.14. NKCC2 abundance do not change with salt loading in WKY or SHRSP.
Total kidney lysates were used to assess NKCC2 activity via Western blotting for total NKCC2 and phosphorylated NKCC2 (pNKCC2), which was represented as a ratio. A representative Western blot is shown on the left-hand side of the figure panel. Individual blot results and signals are shown for pNKCC2 and total NKCC2 in the middle and right-hand side scatter graphs. The NKCC2 and pNKCC2 signals were normalised to β-actin as a loading control. NKCC2 gene was measured by qPCR (bottom right of the panel) and expressed as delta CT (difference from housekeeping β-actin gene). *n* = 9 for Western blotting and *n* = 18 for mRNA (gene expression) for each of the following groups: NS: normal salt, HS: high salt (1% salt) and HS-Nif: high salt with nifedipine. Data are expressed as mean ± SEM. Symbols with grey fill symbolise female sex.

To dissect the effects of blood pressure on urinary UMOD excretion rate, we assessed whether nifedipine influences the salt-induced decrease in urinary UMOD excretion. Nifedipine resulted in a further decrease in urinary UMOD excretion rate in salt-loaded SHRSP compared to respective control rats (fold change, 0.5; p 0.004) (Figure 3.11) as well as a 67% total reduction from baseline (Figure 3.12). This implied that salt reduces urinary UMOD excretion regardless of a chronic hypertensive background or blood pressure-lowering treatments.

3.3.4 UMOD mRNA and total kidney proteins levels do not match changes in urinary UMOD excretion

In order to determine the underlying cause of the decrease in urinary UMOD excretion rate following salt loading, we analysed UMOD transcription, translation, and post-translation. In whole kidneys extracted from WKY and SHRSP, UMOD protein levels were higher in the latter strain at baseline. Notably, total kidney UMOD protein levels did not alter after salt loading in either strain (Figure 3.15).

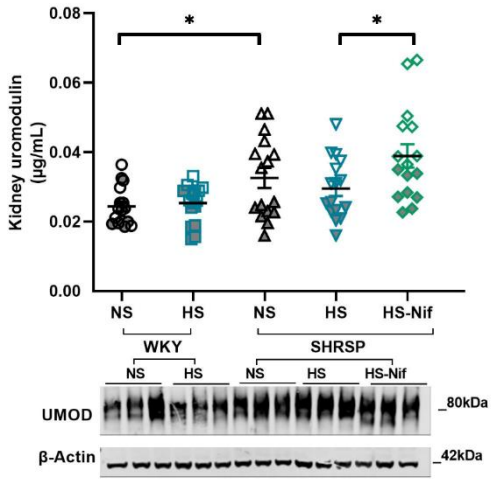

Figure 3.15. Total kidney intracellular UMOD levels are unchanged with salt loading in WKY and SHRSP. Total kidneys were isolated from WKY and SHRSP rats and cut along the sagittal plane, before being cut into two halves again, to yield one fourth of kidney. This was subsequently used to isolate total protein, which was used for an ELISA (top half of the figure) and Western blotting (bottom half of the figure, representative image shown) for UMOD. The ELISA was normalised to total protein whereas the Western blot was normalised to the β-actin loading control. NS: normal salt, HS: high salt (1% salt) and HS-Nif: high salt with nifedipine (*n* = 16 per group). Data are expressed as mean ± SEM. Symbols with grey fill symbolise female sex. *p<0.05 (Brown-Forsythe Welch ANOVA test).

With regards to UMOD mRNA levels, there was a slight decrease after salt loading in WKY and SHRSP, although this was only statistically significant in the SHRSP (relative fold change to the normal salt control, p<0.001) (Figure 3.16 and Figure 3.17). Given the lack of changes in UMOD protein and mRNA expression levels suggested that salt loading is impacting UMOD cellular secretion.

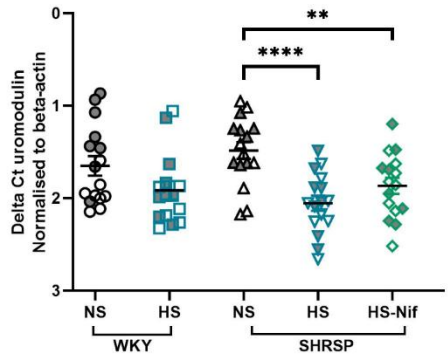

Figure 3.16. The total kidney UMOD mRNA levels slightly decrease in salt loaded SHRSP. Total kidneys were isolated from WKY and SHRSP rats and cut along the sagittal plane, before being cut into two halves again, to yield one fourth of kidney. This was subsequently used to isolate RNA, which was analysed by qPCR for UMOD gene expression. Shown is the comparison of delta Ct *Umod* normalised to β-actin within strains. NS: normal salt, HS: high salt (1% salt) and HS-Nif: high salt with nifedipine (*n* = 16 per group). Data are expressed as mean ± SEM. Symbols with grey fill symbolise female sex. **p<0.01, ****p<0.0001 (Brown-Forsythe Welch ANOVA test).

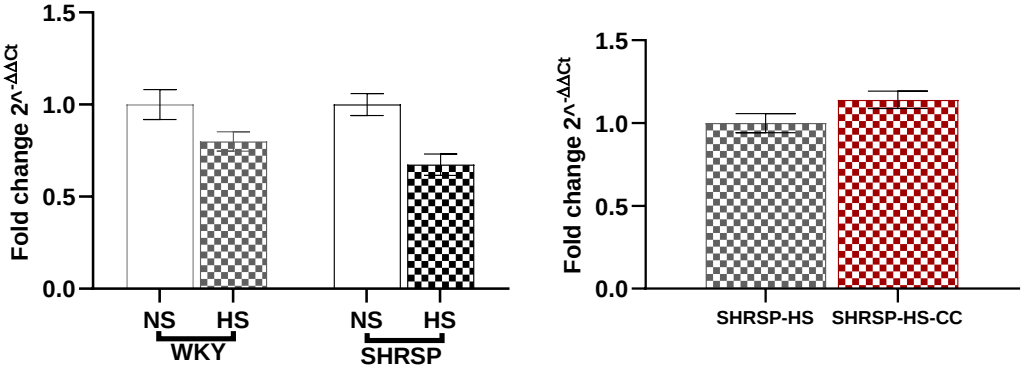

Figure 3.17. The total kidney UMOD mRNA fold-change remained unchanged in both WKY and SHRSP with salt loading.
Total kidneys were isolated from WKY and SHRSP rats and cut along the sagittal plane, before being cut into two halves again, to yield one fourth of kidney. This was subsequently used to isolate RNA, which was analysed by qPCR for UMOD gene expression. Shown is the fold-change of salt-loaded rats relative to the normal salt controls for each strain. NS: normal salt, HS: high salt (1% salt) and HS-CC: high salt with nifedipine (*n* = 16 per group). Data are expressed as mean ± SEM.

In salt loaded SHRSP treated with nifedipine, UMOD mRNA levels remained unchanged however total kidney UMOD protein levels increased by 32% (p=0.027) compared to controls (Figure 3.15). This would suggest a compensatory mechanism, whereby salt loading increases UMOD intracellularly to adjust for the decrease in UMOD excretion rate seen in these SHRSP. It should be noted that as WKY rats can become hypotensive when administered nifedipine (Rakusan et al., 1994, Lemay et al., 2001), none of the WKY groups were given nifedipine in this study.

To test whether nifedipine had any direct effects on TAL tubules, we isolated TAL tubules from kidneys in WKY and SHRSP for ex-vivo incubations with nifedipine. Looking at UMOD protein levels in the media to assess secretion, we found no changes with nifedipine incubation in either strain (Figure 3.18). Similarly, cell lysate (intracellular) UMOD protein levels showed no significant difference with nifedipine for WKY or SHRSP tubules (Figure 3.19). This data indicates that while nifedipine has blood pressure lowering effects in the salt loaded SHRSP, it does not appear to have any direct effects on UMOD trafficking in TAL tubules. This is in line with that fact that there is a lack of L-type calcium channels in the TAL (Zhou and Greka, 2016).

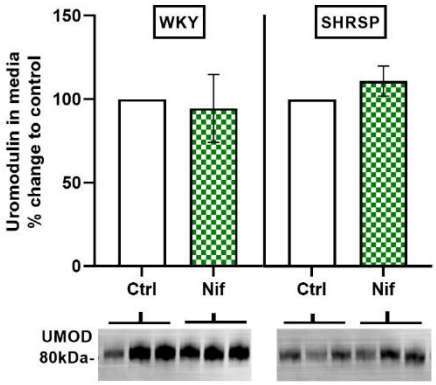

Figure 3.18. Nifedipine has no direct effect on UMOD secretion from isolated medullary TAL tubules in WKY and SHRSP.
Western blots for UMOD were performed on media isolated from an ex-vivo medullary TAL tubule experiments. The tubules were isolated from kidneys of WKY and SHRSP rats at 12 ± 3 weeks old). These were then incubated in 10mM nifedipine (Nif) for 6 hours or basal media (control; ctrl) at 37°C. Representative Western blots are shown for UMOD, with the graphs representing two experimental replicates (WKY, *n* =4; SHRSP, *n* = 6). Data are expressed as mean percentage change to control group of each strain ± SEM.

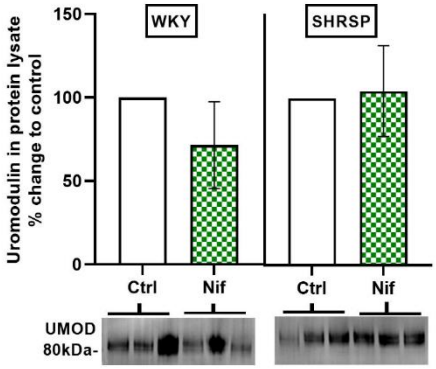

Figure 3.19. Nifedipine does not directly affect UMOD intracellular protein levels in isolated medullary TAL tubules from WKY and SHRSP.
Western blots for UMOD were performed on cell lysates isolated from an ex-vivo medullary TAL tubule experiments. The tubules were isolated from kidneys of WKY and SHRSP rats at 12 ± 3 weeks old). These were then incubated in 10mM nifedipine (Nif) for 6 hours or basal media (control; ctrl) at 37°C. Representative Western blots are shown for UMOD, with the graphs representing two experimental replicates (WKY, n =4; SHRSP, n = 6). Data are expressed as mean percentage change to control group of each strain ± SEM.

Given that total kidney UMOD protein levels remained unchanged with salt loading despite a lower excretion rate, we hypothesized that there should be a compensatory mechanism for maintaining stable intracellular UMOD levels. After intracellular maturation of UMOD, it is anchored to the apical membrane of TAL via a glycosylphosphatidylinositol region. This is later cleaved via the serine protease hepsin prior to secretion into urine (Brunati et al., 2015). In the context of salt loading, a recent study demonstrated that hepsin cleaving of UMOD is key to salt sensitivity using hepsin-inactive $Hpn^{Hlb320/Hlb320}$ mice (Hlb320) (Olinger et al., 2019). Therefore, we measured renal hepsin in both WKY and SHRSP. The WKY rats had significantly higher levels of hepsin compared to SHRSP at baseline (fold-change=1.4, p 0.010), however salt loading did not

alter hepsin expression in either strain (Figure 3.20). These findings led to the conclusion salt is not influencing hepsin in these rat models and that lowering of UMOD excretion rate cannot be explained by altered hepsin expression levels.

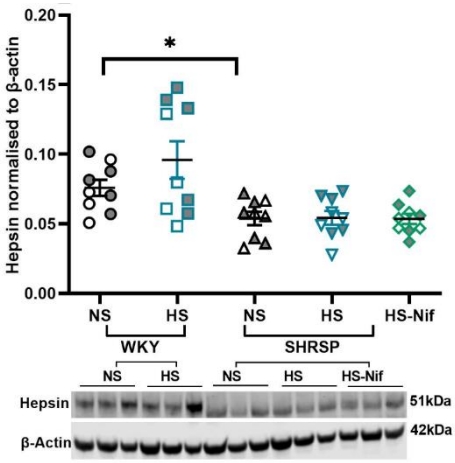

Figure 3.20. Salt loading does not significantly alter hepsin expression in kidneys isolated from WKY and SHRSP rats.
Total kidneys were isolated from WKY and SHRSP rats and cut along the sagittal plane, before being cut into two halves again, to yield one fourth of kidney. This was subsequently used to isolate total protein, which was used for Western blotting for hepsin. This was normalised to the β-actin loading control. NS: normal salt, HS: high salt (1% salt) and HS-Nif: high salt with nifedipine (n = 9 per group). There is a significant strain difference, with SHRSP controls showing higher expression of hepsin compared to WKY controls. Data are expressed as mean ± SEM. Symbols with grey fill symbolise female sex. *$p<0.05$ (Brown-Forsythe Welch ANOVA test).

3.3.5 Salt loading increases the renal intracellular accumulation of UMOD in SHRSP

UMOD consists of a complex tertiary structure consisting of multiple disulphide bonds and undergoes heavy glycosylation along its maturation process. In this regard, the rate limiting step in the maturation of UMOD is its release from the endoplasmic reticulum (ER) (Rampoldi et al., 2011). Therefore, we postulated that UMOD accumulates in cellular compartments of TAL upon salt loading. To investigate this and understand the distribution of UMOD in the medullary TAL, we conducted co-localization immunofluorescence analysis using calnexin, an ER marker. Analysis of UMOD in the ER of SHRSP showed increased accumulation at baseline compared to WKY (Figure 3.21 and Figure 3.22). This is further exacerbated with salt loading. Nifedipine treatment of salt loaded SHRSP did not lower ER accumulation of UMOD, in fact it was similar to the accumulation seen in normal salt and high salt SHRSP groups (Figure 3.22). Interestingly, looking at individual cellular compartments in the WKY and SHRSP revealed a higher UMOD intensity on the luminal membrane rather than ER accumulation in salt loaded WKY (Figure 3.21).

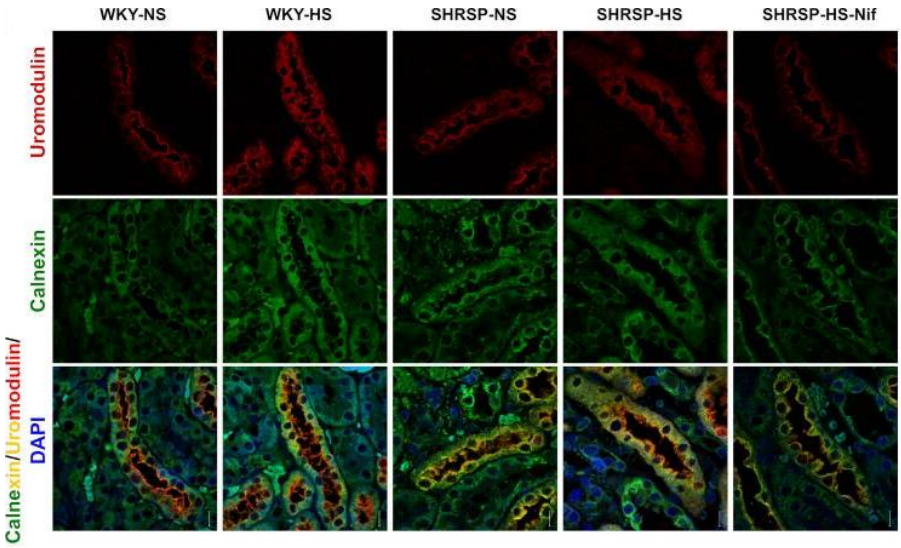

Figure 3.21. Salt loading increases intracellular accumulation of UMOD in both WKY and SHRSP.
Panel showing immunofluorescence analysis of UMOD (red) and ER marker calnexin (green) in rat kidney sections (2µm) from WKY and SHRSP, with a specific focus of medullary TAL tubules. Yellow foci represent areas of co-localization of UMOD and calnexin. Nuclei are stained with DAPI (blue). Scale bar represents 20µm. The following groups are shown NS: normal salt, HS: high salt (1% salt) and HS-Nif: high salt with nifedipine.

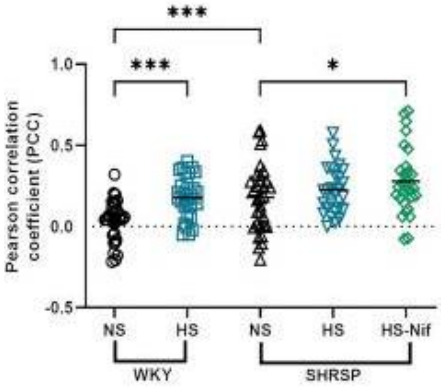

Figure 3.22. SHRSP have higher UMOD in the ER compared to WKY rats.
Pearson's correlation coefficient was calculated from immunofluorescence images obtained from WKY and SHRSP rat kidney sections stained for UMOD and calnexin, as described in Figure 3.21. The data was calculated for four representative tubules by defining a region of interest (ROI) and taking fluorescence intensity values from eight samples per group. One-way ANOVA was used to determine statistical significance between groups. *P<0.05, **P<0.01 and ***P<0.001. Data is represented as mean ± SEM. Symbols with grey fill symbolise female sex.

Next, to further validate these findings, medullary TAL tubules isolated from WKY and SHRSP were incubated with 154mM NaCl (in addition to the basal NaCl in the media) in an ex-vivo experiment. Subcellular fractionation of these tubules revealed a decrease in UMOD in the membrane fraction and an increase in the cytosolic fraction of salt loaded SHRSP (Figure 3.23). In contrast, WKY tubules showed an increased membrane UMOD levels. As mentioned earlier, UMOD exists in an immature form in the ER before undergoing multiple modifications and glycosylation. In our Western blot images, we observed a second, lower molecular weight band consistent with the immature (precursor) UMOD (<80kDa) in salt incubated TAL of both strains (Figure 3.23). The UMOD precursor band existed in the tubule lysate after salt stress which would suggest that salt has some part to play in regulating UMOD maturation and trafficking in the TAL.

Calnexin was highly expressed in the medullary TAL tubules of SHRSP relative to the WKY tubules from the colocalization results. Given that UMOD is a GPI-anchored and N-glycosylated protein it must go through the calnexin-calreticulin cycle for proper folding in the ER as would other proteins of this nature (Ma et al., 2012). We hypothesised that changes in the expression of calnexin and calreticulin would be indicative of any changes in the maturation (i.e.) folding of UMOD. There was a strain difference in calnexin, with a higher expression of calnexin in SHRSP relative to WKY (Figure 3.25). Expression of calnexin also increased significantly with salt loading in SHRSP ($p = 0.04$). Protein levels of calreticulin levels in WKY and SHRSP, however, remained unchanged with or without salt loading (Figure 3.26).

Increased ER accumulation of UMOD in salt loaded SHRSP, led us to investigate whether UMOD is misfolded. An ER matured properly folded glycosylated UMOD reaches the membrane in polymerization incompetent form, where it is cleaved by hepsin (by cleaving the polymerization inhibitory motif) to form the polymers. To check this, we deglycosylated urinary UMOD from salt-loaded animals, and observed that both strains showed increased levels of polymerization-incompetent UMOD (Figure 3.27).

Altogether, it would imply that salt is affecting UMOD maturation and trafficking through yet to be explored signalling pathways in the TAL.

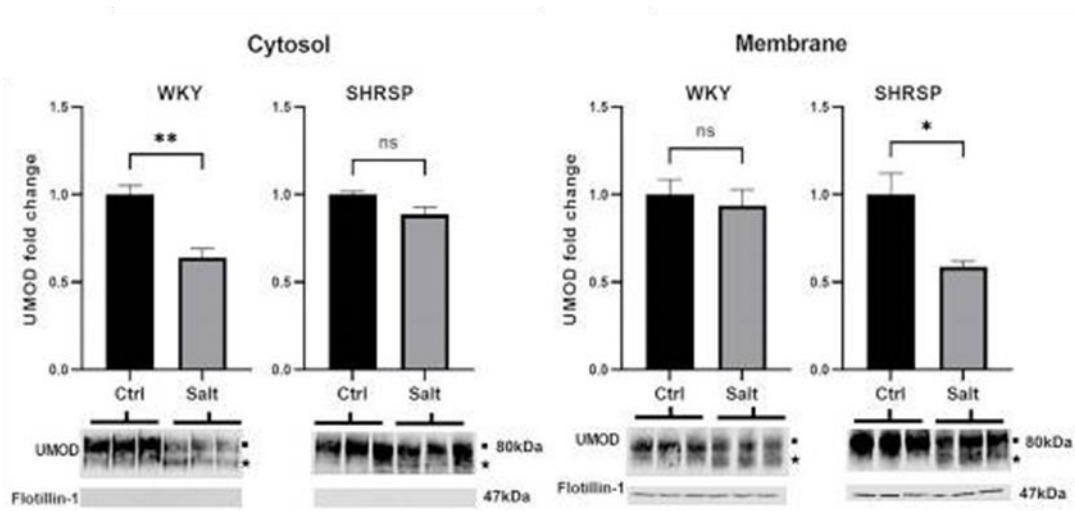

Figure 3.23. Salt loading altered membrane and cytosolic levels of UMOD in WKY and SHRSP medullary TAL tubules.
Medullary TAL tubules were isolated from WKY and SHRSP rats and incubated with an additional 154mM of NaCL in the basal media (Salt) or basal media only (Ctrl) for 6h at 37°C. The cell lysate was then fractionated into membrane and cytosolic fractions. Western blotting was performed for UMOD, and representative images are shown. WKY; $n = 4$ and SHRSP; $n = 4$. Flotillin was used as a plasma membrane marker and UMOD signals were normalised to total protein intensity using Revert 700 staining. ns: non-significant, *P<0.05 and **P<0.01 (Student's t test). Data is expressed as mean ± SEM.

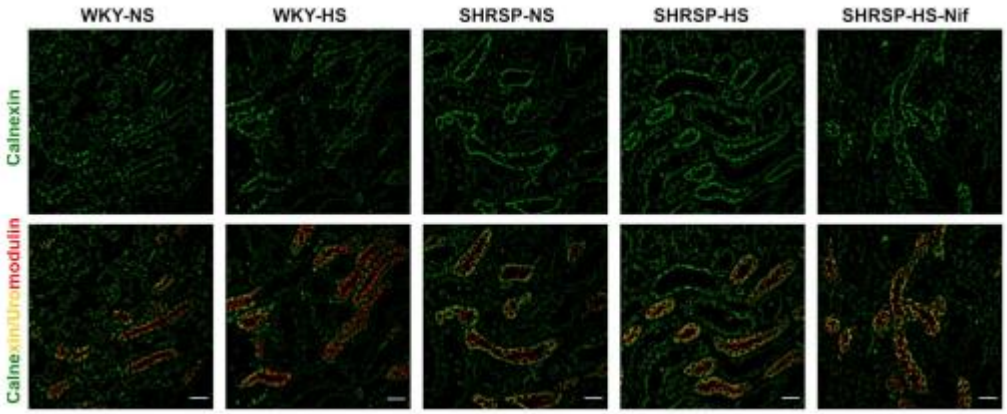

Figure 3.24. Calnexin expression is increased in medullary TAL tubules expressing UMOD after salt loading. Immunofluorescence images of medullary TAL tubules in kidney sections (2µm) extracted from WKY and SHRSP rats. There is staining of ER calnexin (green) and UMOD (red). The following groups are present: NS: normal salt, HS: high salt (1% salt) and HS-Nif: high salt with nifedipine. In total, 4 rats per group were analysed with n = 8 tubules per kidney section. The scale bar represents 50µm. Yellow indicates areas of calnexin and UMOD overlap.

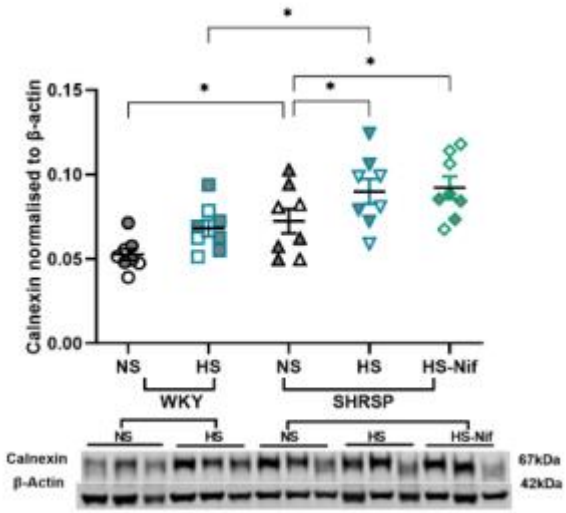

Figure 3.25. Calnexin protein expression is increased in kidneys of salt loaded WKY and SHRSP. Total kidney lysates were extracted from WKY and SHRSP rats. Western blotting was performed for calnexin and protein signal normalised to β-actin. Representative images of the Western blots are shown. The following groups are present on the scatter plots: NS: normal salt, HS: high salt (1% salt) and HS-Nif: high salt with nifedipine. n = 8 per group. Brown-Forsythe Welch ANOVA was used to determine statistical significance between groups. *P<0.05. Data is represented as mean ± SEM. Symbols with grey fill symbolise female sex.

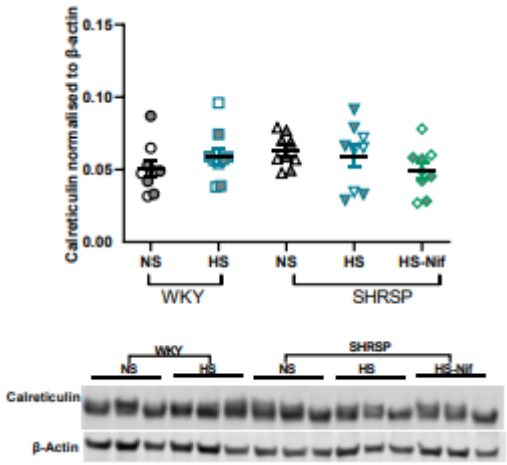

Figure 3.26. Calreticulin protein expression remains unchanged with salt loading in WKY and SHRSP. Total kidney lysates were extracted from WKY and SHRSP rats. Western blotting was performed for calreticulin and protein signal normalised to β-actin. Representative images of the Western blots are shown. The following groups are present on the scatter plots: NS: normal salt, HS: high salt (1% salt) and HS-Nif: high salt with nifedipine. *n* = 8 per group. Brown-Forsythe Welch ANOVA was used to determine statistical significance between groups. *P<0.05. Data is represented as mean ± SEM. Symbols with grey fill symbolise female sex.

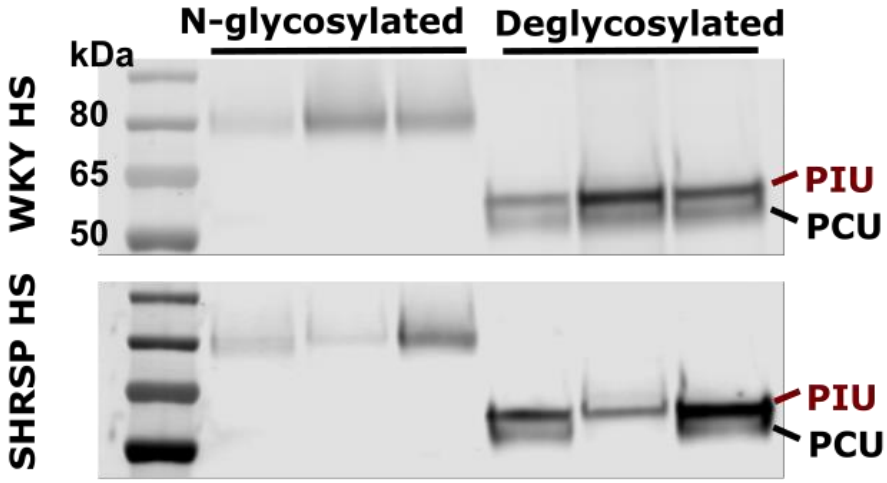

Figure 3.27. Salt loading increases the polymerisation incompetent form of UMOD in both WKY and SHRSP. Representative Western blots of N-glycosylated and deglycosylated urinary UMOD of salt-loaded WKY and SHRSP (*n* = 3; each pool of three rats) are shown. Labels: PIU: polymerization incompetent UMOD, PCU: polymerization competent UMOD, NS: normal salt, HS: high salt (1% NaCl) and HS-Nif: high salt with nifedipine.

3.4 Discussion

The findings presented in this chapter demonstrate the role of salt as a regulator of UMOD excretion and expression in both a normotensive WKY and chronic hypertensive SHRSP background. We have previously published work on renal salt homeostasis and dietary salt intake (Rossitto et al., 2021). With this work, we specifically focus on the role of UMOD and the medullary TAL region. We show salt loading lowers the urinary UMOD excretion rate (that is to say, over 24 hours) and leads to ER retention (i.e., a change in UMOD trafficking) in the chronic hypertensive model. Furthermore, we highlight the reduced

ability to handle salt and increased renal injury in chronic hypertensive models upon salt stress compared to normotensive models.

In the present study, we establish that salt loading lowers UMOD excretion despite any concomitant blood pressure changes. Previous studies have demonstrated an association of high salt intake with increased activity of NKCC2 on the TAL, which leads to greater reabsorption of sodium (Trudu et al., 2013b). Moreover, UMOD plays an important role in enhancing the activity of NKCC2 (Mutig et al., 2011a). It may therefore be postulated that under conditions of high salt, lowering UMOD excretion serves a protective role in that it reduces sodium reabsorption. This is further corroborated by studies in global UMOD knockout mice (*UMOD*$^{-/-}$), which show higher urinary sodium excretion (Graham et al., 2014). The close interaction between UMOD and salt becomes more evident by the fact that blood pressure does not directly impact it. This is highlighted by the fact that nifedipine treatment mitigated a high blood pressure after salt loading in SHRSP yet failed to reverse the lowering of UMOD excretion. This matches results seen in the WKY, whereby UMOD excretion is lowered after salt loading without any change in blood pressure.

There has been a limited number of studies focusing on the salt-UMOD interaction in rat models. Previously it has been reported in kidneys of male Sprague-Dawley (SD) rats, that when administered with 8% dietary salt, there was increased UMOD mRNA and protein levels (Ying and Sanders, 1998). Urinary UMOD excretion levels were never published, however. In the context of our results, UMOD mRNA and protein levels were not impacted by 1% salt loading in either normotensive or chronic hypertensive rat models. It should be mentioned that the study with SD rats utilised protein obtained from membrane fractions of isolated medulla (Ying and Sanders, 1998), whereas here we used total kidney lysates which encompass all intracellular UMOD proteins (both plasma membrane and cytosolic).

A potential hint towards the mechanisms underlying the effect of salt on UMOD lies in that trafficking of UMOD. It is well understood that high dietary salt intake increases vascular oxidative stress and worsens renal damage via increased inflammation in the kidney (Di Castro et al., 2013, Sironi et al., 2001, Gigante et al., 2003). The renal response to salt stress varies in WKY and SHRSP, which is reflected by differences in UMOD maturation, folding, and trafficking. Aberrant UMOD trafficking is a hallmark of disease, such as in the case of uromodulin-associated kidney diseases (UAKD) whereby mutant UMOD is retained in the ER (Rampoldi et al., 2011, Bernascone et al., 2006). If

unchecked, the increased UMOD ER retention leads to ER stress which is a key proponent in *UMOD*-related autosomal dominant tubulointerstitial kidney disease (ADTK-*UMOD*) (Schaeffer et al., 2017). A possible hypothesis would thus be that salt-induced UMOD accumulation in the ER, in combination with ER stress, could lead to renal tubular cell death and ultimately kidney dysfunction as well as progressive renal failure. This would tie in with the development of hypertension, as ER stress is a known contributor to this disease (Young, 2017, Hasty and Harrison, 2012). Salt supplementation has been reported to be key to renal ER stress processes in multiple animal studies (Xu et al., 2014, Yum et al., 2017, Griffin et al., 2001, Hye Khan et al., 2013a). In SHRSP specifically, prior studies have demonstrated the important of ER stress, oxidative stress, and inflammation in the development of vascular dysfunction (Kerr et al., 1999, Collett et al., 2015, Camargo et al., 2018). Furthermore, proteinuria and NGAL upregulation following increases in blood pressure and salt supplementation have been associated with induction of ER stress in kidneys (Yum et al., 2017, Ying and Sanders, 1998). Together, they begin to provide a molecular mechanism wherein salt induced UMOD accumulation in the ER could contribute to hypertension progression and warrants further investigation.

It should be stated that the studies described in this chapter contain a number of limitations that require addressing. While the acute impact of salt loading (with 1 % NaCl) is a significant reduction in UMOD excretion rate, it remained unclear what the long-term effects of salt loading would be on UMOD and the kidney function. This will be explored in the following chapter. This would also more closely follow human patterns of salt intake and provide relevant translational results. Long-term UMOD accumulation in the ER with continuous salt loading may have detrimental effects on renal physiology, even in a normotensive setting. In the current model discussed here, we have not elaborated on how systemic or renal ER stress can culminate in high blood pressure and the degree to which this may occur (i.e., primary or secondary outcome). This requires more research.

To conclude, it was demonstrated that salt loading decreases UMOD excretion and increases its ER retention in a chronic hypertensive rat model. This reveals a novel role of salt as a modulator of UMOD trafficking. This finding is of clinical importance, given that hypertensive patients with high-risk *UMOD* alleles will be overexpressing UMOD and therefore are more predisposed to ER stress induced by accumulation of UMOD if exposed to environmental stressors such as increased dietary salt. An early intervention for these patients could be of great benefit to their health. This would involve a urine screen for UMOD in these patients, followed by prescription of drugs that target ER secretion and

therefore, in theory, alleviation of the potential UMOD accumulation-induced kidney damage. This would occur alongside normal anti-hypertensive treatment regimes.

Chapter 4: Effects of Intermittent Salt Loading on UMOD Trafficking

4.1 Introduction

The relationship between salt and UMOD has been explored in only a handful of models, mostly in mice and at high salt concentrations (Ying and Sanders, 1998, Olinger et al., 2019, Graham et al., 2014). Although these studies are useful in teasing out the effects of UMOD on renal salt handling, the salt concentrations do not match physiological concentrations found in humans and would hinder studying the reverse; the effects of salt on UMOD. Moreover, if transgenic animals are used, the influence of salt on UMOD would be impacted by confounding factors such as hypertension. Our own study (Mary et al., 2021) and the findings of our previous chapter demonstrate that salt loading at a physiological concentration of 1% salt reduces UMOD urinary excretion rate in normotensive WKY rats after 3 weeks of salt loading. The normotensive WKY rats are an ideal model for studying the effects of salt on UMOD, as there are no background genetic factors or pre-disposition to kidney damage that would modulate results (Mary et al., 2021). To this extent, it lends itself as a model for studying whether salt has a direct and reversible effect on UMOD secretion from the TAL. This would provide further molecular understanding of the interactions between sodium and salt, as well as how these processes may become aberrant in pathophysiological settings such as in chronic hypertension.

From our earlier study (Chapter 3), we identified that salt lowers urinary UMOD excretion rate independent of blood pressure changes. We next wanted to analyse in closer detail the acute effects of salt on UMOD excretion by performing intermittent salt loading on normotensive WKY rats to remove hypertension as a confounding factor. To investigate this, we performed an intermittent salt loading study whereby WKY rats were given 1% salt in an on-off-on pattern over 3 weeks (1 week of salt loading, 1 week of normal water, 1 week of salt loading). This chapter hypothesizes that salt has a reversible effect on UMOD secretion and that this would be reflected in its altered trafficking in the TAL cell. A point of terminology should be reiterated here, whereby “secretion” refers to secretion of UMOD from cells, whereas “excretion” refers to rate of secretion of UMOD in the urine.

4.2 Materials and Methods

General Materials and Methods can be found in Chapter 2.

4.2.1 Animals and intermittent salt loading

This chapter utilized male WKY rats (n=10) at 11 weeks of age (hereafter referred to as ‘baseline’). At 12 weeks of age, littermates were randomized into groups of normal drinking water and salt-loaded (*n*=4 control, and *n*=6 for salt), whereby the salt-loaded group received 1% salt intermittently in a 1 week on, 1 week off, and 1 week on pattern (hereafter referred to as the intermittent salt study). Urine (24 hour) and blood samples, as well as SBP readings, were collected every week, as detailed in the General Material and Methods Section. Tissue kidney samples were collected at the end point of the study.

4.3 Results

4.3.1 Blood pressure and overall physiology of salt-loaded animals is unaffected

In order to explore the effects of intermittent salt loading on the physiology and systemic health of the WKY rats, we characterised a number of parameters associated with hypertension and renal health. Systolic blood pressure was not significantly increased or altered on any salt loading week (Figure 4.1). This would be expected with salt insensitive normotensive WKY.

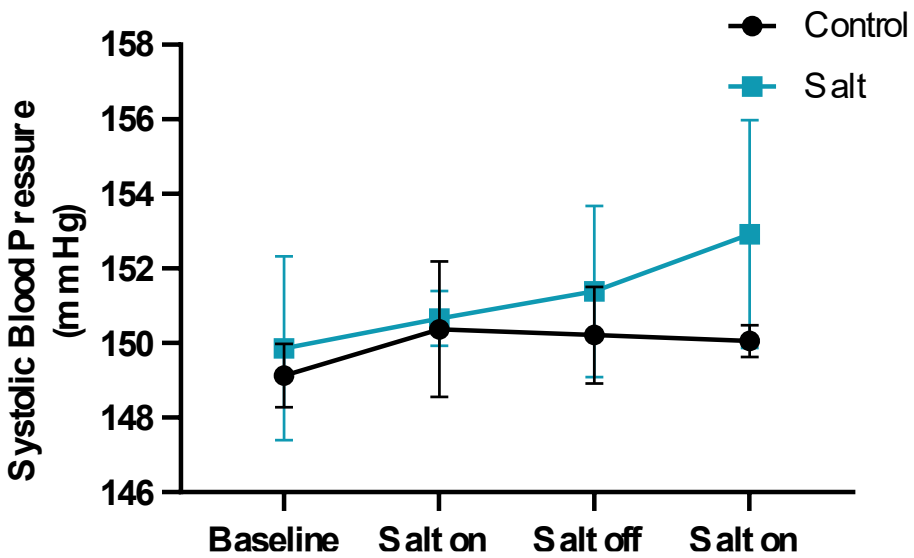

Figure 4.1. Systolic blood pressure was not significantly altered with intermittent salt loading.
Systolic Blood Pressure (SBP) was assessed by tail -cuff measurements. The graph shows the difference in SBP in WKY from baseline measurements in control (*n*=4) and intermittent salt-loaded groups (*n*=6). Data is represented as mean ± S.E.M.

To assess any gross morphological changes upon intermittent salt loading in the WKY rats, body weight was measured every week. We observed a gradual increase in body weight with time, as would be expected with age Figure 4.2. However, there was no significant difference between control and salt-loaded groups at any time point.

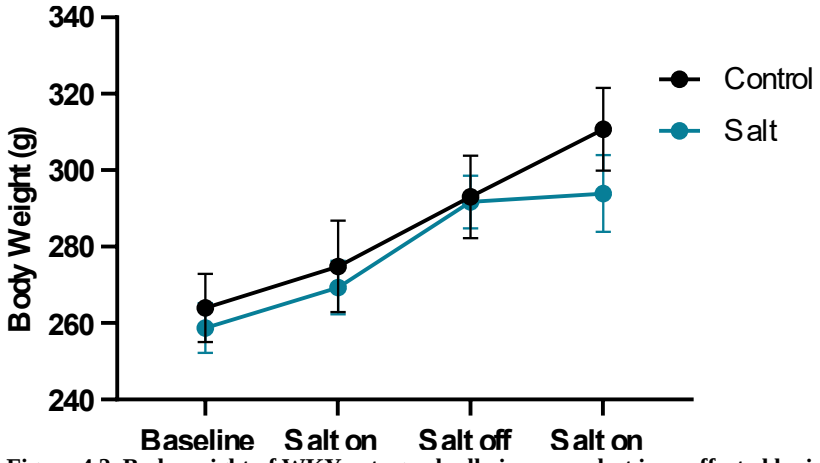

Figure 4.2. Body weight of WKY rats gradually increases but is unaffected by intermittent salt loading. Data are shown for each group over the 3 weeks of intermittent salt loading. Body weight measured each week during salt loading and normal drinking water weeks (control n=4, salt n=6). Data are expressed as mean ± S.E.M.

Since kidneys are a major site of sodium handling and reabsorption, and UMOD is synthesised by TAL cells, we measured kidney weight of the rats at the end of the intermittent salt loading study. There was a trend towards increased kidney weight in the salt loaded WKY rat group (Figure 4.3). Notably, there was some batch variability within each group.

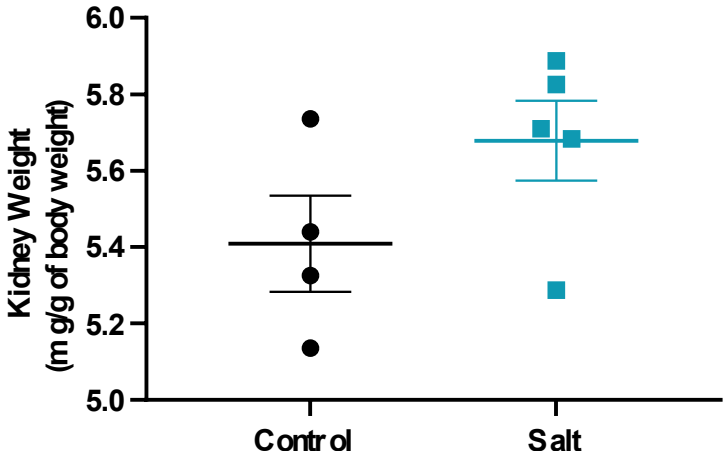

Figure 4.3. Kidney weight is unchanged with intermittent salt loading in WKY rats. The weight of both kidneys was measured at the end of the intermittent salt-study period. The total kidney weight was normalised to body weight. The mean kidney weight is shown for each group ± S.E.M.

In order to examine hydration status of the WKY rats, we analysed the proportion of red blood cells in each animal via haematocrit during each week of the study (via tail-vein puncture), as well as at the end (cardiac puncture). This is indicated by the packed cell volume (PCV). As these rats do not have any specific form of anaemia, changes in PCV directly represent changes in extracellular volume. There was no significant difference in the proportion of red blood cells between control and salt-loaded groups at any one time point (Figure 4.4A and B).

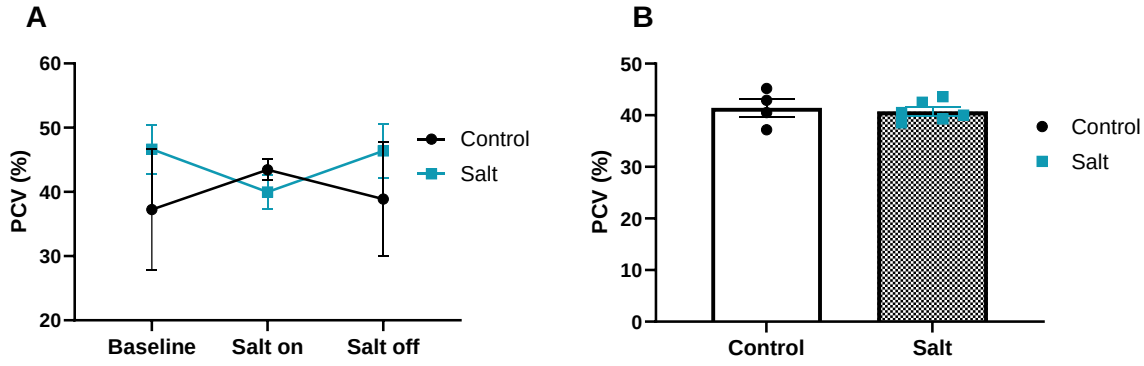

Figure 4.4. The percentage of red blood cells is unaffected after intermittent salt loading period.
Data from (A) tail-vein blood collection during the intermittent study and (B) cardiac puncture at the end of the study. Collected 10% of plasma from each animal prior to cull. Packed Cell Volume (PCV) to show percentage of red blood cells. Data shown as mean ± S.E.M (control *n*=4, salt *n*=6).

Taken together, these characterisation findings suggest that intermittent salt loading with 1% salt do not lead to major morphological or physiological changes.

4.3.2 Intermittent salt loading does not significantly alter electrolyte homeostasis or renal parameters

To better understand the effects of intermittent salt loading on renal excretion and physiology in the WKY rats, we analysed a series of parameters relevant to sodium (Na^+) and water homeostasis. After 1 week of salt loading, a significant increase in urinary output was observed in the WKY rats receiving 1% salt compared to the baseline (Figure 4.5). Upon return to normal water, the urinary output decreased to baseline levels, before increasing again with salt loading in the final week. This behaviour closely matched the water intake values, which increased significantly after salt loading compared to the baseline, decreased in the wash-out week, and increased again upon continuation of salt loading (Figure 4.6).

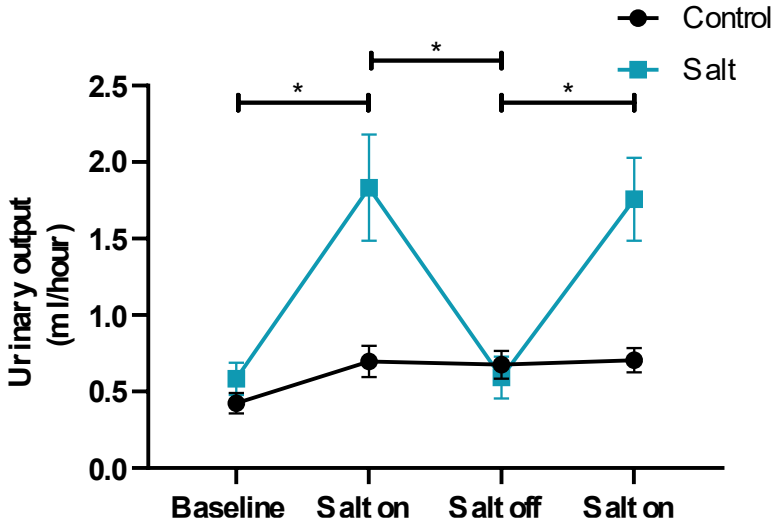

Figure 4.5. Urinary output increases during salt loading week in WKY.
Urinary output of WKYs as measured by metabolic cages at every week of intermittent salt loading period. Urinary output increased significantly during salt loading period ("Salt on") and decreased in the wash out period with normal water ("Salt off"). Data expressed as mean ± S.E.M (control *n*=4, salt *n*=6). *p<0.05 (Mixed-effects analysis with Šídák's multiple comparisons test).

e

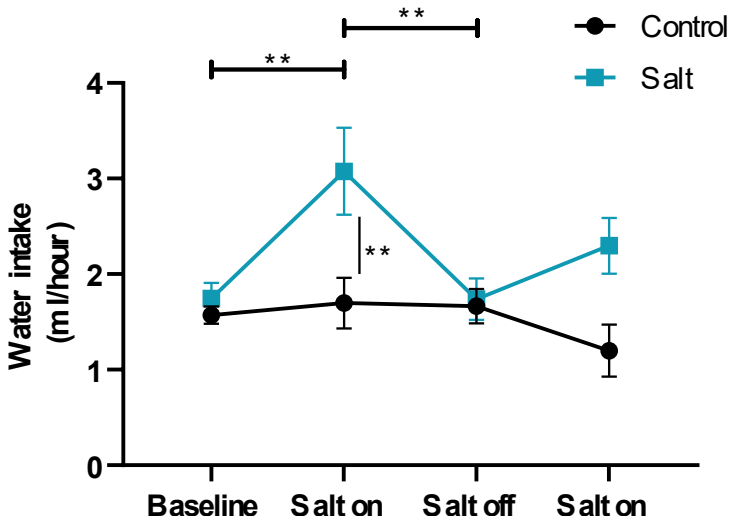

Figure 4.6. Water intake increases during salt loading week in WKY.
Water intake of WKYs as measured by metabolic cages at every week of intermittent salt loading period. Water intake increased significantly during salt loading period ("Salt on") and decreased in the wash out period with normal water ("Salt off"). Data expressed as mean ± S.E.M (control n=4, salt n=6). **p<0.01 (Mixed-effects analysis with Šídák's multiple comparisons test).

Given the importance of kidneys in electrolyte handling and the role of UMOD in sodium reabsorption (Zacchia and Capasso, 2015), we analysed plasma and urinary electrolyte levels. With regards to salt, plasma sodium was significantly higher in the salt-loaded group after the final week of salt loading compared to the control group (2.0 ± 1.2 vs. 0.2 ± 0.6 mmol/L, p<0.05) (Table 4.1). Equally, plasma chloride was also increased in the salt-loaded group (2.0 ± 1.8 and 0.2 ± 0.7 mmol/L, p<0.05). The amount of sodium secreted into the urine was also increased after the first week of salt loading compared to controls

(11.1 ± 1.6 vs 1.0 ± 0.1, p<0.01) as well as to the baseline (11.1 ± 1.6 vs 1.0 ± 0.1, p<0.01). This difference equalised during the wash out period, and again was higher after a week of salt loading when compared to controls (10.2 ± 1.3 vs 0.9 ± 0.1, p<0.01) and baseline (10.2 ± 1.3 vs 1.0 ± 0.1, p<0.01). The fractional excretion of sodium was also higher as measured in the final week (the difference between plasma and urine excretion) compared to controls (2.0 ± 0.2 vs 0.2 ± 0.0, p<0.05). Chloride urinary excretion followed a similar pattern, increasing in the first week of salt loading compared to controls (14.55 ± 1.5 vs 2.0 ± 0.1, p<0.01) and baseline (14.55 ± 1.5 vs 1.8 ± 0.1, p<0.01). And again, in the second week of salt loading relative to controls (13.7 ± 1.3 vs 1.8 ± 0.2, p<0.01) and baseline (13.7 ± 1.3 vs 1.8 ± 0.2, p<0.01). Fractional chloride excretion was also higher in the salt-loaded groups compared to controls (3.8 ± 0.2 vs 0.86± 0.0, p<0.05).

Intermittent Salt Study								
	Baseline		Salt on		Salt off		Salt on	
Parameters	Control	Salt	Control	Salt	Control	Salt	Control	Salt
n	4	6	4	6	4	6	4	6
Body weight (BW, g)	264.0 ± 8.9	258.7 ± 6.5	274.8 ± 11.9	269.3 ± 7.0	293.0 ± 10.8**	291.7 ± 6.9***	310.7 ± 10.8***	293.9 ± 10.1
Water intake (mL/h)	1.6 ± 0.1	1.7 ± 0.2	1.7 ± 0.3	3.1 ± 0.5	1.7 ± 0.2	1.7 ± 0.2	1.2 ± 0.0	2.3 ± 0.4
Urine output (mL/h)	0.4 ± 0.1	0.6 ± 0.1	0.7 ± 0.1	1.8 ± 0.3*	0.7 ± 0.1	0.6 ± 0.1	0.7 ± 0.1	1.8 ± 0.3*
p-urea (mmol/L)	4.2 ± 0.3	4.2 ± 0.2	3.9 ± 0.1	3.1 ± 0.2*,#	4.4 ± 0.3	4.4 ± 0.1	4.2 ± 0.4	3.1 ± 0.4*
p-creatinine (mmol/L)	24.3 ± 2.6	24.5 ± 1.7	22.5 ± 1.2	22.2 ± 0.8	24.3 ± 1.8	26.2 ± 1.3	22.0 ± 0.7	20.3 ± 0.5
p-calcium (mmol/L)	2.4 ± 0.0	2.4 ± 0.0	2.4 ± 0.0	2.4 ± 0.0	2.4 ± 0.0	2.4 ± 0.0	2.4 ± 0.0	2.1 ± 0.1
p-magnesium (mmol/L)	0.8 ± 0.0	0.8 ± 0.0	0.8 ± 0.0	0.8 ± 0.0	0.8 ± 0.0	0.8 ± 0.0	0.7 ± 0.0	0.6 ± 0.0
p-phosphate (mmol/L)	1.8 ± 0.2	1.8 ± 0.0	1.7 ± 0.1	2.3 ± 0.1##	1.6 ± 0.0	1.7 ± 0.1	1.5 ± 0.0	1.6 ± 0.1
p-albumin (mg/L)	12.3 ± 0.5	11.9 ± 0.1	12.5 ± 0.1	12.2 ± 0.1	12.7 ± 0.4	12.1 ± 0.2	9.7 ± 0.8	8.9 ± 0.4**
p-potassium (mmmol/L)	7.6 ± 0.4	7.0 ± 0.4	7.1 ± 0.3	6.9 ± 0.4	7.2 ± 0.6	6.7 ± 0.4	5.8 ± 0.5	5.1 ± 0.2*
p-sodium (mmol/L)&							0.2 ± 0.6	2.0 ± 1.2#
p-chloride (mmmol/L)&							0.2 ± 0.7	2.0 ± 1.8#
u-urea (mmol/day)	3.9 ± 0.5	4.1 ± 0.4	4.4 ± 0.4	4.5 ± 0.2	4.9 ± 0.4	3.2 ± 0.8	5.1 ± 0.3	4.9 ± 0.3
u-creatinine (mmol/day)	51.9 ± 7.3	59.5 ± 2.5	66.5 ± 3.1	67.5 ± 11.2	66.5 ± 16.9	47.9 ± 4.6	67.5 ± 0.1	75.3 ± 0.1
u-albumin (mmol/day)	54.7 ± 4.9	67.4 ± 14.2	61.9 ± 5.6	45.4 ± 9.4	61.9 ± 5.2	43.5 ± 14.8	45.4 ± 15.4	59.1 ± 16.2
u-sodium (mmol/day)	1.0 ± 0.1	1.0 ± 0.1	1.0 ± 0.1	11.1 ± 1.6**,##	1.0 ± 0.0	0.9 ± 0.2	0.9 ± 0.1	10.2 ± 1.3**,##
u-potassium (mmol/day)	1.7 ± 0.3	1.8 ± 0.2	1.9 ± 0.2	2.0 ± 0.1	1.9 ± 0.0	1.4 ± 0.3	2.0 ± 0.1	2.3 ± 1.3
u-calcium (mmol/day)	0.1 ± 0.0	0.1 ± 0.0	0.2 ± 0.0	0.2 ± 0.0*	0.2 ± 0.0	0.2 ± 0.0	0.2 ± 0.1	0.2 ± 0.0
u-magnesium (mmol/day)	0.2 ± 0.0	0.2 ± 0.0	0.3 ± 0.0	0.3 ± 0.0	0.3 ± 0.0	0.2 ± 0.1	0.3 ± 0.0	0.4 ± 0.0
u-phosphate (mmol/day)	0.0 ± 0.0	0.0 ± 0.0	0.0 ± 0.0	0.0 ± 0.0	0.0 ± 0.0	0.0 ± 0.0	0.0 ± 0.0	0.0 ± 0.0
u-chloride (mmol/day)	1.8 ± 0.3	1.8 ± 0.1	2.0 ± 0.1	14.55 ± 1.5**,##	2.0 ± 0.1	1.5 ± 0.4	1.8 ± 0.2	13.7 ± 1.3**,##
u-ACR (mmol/day)	1.2 ± 0.1	1.4 ± 0.2	1.0 ± 0.2	1.0 ± 0.2	1.0 ± 0.1	1.0 ± 0.2	1.0 ± 0.1	0.8 ± 0.2
FE_calcium	2.2 ± 0.3	2.1 ± 0.4	2.7 ± 0.6	2.9 ± 0.5	2.7 ± 0.4	3.5 ± 0.2	2.9 ± 0.5	2.7 ± 0.3
FE_magnesium	0.1 ± 0.0	0.1 ± 0.0	0.1 ± 0.0	0.1 ± 0.0	0.1 ± 0.0	0.1 ± 0.0	0.1 ± 0.0	0.2 ± 0.0
FE_phosphate	0.1 ± 0.0	0.1 ± 0.0	0.1 ± 0.0	0.0 ± 0.1	0.1 ± 0.0	0.0 ± 0.0	0.0 ± 0.0	0.1 ± 0.1
FE_urea	44.3 ± 5.7	45.9 ± 3.1	40.2 ± 3.8	44.8 ± 1.4	40.2 ± 2.8	41.8 ± 3.1	44.8 ± 10.4	46.6 ± 6.3
FE_water	0.5 ± 0.1	0.7 ± 0.1	0.6 ± 0.1	0.6 ± 0.3	0.6 ± 0.0	0.6 ± 0.1	0.6 ± 0.1	1.0 ± 0.1
FE_potassium	10.5 ± 1.8	12.8 ± 2.1	10.4 ± 0.8	11.9 ± 1.2	10.4 ± 1.6	11.6 ± 1.0	11.9 ± 1.2	12.4 ± 0.4
FE_sodium&							0.2 ± 0.0	2.0 ± 0.2#
FE_chloride&							0.6 ± 0.0	3.8 ± 0.2#
Packed Cell Volume (PCV) %							41.45 ± 1.7	40.73 ± 0.80

Table 4.1. Plasma and urine electrolyte levels before and after intermittent salt loading.
Data collected from metabolic cage study. p: plasma, u: urine, ACR: albumin-creatinine ratio, FE: fractional excretion. Data represented as mean ± S.E.M. Performed 2-way ANOVA or Welch's t-test as appropriate. *p<0.05, **p<0.01, ***p<0.001, ****p<0.001 compared to baseline for control or salt groups. #p<0.05, ##p<0.01, ###p<0.001, ####p<0.001 control group compared to salt group. Due to unavailability of plasma at baseline (10% of body weight collected at end of study, could not obtain at baseline due to ethical issues), only end-point plasma was collected (marked by "&"). Packed Cell Volume (PCV) to show percentage of red blood cells from each group derived from cardiac puncture at the end of the study. Data shown as mean ± S.E.M (control *n*=4, salt *n*=6).

Other electrolytes and proteins also showed significant variations after intermittent salt loading. Plasma phosphate levels were significantly higher than controls in the first week of salt loading relative to controls (2.3 ± 0.1 vs 1.7 ± 0.1, $p<0.01$). Interestingly, it did not rise again after the wash-out period and the second salt loading week. Plasma albumin decreased in the salt-loaded group after the final week of salt loading compared to baseline (8.9 ± 0.4 vs 11.9 ± 0.1, $p<0.01$). Plasma urea levels were also decreased in the first week of salt loading compared to controls (3.1 ± 0.2 vs 3.9 ± 0.1, $p<0.05$) and baseline values (3.1 ± 0.2 vs 4.2 ± 0.2, $p<0.05$), as well as the second week of salt loading relative to controls (3.1 ± 0.4 vs 4.2 ± 0.4, $p<0.05$). In summary, urinary excretion of sodium and chloride showed the most amount of variation; both increasing after salt loading and decreasing during the wash out period.

4.3.2.1 KIM-1 and NGAL kidney injury markers expression is not significantly altered with intermittent salt loading

Next, we assessed for the expression of kidney injury markers (KIM-1; proximal tubule) and neutrophil gelatinase-associated lipocalin (NGAL; TAL and distal tubule) in the intermittent salt-loaded WKY rats. KIM-1 expression was significantly decreased by approximately 50% compared to controls in the total kidney (1.02 fold-change ± 0.11 vs 0.56 fold-change ± 0.06, $p<0.05$) (Figure 4.7). The fold-change expression of NGAL (Figure 4.8) showed no biologically significant differences relative to controls. In combination with the lack of change in kidney weight (Figure 4.3), it would suggest that intermittent salt loading is not detrimental to kidney health in normotensive animals.

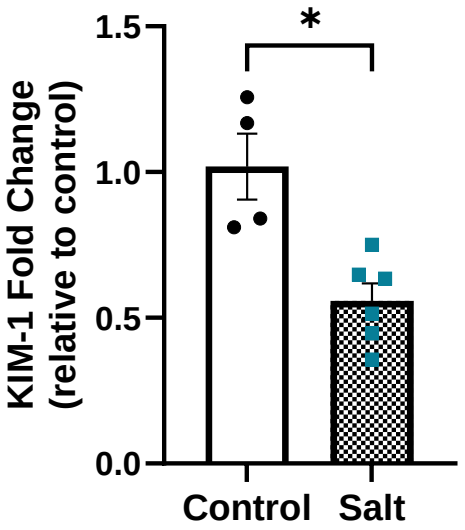

Figure 4.7. Intermittent salt loading does not significantly influence KIM-1 expression.
Gene expression was measured in total kidneys of WKYs after intermittent salt loading. Gene expression is represented as fold change to mean of control ± S.E.M of kidney injury marker-1 (KIM-1) (*n*=4 control, *n*=6 for salt). This is a marker of proximal tubule injury. mRNA levels were normalised to Ubiquitin C (*Ubc*) expression. *p<0.05 (Welch's t-test).

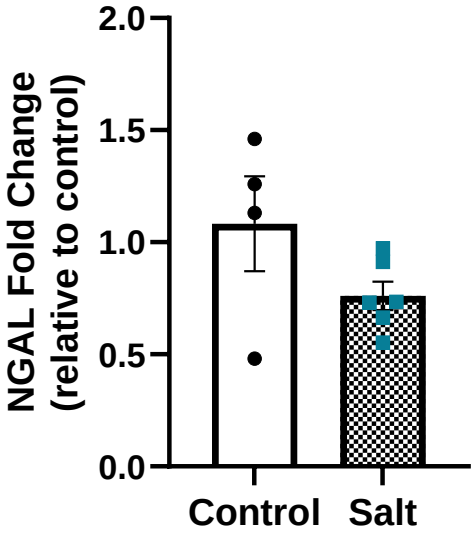

Figure 4.8. Intermittent salt loading does not significantly influence NGAL expression.
Gene expression was measured in total kidneys of WKYs after intermittent salt loading. Gene expression is represented as fold change to mean of control ± S.E.M of neutrophil gelatinase-associated lipocalin (NGAL) (n=4 control, n=6 for salt). This is a marker of distal tubule injury. mRNA levels were normalised to Ubiquitin C (Ubc) expression.

4.3.3 Intermittent salt loading lowers urinary UMOD excretion rate

Given that salt loading significantly lowered urinary UMOD excretion after 3 weeks of salt loading in WKY (see Chapter 3), we next investigated the impact on UMOD excretion after intermittent salt loading (i.e., a week-by-week basis) to better understand whether salt has a direct and reversible effect on UMOD. The urinary UMOD excretion rate is significantly lower than control rats at all time points following salt loading (Figure 4.9). Even after the wash out week ("Salt off"), the UMOD excretion rate did not return to

control levels and remained significantly lower than the respective controls. This would suggest that the effect of salt loading on UMOD excretion rate is acute.

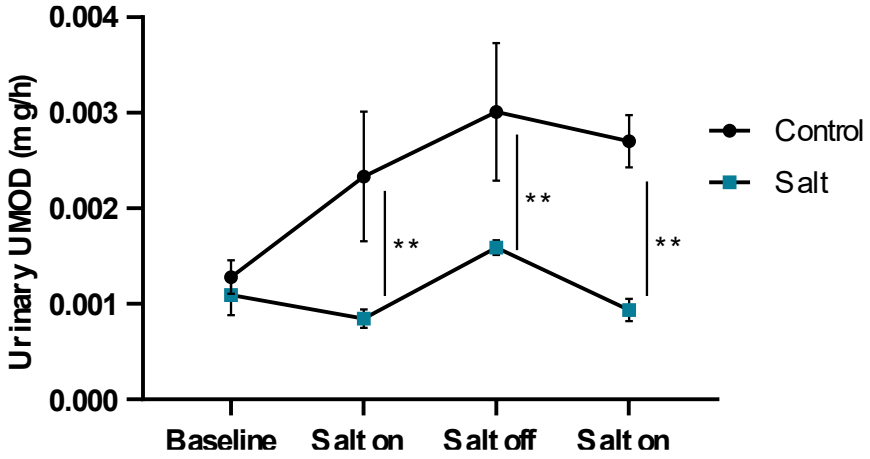

Figure 4.9. Intermittent salt loading-acutely decreases urinary UMOD excretion rate.
Urine samples were collected over 24 hours over 4 time points in the study using metabolic cages. Urinary UMOD concentration was quantified by ELISA. Urinary UMOD was normalised to 24-hour output and represented as excretion rate (mg/h). Graph represents urinary UMOD excretion rate for the intermittent salt study (*n*=4 control, *n*=6 salt). Data is shown as mean ± S.E.M. **p<0.01 (Mixed-effects analysis), comparison between control and salt groups at each time point.

4.3.4 Trafficking of UMOD is not altered with intermittent salt loading

The acute effect of salt loading on UMOD excretion led us to investigate whether this is a reflection of its trafficking within the kidneys. To do this, we aimed to characterise potential changes in UMOD at a transcriptional and translational level. After intermittent salt loading, there was no significant change in UMOD mRNA expression relative to control in the total kidney (Figure 4.10). Similarly, total kidney UMOD protein expression as measured by Western blotting did not show any significant differences between salt-loaded and control groups (Figure 4.11). This would suggest that the salt-induced lowering effect on UMOD excretion is occurring at a trafficking level, which would align with the findings from the previous chapter (Chapter 3).

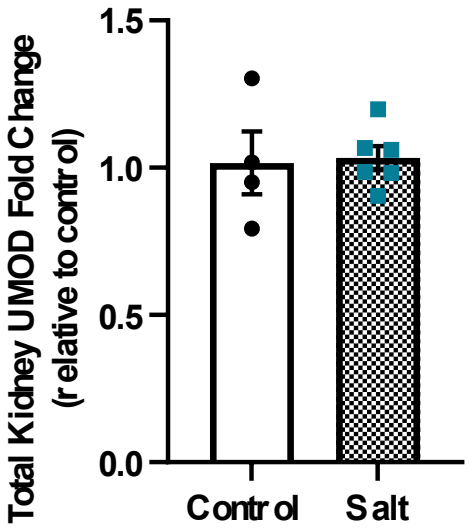

Figure 4.10. Total Kidney UMOD mRNA levels did not change with intermittent salt loading.
Total kidney (cortex and medulla) was used for analysis of UMOD mRNA levels. UMOD mRNA levels were expressed as a scatter plot of fold change relative to the mean of the control (± S.E.M). (*n*=4 control, *n*=6 salt). mRNA levels were normalised to Ubiquitin C (Ubc) expression.

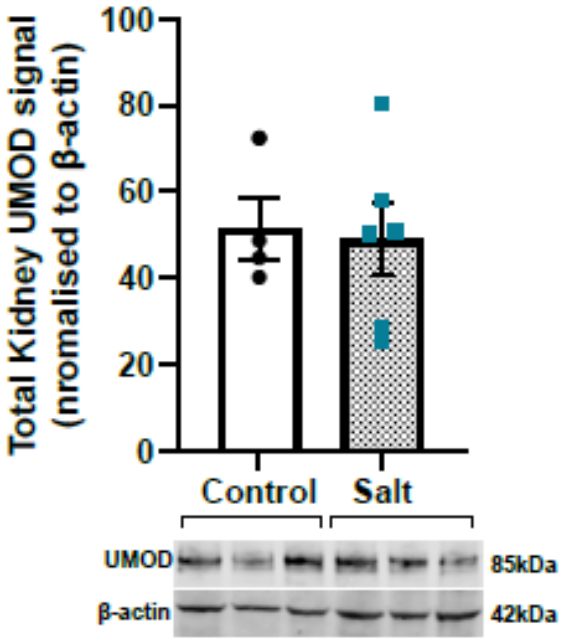

Figure 4.11. Total kidney UMOD protein levels were not altered with intermittent salt loading.
Total kidney (cortex and medulla) lysate was utilised for measuring UMOD protein levels. Total kidney UMOD protein levels and representative Western blot of each group of the intermittent study (*n*=4 control, *n*=6 salt). β-actin was utilised as a loading control. Data expressed as mean ± S.E.M.

The TAL are the primary site of UMOD excretion in the medulla of the kidneys (Devuyst et al., 2017) and thus the region of interest for salt and UMOD interactions. We therefore investigated the levels of UMOD protein in the TAL by isolating the medullary region from the kidneys of the intermittent salt-loaded and control WKY rats. Analysis of UMOD protein expression demonstrated no statistically significant difference between salt-loaded and control groups (Figure 4.12).

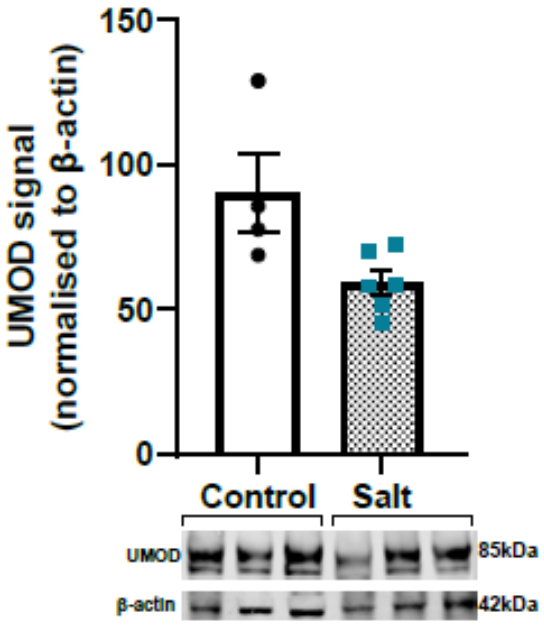

Figure 4.12. The medullary UMOD levels were not significantly different compared to controls after intermittent salt loading.
The medulla region was isolated from total kidneys of WKY rats from the intermittent salt study. UMOD protein levels and representative Western blot of each group of the intermittent study (n=4 control, n=6 salt) are shown. β-actin was utilised as a loading control. Data expressed as mean ± S.E.M. The second lower molecular weight band in the Western blots for UMOD is non-specific.

In order to further interrogate potential changes in localisation of UMOD in the TAL after intermittent salt loading, we performed subcellular fractionation on the medullary region of these rats. There was no change in the membrane fraction (Figure 4.13) and a trend towards decreased UMOD levels in the cytosolic fraction (Figure 4.14). Flotillin-1 was used as a marker of the plasma membrane and only was detectable in the membrane fraction (Figure 4.13), indicating that isolation of individual fractions was successful.

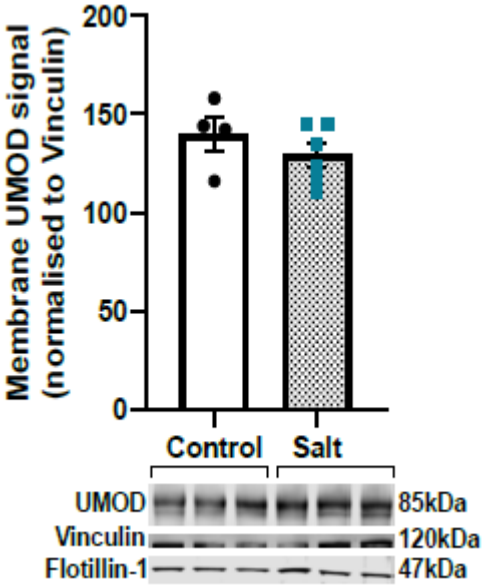

Figure 4.13. Membrane UMOD protein levels in the medullary region were not changed with intermittent salt loading.
The medulla region was isolated from total kidneys of WKY rats from the intermittent salt study. These regions were subfractionated into plasma membrane compartments of the cells. Isolation of membrane fraction was confirmed with membrane marker Flotillin-1. UMOD protein levels and representative Western blots are shown from control (*n*=4) and salt-loaded groups (*n*=6). Data expressed as mean ± S.E.M. The second lower molecular weight band in the Western blots for UMOD is non-specific.

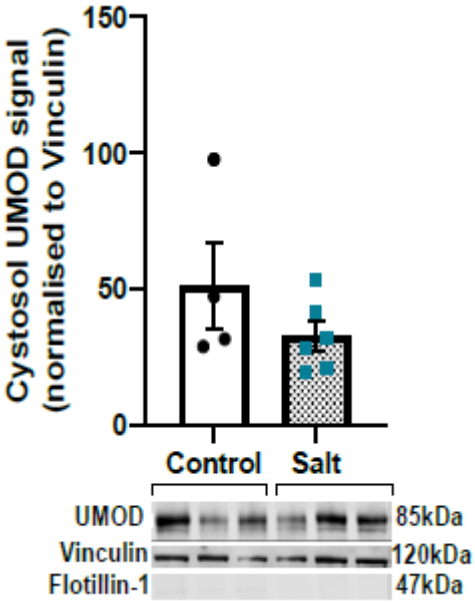

Figure 4.14. There was a trend towards decreased cytosolic UMOD levels in intermittent salt loaded WKY rats.
The medulla region was isolated from total kidneys of WKY rats from the intermittent salt study. These regions were subfractionated into cytosolic compartments of the cells. To confirm isolation of the pure cytosolic fraction, we used the plasma membrane marker Flotillin-1. Lack of bands present for Flottilin-1 on Western blots demonstrates purity of isolated cytosolic fraction. UMOD protein levels and representative Western blots are shown from control (*n*=4) and salt-loaded groups (*n*=6). Data expressed as mean ± S.E.M. The second lower molecular weight band in the Western blots for UMOD is non-specific.

4.4 Discussion

In this chapter, we found that salt influences UMOD excretion acutely and it may potentially be reversible. This is accompanied by disturbances in urine and plasma

electrolytes balances, especially with sodium and chloride levels. We demonstrated that intermittent salt loading, over a shorter time period, does not lead to intracellular UMOD accumulation in a normotensive background. These findings will be explored in greater detail in the following chapter in the context of long-term salt loading.

Here we establish that UMOD excretion rate is acutely lowered with salt loading, highlighting the importance of UMOD in maintaining kidney homeostasis. It is well understood that UMOD plays a key role in salt reabsorption along the TAL (Zacchia and Capasso, 2015). Key to sodium reabsorption in the nephron is NKCC2, which facilitates 20-25% of reuptake of the total filtered NaCl load (Castrop and Schiessl, 2014), and its activity is regulated by UMOD (Mutig et al., 2011a). In this regard, a quick response to salt loading, and by extension UMOD excretion, is critical for maintenance of kidney physiology. Failure to regulate UMOD urinary excretion could lead to hyperosmolarity and a limited ability to concentrate urine (Pruijm et al., 2016a, Segar, 1966). This is a hallmark of kidney damage, which is prevalent in the chronic hypertensive SHRSP model after 3 weeks of salt loading (Chapter 3). There appears to be some reduction in KIM-1 expression in the WKY rats, which may be a protective effect of the kidney to prevent early kidney damage. Studying the kinetics of continued intermittent salt loading on KIM-1 expression would provide further insights into physiology of kidney salt-handling. There remain challenges, however, in interpreting the effect of intermittent salt loading on UMOD excretion due to instability in the control group. A potential contributor to this variation could be the fact that urinary UMOD excretion naturally increases with age (Ollier-Hartmann et al., 2008, Duława et al., 1998). Also, the large standard error may be explained by the relatively low sample number (n = 4) in the control group compared to the salt-loaded group (n =6). It is reasonable to presume that increasing sample number would help limit this variability. Nonetheless, the WKY model used here is suitable for exploring salt-induced effects on UMOD outside of any blood pressure effect and will be key to unravelling the molecular mechanisms underlying this process in future investigations.

The acute changes in urinary UMOD excretion combined with the wide effect on urinary and plasma electrolyte levels following short-term salt loading demonstrates the importance of UMOD in renal electrolyte handling. Outside its regulation of NKCC2, UMOD has also been associated with the activity of renal outer medullary potassium (ROMK) channel (Renigunta et al., 2011), which is expressed along the TAL and the distal convoluted tubule (DCT). It plays a key role in potassium secretion, to maintain a potential difference to allow transepithelial current flow and paracellular Na^+ and Ca^{2+} reabsorption

(Welling and Ho, 2009). Together, it would explain the differences in urinary and plasma sodium and chloride seen in the salt loaded WKY rats. Interestingly, salt loading altered plasma urea and albumin levels, especially in the final week after the wash out period. This may be an early stress marker, as *Umod* knockout mice also exhibit increased plasma urea levels, alongside impaired urinary concentration, reduced fractional excretion of uric acid and neuropathological alterations similar to the Uromodulin-associated kidney disease (UAKD) phenotype seen in humans (Kemter et al., 2013). We postulate that the response of TAL to reduce UMOD secretion is a protective effect, which is staggered to enable kidney electrolyte homeostasis to return to equilibrium. This would explain why the urinary UMOD excretion rate was still significantly lower compared to controls, even after a week of receiving normal water. It would be reasonable to assume that UMOD excretion rates would return to normal after longer periods of time without salt loading (e.g., after 1 month), however this would require further validation.

The intermittent salt loaded WKY rats demonstrated a trend towards greater UMOD protein levels at the membrane, similar to the WKY rats under 3 weeks of salt loading in Chapter 3. Direct imaging of salt effects on the lipid bilayer showed that sodium penetrates deeply into the headgroup region and binds to the lipids (Ferber et al., 2011). Lipid molecules were shown to re-order non-isotropically under the influence of sodium (Ferber et al., 2011). The altered molecular structure of the lipid bilayer in salt-loaded rats at the plasma membrane of the TAL caused by sodium interactions in the urine may be a natural mechanism by which UMOD is retained and secretion reduced. Further experiments with UMOD at a sub-molecular resolution, together with its interaction with sodium, would be needed to prove this. Nonetheless, our findings indicate that UMOD trafficking has more sites of regulation than previously known and that this ties in with the normal functioning of the kidneys.

The strength of this study lies in the fact that it provides proof of the acute influence of salt on UMOD secretion from the TAL, without the background of chronic hypertension, as described in the previous chapter. It describes a model that may be used to unravel the precise molecular mechanisms of the influence of salt on renal physiology. That being said, there are a few limitations to the conclusions of this chapter. We are presuming that the effect of salt is reversible on UMOD secretion, however further experimentation with longer wash out periods are required to prove this. Also, it would be interesting to expand the investigation to cover long-term intermittent salt loading and what effects this has on kidney function. This would more closely match human diets, which usually vary in salt-

load over time (Meneton et al., 2005). This would also increase translatability of our findings.

To conclude, this chapter demonstrate the intermittent effects of salt loading on the secretion of UMOD in the TAL. The short response time for changing of UMOD secretion by the kidney, highlights the importance of UMOD in regulating normal renal function. This increases the need for the discovery of regulatory mechanisms behind salt induced UMOD trafficking alterations, as these will be significantly aberrant in diseases such as hypertension.

Chapter 5: Long-term Effects of Salt Loading on UMOD trafficking

5.1 Introduction

Dietary sodium has been linked to cardiovascular disease risk and hypertension, with certain cohorts being particularly salt-sensitive (He and MacGregor, 2010, MacGregor, 1985, Freis, 1992, Whelton et al., 1998, He et al., 1999, Sacks et al., 2001b, O'Donnell et al., 2014b). However, high salt is a risk factor for many other pathologies, including kidney diseases such as CKD (Borrelli et al., 2020). Moreover, it is known that salt has an impact on function of immune cells with negative effects in onset and progression of diseases like obesity, cancer, metabolic syndrome, and autoimmune diseases (Willebrand and Kleinewietfeld, 2018). It is reasonable to postulate that higher salt-intake would therefore contribute to kidney injury, although the mechanisms behind this relationship are complex. There is growing evidence that UMOD is strongly associated with sodium homeostasis and hypertension (Trudu et al., 2013b, Graham et al., 2014). Therefore, UMOD is an optimal candidate to help elucidate, at least in part, the molecular link between salt, kidney injury and hypertension.

A key process to the maturation of UMOD along its secretory pathway is its correct folding in the ER. ER stress is the process by which the inward flux of nascent polypeptides into the ER can overwhelm the protein-folding machinery, leading to an imbalance and the accumulation of misfolded protein, which is toxic for the cell. There are several factors that contribute to ER stress, including deficiencies in post-translational modifications, aberrations in calcium levels and redox homeostasis, aberrant ER-associated degradation (ERAD), lipid biolayer stress, and hypoxia (Adams et al., 2019). ER accumulation of UMOD is intrinsic to certain disease pathologies. The protein coding mutations driving autosomal dominant tubulointerstitial kidney disease cause misfolding in UMOD and subsequently it accumulates in the ER, causing increased intracellular accumulation, ER-stress, and reduced UMOD excretion (Rampoldi et al., 2003). High salt intake has been associated with renal damage and oxidative stress, whereby inflammation is accelerated in the kidneys (Di Castro et al., 2013, Sironi et al., 2001, Gigante et al., 2003). Moreover, ER stress has been highlighted as a significant contributor to the pathogenesis of hypertension (Hasty and Harrison, 2012, Young, 2017). High dose salt supplementation has been demonstrated to induce kidney ER stress (Xu et al., 2014, Yum et al., 2017, Griffin et al., 2001, Hye Khan et al., 2013b). Further, the association of

proteinuria and NGAL with increased SBP and salt intake, together with ER stress in the kidney highlights the important role of salt balance by the kidneys to maintain normal physiology. We hypothesised that salt would influence processes related to ER release, including kidney damage, and ultimately secretion of UMOD from the TAL cell (Yum et al., 2017, El Karoui et al., 2016).

In the Chapter 3 it was demonstrated that salt loading with 1% salt for 3 weeks significantly lowers urinary UMOD excretion in normotensive WKY rats and to a greater extent in chronic hypertensive SHRSP. This physiologically relevant concentration of salt did not lead to kidney injury and blood pressure differences in the WKY rats, and for this reason, this concentration of salt was chosen for the current study. A difference in UMOD trafficking with salt loading accompanied by its intracellular retention in the TAL in SHRSP rats was noted in Chapter 3. This suggested a pathophysiological mechanism involving UMOD, whereby salt loading is exacerbating the impacts of hypertension. In this chapter, it was hypothesized that long-term salt loading would significantly alter renal physiology and UMOD trafficking to an extent that may match the phenotype seen in the chronic hypertensive SHRSP model. Thus, the main aim of this study was to investigate effects of long-term salt exposure on WKY rats.

5.2 Materials and Methods

General Materials and Methods can be found in Chapter 2.

5.2.1 Animals and long-term salt loading

This chapter utilized male WKY rats (n=12) at 11 weeks of age (hereafter referred to as ‘baseline’). At 12 weeks of age, littermates were randomized into groups of normal drinking water and salt-loaded (*n*=6 control, and *n*=6 for salt), whereby the salt-loaded group received 1% Salt (Sigma, Dorset, UK) continuously over a period of 3 months (referred to as long-term salt study). Kidney tissue, 24-hour urine, blood samples, as well as systolic blood pressure readings, were collected as detailed in the General Material and Methods Section. Blood and urine were collected at four time points (at baseline, 1-month, 2-month, and 3-month times points).

5.2.2 UMOD GFP MDCK Cells

Madin-Darby Canine Kidney (MDCK) cells stably expressing human uromodulin fused with green fluorescent protein (GFP) were gifted by Prof. Luca Rampoldi (Schaeffer et al., 2017). These are referred hereafter as UMOD-GFP MDCK cells. Cells were cultured in

Dulbecco's Modified Eagle's Medium (DMEM) (ThermoFisher Scientific, Paisley, UK) supplemented with 10% foetal bovine serum (FBS, ThermoFisher Scientific, Paisley, UK) and 1% Penicillin/Streptomycin (ThermoFisher Scientific, Paisley, UK) at 37°C and 5% CO_2. After confluency, the cells were incubated in DMEM supplemented with 60mM salt or 120mM mannitol (as osmotic control) and incubated for 18h at 37°C, 5% CO_2. Media and cells were collected for UMOD quantification.

5.2.3 Immunofluorescence analysis of UMOD-GFP MDCK cells

Cells were fixed in neutral buffered formalin at room temperature for 1 hour after washes in PBS. Cells were then permeabilised with PBS containing 0.1% Triton X-100 for 10 minutes, before being blocked with 1X Carbo-Free Blocking Solution (Vector Laboratories, Oxfordshire, UK) supplemented with 0.1% Tween-20 for 1h at room temperature. These were then directly mounted with Mounting Medium with DAPI – Aqueous, Fluoroshield (Abcam, Cambridge, UK). For antibodies used, image acquisition, and post-imaging analysis, refer to the General Materials and Methods chapter.

5.3 Results

5.3.1 Long-term salt loading results in only minor blood pressure and systemic physiological changes in the WKY rats

To gain an understanding of systemic changes that may occur during long-term salt loading, we assessed blood pressure, body weight, and renal health of the WKY rats. There was no significant change in systolic blood pressure when compared to group baseline values in either the control or salt-loaded groups after the 3 months (Figure 5.1). This further highlights that these rats are not sensitive to salt-induced blood pressure changes, as seen for the previous chapter.

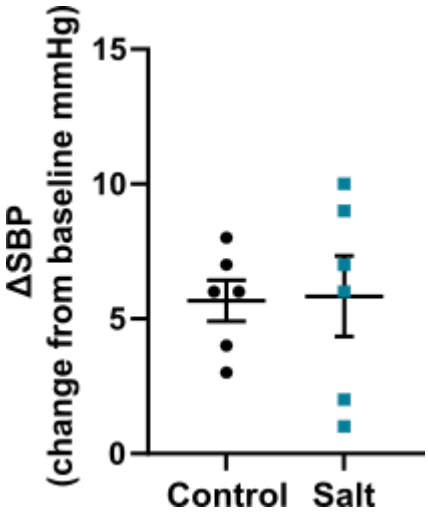

Figure 5.1. Systolic Blood Pressure was not significantly different after 3 months of salt loading compared to controls.
Systolic Blood Pressure (SBP) was assessed by tail -cuff measurements. The difference in SBP is shown for each respective group from baseline measurements to the end of the study (at the 3 months timepoint) in control (n=6) and 3-month (*n*=6) salt-loaded groups. The comparison is being made between experimental groups at these two time points. Data are represented as mean ± S.E.M.

Body weight was monitored throughout the 3-month salt loading period as a measure of health of the WKY rats. There was no significant difference between control and salt-loaded groups at a given timepoint with regards to body weight (Figure 5.2). Although, body weight did increase with age of the animals, as would be expected.

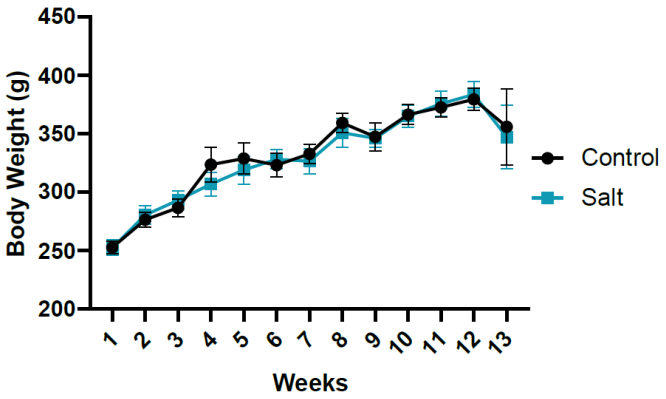

Figure 5.2. Body weight increased with age in WKY rats in both control and salt-loaded groups.
Body weight was measured every week for each group over 3 months of salt loading (starting at week: 11-week-old rats). There are no significant differences between experimental groups at any given timepoint. Each data point represents mean ± S.E.M (*n*=6 per group).

As for the previous chapter, kidney weight was measured at the end of the study due to their importance in electrolyte handling and being the site of UMOD production and secretion. The salt-loaded WKY rats exhibited a trend towards increased kidney weight after 3 months compared to controls, although this was not statistically significant (Figure 5.3).

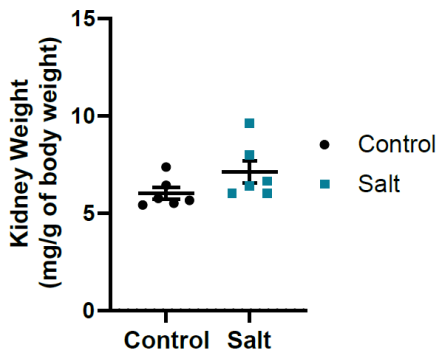

Figure 5.3. Kidney weight remained unchanged in WKY rats after 3 months of salt loading.
Kidney weight of both kidneys from WKY rats at the end of the 3-month salt loading period for both groups (*n*=6). There is no significant difference between experimental groups at this timepoint. Data shown as mean ± S.E.M.

Next, the haematocrit of each of the WKY rats was analysed to understand changes in hydration status, which is to say differences in extracellular volume, during and after long-term salt loading periods. There was no statistically significant difference in PCV between control and salt-loaded groups at any time point throughout (Figure 5.4) and at the end of study Figure 5.5). Although, a crossover occurs at week 9 where PCV appears to be higher in the week 9 salt-loaded WKY rats compared to controls at the same timepoint, and this is maintained until the end of the 3 month study (Figure 5.4). This may suggest a physiological adjustment of extracellular volume as a result of increased plasma sodium content due to the long period of salt exposure in the long-term salt loaded WKY rats.

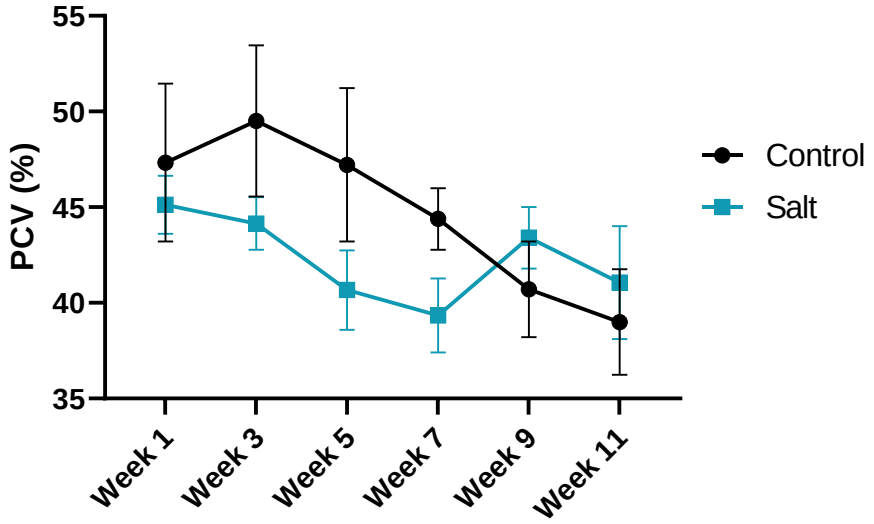

Figure 5.4. The percentage of red blood cells is unchanged during long-term salt loading
Data collected from tail-vein blood collection and after haematocrit. Collected 250µL of plasma from each animal throughout the study, in line with ethical guidelines. Packed Cell Volume (PCV) to show percentage of red blood cells. There are no significant differences in PCV between experimental groups at any given time point. Data shown as mean ± S.E.M (control *n*=6, salt *n*=6).

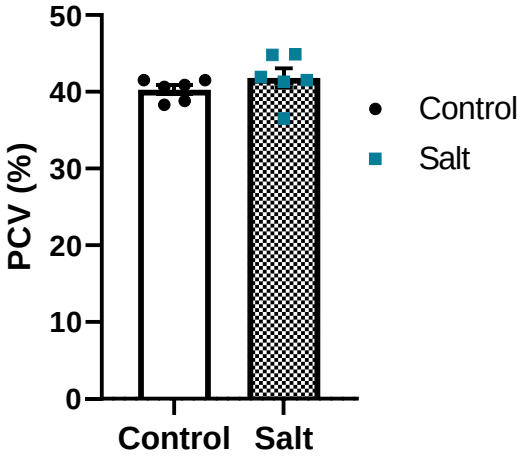

Figure 5.5. There is no statistically significant difference in percentage of red blood cells in WKY after 3 months of salt loading.
Data collected from cardiac puncture and after haematocrit at the end of the long-term salt study. Collected 10% of plasma from each animal prior to cull. Packed Cell Volume (PCV) to show percentage of red blood cells. There are no significant differences in PCV between experimental groups at this timepoint. Data shown as mean ± S.E.M (control *n*=6, salt *n*=6).

As for the previous chapters, these findings further highlight that 1% salt loading is a suitable physiological concentration for the WKY rats without inducing any gross salt stress injuries or blood pressure.

5.3.2 There is a considerable impact on electrolyte balances in long-term salt loaded WKY rats

Given the lack of gross morphological changes with 1% salt loading, the next assessment involved characterising potential differences in renal outputs and sodium handling. Salt loading significantly increased urinary output compared to baseline and relative to control animals at all timepoints (Figure 5.6). It should be noted that “baseline” refers to comparisons within the same groups relative to week 1 timepoint whereas “controls” refers to comparisons between groups at one timepoint. Similarly, water intake was also significantly higher after 3 months of salt loading compared to controls at the same timepoint (Figure 5.7). Water intake was not significantly higher than controls in week 9, although there was a trend towards higher intake in the salt-loaded group (Figure 5.7).

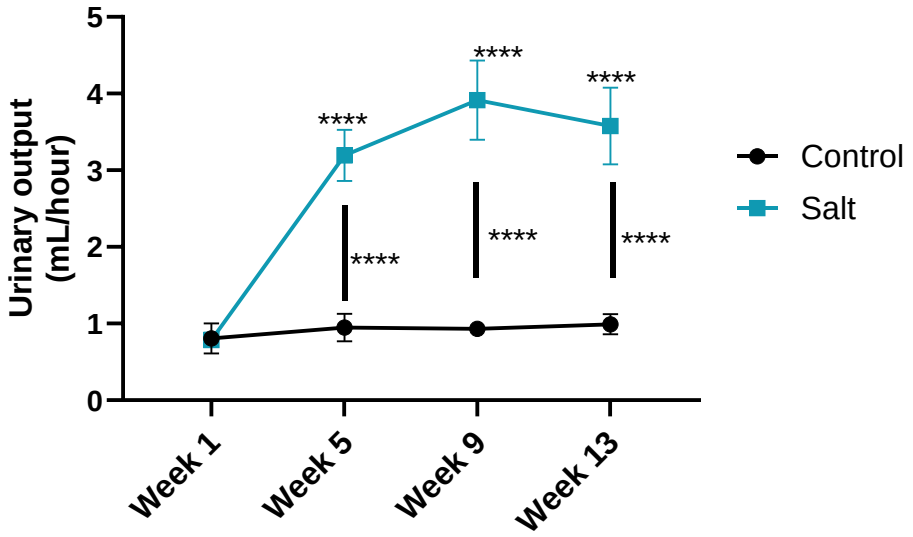

Figure 5.6. Urinary output is significantly increased after 3 months of salt loading both between control groups and compared to week 1.
Urinary output was measured by metabolic cages over 4 time points throughout the long-term salt loading period. Urinary output WKY rats were significantly increased during 3 months of salt loading. Data represent mean ± S.E.M. (control *n*=6, salt *n*=6). ****p<0.0001 (Mixed-effects analysis with Šídák's multiple comparisons test). Comparisons shown are between salt and control groups (asterisks next to vertical line), as well as intra-salt group comparisons (asterisks above data point) to baseline values (at week 1).

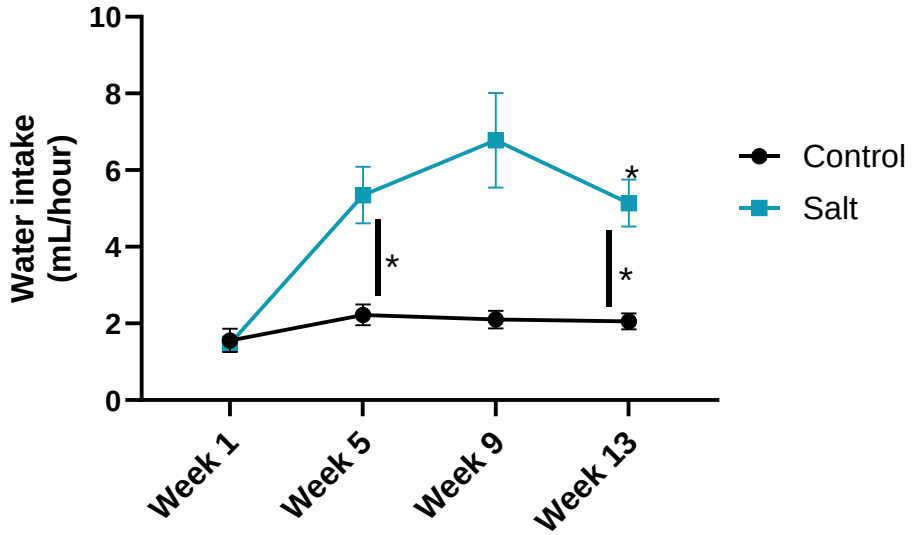

Figure 5.7. Water intake increased significantly in WKY after 3 months of salt loading.
Water intake was measured by metabolic cages over 4 time points throughout the long-term salt loading period. Water intake for WKY rats was significantly increased after 3 months of salt loading. Data represent mean ± S.E.M. (control *n*=6, salt *n*=6). *p<0.05 (Mixed-effects analysis with Šídák's multiple comparisons test). Comparisons shown are between salt and control groups (asterisks next to vertical line), as well as intra salt group comparisons (asterisks above data point) to baseline values (at week 1).

In order to explore the effects of long-term salt loading on renal excretion and physiology in the WKY rats, we characterised parameters relevant to Na^+ and water homeostasis. The salt-loaded rats were provided with 1% salt which equivalates to 1.22g of NaCl per day or

0.48g of sodium per day (based on an average water intake of 122mL/day). The rats receiving long-term salt loading secreted 0.463g of NaCl per day. My group have previously demonstrated that sodium accumulates in the skin and other organs (Rossitto et al., 2021). Also, roughly 10% of sodium is excreted via the faeces (Armanini et al., 2019). These sodium losses have not been accounted for here as the focus is on urinary UMOD. To compare this to humans, several blood pressure guidelines recommend low sodium intake (<2.3g of sodium intake, or 5.8g/day of NaCl) (O'Donnell et al., 2020). Biochemical analysis revealed a significant increase in urinary sodium excretion in the long-term salt loaded WKY rats compared to controls when looking within experimental groups (change from baseline values, salt: 12.8 ± 2.20 and control: 1.47 ± 0.52 mmol/day, p<0.001) (Figure 5.8 and Table 5.1).

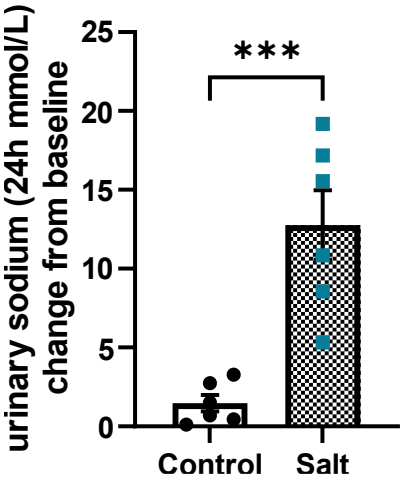

Figure 5.8. Urinary sodium excretion was significantly increased in the salt-loaded group after long-term salt loading.
Urinary sodium was measured in urine samples collected by metabolic cage. This represents the final urine sample taken from control and salt-groups at the end of the study. Data are represented as the delta change from baseline values for control and 3-month salt-loaded groups (*n*=6) (± S.E.M) (i.e. comparison between experimental groups at these two timepoints). ***p<0.001 (Unpaired t-test).

Examination of plasma sodium also revealed an increase in the salt-loaded group relative to controls at the 3-month timepoint (136.3 ± 0.3 vs. 134.3 ± 8.3 mmol/L, p<0.05) (Table 5.1). Similarly, urinary and plasma chloride was significantly higher in salt-loaded groups compared to controls at the 3-month timepoint (urinary: 15.3 ± 3.9 vs. 1.8 ± 0.6 mmol/day, p<0.01; plasma: 10.2.0 ± 0.5 vs. 99.7 ± 5.9 mmol/L, p<0.05). Additionally, other major electrolytes were also analysed to determine any major disturbances in renal electrolyte handling post long-term salt loading. The excretion of potassium into the urine was significantly higher in the long-term salt-loaded group when compared to baseline (i.e. week 1) (3.5 ± 0.6 vs. 1.7 ± 0.2 mmol/day, p<0.05) and to controls (3.5 ± 0.6 vs. 2.0 ± 0.5 mmol/day, p<0.05) (Table 5.1). For plasma potassium, there was a significant difference between salt and control groups at baseline (5.8 ± 0.4 vs. 7.6 ± 0.3 mmol/L, p<0.01), although this significance was lost after 3 months. Urinary magnesium excretion was

upregulated in the long-term salt loaded groups both relative to baseline (0.5 ± 0.1 vs. 0.2 ± 0.0 mmol/day, $p<0.01$) and to control groups at that timepoint (0.5 ± 0.1 vs. 0.3 ± 0.1 mmol/day, $p<0.01$). The levels of magnesium in the plasma were significantly higher in the long-term salt-loaded group compared to controls at the 3-month timepoint (0.8 ± 0.0 vs. 0.7 ± 0.0 mmol/L, $p<0.05$). Also, the control group had lower plasma magnesium after 3 months compared to its corresponding baseline values (0.7 ± 0.0 vs. 0.8 ± 0.0 mmol/L, $p<0.05$). Furthermore, urinary phosphate excretion levels were increased in the salt-loaded group when compared to baseline (0.207 ± 0.057 vs. 0.017 ± 0.014 mmol/day, $p<0.01$) and control groups at the 3-month timepoint (0.207 ± 0.057 vs. 0.0 ± 0.013 mmol/day, $p<0.01$). While plasma levels of phosphate remained unchanged, the fractional excretion of phosphate was significantly higher in the long-term salt-loaded group relative to baseline values (1.93 ± 0.01 vs. 0.24 ± 0.03, $p<0.05$) and controls at the 3-month timepoint (1.93 ± 0.01 vs. 0.01 ±0.01, $p<0.05$). While urinary calcium levels were not significantly affected, plasma calcium levels in the long-term salt loaded group were higher in the salt-loaded group compared to baseline (2.5 ± 0.0 vs. 2.3 ± 0.2 mmol/L, $p<0.05$) and controls at the 3-month timepoint (2.5 ± 0.0 vs. 2.2 ± 0.2 mmol/L, $p<0.01$). Also, fractional excretion of calcium was altered with lower values in the salt-loaded group after 3 months relative to baseline values (1.1 ± 0.3 vs. 3.6 ± 0.9, $p<0.05$). Finally, urinary urea levels were also altered with long-term salt loading, showing increased values compared to baseline (12.0 ± 2.4 vs. 3.8 ± 0.5 mmol/day, $p<0.05$) and controls at the 3-month timepoint (12.0 ± 2.4 vs. 5.1 ± 1.7 mmol/day, $p<0.05$).

Long-term Salt Study				
	Baseline		3 months	
Parameters	Control	Salt	Control	Salt
n	6	6	6	6
Body weight (BW, g)	252.7 ± 5.3	252.5 ± 6.7	383.9 ± 30.5****	374.8 ± 18.6****
Water intake (mL/h)	1.6 ± 0.3	1.5 ± 0.1	2.1 ± 0.2	5.1 ± 0.6****,####
Urine output (mL/h)	0.8 ± 0.2	0.8 ± 0.1	1.0 ± 0.1	3.6 ± 0.5****,####
p-urea (mmol/L)	4.2 ± 0.4	4.3 ± 0.3	4.2 ± 3.7	4.7 ± 2.9
p-creatinine (mmol/L)	24.3 ± 1.4	22.0 ± 2.1	25.7 ± 1.2	25.2 ± 2.2
p-calcium (mmol/L)	2.4 ± 0.0	2.3 ± 0.0	2.2 ± 0.2	2.5 ± 0.0*,##
p-magnesium (mmol/L)	0.8 ± 0.0	0.8 ± 0.0	0.7 ± 0.0*	0.8 ± 0.0#
p-phosphate (mmol/L)	1.8 ± 0.1	1.9 ± 0.1	1.5 ± 0.1	1.7 ± 0.1
p-albumin (mg/L)	12.3 ± 0.3	11.5 ± 0.3	9.7 ± 0.9*	10.6 ± 0.2
p-potassium (mmol/L)	7.6 ± 0.3	5.8 ± 0.4##	5.8 ± 0.4*	5.6 ± 0.2
p-sodium (mmol/L)&			134.3 ± 8.3	136.3 ± 0.3#
p-chloride (mmol/L)&			99.7 ± 5.9	102.0 ± 0.5#
u-urea (mmol/day)	3.9 ± 0.1	3.8 ± 0.5	5.1 ± 1.7	12.0 ± 2.4*,#
u-creatinine (mmol/day)	51.9 ± 9.6	56.7 ± 6.5	50.6 ± 25.8	185.4 ± 38.1**,#
u-albumin (mmol/day)	54.7 ± 23.1	40.7 ± 7.3	45.4 ± 19.7	241.8 ± 98.9
u-sodium (mmol/day)	1.0 ± 1.4	3.9 ± 1.5	0.9 ± 0.6	12.6 ± 3.3##
u-potassium (mmol/day)	1.7 ± 0.1	1.7 ± 0.2	2.0 ± 0.5	3.5 ± 0.6*,#
u-calcium (mmol/day)	0.1 ± 0.0	0.2 ± 0.0	0.1 ± 0.0	0.1 ± 0.0
u-magnesium (mmol/day)	0.2 ± 0.0	0.2 ± 0.0	0.3 ± 0.1	0.5 ± 0.1**,##
u-phosphate (mmol/day)	0.003 ± 0.051	0.017 ± 0.014	0.000 ± 0.013	0.207 ± 0.057**,##
u-chloride (mmol/day)	1.8 ± 1.6	5.8 ± 2.1	1.8 ± 0.6	15.3 ± 3.9,##
u-ACR	1.2 ± 0.2	0.8 ± 0.1	1.0 ± 0.9	1.2 ± 0.3
FE_calcium	2.2 ± 0.9	3.6 ± 0.9	2.9 ± 0.3	1.1 ± 0.3*
FE_magnesium	0.11 ± 0.02	0.15 ± 0.03	0.14 ± 0.01	0.09 ± 0.01
FE_phosphate	0.07 ± 0.02	0.24 ± 0.03	0.01 ± 0.01	1.93 ± 0.01*,#
FE_urea	44.32 ± 0.02	41.80 ± 0.03	44.75 ± 0.01	35.28 ± 0.01
FE_water	0.50 ± 0.11	0.92 ± 0.18	0.58 ± 0.42	1.31 ± 0.23
FE_K	10.1 ± 0.1	14.4 ± 0.2	9.5 ± 0.4	9.1 ± 0.2
FE_Na&			1.7 ± 1.0	1.8 ± 0.6
FE_Cl&			2.6 ± 1.4	2.9 ± 0.9
Packed Cell Volume (PCV) %			40.28 ± 0.56	41.83 ± 1.3

Table 5.1. Plasma and urinary electrolyte levels before and after long-term salt loading.
Data collected from metabolic cage study. p: plasma, u: urine, ACR: albumin-creatinine ratio, FE: fractional excretion. Data represented as mean ± S.E.M. Performed 2-way ANOVA or Welch's t-test as appropriate. *p<0.05, **p<0.01, ***p<0.001, ****p<0.001 refer to comparisons to baseline values for within each experimental group. p<0.05, ##p<0.01, ###p<0.001, ####p<0.001 refer to comparisons made between controls and salt groups at a given timepoint (in this case at 3 months). Due to unavailability of plasma at baseline (10% of body weight collected at end of study, could not obtain at baseline due to ethical issues), only end-point plasma was collected (marked by "&"). Packed Cell Volume (PCV) representing percentage of red blood cells from each group derived from cardiac puncture at the end of the 3-month salt loading period. Data shown as mean ± S.E.M (control *n*=6, salt *n*=6).).

5.3.3 Long-term salt loading does not induce kidney damage in the normotensive WKY rats

To examine whether long-term salt loading has any negative impacts on the kidneys with regards to injury, a gene expression analysis of kidney injury markers KIM-1 (proximal tubule marker) and NGAL (TAL and distal tubule marker) was performed on total kidneys isolated from long-term salt-loaded WKY rats. Both KIM-1 (Figure 5.9) and NGAL mRNA expression (Figure 5.10) was unchanged with long-term salt loading relative to controls at the 3-month timepoint. Notably, there was considerable batch variation within each group.

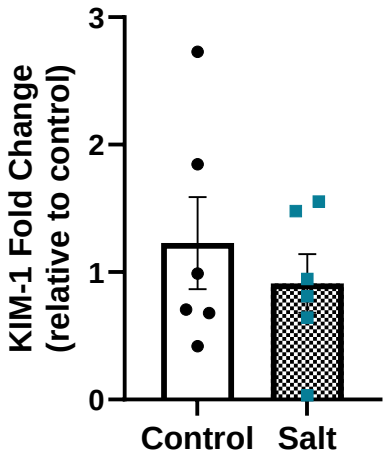

Figure 5.9. Long-term salt loading does not significantly influence kidney KIM-1 expression.
Gene expression represented as fold change to control ± S.E.M of kidney injury marker-1 (KIM-1). Total kidneys were isolated from control and salt-loaded groups at the 3-month timepoint. *n*=6 per group. mRNA levels were normalised to Ubiquitin C (*Ubc*) expression.

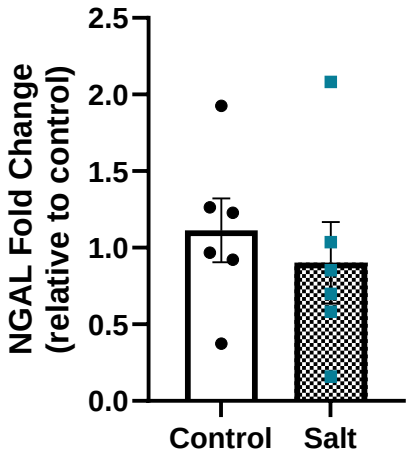

Figure 5.10. Long-term salt loading does not significantly influence kidney NGAL expression.
Gene expression represented as fold change to control ± S.E.M of neutrophil gelatinase-associated lipocalin (NGAL). Total kidneys were isolated from control and salt-loaded groups at the 3-month timepoint. *n*=6 per group. mRNA levels were normalised to Ubiquitin C (*Ubc*) expression.

5.3.4 Long-term salt loading directly and consistently lowers the urinary UMOD excretion rate

It has been established that salt loading lowers urinary UMOD excretion rate on an acute basis in WKY rats (Chapter 3) and to some extent this is reversible (Chapter 4). Here the effects of long-term salt loading (i.e., over 3 months) on the urinary UMOD excretion were characterised by performing UMOD ELISA. Long-term salt loading significantly attenuated urinary UMOD excretion rate over 3 months (Figure 5.11). Urinary UMOD levels were significantly lower in the first month of salt loading compared to baseline (4.06 x 10^{-4} ± 1.45 x 10^{-4} vs. 0.002 ± 0.001 mg/h, p<0.01) and relative to control at the same time point (4.06 x 10^{-4} ± 1.45 x 10^{-4} vs. 0.003 ± 0.0004 mg/h, p<0.01). Likewise, at month 2 of salt loading, urinary UMOD excretion rate was lower compared to baseline (week 1 timepoint) (0.001 ± vs. 1.42 x 10^{-4} vs. 0.002 ± 0.001 mg/h, p<0.01) and the control group at the 3-month timepoint (0.001 ± vs. 1.42 x 10^{-4} vs. 0.002 ± 0.0005 mg/h, p<0.01). The final month also showed significantly attenuated levels of urinary UMOD excretion in the salt-loaded groups, relative to both baseline values at week 1 within each experimental group (0.001 ± 1.88 x 10^{-4} vs. 0.002 ± 0.001 mg/h, p<0.01) and controls at the 3-month time point (0.001 ± 1.88 x 10^{-4} vs. 0.004 ± 0.0005 mg/h, p<0.01). This suggests salt is consistently lowering urinary UMOD excretion rate.

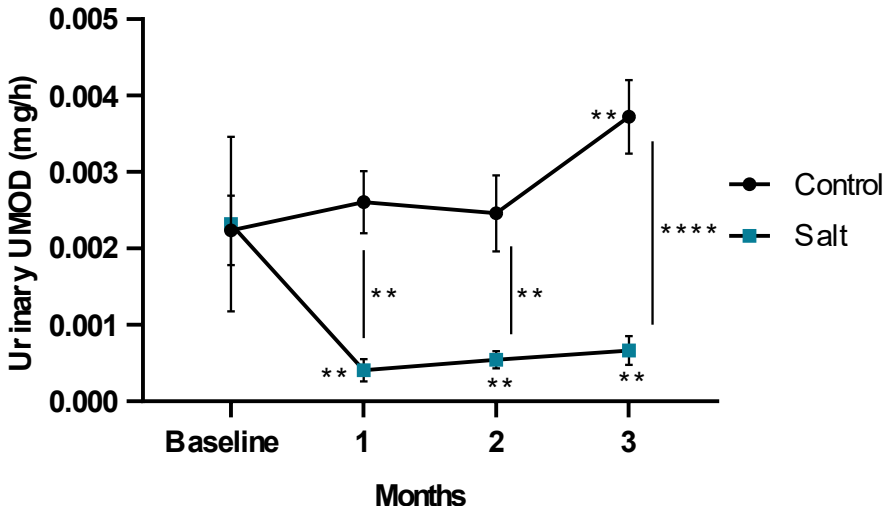

Figure 5.11. Long-term salt loading consistently lowers urinary UMOD excretion rate.
Urine samples were collected over 24 hours over 4 time points in the study using metabolic cages. Urinary UMOD concentration was quantified by ELISA. Urinary UMOD was normalised to 24-hour output for urine and represented as excretion rate (mg/h). Graph represents urinary UMOD excretion rate for the long-term salt study (*n*=6 control, *n*=6 salt). Data are shown as mean ± S.E.M. **p<0.01, ****p<0.0001 (Mixed-effects analysis).

To determine whether this change in urinary UMOD excretion rate is reflected in the serum UMOD levels, we analysed serum UMOD using an ELISA. This demonstrated that there was no significant difference in protein levels of serum UMOD between control and salt loaded WKY groups at the 3-month timepoint (Figure 5.12).

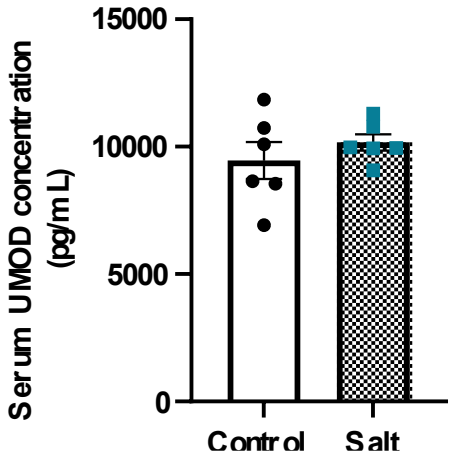

Figure 5.12. Serum UMOD levels were unaltered after 3 months of salt loading compared to controls.
Blood was collected at the end of the study by cardiac puncture. Serum UMOD concentration was quantified by ELISA. Serum UMOD levels after 3 months in WKY rats of the long-term salt study are unchanged (*n*=6 control, *n*=6 salt). Data are shown as mean ± S.E.M.

To confirm whether this effect of salt on reduction in urinary excretion rate is specific to UMOD, the levels of excretion of Epidermal Growth Factor (EGF) protein was assessed, another glycosylated protein known to be excreted by the TAL, with the same molecular weight as UMOD, and secreted into the urine (Salido et al., 1991). EGF levels in the urine did not alter significantly following 3 months of salt loading when compared to controls (Figure 5.13). Likewise, when EGF protein expression was analysed in total kidneys from WKY rats, there was no statistically significant difference between control and salt-loaded groups (Figure 5.14). In summary, these data suggest salt is influencing UMOD directly at the excretion level.

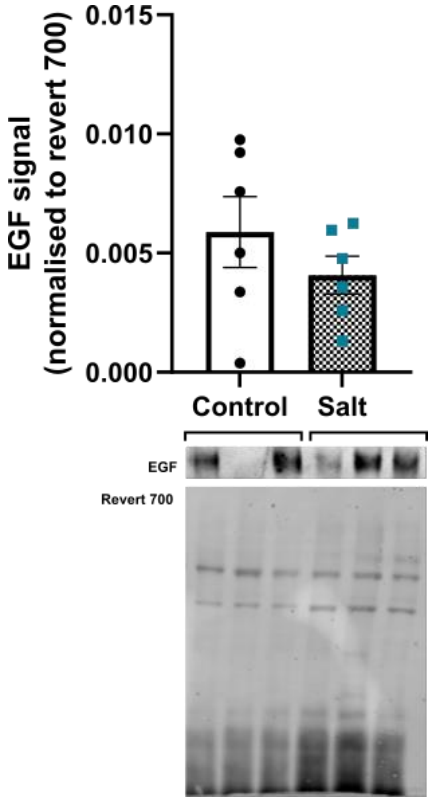

Figure 5.13. The urinary excretion of epidermal growth factor (EGF) after long-term salt loading were unchanged.
EGF protein levels were quantified in urine samples after 3 months of salt loading using Western blotting for urine samples. (*n*=6 control, *n*=6 salt). Data are shown as mean ± S.E.M. Urine samples were normalised to total protein stain revert 700.

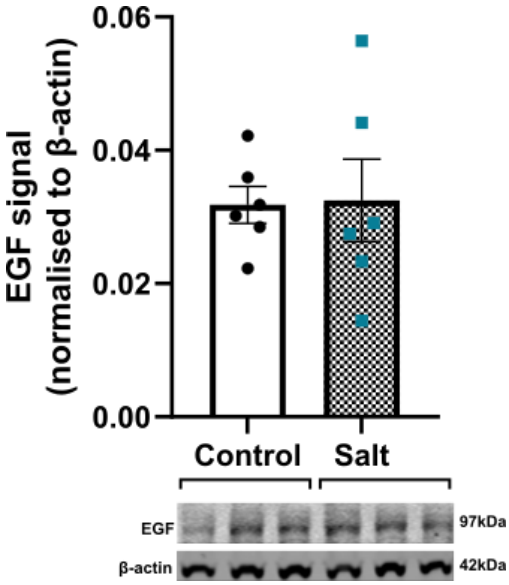

Figure 5.14. The intracellular levels of epidermal growth factor (EGF) in TAL region of kidneys from WKY rats after long-term salt loading were unchanged.
EGF protein levels were quantified after 3 months of salt loading using Western blotting for total kidney lysates from WKY rats in the long-term salt study. (*n*=6 control, *n*=6 salt). Data are shown as mean ± S.E.M. The data were normalised to β-actin.

5.3.5 UMOD accumulates in the ER of long-term salt loaded WKY rats

UMOD trafficking was impacted significantly in the salt loaded SHRSP after 3 weeks (Chapter 3), however this was not the case with intermittent salt loading in WKY rats

(Chapter 4). To test whether salt impacts UMOD trafficking in the normotensive models in the long-term, transcriptional, translational, and post-translational changes in UMOD were analysed in kidneys of the 3-month salt-loaded WKY rats. Gene expression analysis revealed no statistically significant difference in UMOD mRNA expression in total kidneys of the salt-loaded group compared to controls (Figure 5.15). However, total kidney UMOD protein levels were considerably upregulated in the salt-loaded group relative to controls (120.7 ± 8.16 vs 89.08 ± 9.89 relative intensity, $p<0.05$) (Figure 5.16). This indicated that slower UMOD excretion rate in long-term salt-loaded animals may be due to the intracellular accumulation.

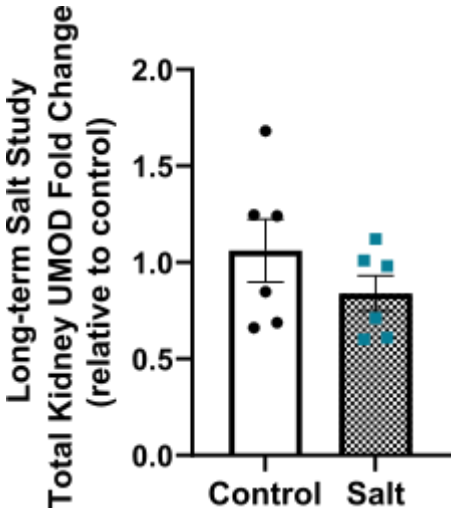

Figure 5.15. Total kidney UMOD mRNA levels did not change significantly after 3 months of salt loading. Total kidney (cortex and medulla) UMOD mRNA expression of long-term salt-loaded group (expressed as a scatter plot of fold change relative to the mean of the control (± S.E.M) *n*=6 control, *n*=6 salt. mRNA levels were normalised to Ubiquitin C (*Ubc*) expression.

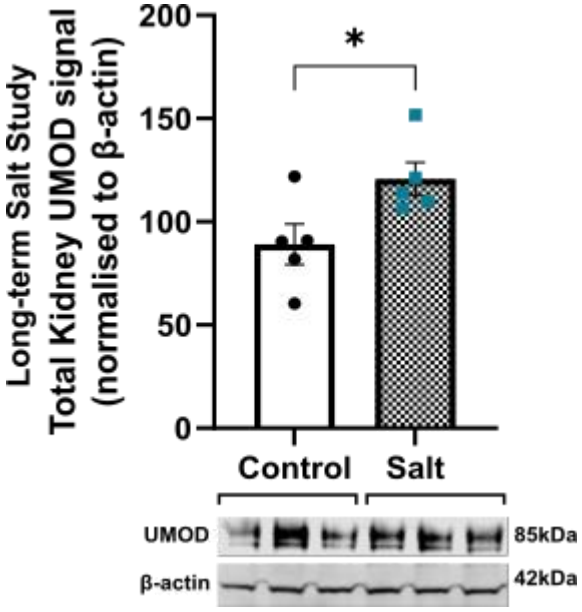

Figure 5.16. Total kidney UMOD protein levels significantly increased in the long-term salt loading group. Total kidney UMOD protein levels and representative Western blot of each group in long-term study (*n*=5 control, *n*=5 salt), showing increased UMOD and intracellular accumulation. Data represented as mean ± S.E.M. *$p<0.05$ (Welch's t-test). β-actin was used as a loading control.

To further interrogate the processes occurring with UMOD trafficking under long-term salt loading, medullary regions were isolated from total kidneys of the WKY rats. These regions contain the majority of TAL cells, which express and secrete a high proportion of UMOD found in the urine (Rampoldi et al., 2011, Chabardes-Garonne et al., 2003). A significant increase in UMOD protein levels was observed in the medullary regions of salt loaded WKY rats compared to controls (202.3 ± 19.55 vs 97.32 ± 20.18 relative intensity, $p<0.01$) (Figure 5.17).

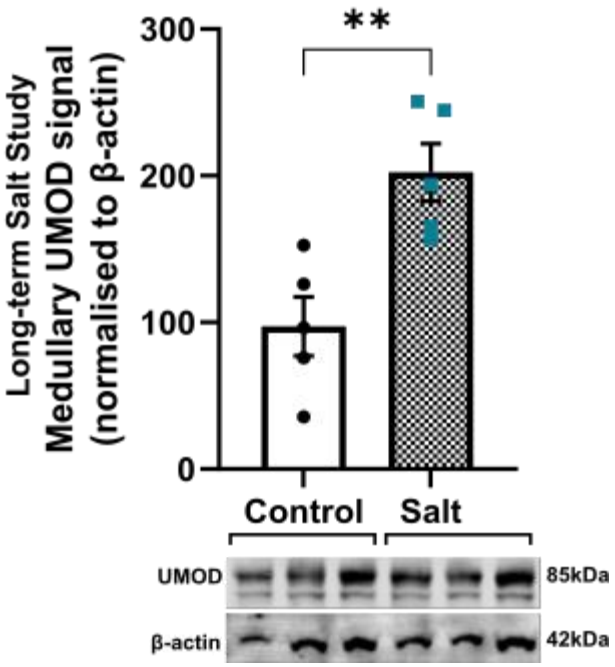

Figure 5.17. Long-term salt loading significantly increased UMOD protein levels in the kidney medullary region. UMOD protein levels and representative Western blots from control (*n*=5) and salt-loaded groups (*n*=5) of the long-term study in the medullary fraction of their kidneys. UMOD protein levels were significantly increased in the salt-loaded group. Data represented as mean ± S.E.M. **$p<0.01$ (Welch's t-test). β-actin was used as a loading control.

Next, in order to study the precise location of UMOD within the TAL cells after long-term salt loading, a subcellular fractionation analysis was conducted on the medullary regions from kidneys isolated from WKY rats. The plasma membrane fraction showed no significant difference after 3 months of salt loading (Figure 5.18A). In contrast, cytosolic levels of UMOD were significantly higher in the salt-loaded group relative to controls (4.74 ± 0.43 vs 3.52 ± 0.28 relative intensity, $p<0.05$) (Figure 5.18B). This implied UMOD is being retained intracellularly in TAL cells after long-term salt exposure.

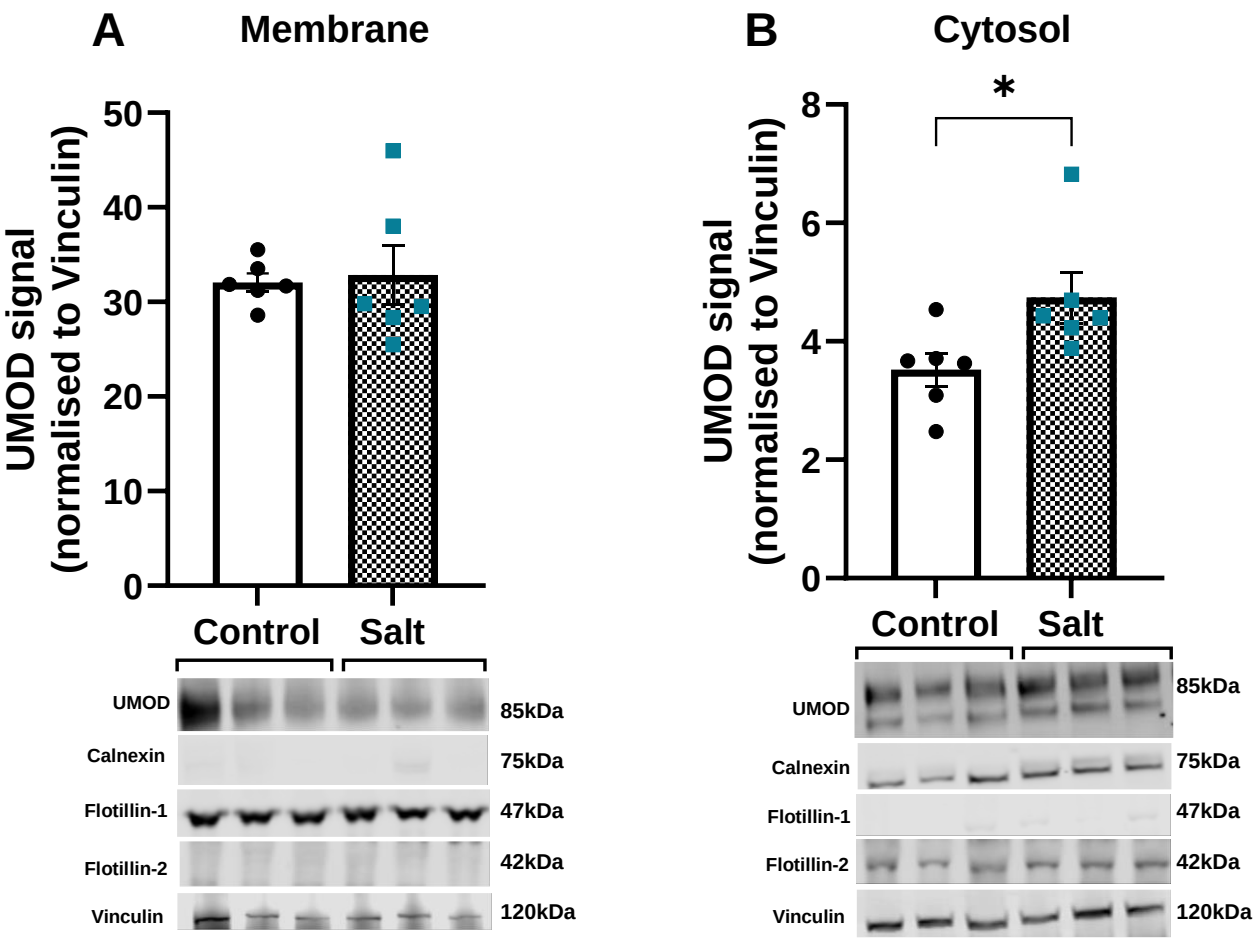

Figure 5.18. Membrane and Cytosolic UMOD protein levels in the medullary region were not changed with long-term salt loading.
Kidneys of control and salt-loaded animals (*n*=6, per group) from the long-term study were isolated. After subcellular fractionation, UMOD protein levels and representative Western blots in (A) membrane fractions and cytosolic (B) isolated from the medullary region of the control (*n*=6) and salt-loaded groups (*n*=6). Data represented as mean ± S.E.M. The plasma membrane (referred to as membrane fraction) was validated by the presence of membrane marker Flotillin-1. The cytosolic fraction contains the contents of all intracellular organelles (e.g., ER, Golgi apparatus, etc.) and the cytoplasm as confirmed by presence of ER chaperone calnexin, and Flotillin-2 as a marker of the cytosol. Vinculin was used as a loading control. *p<0.05, and **p<0.01 (Welch's t test).

Since UMOD is being retained intracellularly, and the rate-limiting step in UMOD secretion is its release from the ER, we looked at UMOD levels in the ER. Co-localization immunofluorescence analysis was performed using calnexin as an ER marker to understand the distribution of UMOD in TAL tubules of the kidney. Salt-loaded WKY TAL regions had significantly higher co-localisation with the ER compared to controls (0.398 ± 0.01 vs 0.362 ± 0.007 Spearman's coefficient, p<0.01) (Figure 5.19).

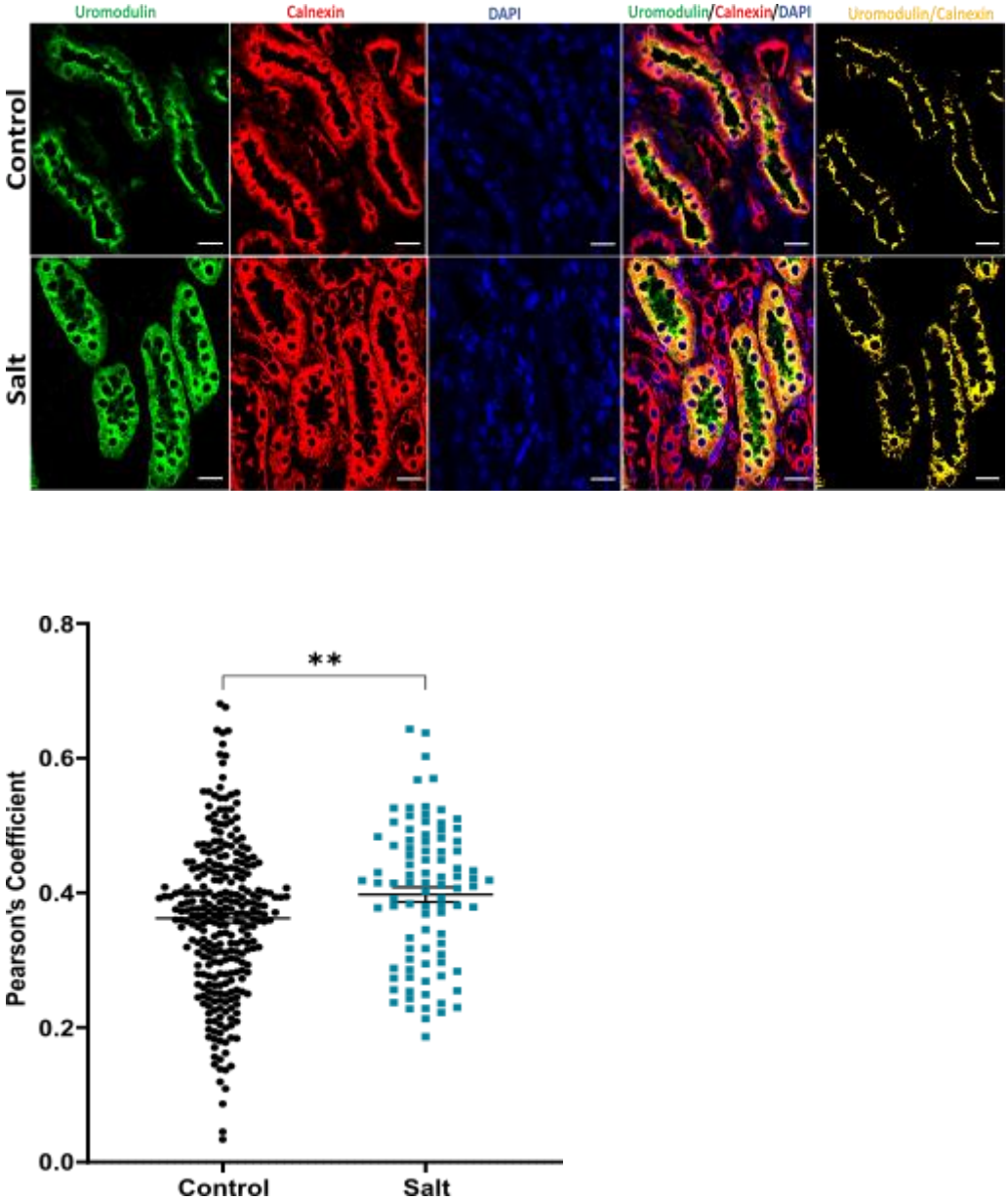

Figure 5.19. Long-term salt loading leads to increased co-localization of UMOD with the ER marker calnexin in the medullary TAL of WKY rats.
Top: Representative immunofluorescence analysis showing UMOD (green) and ER marker calnexin (red) in from medulla of rat kidney sections. Co-localization of UMOD and calnexin is represented by yellow. Nuclei are stained in blue with DAPI. Scale bar represents 20 µm. Bottom: The scatter plot represents Pearson's correlation coefficients which were calculated for four representative tubules (ROI, regions of interest) from 5 samples per group. Error bars represent mean ± S.E.M. **$p<0.01$ (Welch's t test). Images were evaluated in a blinded fashion.

UMOD undergoes a number of glycan modifications along its secretory pathway, and this can be utilised to differentiate between different stages of UMOD maturation. To this extent, an Endo H enzymatic assay was conducted on UMOD protein isolated from the medullary region of kidneys harvested from WKY rats. The Endo H enzyme cleaves simple N-glycans but cannot cleave complex N-glycans. There was a significant increase in the ER (immature) form of UMOD (consisting of simple N-glycans) in the salt-loaded group compared to the membrane (mature) form (Endo-H resistant containing complex N-glycans) (1.19 ± 0.12 vs 1.00 ± 0.03 signal ratio to control, $p<0.05$) (Figure 5.20). The significant UMOD accumulation in the ER of the long-term salt-loaded animals, suggests

that salt regulates the maturation of UMOD in TAL cells and leads to its retention if continued for longer periods of time.

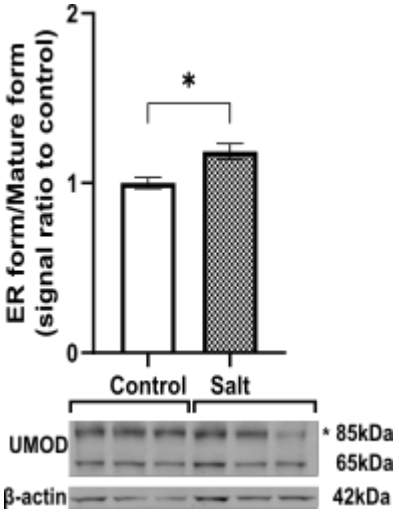

Figure 5.20. There is an accumulation of immature UMOD in the ER of medullary TAL of WKY rats. Endo H assay of the medulla samples from the control (*n*=6) and long-term salt-loaded (*n*=6) animals. Western blot shows representative bands of the endo H-resistant UMOD with complex glycans (mature, top band represented by "*") and the ER form of UMOD (immature, bottom band). The data is expressed as a comparison of the average ER-form UMOD band signal to the average mature UMOD band signal, shown as a single ratio value. Error bars represent mean ± S.E.M. *p<0.05. (Welch's t test). β-actin was used as a loading control.

5.3.6 The reduction in UMOD secretion is a result of salt-induced effects rather than changes in osmotic pressure

As to further evaluate the direct effects of on UMOD trafficking in the WKY kidneys, an *in vitro* model of constitutively expressing human UMOD-GFP MDCK cells was used. Since there is no current TAL cell model available, UMOD-GFP MDCK cells served as a suitable replacement model. To account for potential osmotic influences provided by salt on the cells, we used the inert molecule mannitol as an osmotic control. Since osmotic pressure could not be controlled in the *in vivo* experiments, this cell model allows for the study of whether salt-driven effects on UMOD secretion by TAL are due to salt itself or osmotic pressure differences. Therefore, the UMOD-GFP MDCK cells were incubated with 60mM salt (in addition to an existing 110mM in DMEM media) or 120mM of mannitol (as an osmotic control) for 18 hours. This more closely replicates conditions for WKY exposed to intermittent salt loading conditions in Chapter 4, rather than the long-term salt-study. The 18-hour incubation time was chosen as it more closely reflects the 24 hour urinary UMOD excretion rate reported in the animal models used in this thesis. Also, a significant reduction in UMOD secretion is observed in cells incubated with salt compared to mannitol controls at this 18-hour time point (0.0958 ± 0.0158 vs 0.174 ± 0.026 relative intensity, $p<0.05$) (Figure 5.21). In contrast, no significant changes were observed in the intracellular UMOD protein levels (Figure 5.22) or UMOD mRNA expression (Figure 5.23).

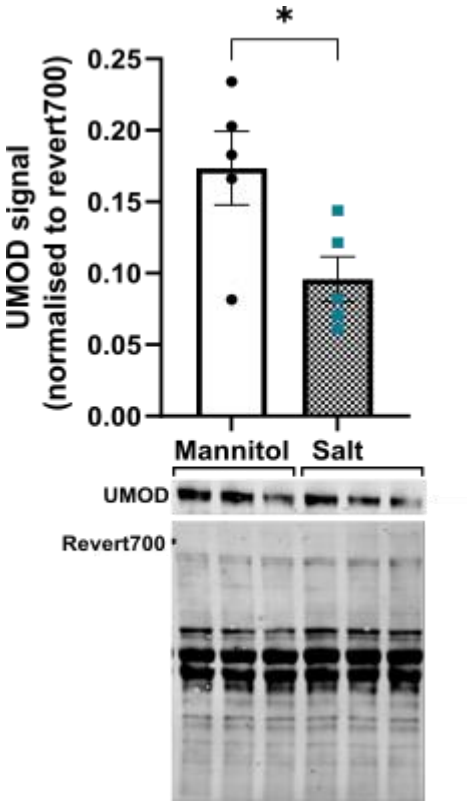

Figure 5.21. MDCK cells have decreased secretion of UMOD into the media with salt incubation for 18 hours. UMOD-GFP MDCK cells were incubated with DMEM media with additional 60mM salt or 120mM mannitol (osmotic control) for 18 hours. Secreted UMOD protein levels in the media and representative Western blots. Media samples were normalised to total protein stain revert 700. Data are represented as mean ± S.E.M. (*n*=5 mannitol, *n*=5 salt). *p<0.05. (Welch's t test).

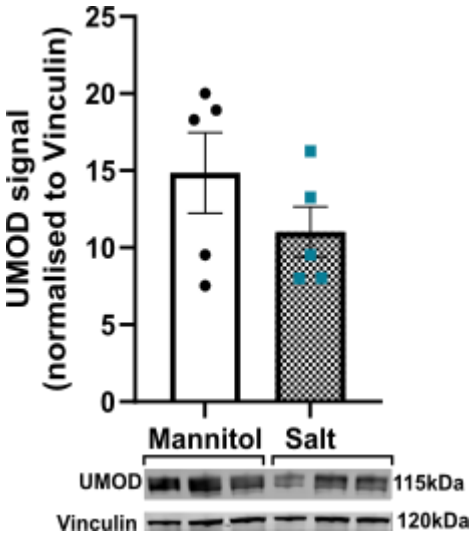

Figure 5.22 Intracellular levels of UMOD remain unchanged in MDCK cells after salt incubation for 18 hours. UMOD-GFP MDCK cells were incubated with DMEM media with additional 60mM salt or 120mM mannitol (osmotic control) for 18 hours. UMOD protein levels in the cell lysate and representative Western blots. UMOD was normalised to Vinculin. Data are represented as mean ± S.E.M. (*n*=5 mannitol, *n*=5 salt).

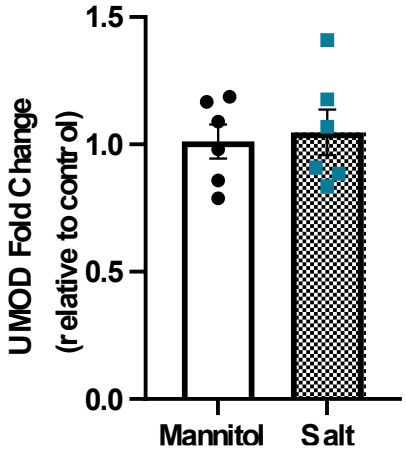

Figure 5.23 The expression of UMOD mRNA levels remains unchanged in MDCK cells after salt incubation for 18 hours.
UMOD-GFP MDCK cells were incubated with DMEM media with additional 60mM salt or 120mM mannitol (osmotic control) for 18 hours. UMOD mRNA expression is shown as fold change relative to mean of control ± S.E.M. Expression was normalised to HPRT housekeeping gene. (*n*=6 mannitol, *n*=6 salt).

As to identify any changes in UMOD trafficking in the salt incubated MDCK cells, immunofluorescence analysis for UMOD was conducted. Specifically, cells were either permeabilised or not permeabilised as to allow differentiation between intracellular and cell surface compartments (i.e., intracellular and membrane UMOD), respectively. There was a significant decrease in the surface membrane UMOD compared to mannitol controls (0.762 ± 0.071 vs 1.190 ± 0.106 relative intensity, $p<0.05$) (Figure 5.24). In contrast, intracellular UMOD levels showed no statistically significant differences (Figure 5.24).

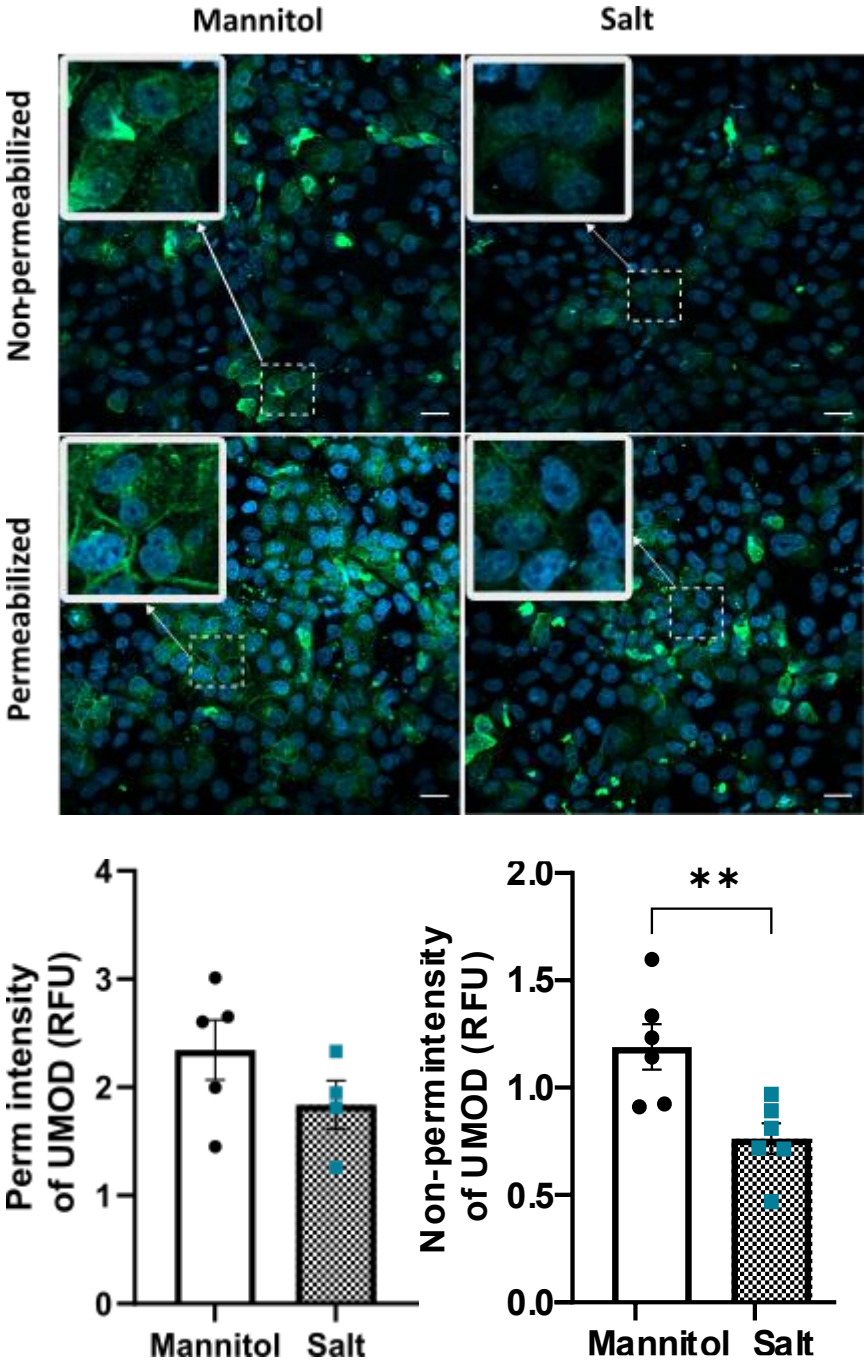

Figure 5.24. There is a reduction in UMOD on the membrane surface of MDCK cells after 18 hours of salt loading.
Immunofluorescence analysis of UMOD in UMOD-GFP MDCK cells after incubation with 60mM salt or 120mM mannitol as an osmotic control for 18 hours at 40X magnification. Representative images of non-permeabilized and permeabilized cells with UMOD (green) are shown and associated relative fluorescence units (RFU) (non-permeabilized ("Non-perm") and permeabilized ("Perm") calculated from the images displayed as scatter plots. White dashed boxes and arrows represent zoomed in regions of interest. Data are represented as mean ± S.E.M (n=6 images per group) **$p<0.01$(Welch's t-test). Scale bar represents 20µm. DAPI used as a nuclear stain (blue). Images were evaluated in a blinded fashion.

5.3.7 Long-term salt exposure induces a medulla-specific ER stress response

Salt is a known inducer of ER stress in kidney tissues (Khadive et al., 2021), which can lead to kidney damage. To examine whether long-term salt loading influences ER environment in the total kidneys (cortex and medulla) of WKY rats, an immunoblot

analysis was performed for common ER stress markers Binding Immunoglobulin Protein (BiP) and Protein Disulphide Isomerase (PDI). There was no statistically significant difference between control and salt-loaded groups in BiP (Figure 5.25) or PDI (Figure 5.26) protein levels in total kidneys of these animals.

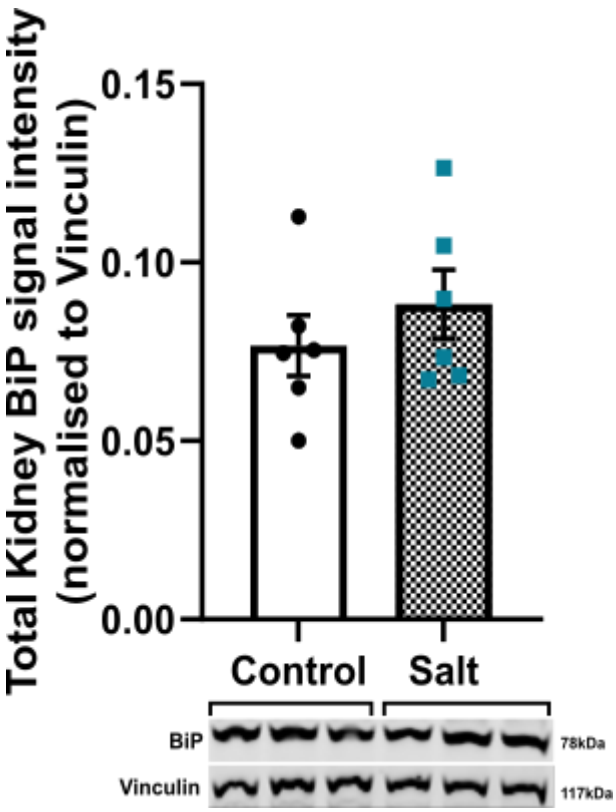

Figure 5.25. BiP protein levels in total kidneys were unchanged after long-term salt loading in WKY rats. Total kidneys were extracted from WKY rats after the long-term salt study. UMOD protein levels and representative Western blots for Binding Immunoglobulin Protein (BiP) for total kidney lysates are shown. Data expressed as mean ± S.E.M. *n*=6 kidney (per group). Data was normalised to Vinculin.

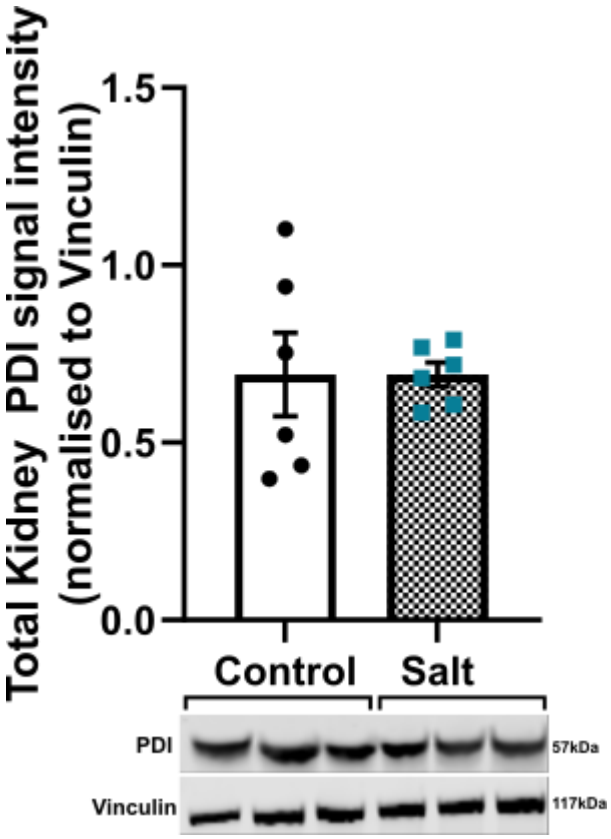

Figure 5.26. PDI protein levels in total kidneys were unchanged after long-term salt loading in WKY rats. Total kidneys were extracted from WKY rats after the long-term salt study. UMOD protein levels and representative Western blots for Protein Disulphide Isomerase (PDI) for total kidney lysates are shown. Data expressed as mean ± S.E.M. *n*=6 kidney (per group). Data was normalised to Vinculin.

Given that the majority of UMOD is produced in the TAL, which are concentrated in the medulla of the kidney, the next analysis was focused on determining protein expression of these ER stress markers in this region. There was a significant increase in BiP in the medulla of salt-loaded rats compared to controls (0.00781 ± 0.00101 vs 0.00496 ± 0.00042 relative intensity, $p<0.05$) (Figure 5.27). Similarly, medullary PDI levels were also significantly upregulated in the salt-loaded relative to controls (4.618 ± 0.367 vs 3.181 ± 0.321 relative intensity, $p<0.05$) (Figure 5.28).

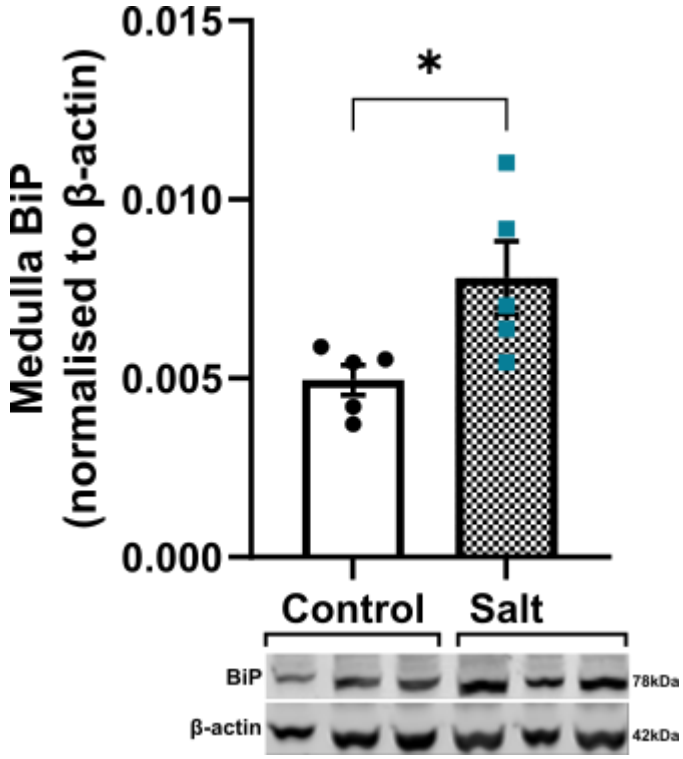

Figure 5.27. BiP protein levels in the medullary region of the kidneys were increased after long-term salt loading in WKY rats.
The medullary lysate was extracted from total kidneys of WKY rats after the long-term salt study. UMOD protein levels and representative Western blots for Binding Immunoglobulin Protein (BiP) are shown. Data expressed as mean ± S.E.M. *n*=6 kidney (per group). Data was normalised to β-actin.

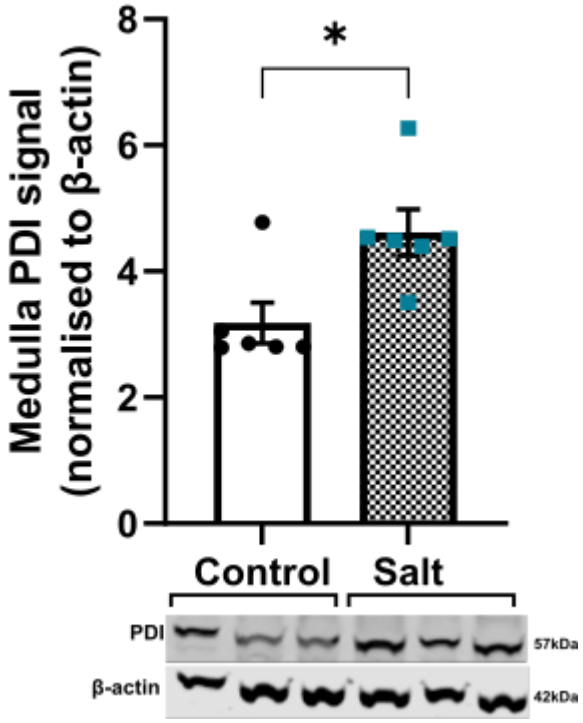

Figure 5.28. PDI protein levels in the medullary region of the kidneys were increased after long-term salt loading in WKY rats.
The medullary lysate was extracted from total kidneys of WKY rats after the long-term salt study. UMOD protein levels and representative Western blots for Protein Disulphide Isomerase (PDI) are shown. Data expressed as mean ± S.E.M. *n*=6 kidney (per group). Data was normalised to β-actin.

To understand whether this increase in ER stress marker levels is a phenomenon of prolonged salt exposure, we compared expression levels of BiP in the long-term salt study to that of the 3-week acute salt study (Chapter 3). BiP was not significantly increased after 3 weeks of salt loading in total kidneys of WKY rats (Figure 5.29). Additionally, when compared to the chronic hypertensive SHRSP model, there was no significant difference in expression of BiP (Figure 5.29). This would suggest that activation of ER stress is localised to the medulla and only occurs after long-term salt loading, as is the case for WKY rats after 3 months.

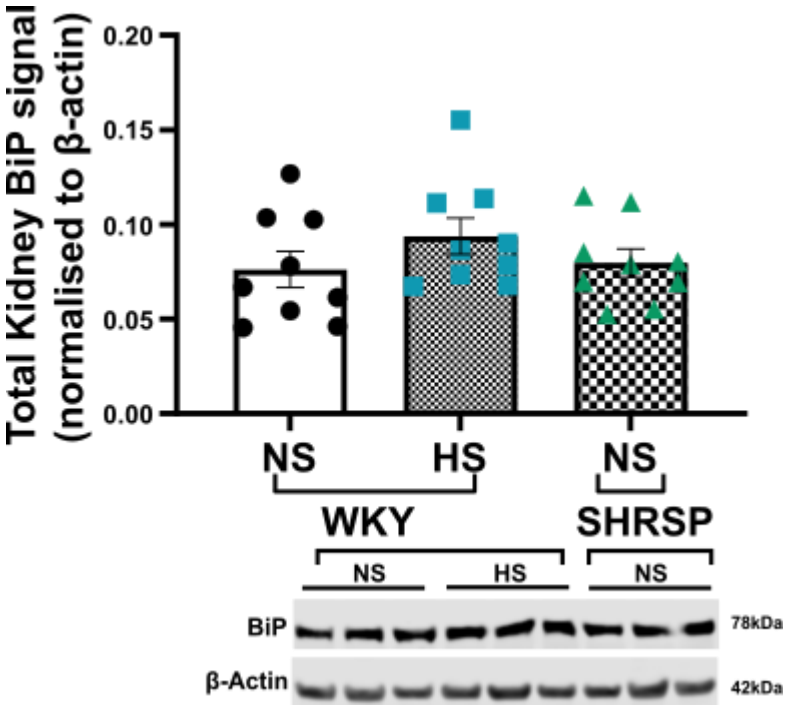

Figure 5.29. Acute salt loading did not significantly alter BiP protein expression in chronic hypertensive SHRSP rats.
The total kidneys of NS: normal salt and HS: high salt (1% salt) loaded animals (*n*=9, per group) in both WKY and SHRSP. Total kidney Bip signal intensity and representative Western blots for BiP and β-actin (loading control) are shown. Bars indicate mean ± S.E.M. The kidneys were collected from the previous study outlined in chapter 3. Animals were administered 1% salt over 3 weeks continuously at 11 weeks of age, for an in-depth methodology refer to chapter 3.

5.4 Discussion

The aim of this chapter was to identify the long-term effects of salt on UMOD retention in a normotensive background. We hypothesized and confirmed that long-term salt loading induces intracellular accumulation of UMOD, specifically within the ER of the epithelial cells in the TAL region. Further, we found markers of early-stage ER stress to be upregulated after long-term salt exposure. This finding highlights the potential of salt to induce ER stress and UMOD accumulation.

The pathophysiology of UMOD accumulation via salt, and whether this contributes to the development of hypertension, remains to be elucidated. One of the main hypotheses of this study was that long-term salt loading substantially impacts UMOD trafficking, which ultimately would cause aberrations in renal physiology. There was also the unanswered question from Chapter 3 and 4, as to whether UMOD accumulation impacts renal ER stress? To remove confounding factors that stem from hypertension, such as kidney injury found in SHRSP (Mary et al., 2021), the present study opted for a salt-resistant and normotensive WKY rat model. Although, it is important to note that the aim of this study was not assess which animal model is most suitable for studying the relationship between salt and UMOD. Given that the focus is on unravelling mechanisms underlying the effects

of salt on UMOD, rather than any specific disease (e.g., hypertension), the WKY rats provide an ideal model in this context. Moreover, this study makes critical use of 24-hour urine sample, which is considered the gold standard for analysing UMOD excretion rates (Youhanna et al., 2014). This removes the need for normalisation to creatinine, as is required for spot urine samples, as was used in other studies of UMOD (Graham et al., 2014, Trudu et al., 2013b). Furthermore, although it may be argued that sex-based differences exist in the effects of salt on UMOD excretion rate, it was demonstrated in Chapter 3 that no discernible differences in UMOD excretion rate exist between male and female rats after salt loading. Therefore, the use of primarily male WKY rats in the present study is justified.

The current scope of research focusing on dietary salt and UMOD excretion in rats is restricted (Ying and Sanders, 1998). Previous studies have demonstrated that higher salt intake leads to increased reabsorption of salt in TAL via NKCC2 activity, and that UMOD regulates this activity (Mutig et al., 2011a). It may be postulated that with higher salt concentrations, the reduction of UMOD secretion by the TAL is a homeostatic response that acts to prevent excess sodium reabsorption. A study with C57/BL6 mice showed demonstrated that high salt loading (2% salt) over 2 months resulted in increased urinary UMOD excretion in the wild-type rats (Olinger et al., 2019). In contrast, in Chapter 3 and Chapter 4 WKY and SHRSP rats exhibited a distinct decrease in urinary UMOD excretion rate following salt loading with 1% salt. In this chapter, it was demonstrated that UMOD excretion rate remains consistently low during longer-term salt loading periods. The key difference between the present study and the study with C57/Bl6 mice (Olinger et al., 2019) is the concentration of salt used. The concentration of 1% salt was chosen as it is more physiologically relevant and those not induce severe kidney damage (demonstrated in Chapter 4). Moreover, there is a lack of influence of this salt concentration on systolic blood pressure in the WKY rats. Albeit the difference in effects of salt on UMOD excretion may be species-dependent. However, it would be prudent to reduce urinary UMOD levels from a physiological standpoint as a form of negative feedback, as a way to reduce hyperosmolarity in the urine caused by higher NaCl concentrations as a result of consistent salt loading.

It may be expected that the extent of reduction of urinary UMOD excretion rate may differ between long-term salt loading carried out in the present chapter and intermittent salt loading in the previous chapter (Chapter 4). UMOD excretion in the salt group of the intermittent salt study was 0.001mg/h (0.024mg/day) compared to controls (0.003 mg/h or 0.072mg/day). Interestingly, when compared to the long-term salt study, rats of the same

age (14-weeks old) showed an identical reduction in urinary UMOD excretion rate in the salt group (0.001mg/h or 0.024mg/day) compared to control rats (0.003 mg/h or 0.072mg/day). In both cases, this is a 66.6% reduction in the urinary UMOD excretion rate. From this, it may be concluded that a reduction of this magnitude for the most abundant protein found in the urine of healthy individuals must impact renal physiology in a considerable way. And thus, highlighting the importance of studying UMOD as a marker of effects of salt loading on the kidneys.

The fact that the reduction in urinary UMOD excretion rate is a specific effect of salt is underlined by the lack of change in the secretion of another TAL protein, specifically EGF (Zeng et al., 2009). The exact molecular mechanisms that are influenced by salt in the TAL are not yet understood. However, it is likely that this an NKCC2-independent mechanism as the UMOD-GFP MDCK cells studied here demonstrate a decrease in UMOD secretion even though they lack NKCC2 expression. The factors involved in retaining UMOD in the ER require further investigation. However, it may still be argued that osmotic pressure changes as a result of variations in NaCl concentrations could be responsible for lowering UMOD secretion by the TAL. The data on the UMOD-GFP MDCK cells indicates otherwise, whereby osmolarity was controlled with mannitol, which showed no influence on the secretion of UMOD. The quick action of salt on UMOD secretion in these cells, with a difference found after 18 hours, could reflect the importance of sodium handling by cells and the role UMOD plays in this. It seems more logical, therefore, that reduction in UMOD excretion observed in the normotensive setting is a result of a direct effect of salt on the epithelial cells of the TAL and occurs irrespective of blood pressure or kidney injury factors. This further supports the findings discussed in Chapter 3 and 4. Of note is the unilateral effect of salt on UMOD trafficking (i.e., an apical trafficking rather than a basolateral), given that serum UMOD levels were unaffected. It may also suggest a different trafficking pathway for basolateral secretion of circulating UMOD. Circulating UMOD has a consistent inverse relationship with hypertension (Wang et al., 2021). It may be hypothesised that serum UMOD excretion will only be changed as a protective measure, as would be prevalent in a pathophysiological scenario (e.g., with kidney injury). However, this is not the case with the WKY rats studied here.

High dietary salt intake increases vascular oxidative stress and contributes to renal damage via increased inflammation (Di Castro et al., 2013, Sironi et al., 2001, Gigante et al., 2003). Since sodium loading influences the pH and redox potential, and these are critical in the correct folding of proteins in the ER (Merksamer et al., 2008). Therefore, it may be proposed that prolonged sodium-loading is a contributor to the misfolding of UMOD. In

normal physiological conditions, these proteins are degraded by ER-associated degradation system (Meusser et al., 2005). However, in periods of continued exposure to sodium, as would be the case for the long-term salt study rats, this system may be overwhelmed. ER chaperone BiP recognises misfolded proteins derived from ribosomes during translation causing their degradation through the ERAD pathway (Cesaratto et al., 2019). The increase in BiP in the WKY exposed to long-term salt loading may be a protective response, as to prevent negative effects of UMOD accumulation. It stands to reason that were this accumulation of misfolded UMOD to continue, under continued salt stress, that this would contribute to overwhelming of the system and eventual kidney damage.

Another major hypothesis of this study postulated that long-term salt loading would change the phenotype of normotensive models to that of the hypertensive SHRSP seen in our previous study with 3 weeks of salt loading (Chapter 3). The oxidative environment of the ER is primed for the formation of disulphide bonds, and UMOD with 24 disulphide linkages requires these conditions for its proper folding. PDI is reduced following the acceptance of electrons form cysteine residues and is known to accumulate during ER stress (Tu et al., 2000). The data exhibited here appears to indicate early signs of transition into this state by the long-term salt loaded WKY rats. PDI has been reported to act as a redox-dependent switch, by functioning as a chaperone rather than a disulphide isomerase in its reduced state, which occurs during ER stress (Tsai et al., 2001). The increasingly reduced ER environment in the long-term salt exposed animals may act as a switch for PDI towards chaperone activity in order to regulate misfolded UMOD. Studies in hepsin-deficient mice treated with high salt for 2 months with increased misfolded UMOD in the ER also reported higher BiP and PDI expression (Olinger et al., 2019). A possible outcome of long-term salt loading may be a trigger of early deleterious processes in the kidneys of normotensive WKY. These processes accumulate to the point of renal injury, as seen in the chronic hypertensive SHRSP (Chapter 3). This is a novel perspective on renal disease mechanisms that might occur in hypertensive patients. Although blood pressure remained unaffected by salt in the normotensive models, UMOD may be indirectly contributing to blood pressure increases in salt-loaded chronic hypertensive models. Chronic hypertensive models may have increased UMOD retention and greater lag periods in ER processing. Real-time imaging of UMOD in both normotensive and hypertensive cells exposed to salt would be key to the molecular understanding of UMOD trafficking in these conditions.

There are a number of caveats to the findings of this chapter that require addressing. It is still unclear which molecular signalling pathways are involved in regulating UMOD trafficking and how exactly salt is impacting them. Further mechanistic studies using the

normotensive WKY rat model in combination with the UMOD-GFP UMOD expressing cell line will be crucial to uncovering the molecular detail behind the interaction of salt and UMOD. There is also availability for further investigation with regards to reversibility of long-term salt loading effects. The phenotype of ER-accumulated UMOD may be rescuable, as was seen to some extent in the intermittent salt study (Chapter 4). This would also have implications for therapeutic interventions in hypertension. While there were salt-induced functional changes in the form of attenuated UMOD excretion, there are no obvious renal structural changes, highlighting the dynamic regulation of UMOD in response to salt. A speculation of a possible sequence of events are: Salt → (ER stress → UMOD accumulation)/ (UMOD accumulation → ER stress) → Kidney damage. Further experiments defining the relationship between ER stress and UMOD will be necessary. This will involve further use of the UMOD-GFP UMOD-expressing cell model, to inhibit certain parts of the ER stress pathways using toxins and small molecular inhibitors. Finally, the findings are somewhat limited by lack of access to human cohorts, which would greatly improve translatability. To this date, however, no such clinical trial is available.

To summarise, this chapter highlights the progressive effect that salt has on UMOD and renal physiology in a normotensive background. Only after continued salt exposure over a longer period of time, in combination with ER accumulation, is an ER stress response triggered. Importantly, UMOD is only one of many points of impact following long exposure of salt, even at a physiological concentration. These need to be considered when considering multifactorial diseases such as hypertension. Unravelling the signalling components involved in salt and UMOD trafficking would hold great promise for future therapeutic targets, not only in hypertension but also other kidney-related diseases such as CKD.

Chapter 6: Cell Culture Models for Studying UMOD Expression

6.1 Introduction

The secretion of UMOD from TAL cells is a complex process that involves several molecular mechanisms, including intracellular trafficking, post-translational modification, and exocytosis (Boder et al., 2021, LaFavers et al., 2022). However, the molecular mechanisms involved in UMOD secretion from TAL cells are not fully understood, and one of the main challenges in studying this process is the lack of suitable cell models. Currently, there are limited options for studying TAL cell biology *in vitro*, and many studies have relied on primary cultured cells or immortalized cell lines that may not fully recapitulate the complexity of the *in vivo* system (Grunewald et al., 2001, Olinger et al., 2019, Bourgeois et al., 2003, Glaudemans et al., 2014).

Recent studies have attempted to address this challenge by generating more physiologically relevant *in vitro* model systems, such as by using organoids or co-culture systems (Garreta et al., 2018, Ward et al., 2011). These model systems have the potential to provide a more accurate representation of the *in vivo* TAL cell microenvironment and may therefore help to elucidate the molecular mechanisms of UMOD secretion. Despite these recent advancements, further research is needed to fully understand the molecular mechanisms involved in UMOD secretion from TAL cells. Improved *in vitro* models, along with advances in imaging and molecular biology technologies, will be critical in advancing our understanding of this process and its role in kidney function.

In this chapter, the aims were to characterize and assess two cell models for the molecular mechanistic study of UMOD trafficking and secretion from TAL cell: 1) primary mTAL cells and 2) immortalized UMOD-YFP expressing 293FT cells. It was hypothesized that primary mTAL cell epithelial cells isolated from kidneys of WKY rats would express and secrete UMOD. It was postulated that salt incubation can influence UMOD trafficking in the primary mTAL cells, similar to what was observed *in vivo* in previous chapters. In addition to this, this chapter aimed to generate a novel inducible cell line based on 293FT cell line (based on a human embryonic kidney cell background) that expresses UMOD tagged with YFP as a fusion protein. Production of the plasmid expression vector expressing UMOD-YFP and expression patterns in the 293FT cells are outlined sand characterized here.

6.2 Materials and Methods

General Materials and Methods can be found in Chapter 2.

6.2.1 Medullary Thick Ascending Limb Tubules

6.2.1.1 Dissection and culture of primary mTAL cells

mTAL tubules were isolated from kidneys harvested from 5-week old male WKY rats. The kidneys were immediately stored in filtered HEPES-Buffered Hank's Balanced Salt Solution (pH 7.4, GIBCO HBSS, ThermoFisher Scientific, UK) supplemented with $NaHCO_3$ (25mM) and kept on ice. For each kidney, the medulla region was excised and placed into filtered Collagen Type IV Collagenase (Sigma-Aldrich, UK) dissolved in HBSS pH 8.4 (ThermoFisher Scientific, UK) where it was cut into smaller pieces using surgical blades to assist digestion and cell detachment. This solution was incubated at 37°C using a water bath for 10 minutes. The supernatant was removed and added to cell culture grade BSA pH 7.4 (Sigma-Aldrich, UK) dissolved in HBSS. Collagenase incubation was repeated until the medulla pieces were fully digested. The tubule suspension was then centrifuged at 200xg for 10 minutes and the pellet resuspended in HBSS. This solution was the filtered through a 53µm nylon mesh (Cole-Parmer, USA) using HBSS for size exclusion of the TAL tubules. The TAL tubules on the nylon mesh were then washed with HBSS, and the subsequent solution centrifuged at 500xg for 10 minutes. The resulting pellet was then resuspended in Renal Epithelial Growth Medium (REGM) (Lonza, UK) with 10% Foetal Bovine Serum (FBS). The cells were cultured on 6-well plates coated in Poly-D-Lysine (ThermoFisher Scientific, UK). Primary cells were incubated at 37ºC at 5% CO_2 for five days or three days, respectively, until a confluent primary mTAL epithelial cell monolayer was formed. A media change was conducted every 48 hours, whereby the media was extracted at stored at -80ºC.

6.2.1.2 Imaging of mTAL Primary Cells

Primary mTAL cell cultures were imaged using the EVOS XL Core Cell Imaging System (Thermo Fisher Scientific) with a 20X objective. Acquisition parameters were kept identical for all cultures. Images were processed using ImageJ software.

6.2.2 Transgenic UMOD expressing FT-293 Cells

6.2.2.1 Cell Line Culture

All cell culture experiments were performed in a Biological Safety Class II vertical laminar flow cabinet using sterile techniques. A phase contrast inverted microscope was used to

examine cultures to confirm the absence of contamination and check the confluence. Flp-In™ T-REx™ 293 cells (293FT, based on Human Embryonic Kidney 293 cells, Thermo Fisher Scientific, UK) were generously provided by Prof William Fuller (University of Glasgow). 293FT cells were maintained between passages 5 and 30 in T75 flasks in a humidified incubator (37°C and 5% CO_2). Cells were passaged between 80-90% confluence to prevent contact inhibition by aspirating the media and washing with pre-warmed sterile phosphate buffered saline (PBS). Cells were passaged by incubation with 0.05% Trypsin-EDTA for 2 minutes. The flasks were gently tapped to dislodge the cells and the trypsin was neutralised by addition of the cell culture medium (Dulbecco's Modified Eagle Medium (DMEM), 10% foetal bovine serum (FBS), 1% penicillin/streptomycin). The cells were then centrifuged for 3 minutes at 1000 rpm, before the remaining supernatant was aspirated, and the pellet suspended in fresh cell culture medium. This was to enable transfer of cells to new flasks or plates. After experimentation, plates were washed with PBS before RIPA lysis buffer (Appendix 8.1.1.5) for each experiment was added. For freezing, the pellet of the cells was resuspended in freezing medium (90% cell culture medium, 10% dimethyl sulfoxide (DMSO) and kept in -80°C.

6.2.2.2 Primer Design

The primers used in a PCR reaction can be used to replicate DNA. It is utilised in this study to amplify the UMOD-Yellow Fluorescent Protein (YFP) plasmid. The primers were designed by Prof William Fuller and prepared by Eurofins (Table 6.1). Primers were designed using Takara's In-Fusion primer design tool which incorporates overlapping ends to the primers to allow the plasmid to be re-circularised or two products to be fused together. These are resuspended in nuclease free water to a stock concentration of 100 µM and used with CloneAmp HiFi PCR kit (Takara Bio, EU).

Table 6.1 Primers for production of the UMOD-YFP plasmid.

Oligo Name	Sequences	Length (Bp)	GC%	Tm (°C)	Gene-Specific Tm (°C)
pcDNA5-F	CTCGAGTCTAGAGGGCCCG	19	68	63.3	63.3
pcDNA5-R	AACGCTAGAGTCCGGAGGCT	20	60	65.2	65.2
UMOD-F	AGCCTCCGGACTCTAGCGTTGCAGAAAGGATGGGGCAGC	39	62	77.3	63.8
UMOD-R	TGCTCACCATCTGAAAAGTCAGGGTCAAGGTGG	33	52	72.3	63.3
YFP-F	GACTTTTCAGATGGTGAGCAAGGGCGAGG	29	55	70.7	64.8
YFP-R	ACGGGCCCTCTAGACTCGAGTTATCTAGATCCGGTGGATCCCGG	44	59	72.2	64.9

6.2.2.3 Production of the UMOD-YFP plasmid

The cloning strategy for the final UMOD-YFP plasmid product was as follows; the human *UMOD* transcript 1 is inserted into the backbone of the pcDNA5 FRT/TO Flp-In expression vector (Invitrogen), specifically between bases 970 and 1335. The In-Fusion HD Cloning Kit (Takara Bio, EU) was used to ligate all these products together after

separate PCR amplification. The human *UMOD* transcript 1 (NM_03361.3) was obtained from GeneScript (OHu21261; in the pcDNA3.1-C-(k)DYK plasmid backbone. The YFP transcript was encoded in the pEYFP-C1 plasmid. The final ligated UMOD-YFP pcDNA5 FRT/TO plasmid encodes the UMOD-YFP fusion protein.

In all cases, the plasmid DNA was linearized using forward and revere primers (see Table 6.1) and CloneAmp Hifi PCR premix (containing dNTPs and DNA polymerase). This was run on the Thermal Cycler on the following programme (Table 6.2).

Table 6.2 Thermal Cycler Programme for DNA amplification of UMOD-YFP products.

Step	Temperature	Time	Cycle
Hot start	98°C	2 minutes	1
Denaturation	98°C	10 seconds	35
Annealing	65°C	15 seconds	
Extension	72°C	5 seconds per kb of plasmid	
Cooling	4°C	Hold	∞

Following the PCR reaction, the mix was incubated with DpnI enzyme (37°C, > 3 hours) to remove parental DNA. A PCR Clean Up Kit (Qiagen, UK) was used to remove excess buffer, enzymes, and primers from the reaction mix. The purified, linearized PCR product was then re-circularised to produce a functional plasmid by incubation of 200ng of PCR product (combined with a molar excess of each insert according to the manufacturer's instructions) with In-Fusion HD Enzyme Premix at 50°C for 15 minutes. This is then kept on ice before transformation. Combination of the PCR products with the In-Fusion HD Enzyme Premix allows fusion of the products into one circularised plasmid product (Figure 6.1).

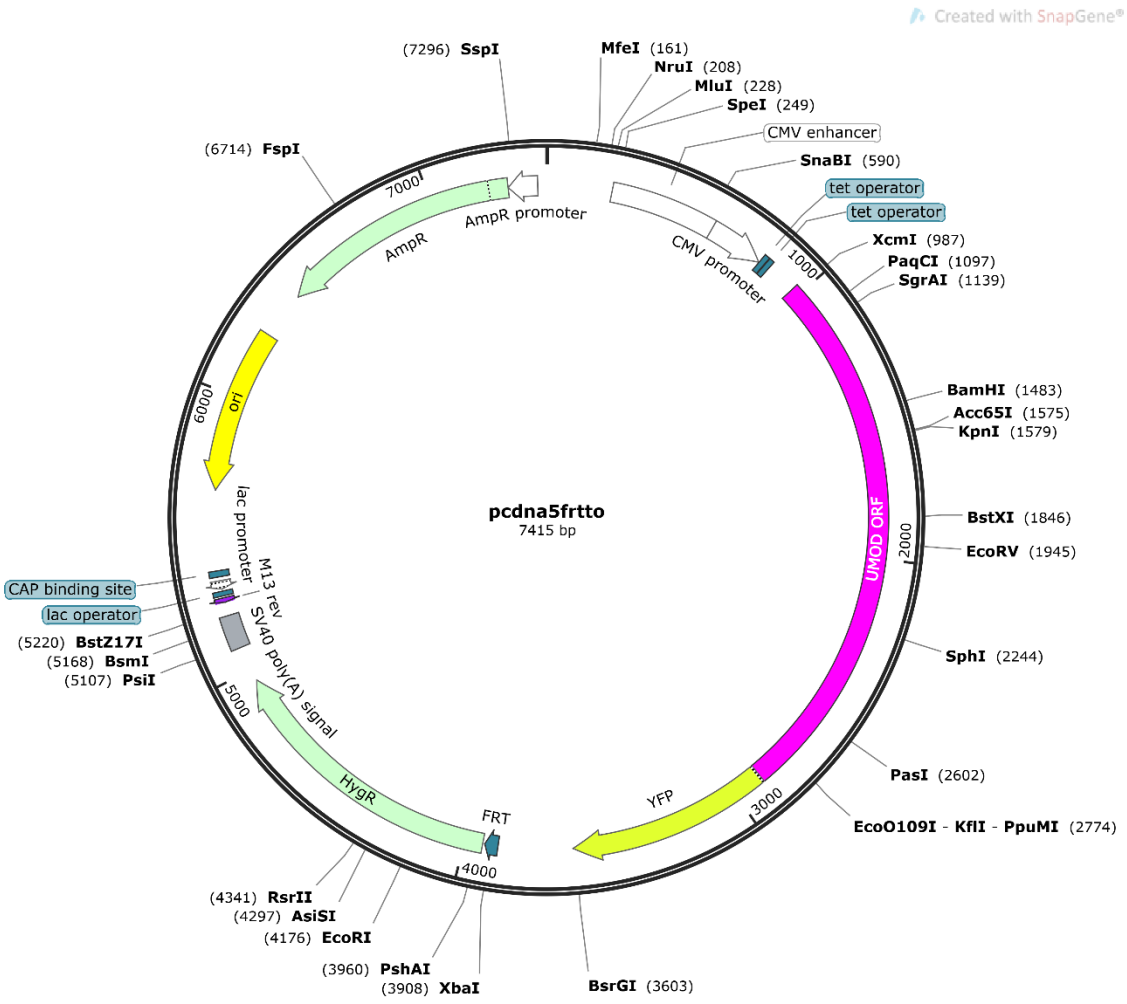

Figure 6.1 The UMOD-YFP insert in the pcDNA5-FRT/TO backbone vector.
The pcDNA FRT/TO backbone plasmid contains the human UMOD transcript 1 open reading frame (ORF) with a Yellow-Fluorescent Protein (YFP) ORF at its C-terminal. Within this 7415 basepair (bp) plasmid are also encoded, ampicillin resistance gene (AmpR) and the Hygromycin resistance gene (HygrR). The tetracycline inducible operator (tet) is present to induce expression of UMOD-YFP fusion. The various available sites for restriction enzymes are shown. This image was created using SnapGene visualisation software.

6.2.2.4 Bacterial Cultures

All bacterial work was carried out under sterile conditions by keeping items under close proximity to a Bunsen flame. Tips, stripettes, and spreaders were sterilised where possible before use. For cultural maintenance Ampicillin (100µg/mL) and Kanamycin (50µg/mL) were thawed on ice. These were added to L-Agar and Luria-Bertani (LB) broth. Plates and cultures were stored at 4°C.

6.2.2.5 Transformation of chemically competent cells

Stellar (Takara Bio) chemically competent cells were thawed on ice prior to incubation with the plasmid DNA. The cells and DNA were gently mixed and incubated for 30 minutes on ice, gently agitating every few minutes. The cells were incubated at 42°C for 30 seconds to encourage DNA uptake (transformation), after which cells were given a recovery period on ice for 5 minutes. The transformed cells were grown in S.O.C. medium

(ThermoFisher Scientific, UK) and incubated at 37°C with orbital shaking at 200xg for 1 hour. These cells were then spread onto Agar plates with the respective antibiotic before inverted overnight incubation at 37°C.

Positively transformed cells were selected by the presence of clear, individual colonies. These were isolated with sterile pipette tips and used to inoculate 5mL of Luria-Bertani (LB) (ThermoFisher Scientific, UK) broth with the respective antibiotic for 18 hours in a shaking incubator (200xg, 37°C). After inoculation, bacteria were either harvested for mini prep and/or transferred to a larger culture for midi prep (see Plasmid Preparation). Overnight cultures were stored as glycerol stocks (1mL of culture suspension in 50% glycerol in sterile water) and snap frozen with dry ice. These were then stored in -80°C for long-term storage.

6.2.2.6 Plasmid Preparation

To amplify plasmid DNA, DNA from individual bacterial colonies was prepared using Qiagen Plasmid Mini/Midi Prep Kits (Qiagen, UK). The bacterial culture was pelleted in a high-speed centrifuge (3200xg for 20 minutes) followed by lysis, neutralisation and precipitation with appropriate buffers provided by the kit. The lysate containing the plasmid DNA is cleared by centrifugation. The supernatant is then collected and transferred to a resin that binds the plasmid DNA. The subsequent bound DNA is washed via vacuum manifold before it was eluted in Tris-EDTA buffer (10mM Tris-Cl, 1mM EDTA; pH 8.0). The concentration of DNA and the purity was determined by NanoDrop 2000 spectrophotometer (Denovix) by measuring absorbance at 260nm. This was used to calculate the concentration in ng/µL and the DNA purity with A260/A280 ratio. These were then stored at -20°C.

6.2.2.7 Agarose gel electrophoresis

In order to check the ligation products and successful amplification of DNA, the samples were resolved according to their size. Also, the products were compared to the parental plasmids to check proper ligation. The agarose gels (1% w/v) were prepared in Tris-acetate-EDTA buffer (40mM Tris-Base, 20mM Acetic Acid, 1mM EDTA in dH_2O, pH 8.5) and boiled until dissolved. To visualise the products, double-stranded DNA was stained with addition of SYBR Green 1 Nucleic Acid Gel Stain (0.1µL/mL). The gel was set at room temperature for 10 minutes, after which the sample were added (final concentration of 150-300ng). The gels were run at 100V for 1 hour (BioRad, UK). The gels were visualised using the BioRad Imaging System and Quantity One software

(BioRad, UK). Plasmids were sequenced using gene specific primers and Eurofins TubeSeq Service to confirm sequence ligation.

6.2.2.8 Stable cell generation

Flp-In™ T-REx™ 293 (293FT) Cell Lines (Thermo Fisher Scientific, UK) were transfected with the FRT/TO-UMOD-YFP the day after plating using Lipofectamine 2000 Reagent (Invitrogen, #10696153) according to manufacturer's instructions in 6-well plates. This is achieved via the Flp-In system and Flp-mediated recombination (Figure 6.2). The pCDNA5-FRT/TO expression vector with UMOD-YFP is cotransfected with the pOG44 plasmid into the Flp-In FT-293 cell lines at 3 different ratios (high: 12µg pOG44 + 1µg pcDNA5-FRT/TO, medium: 9µg pOG44 + 1µg pcDNA5-FRT/TO, and low: 5µg pOG44 + 1µg pcDNA5-FRT/TO). The Flp recombinase from pOG44 catalyses homologous recombination event between the FRT sites in the host cells and the pcDNA5/FRT expression vector. This integration confers Hygromycin resistance and Zeocin sensitivity. The Lipofectamine 2000 Reagent was added at a volume of 3µL to a 12-well plate to Opti-MEM. In a separate 1.5 mL Eppendorf tube, 1µg of plasmid DNA was added to 125µL of Opti-MEM. These were incubated at room temperature for 5 minutes, before the combining both solutions in the wells of the 12-well plate. This was left to incubate at room temperature for 30 minutes. The resulting transfection mixture was added to the FT-293 cell culture in the 6-well plates in a dropwise manner and left to incubate for 24 hours at 37°C.

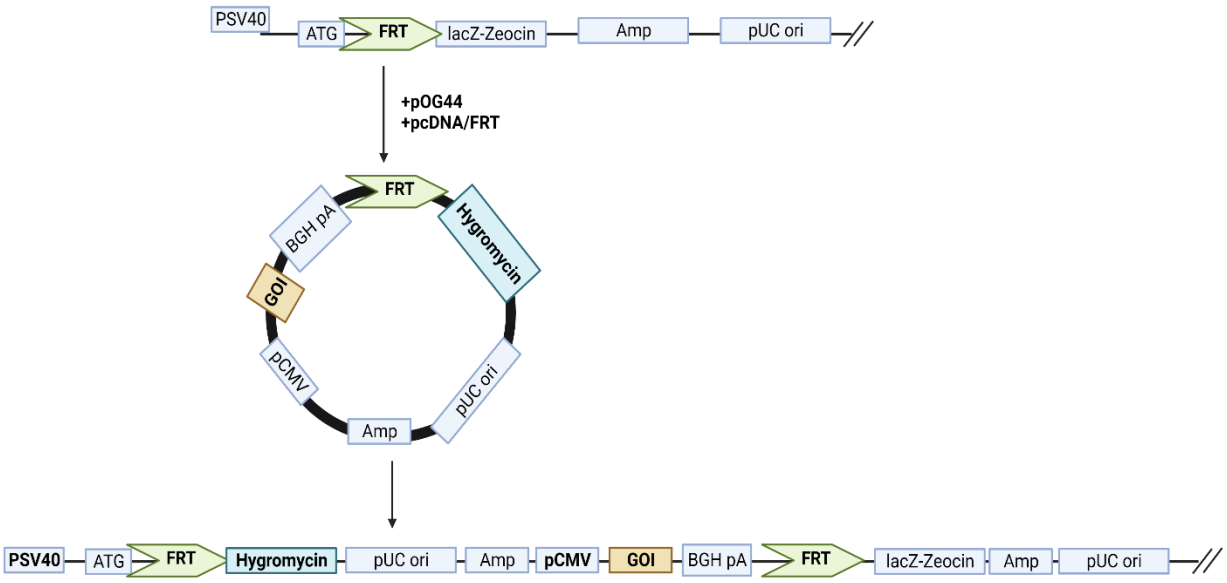

Figure 6.2 Diagrammatic Representation of The Flp-In System
Diagram of explaining the key steps in the Flp-In System (ThermoFisher Scientific, UK). In this system, the pFRT/lacZeo site is transfected into the HEK-293 cells the generate the stably expressing Flp-In™ T-REx™ 293 Cell Lines (ThermoFisher Scientific, UK). Following this, the pcDNA5/FRT expression vector containing the gene of interest (GOI), in this case: UMOD-YFP) is co-transfected alongside pOG44 into the Flp-In™ T-REx™ 293 Cell Line. The Flp recombinase enzyme expressed in the pOG44 catalyses the homologous recombination of FRT sites between the host cell and expression vector. Integration of this plasmid construct into the host genome confers hygromycin resistance and Zeocin™ sensitivity following transcription of the gene of interest (GOI). PSV40, mutated SV40 early promoter that controls expression of hygromycin resistance; ATG, initiation codon of the Invitrogen™ lacZ-Zeocin™ fusion gene; FRT, Flp Recombination Target; Amp, Ampicillin Resistance Gene; pUC ori, origin of replication; BGH pA, BGH polyadenylation signal; pCMV, CMV promoter that controls stable expression of the GOI. Image was adapted from ThermoFisher Scientific, UK.

The ratio of pcDNA5 and pOG44 that shows the most viability under an inverted microscope is then subcultured into a T25 flask using Trypsin/EDTA. Successfully transfected FT-293 cells were grown in DMEM media (as mentioned earlier) and selected for by addition of 50µL of Hygromycin stock (100mg/mL) after 4-5 days. Growth is monitored daily under phase contrast inverted microscope. Once visible colonies form, 75µL of Blasticidin stock (10 mg/mL) is added to the DMEM with Hygromycin (concentration 50µg/mL).

For induction of UMOD-YFP expression, cells were administered 1:1000 tetracycline HCL (10mg/mL stock) to the working DMEM once cells had reached 80% confluence. This was maintained for 24 hours at 37°C. See individual chapter methods for further analyses performed on these cells.

6.3 Results

6.3.1 Characterisation of primary TAL cell lines

A series of optimisation experiments were performed to ensure optimum growth of primary mTAL cells in culture. We observed that primary mTAL cells cannot grow in culture flasks and prefer growth on 6-well or 12-well plates coated with a poly-D-lysine substrate. In addition, these cells cannot be subcultured, whereby conditions of trypsinisation causes cell death. In terms of conditions of growth, it was observed that these cells prefer growth on a poly-d-lysine substrate. The cells grow into a confluent monolayer after 3-5 days in culture, with an optimum concentration of 10% FBS. The speed of confluency may be influenced by the type of media used, specifically REGM media produced by PromoCell was found to be most efficient, with cells reaching confluency in 3 days. Overnight or 2-hour starvation periods prior to salt loading is impossible due to increased stress of cells and was thus discontinued. The primary mTAL culture begins as individual tubules in suspension (Figure 6.3), before outward expansion of epithelial cells and dome structure formation at day 2 (Figure 6.3), and ultimately resulting in confluent monolayers by joining of dome structures at days 3-5 (Figure 6.3).

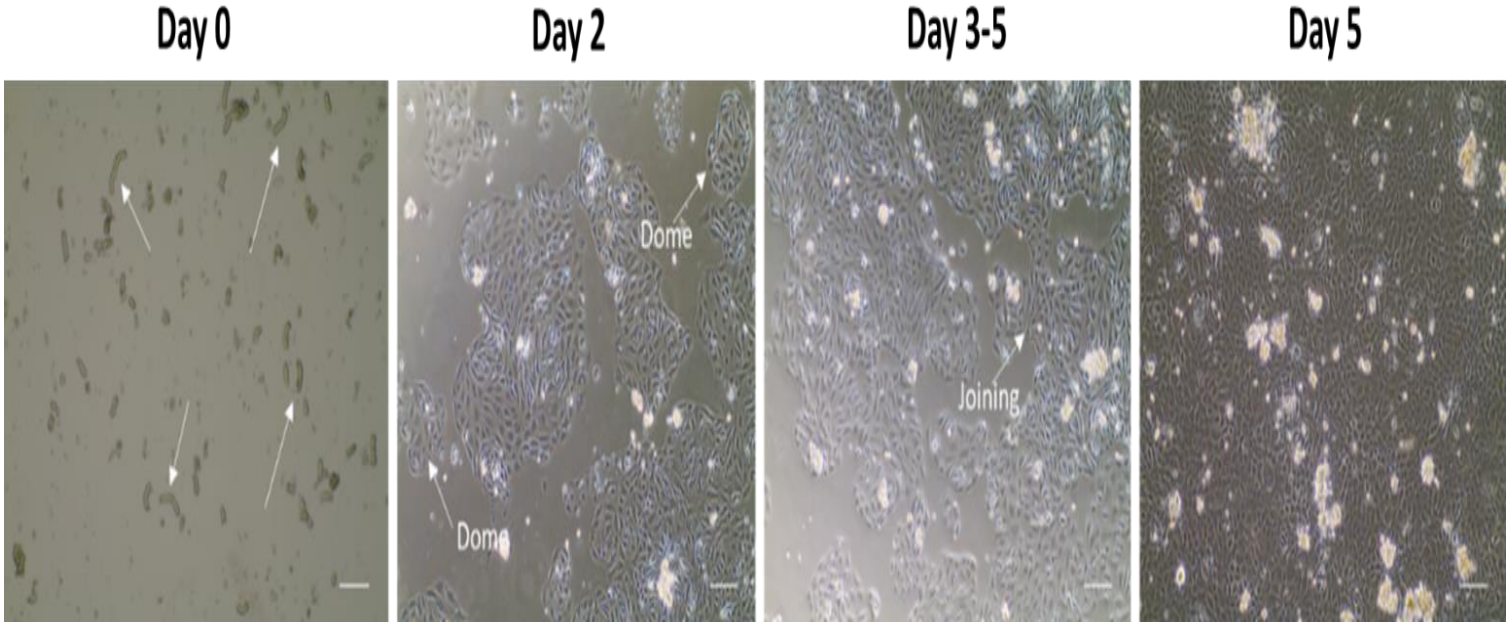

Figure 6.3. Characterisation of the growth of primary mTAL epithelial cell cultures over 5 days. Inverted phase-contrast microscope images of mTAL primary cell cultures at various stages (day 1 to day 5) of their growth *in vitro.* At day 0, white arrows highlight the individual tubules floating in suspension after isolation from the medullary region in kidneys of 5-week-old WKY rats. Day 2 shows the expansion of epithelial cells growing outwards from the initial tubules and forming characteristic dome structures. Day 3-5 exhibits the joining of these dome structures and reaching of confluency of the mTAL epithelial cells. At day 5, the cells have reached 90-100% confluency and form a monolayer. At this stage, cells would be incubated with compounds, such as NaCl or calcium, for testing. Images are taken at 20X magnification and scalebar is equivalent to 100µm.

It has previously been demonstrated that calcium and the G-protein coupled receptor calcium-sensing receptor (CaSR) plays a key role in the excretion of uromodulin by the

TAL (Tokonami et al., 2018a). To determine optimum composition of calcium in the media for growth of the primary mTAL cells, we performed optimisation experiments with a range of extracellular calcium concentrations. An initial characterisation study revealed no major changes in mTAL cell morphology following NaCl loading with no calcium (0mM), physiological calcium (1mM) or higher calcium levels (3mM) compared to pre-incubation images Figure 6.4 Given that 1mM of calcium is considered the typical physiological concentration (Bagur and Hajnóczky, 2017), this concentration was chosen for future experiments.

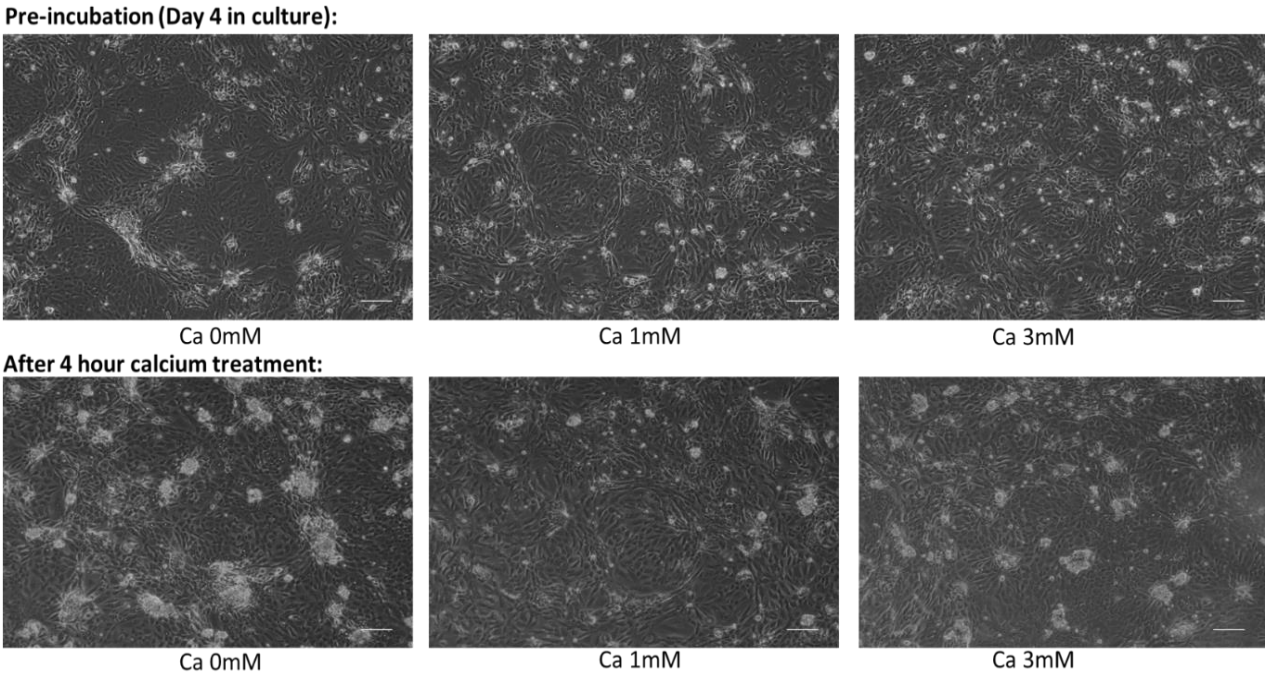

Figure 6.4. Calcium at varying concentrations does not influence the morphology of primary mTAL epithelial cell cultures.
Inverted phase-contrast microscope images of mTAL primary cell cultures incubated with calcium (0, 1, and 3mM) for 4 hours. There are no major differences in the cells after the calcium incubation period. Images are taken at 20X magnification and scalebar is equivalent to 100µm.

6.3.2 Effect of salt stress on UMOD secretion from primary TAL cells

To determine the effects of salt stress on mTAL primary cells, confluent primary mTAL cells were exposed to media with an increased salt content (+154mM NaCl) for 4 hours and compared to controls that received basal media. An increased salt concentration resulted in gross morphological changes in the cell monolayer relative to controls, with large gaps present between cells and increased cell debris (Figure 6.5). This would suggest that the cells are undergoing significant stress.

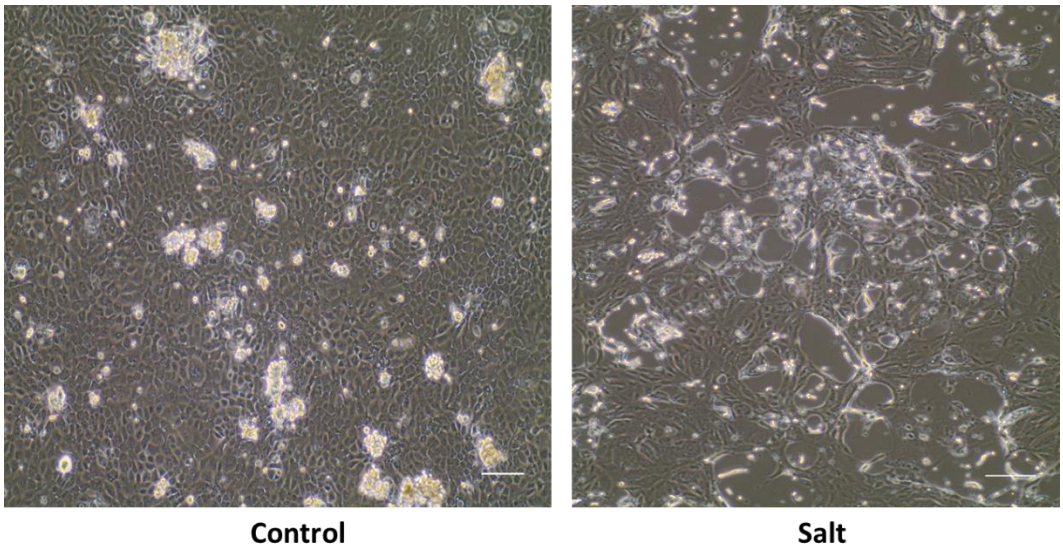

Figure 6.5. Salt stress alters the morphology of primary mTAL epithelial cells.
Inverted phase-contrast microscope images of mTAL primary cell cultures incubated with salt (an additional 154mM to the NaCL found in the basal media) for 4 hours. The control received only basal media. The salt-incubated cells show a change from a typical polygonal shape with a centrally located nucleus (cuboidal epithelial cells) observed in the controls to stretched out cells with large gaps in the monolayer. This is indicative of stress in the cells. Images are taken at 20X magnification and scalebar is equivalent to 100µm.

To analyse the effects of salt stress on UMOD protein expression and trafficking, mTAL primary cells were subfractionated into membrane and cytosolic fractions. There was no statistically significant difference in UMOD protein levels in the membrane fraction after salt stress (Figure 6.6). However, the proportion of UMOD in the cytosol was significantly lower in the salt exposed cells compared to the controls (26.82 ± 7.14 vs. 68.70 ± 4.02, $p<0.05$) (Figure 6.7). This would suggest a retention of UMOD in the cells of the salt-stressed mTAL cells.

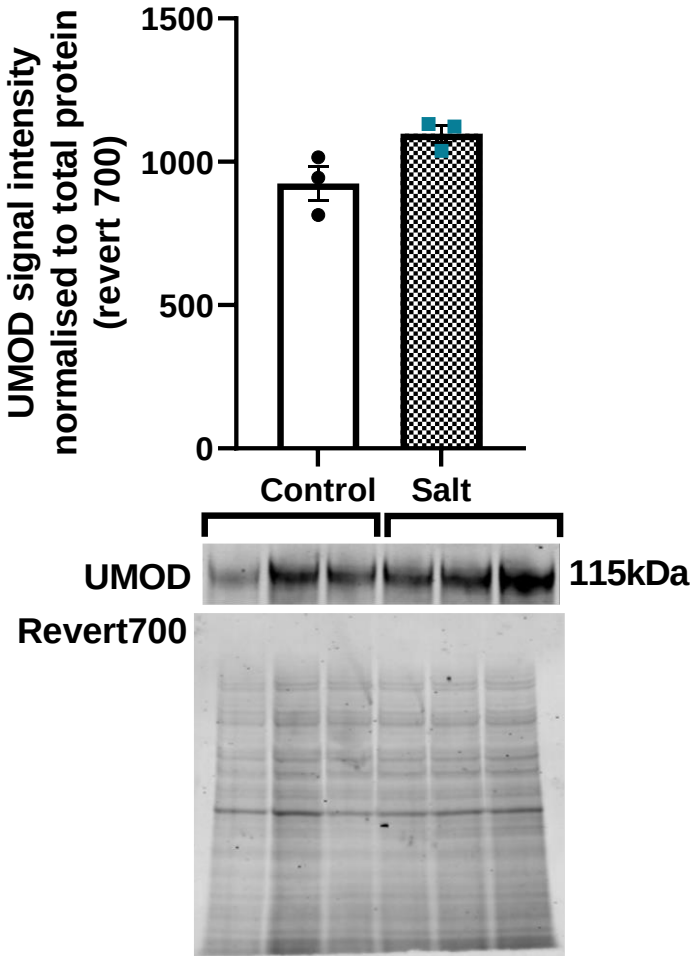

Figure 6.6. Salt incubation does not alter UMOD protein levels in the plasma membrane of primary mTAL epithelial cells.
Primary mTAL epithelial cell cultures were subjected to 4 hours of higher salt concentrations in the media (+154mM NaCl on top of basal content, Salt) or basal media (Control). Cells were lysed and subfractionated into plasma membrane portions of the cells. Representative Western blot images are shown for immunoblots for UMOD. The UMOD signal was normalised to total protein stain (Revert700).

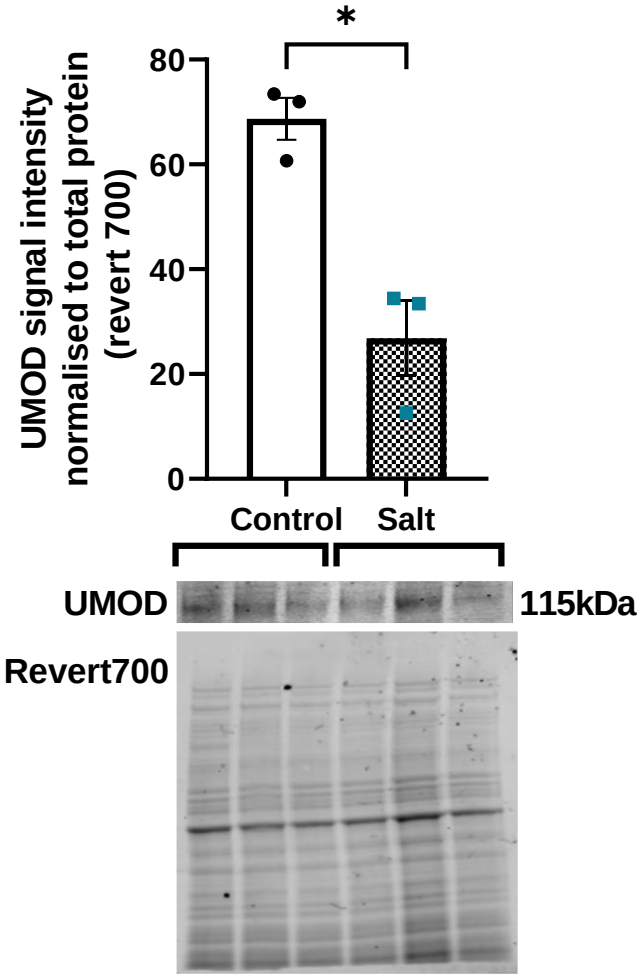

Figure 6.7. Salt incubation lowers UMOD protein levels in the cytosol of primary mTAL epithelial cells. Primary mTAL epithelial cell cultures were subjected to 4 hours of higher salt concentrations in the media (+154mM NaCl on top of basal content, Salt) or basal media (Control). Cells were lysed and subfractionated into cytosolic portions of the cells. Representative Western blot images are shown for immunoblots for UMOD. The UMOD signal was normalised to total protein stain (Revert700).

To characterise the suitability of primary mTAL cells as a model for the molecular study of UMOD, the expression of UMOD was monitored over several passages. There was a considerable reduction in the expression of UMOD with the higher passage number, reaching to almost undetectable delta Ct values at p8 (Ct 34 (Figure 6.8). This would imply that UMOD expression is lost during subculturing.

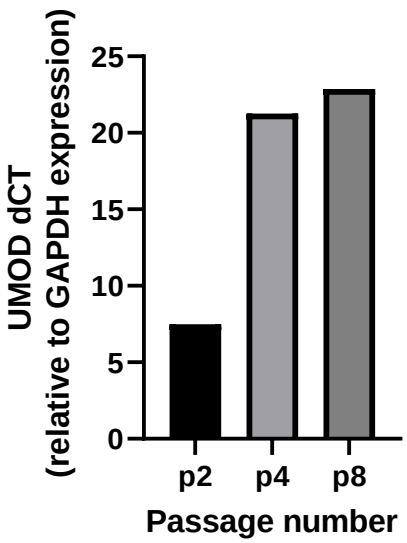

Figure 6.8. Primary mTAL epithelial cells have reduced UMOD mRNA expression with increasing passage number.
The graph shows UMOD mRNA expression levels in primary mTAL epithelial cells at varying subculturing stages (p=passage number). UMOD mRNA expression is normalised to GAPDH housekeeping expression.

6.3.3 Characterisation of HEK UMOD-YFP cell line

Since the primary mTAL cell line was not suitable for the molecular study of UMOD, a separate cell model was required with stable expression of UMOD. For this reason, a transgenic UMOD expressing 293FT cell line was generated. The details of the generation of the UMOD expressing 293FT cells can be found in the methods section (Section 6.2.2). Following amplification of YFP, UMOD, and pcDNA5 FRT/TO Flp-In expression vectors, the appropriate products was confirmed by band size on agarose gels (Figure 6.9). The UMOD band size corresponded to 2kb, whereas YFP at 0.8kb (Figure 6.9). The pcDNA5 FRT/TO vector corresponded to approximately 5500kb (Figure 6.9). These all aligned with their expected sizes.

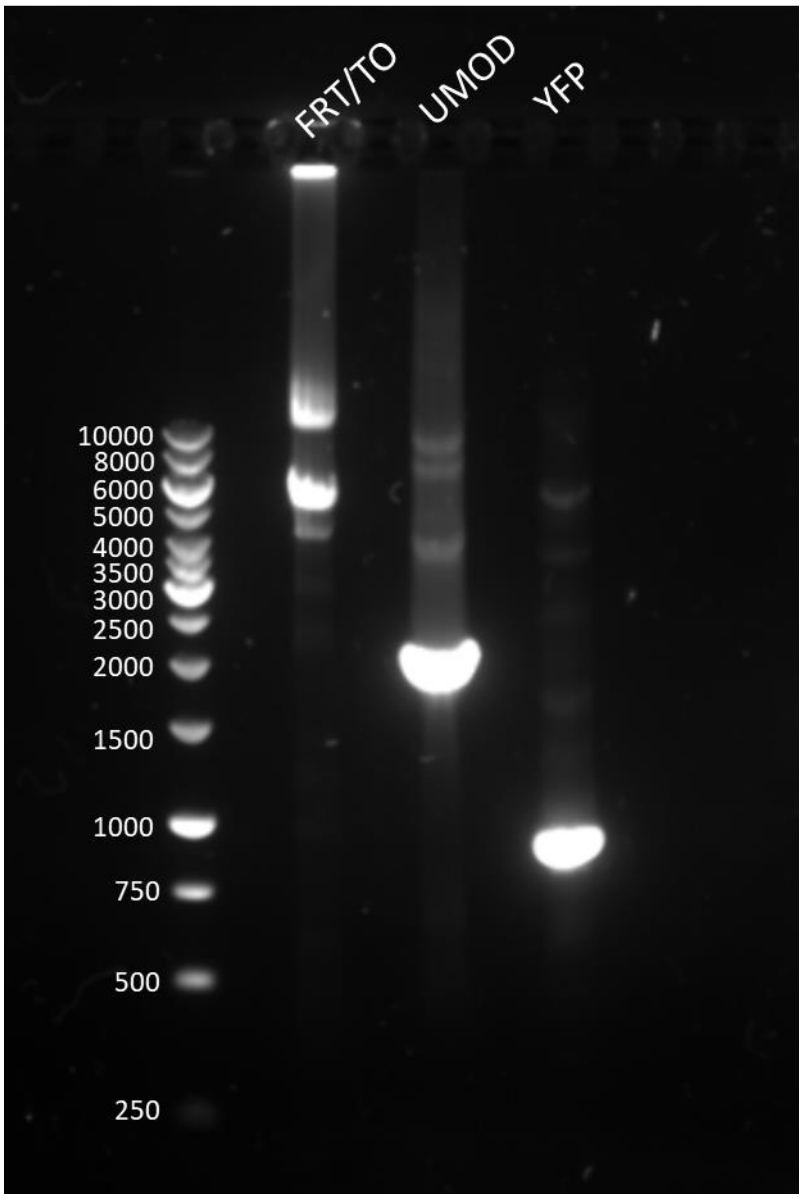

Figure 6.9. Agarose gel confirming PCR products of YFP, UMOD, and pcDNA5 FRT/TO expression vectors. A 1% agarose gel was used for the separation of the PCR products by size, with the ladder on the left-hand side representing markers in base pairs (bp). Gel was stained with SYBR Green 1 Nucleic Acid Gel Stain. The FRT/TO plasmid band corresponds to 5500 bp, the UMOD cDNA is 2000 bp in size, and the YFP band is 800 bp.

Following amplification of the vectors and inserts, as well as In-Fusion ligation of the resulting PCR products, the ligated UMOD-YFP vector was amplified using *E. coli* Stellar™ competent cells after transformation. After confirmation of correct plasmid amplification with colony PCR, whereby DNA is extracted from the *E. coli* and resolved on an agarose gel (resulting band is 3 kilo basepairs (kbp) larger than the pcDNA5 FRT/TO vector), the DNA was further amplified using Mini and Midi Prep. Next, the UMOD-YFP plasmid was transfected into 293FT cells, which allow transient expression of the human UMOD-YFP fusion protein upon tetracycline induction. To test for successful transformation of 293FT cells, an immunoblot for UMOD was conducted and the

appropriate size band at 115kDa was detected (Figure 6.10). Similarly, to check that the YFP was indeed fused to UMOD, an immunoblot was performed and the band size of 115kDa observed (Figure 6.10). This would suggest that UMOD-YFP was being successfully expressed from the 293FT cells.

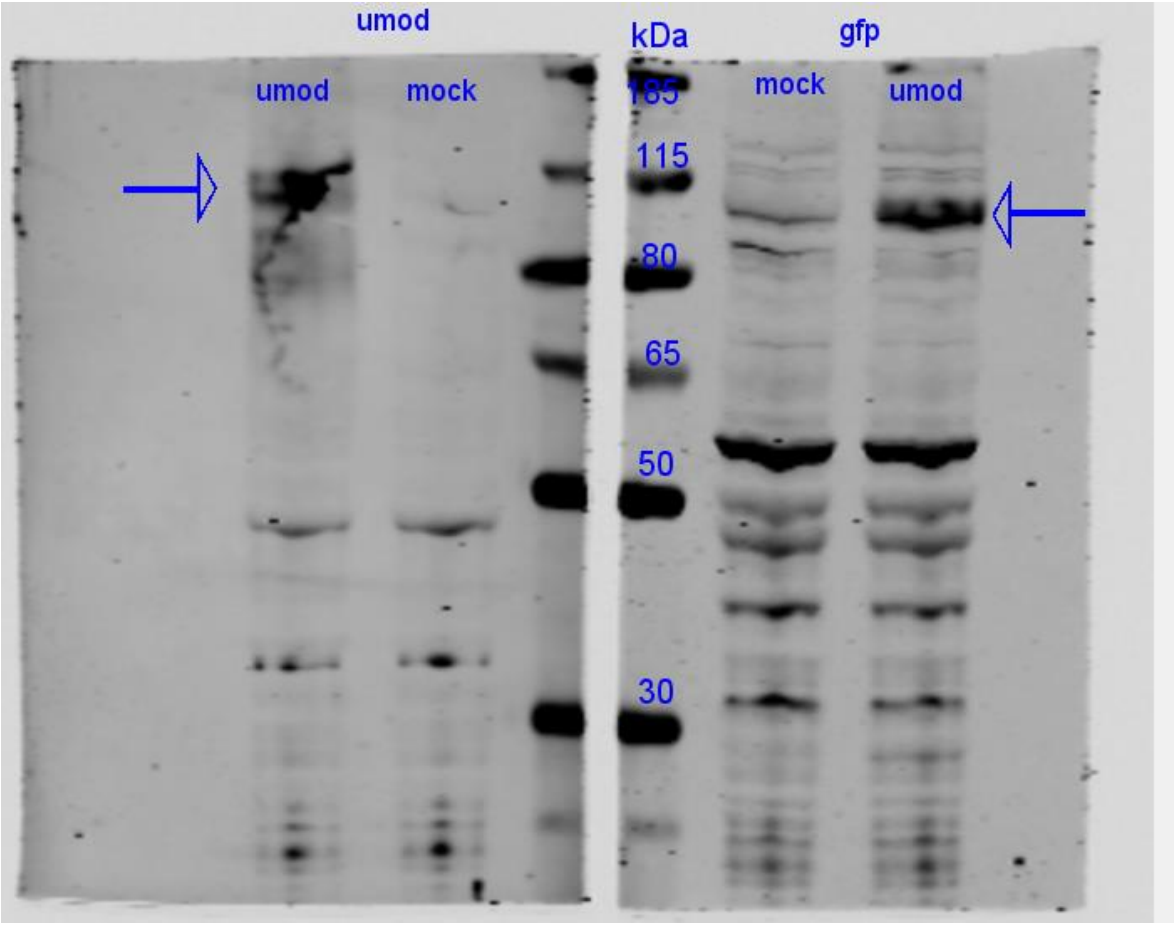

Figure 6.10. Confirmation of expression of UMOD-YFP fusion protein in 293FT lysate after induction with tetracycline.
Western blot for UMOD (labelled "umod") and YFP (labelled "gfp") using protein lysate of UMOD-YFP expressing 293FT cells after induction by 24 hours incubation with tetracycline. Protein marker and relative sizes in kDa are shown in the centre of the image. Blue arrows point to the band that represents UMOD-YFP.

To further confirm successful transfection and induction of UMOD-YFP expression in the 293FT cells, an immunofluorescence analysis for YFP fluorescence was performed (Figure 6.11). There were roughly 40% successfully transfected cells based on fluorescence analysis alone (Figure 6.11), which is to be expected for transient transfection. Therefore, the next stage was to generate stably expressing UMOD-YFP 293FT cells.

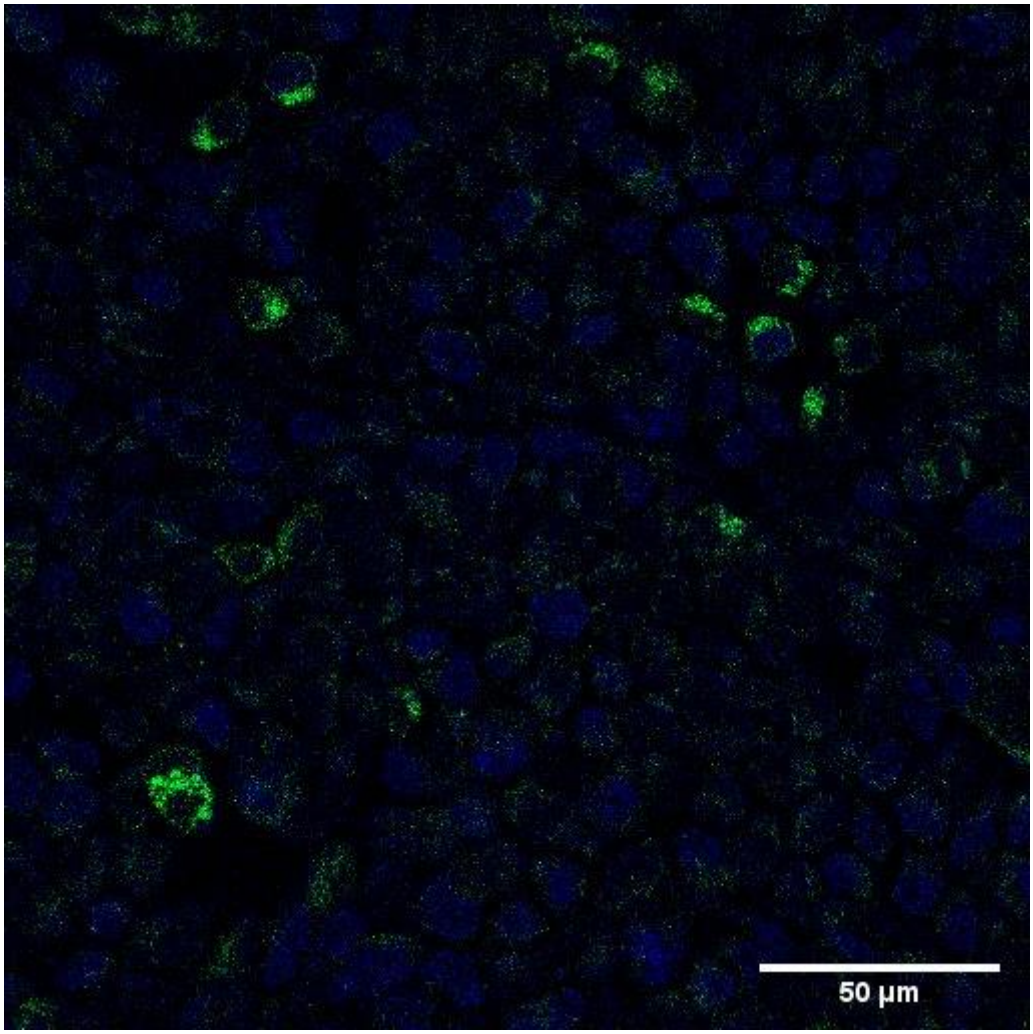

Figure 6.11. Immunofluorescence analysis confirms UMOD expression in tetracycline-induced UMOD-YFP 293FT cells after transient transfection.
Representative immunofluorescence image showing YFP (green) representing UMOD expression in tetracycline-induced 293FT cells after transfection with the UMOD-YFP expression vector. Image at 40X magnification and scale bar represents 50µm.

The Flp-In^{TM} recombination system was utilised and is detailed in the methods section (Section 6.2.2). Briefly, the system uses homologous recombination to integrate the UMOD-YFP expression vector into the genome of the 293FT cells, as well as conferring Hygromycin antibiotic resistance to the cells to allow for selection. Immunofluorescence analysis for UMOD was performed after tetracycline induction for 24 hours on positively selected 293FT cells. There was a clear pattern of expression of UMOD in the cytosol of the cells and near the ER, as proven by overlap with the ER marker calnexin (Figure 6.12). The negative control without tetracycline induction showed no UMOD expression, which suggests UMOD expression is selective and inducible.

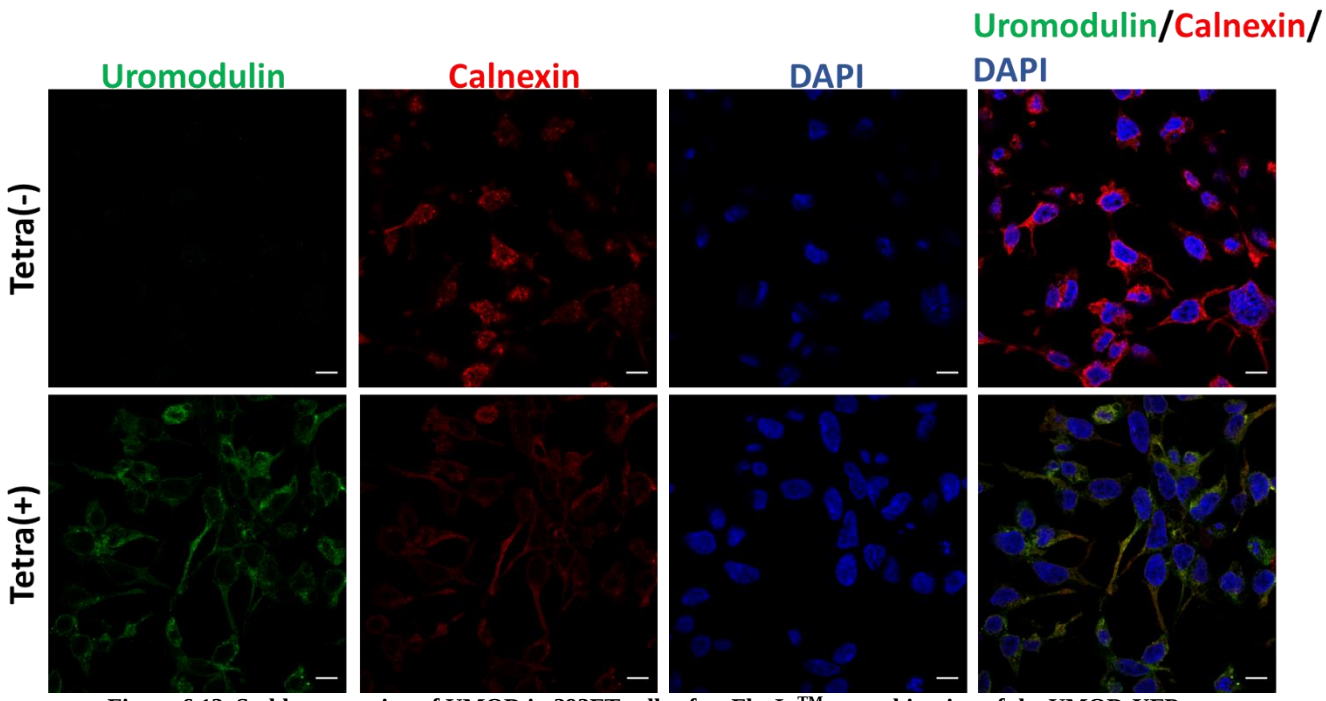

Figure 6.12. Stable expression of UMOD in 293FT cells after Flp-In^{TM} recombination of the UMOD-YFP vector. Confocal imaging of 293FT cells that are stabling expressing the integrated UMOD-YFP expression vector under a tetracycline promoter. UMOD (green), the ER marker calnexin (red), nuclear DAPI staining (blue) and an overlay of both UMOD + calnexin (yellow) signals are shown. Representative images are shown of cells incubated with tetracycline for 24 hours ("Tetra(+)") and without ("Tetra(-)"). Images were taken at 40X magnification and scale bar represents 50µm.

6.4 Discussion

The previous chapters focused on establishing the relationship between UMOD trafficking and salt but lacked a suitable cell model for further molecular studies. The characterisation studies with primary mTAL epithelial cells in this chapters have demonstrated the challenges stemming from their culture and the stability of their expression of UMOD. Exposure of salt to primary mTAL cells has an opposite effect on UMOD compared to *in vivo* findings shown in earlier chapters, whereby its trafficking to the membrane is increased. This is paralleled by significant changes in cell morphology. The fact that UMOD expression is lost with subculturing of primary mTAL cells makes them unsuitable models for the molecular mechanistic studies of UMOD. Instead, a transgenic cell model was generated: UMOD-YFP expressing 293FT cells. This model offers the ability to induce UMOD expression via tetracycline at user-defined timepoint. Moreover, YFP-tag enables multiple experimental advantages, from live cell imaging to immunoprecipitation assays.

Our study has started to unravel the effect of extracellular regulators on UMOD secretion, in this case calcium. We demonstrate that calcium has no effect on mTAL cell morphology. Prior studies have associated apical calcium-sensing receptor (CasR)

signalling has with the secretion of uromodulin in mTAL (Tokonami et al., 2018a). More specifically, mice with activating mutations in CaSR showed a lower urinary secretion of UMOD, whereas mice with inactivating mutations in the receptor had enhanced UMOD secretion (Tokonami et al., 2018a). Therefore, further investigations into the CaSR signalling mechanisms and their involvement in the UMOD secretory pathway will be necessary using the primary mTAL cell model. It will be important to consider and regulate calcium levels in media compositions of cell models for the molecular study of UMOD secretion.

The drastic changes in mTAL morphology upon salt incubation clearly demonstrates stress and does not match physiological conditions. Salt stress can cause significant damage to renal cells by disrupting homeostasis and inducing apoptosis. Exposing renal cells to high salt concentrations induces oxidative stress, leading to cellular damage, apoptosis, and inflammation (Araujo and Wilcox, 2014). Other studies have shown that high salt concentrations also affect the cellular functions of renal cells, such as ion transport and protein synthesis (Barnett et al., 2022, Wang et al., 2016). (It is likely for these reasons that drastic changes in mTAL primary cell morphology are observed, even within the short time frame of 4 hours. Although, TAL tubules are exposed to higher osmotic pressures *in vivo*, reaching up to 1200 mOsm/kg in TAL at the tip of the medulla in humans (Zacchia et al., 2018) compared to the 600 mOsm in the cell culture experiments performed in this chapter . It is likely that the 3D environment and tissue organisation are contributing to the higher osmotic pressure resistance *in vivo* (Kourouklis et al., 2023). In this regard, the 2D primary mTAL cell model are not suitable for the molecular mechanistic studies of the effects of salt on UMOD trafficking.

A significant disadvantage to primary mTAL cells is the loss of UMOD expression with passaging. The transgenic UMOD-YFP expressing 293FT cell model generated here offers a suitable solution to this challenge. The cell model is inducible and UMOD is fluorescently-tagged, which would lend itself to live cell tracking experiments (Wiedenmann et al., 2009). This would greatly enhance the understanding of UMOD trafficking from the ER to the plasma membrane, and the dynamics of retention with salt loading as shown in previous chapters. In addition, the YFP tag will allow for co-immunoprecipitation assays with GFP-trap beads to determine protein-protein interactions of UMOD and whether these change with salt loading (Yilmazer et al., 2023). There is a current lack of understanding of UMOD interactors and regulators in the TAL, as well as signalling components involved. For these reasons, this cell model would be the most ideal model for studying the relationship between salt and UMOD trafficking.

There are, however, a number of limitations associated with the UMOD-YFP 293FT cell model presented in this chapter that require addressing. For one, the limitations of a 2D cell model still apply, including the lack of understanding of the effects of salt and UMOD on the cells other than TAL in the nephron. To this extent, a 3D kidney cell model would be more beneficial as it takes into account the microenvironment of the whole kidney, as well as replicating certain disease conditions more closely (Kourouklis et al., 2023). Next, while the cells are based on kidney cells, they are not TAL epithelial cells. This makes it difficult to make one-to-one comparisons, as signalling systems and mechanisms may differ slightly. A potential solution to this may be to transfect the UMOD-YFP plasmid generated here into the primary mTAL epithelial cells, thereby overcoming the loss of endogenous UMOD expression with subculturing.

In conclusion, this chapter presents a novel transgenic UMOD cell model for the molecular study of UMOD. This cell model holds several advantages over primary mTAL cells, the prime benefit being the inducible nature of UMOD expression. The model will not only be useful for unravelling the interactions of salt with UMOD, but also has the potential to uncover several other signalling components and interactors for many disease contexts, including hypertension. Future experiments will need to focus on characterising the effects of various salt concentrations on the UMOD 293FT cells and whether they undergo similar stress effects as seen for the primary mTAL cells.

Chapter 7: General Discussion

Understanding the relationship between salt, UMOD, and hypertension is of growing interest to kidney research (Mary et al., 2022). However, studies are often contradictory and lack mechanistic insights. The work detailed in this thesis identified novel effects of salt loading at a physiologically relevant concentration on UMOD excretion and blood pressure in chronic hypertensive SHRSP rat models. There is a distinct decrease in urinary UMOD excretion with salt loading independent of blood pressure changes, which is paralleled by retention of UMOD in the ER of the TAL region in hypertensive animals. Previously, only the reverse had been studied; the effect of UMOD on sodium homeostasis (Graham et al., 2014, Pruijm et al., 2016a, Trudu et al., 2013b). Clinical studies investigating the relationship between salt and UMOD excretion are currently limited and would greatly enhance the translatability of the findings discussed in this thesis. An interventional study in a family-based Chinese cohort reported that a high salt intake (7g of salt for 7 days, followed by 18g for an additional 7 days) resulted in a reduction in 24-hour urinary UMOD excretion (Du et al., 2021). Future studies should be conducted in more diverse participants, exposed to longer salt loading periods. Also, both normotensive and hypertensive individuals should be analysed to identify any notable differences in urinary UMOD excretion.

The importance of salt in regulating urinary UMOD excretion

This thesis provides further insights into the changes in UMOD excretion without the confounding effects of blood pressure, specifically with intermittent and long-term salt loading in normotensive WKY models. Regulating UMOD urinary excretion rate is one of the first points of influence for salt, and this is reversible to an extent. This is especially pertinent given that previous studies have utilised very high, non-physiological concentrations of salt (>1%) that would often be accompanied by significant kidney damage (Ying and Sanders, 1998, Olinger et al., 2019). In this regard, it would be reasonable to assume that the use of 1% NaCl in experiments reported in this thesis is more accurate to regular human salt intake and therefore a better representation of the UMOD excretion patterns.

A critical point of influence for salt on UMOD is retention in the ER, although the precise molecular dynamics and components involved in this process remain unknown. The fact that urinary UMOD excretion is occurring also in high-salt conditions, but at a reduced rate, suggests that salt is directly impacting release of UMOD from the ER, the rate-

limiting step in UMOD secretion. The fact that BiP and PDI expression were upregulated in long term salt loaded WKY indicates the importance of the chaperone and folding systems in UMOD retention times. This is highlighted by studies with immortalised mouse TAL cells expressing ADTKD-UMOD, which contains mutations that results in ER accumulation of UMOD (Schaeffer et al., 2017). In this case, BiP and PDI expression was also significantly increased (Schaeffer et al., 2017). It may be postulated that UMOD enters the calnexin cycle to be properly folded (Ellgaard and Helenius, 2003). In the calnexin cycle, proteins carrying monoglucosylated glycans bind to lectin chaperones calnexin and calreticulin, which recruit a variety of function-specific chaperones to mediate protein disulphide formation, proline isomerisation, and general protein folding (Kozlov and Gehring, 2020). By directly binding the N-glycan on proteins, calnexin has been demonstrated to retain GPI-anchored proteins such as UMOD in the ER until they are correctly folded (Guo et al., 2020). It may be hypothesised that increased sodium within the TAL cells, resulting from salt loading, is directly interacting with the components of the calnexin cycle thereby retaining UMOD as a natural homeostatic mechanism to prevent salt stress damage. However, with continued exposure to salt stress this overwhelms the folding system resulting in ER stress and ultimately kidney damage. Intracellular molecular imaging would provide nanometre resolution of UMOD trafficking dynamics in the ER following salt exposure and precise retention times (Crivat and Taraska, 2012), which would greatly be facilitated by the UMOD-YFP 293FT cell model generated as part of my studies.

The influence of salt on circulating UMOD

Although it is well established that salt influences UMOD urinary excretion, the role of salt in regulating serum UMOD is still unclear. It has previously been reported that higher serum UMOD levels are associated with a lower risk of mortality and CVD in older adults (Steubl et al., 2020a). It may be that the lack of change in serum UMOD in the long-term salt-loaded normotensive rats in this work may be due to the low severity of the phenotype, unlike in the chronic hypertensive SHRSP rats. This is also apparent in human populations, whereby severe disease phenotypes show significant changes in serum UMOD; such as the inverse association of serum UMOD with aortic stiffness reported in type 1 diabetic adolescent individuals (Wiromrat et al., 2019a). It is clear that serum UMOD has key protective roles in renal physiology, given that renal transplant recipients with lower circulating UMOD levels face higher risk of organ failure or rejection (Bostom et al., 2018, Steubl et al., 2017). It has also been demonstrated to act as a kidney and systemic oxidative stress inhibitor through the inactivation of the TRPM2 channel (LaFavers et al., 2019). It is

highly possible that the answer to the relationship between serum UMOD and urinary UMOD lies within its intracellular trafficking within the TAL epithelial cells and unravelling potential mechanisms will be paramount to future investigations. Glycosylation is likely to play a critical role in the polarised trafficking UMOD, given that 30% of the molecular mass of UMOD is made of glycan residues (van Rooijen et al., 1999). In fact, N-glycans are responsible for the apical targeting of GPI-anchored proteins in polarised epithelial cells (Pang et al., 2004). A study using aptamer-based assays reported enzymes that write glycan marks on UMOD that may be related to its complex glycosylation pattern and clearance (Li et al., 2022). It is conceivable that these glycan marks differ between serum and urine forms of UMOD and could be recognised by differing receptors. Deciphering these glycan signals on UMOD will require proteomic analyses to identify individual glycan chains, and following this, cell mutagenic experiments expressing different forms of the glycan chains on UMOD to understand the function of each glycan chain.

The limitations of the WKY model

The normotensive WKY rat by definition is salt-insensitive (Clark et al., 1996) and does not fully recapitulate the chronic hypertensive SHRSP model. Microarray expression profiling and qPCR experiments identified a 6-Mbp region harbouring genes responsible for salt-sensitive blood pressure regulation specific to the SHRSP compared to WKY, including physiological candidate genes *Edg1* and *Vcam1* (Graham et al., 2007). WKY rats were chosen in this thesis to remove blood pressure as a confounding factor to uncover mechanisms involved in salt and its influence on UMOD trafficking and secretion. However, what are the other background factors that may be present in the chronic hypertensive background of the SHRSP that could influence UMOD trafficking? To further elaborate on the long-term salt loading findings presented in this work, an untargeted proteomic approach should be undertaken to uncover novel molecular components that may differ between WKY and SHRSP models, and by extension drive the SHRSP phenotype (Sobsey et al., 2020). Moreover, advancements in mass spectrometry technologies have enabled untargeted approaches on single-cells, meaning that individual TAL epithelial cells could be isolated from WKY and SHRSP kidneys before and after salt loading to reveal novel biological systems involved in UMOD trafficking (Beck and Geiger, 2022). A key example of the power of this approach is the peptidome analyses that have uncovered a range of UMOD peptides in the urine of various diseases (Mary et al., 2017, Krochmal et al., 2017a, Van et al., 2020, Wu et al., 2010, Pejchinovski et al., 2018).

Similarly, mass-spectrometry approaches will be paramount to discovering molecular regulators of UMOD trafficking and interactors with salt.

The role of inflammation and UMOD trafficking

The importance of inflammation in hypertension and vascular disease has been appreciated for decades (De Miguel et al., 2015) and TNFα production, a cytokine with proinflammatory and immunoregulatory effects, is increased in kidneys with salt loading (Ferreri et al., 2012) and attenuates levels of NKCC2 and UMOD mRNA in the TAL (Graham et al., 2014, Heitmeier et al., 2014). This thesis highlights ER stress as a potential driver of UMOD retention that underpins the chronic hypertensive phenotype. Importantly, ER stress is a known an activator of inflammation (Chipurupalli et al., 2021). A subsequent question that remains to be answered: what is the role of inflammation in salt loading, UMOD trafficking and ER retention, ER stress, and ultimately the progression of hypertension? It is understood that UMOD directly interacts with TNFα, though the molecular basis of such interaction is yet to be elucidated (Sherblom et al., 1988, Wu et al., 2012a). Studies have shown that NKCC2-dependent activation of NFAT5 is part of a signalling pathway that triggers TNFα production, thereby inhibiting NKCC2 activity by a negative feedback loop (Hao et al., 2013). It may be postulated that TNFα mediates Na^+ homeostasis by maintaining NKCC2 function, and that ER stress and continued TNFα would hinder this process, thereby leading to chronic hypertensive phenotype. Further molecular studies with inhibitors of TNFα are required to investigate the effects on UMOD trafficking and kidney damage during salt loading.

Complex 3D *in vitro* models as the future of UMOD studies

The nephron is a complex set of tissues, comprising multiple microenvironments that crosstalk with one another to maintain homeostasis (Khoshdel-Rad et al., 2022). This context is especially prevalent for UMOD, given that it interacts with proteins both within TAL and outside, such as the DCT (Voets et al., 2004, Nie et al., 2018, Boder et al., 2021). It is therefore prudent that model systems for the molecular study of UMOD trafficking would need to take these factors into account. The UMOD-YFP expressing cell model generated in this thesis will be limited by factors common to 2D cell cultures, including lack of cell-cell and cell-extracellular environment interactions, no *in vivo*-like microenvironment, changed morphology and way of divisions, loss of phenotype and polarity (especially in TAL with apical and basolateral compartments), and do not mimic physiological structure of tissues (Kapalczynska et al., 2018). In this regard, the use of 3D human kidney organoids would offer several advantages over 2D renal cell models, such as

multiple cell types (renal epithelial, stromal, and vascular cell types), modelling cellular physiology of the human kidney, high-throughput testing, modelling complex diseases such as AKI, as well as ability to generate patient-derived organoids for personalized medicine (Nunez-Nescolarde et al., 2022). The generation of 3D kidney organoids has been reported on in detail by the group Prof Nuria Montserrat (Selfa et al., 2021). hPSCs are induced for a short period of 4 days in a two-dimensional (2D) culture fashion toward posterior IM-like (PIM) cells that are then aggregated into 3D spheroids and cultured under organotypic conditions for 16 additional days. After aggregation, PIM-committed spheroids are kept in the presence of growth factors for 5 days to induce NPC commitment. Three additional days are then required for the formation of renal vesicle (RV) structures—the precursor structures of the nephrons—that appear within the organoids 24 h after complete growth factor removal due to a process of mesenchymal to epithelial transition. During the following 8 days, RVs acquire proximal–distal polarity and develop into nephron-like structures by recapitulating in vitro the process known as nephron patterning. Day 16 kidney organoids reveal the presence of segmented nephron-like structures containing glomerular-like structures with presumptive podocyte-like cells and tubular-like structures (including proximal and distal fates). It is at this point, UMOD expression has been reported in the early TAL structures of the kidney organoids (Garreta et al., 2019). A placement project was carried out in the laboratory of Prof Montserrat, outside of the work reported in this thesis, wherein the use of kidney organoids was investigated as a model for studying UMOD trafficking. Wholemount and paraffin section immunofluorescence staining for UMOD were conducted on day 23 hPSCs derived organoids, which showed punctate staining versus the clear pattern of UMOD expression around TAL structures seen *in vivo*. Moreover, expression of UMOD mRNA levels and protein levels were found to be very low, indicating that perhaps the model is still too immature for the study of UMOD at 23 days. Further maturation periods, for example for longer than 40 days as has been reported previously (Carrisoza-Gaytan et al., 2023), may improve expression of UMOD in these kidney organoids. Although the 3D human kidney organoid model is not yet fully established for the study of UMOD, it will be pivotal for future molecular studies of UMOD trafficking given its greater translatability to *in vivo* systems.

7.1 Final Conclusions

This thesis provides novel evidence on the effects of salt loading on UMOD trafficking in both normotensive and chronic hypertensive models. Salt is driving UMOD retention in the ER, thereby reducing urinary UMOD excretion. This process is accompanied by ER

stress over prolonged exposure to salt in the normotensive models, which matches the phenotype seen in chronic hypertensive rats, providing new perspectives into the development of hypertension and renal pathophysiology. The inducible UMOD-YFP expressing 293FT cell model generated here will be key in the next stage of research in unravelling the relationship between salt and UMOD, by providing molecular insights into the components involved in UMOD trafficking in both physiological and disease settings. The translation value of this research lies in the preclinical WKY rat and UMOD-YFP 293FT cell models, as well as the 3D kidney organoids, which will serve to discover new molecular mechanisms involved in salt and UMOD trafficking in the kidneys. Although these findings offer no immediate pathway to development of new therapies, they can then act as a stimulus for future clinical studies.

Chapter 8: Appendix

This Chapter outlines laboratory practices and methods common to more than one Chapter. Each subsequent results Chapter has a specific materials and methods section.

8.1 Materials

8.1.1 Laboratory-Prepared solutions

8.1.1.1 Phosphate Buffered Saline – PBS (20X)

For 1L:

Dissolve:

NaCl (Sigma-Aldrich, UK) - 160g

KCl (Sigma-Aldrich, UK) - 4g

KH_2PO_4 (Sigma-Aldrich, UK) – 4g

Na_2HPO_4 (Sigma-Aldrich, UK) – 23g

in 800 mL dH_2O. Mix using magnetic stirrer.

Adjust pH to 7.4.

Make up final volume of 1L with dH_2O.

Keep at room temperature for up to 24 months.

8.1.1.2 Phosphate Buffered Saline - PBS (1X)

For 1L:

Dilute 50mL of 20X PBS in 950mL of dH_2O.

Keep at room temperature for up to 24 months.

8.1.1.3 Tris-Buffered Saline – TBS (20X)

For 1L:

Dissolve:

Tris-HCl (Fisher Scientific, UK) - 48.46g

NaCl (Sigma-Aldrich) - 160.12g

in 800mL dH_2O and mix with magnetic stirrer.

Adjust to pH 7.6 using 1M HCl.

Make up final volume of 1L with dH_2O.

Keep at room temperature for 12 months.

8.1.1.4 Tris-Buffered Saline - TBS (1X)

For 1L:

Dilute 50mL of 20X TBS into 950mL of dH_2O.

8.1.1.5 RIPA Buffer

Prepare 10mL stock solutions of:

1M Tris-HCl: Dissolve 1.21 g Tris-HCl (Fisher Scientific, UK) in 10mL of dH_2O.

5 M NaCl: Dissolve 2.9 g NaCl (Sigma-Aldrich, UK) in 10mL dH_2O.

0.5 M EDTA: Dissolve 1.86 g EDTA (Sigma-Aldrich, UK) in 10mL dH_2O.

To make 100mL of RIPA buffer:

Sodium deoxycholate (Fisher Scientific, UK) - 0.5g

1 M Tris-HCl - 5 mL

5 M NaCl - 3 mL

0.5 M EDTA - 0.2 mL

to 75 mL of dH_2O.

Adjust pH to 8.8 using 2M NaOH.

Add: 10% SDS for final concentration of 1%

10% NP-40 - 1mL

0.1% OTG

Add PhosSTOP (Sigma-Aldrich, UK) and cOmplete Protease inhibitor cocktail (Merck, UK) at 1X

Top up to 100mL with dH_2O.

8.1.1.6 Sodium Citrate Buffer (10X)

For 1L:

Tri-sodium citrate (dihydrate) (Sigma-Aldrich, UK) – 29.4g

Add 800mL of dH_2O.

Mix to dissolve with magnetic stirrer.

Adjust pH to 6.0 with 1M HCl.

Top up volume to 1L with dH_2O.

Store this solution at room temperature for 3 months or at 4°C for longer storage (up to 12 months).

8.1.1.7 Sodium Citrate Buffer (1X)

Must be made fresh every experiment.

For 1L:

Take 100mL of 10X Sodium Citrate Buffer and add to 900mL of dH_2O.

8.1.1.8 Gel Loading SDS Sample Buffer (6X)

For 50mL:

Sodium Dodecyl Sulphate (SDS (Sigma-Aldrich, UK) – 6g in 8.75mL 1M Tris-HCL at pH 6.8

Dissolve by heating and vortexing.

Add glycerol (Sigma-Aldrich, UK) – 37.6g

Leave to dissolve.

Check pH and adjust with 1M HCl.

Add 46 mg of bromophenol blue (Sigma-Aldrich, UK) and dissolve.

Aliquot as necessary and store in -20°C as stock.

8.2 Tissue Harvest Protocol

Table 8.1 Tissue harvest protocol sheet for rat culls.

Date	

Strain	
Animal ID	
Rat Weight	
Tibia length	
Tissue details	
Blood	☐ EDTA ☐ Heparin
Aorta	☐ Freeze
Heart	Weight : ☐ RNA ☐ Prt ☐ Histology
Lungs	Weight : ☐ Prt ☐ ☐ Histology
Mesenteries	☐
Pancreas	☐ Freeze
Kidney	Left Weight : Right Weight : ☐ RNA ☐ Prt ☐ ☐ Histology
Adrenal gland	☐ Freeze ☐ Histology
Spleen	Weight : ☐ Freeze ☐ Histology
Liver	Weight : ☐ RNA ☐ Prt ☐ Na+ ☐ Histology

References

ABDULLAH, H. I., PEDRAZA, P. L., HAO, S., RODLAND, K. D., MCGIFF, J. C. & FERRERI, N. R. 2006. NFAT regulates calcium-sensing receptor-mediated TNF production. *Am J Physiol Renal Physiol,* 290**,** F1110-7.

ABDULLAH, H. I., PEDRAZA, P. L., MCGIFF, J. C. & FERRERI, N. R. 2008. Calcium-sensing receptor signaling pathways in medullary thick ascending limb cells mediate COX-2-derived PGE2 production: functional significance. *Am J Physiol Renal Physiol,* 295**,** F1082-9.

ADAMS, C. J., KOPP, M. C., LARBURU, N., NOWAK, P. R. & ALI, M. M. U. 2019. Structure and Molecular Mechanism of ER Stress Signaling by the Unfolded Protein Response Signal Activator IRE1. *Front Mol Biosci,* 6**,** 11.

AKESSON, I., HAUGEN, H. & ENGER, E. 1978. Quantification of uromucoid: a simplified method. *Scand J Clin Lab Invest,* 38**,** 93-5.

AL GHOULEH, I., KHOO, N. K., KNAUS, U. G., GRIENDLING, K. K., TOUYZ, R. M., THANNICKAL, V. J., BARCHOWSKY, A., NAUSEEF, W. M., KELLEY, E. E., BAUER, P. M., DARLEY-USMAR, V., SHIVA, S., CIFUENTES-PAGANO, E., FREEMAN, B. A., GLADWIN, M. T. & PAGANO, P. J. 2011. Oxidases and peroxidases in cardiovascular and lung disease: new concepts in reactive oxygen species signaling. *Free Radic Biol Med,* 51**,** 1271-88.

ALGHARABLY, E. A. H., BOLBRINKER, J., LEZIUS, S., REIBIS, R., WEGSCHEIDER, K., VÖLLER, H. & KREUTZ, R. 2017. Uromodulin associates with cardiorenal function in patients with hypertension and cardiovascular disease. *J Hypertens,* 35**,** 2053-2058.

ANDERSON, R. J., BERL, T., MCDONALD, K. M. & SCHRIER, R. W. 1976. Prostaglandins: effects on blood pressure, renal blood flow, sodium and water excretion. *Kidney Int,* 10**,** 205-15.

ARAUJO, M. & WILCOX, C. S. 2014. Oxidative stress in hypertension: role of the kidney. *Antioxid Redox Signal,* 20**,** 74-101.

ARES, G. R., CACERES, P. S. & ORTIZ, P. A. 2011. Molecular regulation of NKCC2 in the thick ascending limb. *Am J Physiol Renal Physiol,* 301**,** F1143-59.

ARES, G. R., HAQUE, M. Z., DELPIRE, E. & ORTIZ, P. A. 2012. Hyperphosphorylation of Na-K-2Cl cotransporter in thick ascending limbs of Dahl salt-sensitive rats. *Hypertension,* 60**,** 1464-70.

ARGADE, S., CHEN, T., SHAW, T., BERECZ, Z., SHI, W., CHOUDHURY, B., PARSONS, C. L. & SUR, R. L. 2015. An evaluation of Tamm-Horsfall protein glycans in kidney stone formers using novel techniques. *Urolithiasis,* 43**,** 303-12.

ARGADE, S. P., VANICHSARN, C., CHENOWETH, M. & PARSONS, C. L. 2009. Abnormal glycosylation of Tamm-Horsfall protein in patients with interstitial cystitis. *BJU Int,* 103**,** 1085-9.

ARIMA, H., BARZI, F. & CHALMERS, J. 2011. Mortality patterns in hypertension. *J Hypertens,* 29 Suppl 1**,** S3-7.

ARMANDO, I., VILLAR, V. A. & JOSE, P. A. 2011. Dopamine and renal function and blood pressure regulation. *Compr Physiol,* 1**,** 1075-117.

ARMANINI, D., BORDIN, L., DONA, G., CECCATO, F., BARBOT, M., SCARONI, C. & SABBADIN, C. 2019. Pitfalls in urinary sodium excretion. *J Clin Hypertens (Greenwich),* 21**,** 1635-1636.

ARMSTRONG, M., KERNDT, C. C. & MOORE, R. A. 2023. Physiology, Baroreceptors. *StatPearls.* Treasure Island (FL) ineligible companies. Disclosure: Connor Kerndt declares no relevant financial relationships with ineligible companies. Disclosure: Ross Moore declares no relevant financial relationships with ineligible companies.

BACHMANN, S., MUTIG, K., BATES, J., WELKER, P., GEIST, B., GROSS, V., LUFT, F. C., ALENINA, N., BADER, M., THIELE, B. J., PRASADAN, K., RAFFI, H. S. & KUMAR, S. 2005. Renal effects of Tamm-Horsfall protein (uromodulin) deficiency in mice. *Am J Physiol Renal Physiol,* 288**,** F559-67.

BADGETT, A. & KUMAR, S. 1998. Phylogeny of Tamm-Horsfall protein. *Urol Int,* 61**,** 72-5.

BAGUR, R. & HAJNÓCZKY, G. 2017. Intracellular Ca(2+) Sensing: Its Role in Calcium Homeostasis and Signaling. *Mol Cell,* 66**,** 780-788.

BARNETT, A. M., BABCOCK, M. C., WATSO, J. C., MIGDAL, K. U., GUTIÉRREZ, O. M., FARQUHAR, W. B. & ROBINSON, A. T. 2022. High dietary salt intake increases urinary NGAL excretion and creatinine clearance in healthy young adults. *Am J Physiol Renal Physiol,* 322**,** F392-f402.

BAI, X., LENHART, K. C., BIRD, K. E., SUEN, A. A., ROJAS, M., KAKOKI, M., LI, F., SMITHIES, O., MACK, C. P. & TAYLOR, J. M. 2013. The smooth muscle-selective RhoGAP GRAF3 is a critical regulator of vascular tone and hypertension. *Nature Communications,* 4**,** 2910.

BAKHOUM, C. Y., ANDERSON, C. A. M., JURASCHEK, S. P., REBHOLZ, C. M., APPEL, L. J., MILLER, E. R., PARIKH, C. R., OBEID, W., RIFKIN, D. E., IX, J. H. & GARIMELLA, P. S. 2021. The Relationship Between Urine Uromodulin and Blood Pressure Changes: The DASH-Sodium Trial. *Am J Hypertens,* 34**,** 154-156.

BANACH, P., DEREZIŃSKI, P., MATUSZEWSKA, E., MATYSIAK, J., BOCHYŃSKI, H., KOKOT, Z. J. & NOWAK-MARKWITZ, E. 2019. MALDI-TOF-MS Analysis in the Identification of Urine Proteomic Patterns of Gestational Trophoblastic Disease. *Metabolites,* 9.

BATES, J. M., RAFFI, H. M., PRASADAN, K., MASCARENHAS, R., LASZIK, Z., MAEDA, N., HULTGREN, S. J. & KUMAR, S. 2004. Tamm-Horsfall protein knockout mice are more prone to urinary tract infection: rapid communication. *Kidney Int,* 65**,** 791-7.

BATTULA, S., HAO, S., PEDRAZA, P. L., STIER, C. T. & FERRERI, N. R. 2011. Tumor necrosis factor-alpha is an endogenous inhibitor of Na+-K+-2Cl-cotransporter (NKCC2) isoform A in the thick ascending limb. *Am J Physiol Renal Physiol,* 301**,** F94-100.

BEARD, D. A., PETTERSEN, K. H., CARLSON, B. E., OMHOLT, S. W. & BUGENHAGEN, S. M. 2013. A computational analysis of the long-term regulation of arterial pressure. *F1000Res,* 2**,** 208.

BECK, L. & GEIGER, T. 2022. MS-based technologies for untargeted single-cell proteomics. *Curr Opin Biotechnol,* 76**,** 102736.

BENNETT, C. M., BRENNER, B. M. & BERLINER, R. W. 1968. Micropuncture study of nephron function in the rhesus monkey. *J Clin Invest,* 47**,** 203-16.

BERNASCONE, I., VAVASSORI, S., DI PENTIMA, A., SANTAMBROGIO, S., LAMORTE, G., AMOROSO, A., SCOLARI, F., GHIGGERI, G. M., CASARI, G., POLISHCHUK, R. & RAMPOLDI, L. 2006. Defective intracellular trafficking of uromodulin mutant isoforms. *Traffic,* 7**,** 1567-79.

BIR, S. C., KOLLURU, G. K., FANG, K. & KEVIL, C. G. 2012. Redox balance dynamically regulates vascular growth and remodeling. *Semin Cell Dev Biol,* 23**,** 745-57.

BLAINE, J., CHONCHOL, M. & LEVI, M. 2015. Renal control of calcium, phosphate, and magnesium homeostasis. *Clin J Am Soc Nephrol,* 10**,** 1257-72.

BODER, P., MARY, S., MARK, P. B., LEIPER, J., DOMINICZAK, A. F., PADMANABHAN, S., RAMPOLDI, L. & DELLES, C. 2021. Mechanistic interactions of uromodulin with the thick ascending limb: perspectives in physiology and hypertension. *J Hypertens,* 39**,** 1490-1504.

BOEDTKJER, E., PRAETORIUS, J., MATCHKOV, V. V., STANKEVICIUS, E., MOGENSEN, S., FUCHTBAUER, A. C., SIMONSEN, U., FUCHTBAUER, E. M. & AALKJAER, C. 2011. Disruption of Na+,HCO(3)(-) cotransporter NBCn1 (slc4a7) inhibits NO-mediated vasorelaxation, smooth muscle Ca(2)(+) sensitivity, and hypertension development in mice. *Circulation,* 124**,** 1819-29.

BOIM, M. A., HO, K., SHUCK, M. E., BIENKOWSKI, M. J., BLOCK, J. H., SLIGHTOM, J. L., YANG, Y., BRENNER, B. M. & HEBERT, S. C. 1995. ROMK inwardly rectifying ATP-sensitive K+ channel. II. Cloning and distribution of alternative forms. *Am J Physiol,* 268**,** F1132-40.

BOKHOVE, M., NISHIMURA, K., BRUNATI, M., HAN, L., DE SANCTIS, D., RAMPOLDI, L. & JOVINE, L. 2016. A structured interdomain linker directs self-polymerization of human uromodulin. *Proc Natl Acad Sci U S A,* 113**,** 1552-7.

BOMFIM, G. F., DOS SANTOS, R. A., OLIVEIRA, M. A., GIACHINI, F. R., AKAMINE, E. H., TOSTES, R. C., FORTES, Z. B., WEBB, R. C. & CARVALHO, M. H. 2012. Toll-like receptor 4 contributes to blood pressure regulation and vascular contraction in spontaneously hypertensive rats. *Clin Sci (Lond),* 122**,** 535-43.

BORRELLI, S., PROVENZANO, M., GAGLIARDI, I., MICHAEL, A., LIBERTI, M. E., DE NICOLA, L., CONTE, G., GAROFALO, C. & ANDREUCCI, M. 2020. Sodium Intake and Chronic Kidney Disease. *Int J Mol Sci,* 21.

BOSTOM, A., STEUBL, D., GARIMELLA, P. S., FRANCESCHINI, N., ROBERTS, M. B., PASCH, A., IX, J. H., TUTTLE, K. R., IVANOVA, A., SHIREMAN, T., KIM, S. J., GOHH, R., WEINER, D. E., LEVEY, A. S., HSU, C. Y., KUSEK, J. W. & EATON, C. B. 2018. Serum Uromodulin: A Biomarker of Long-Term Kidney Allograft Failure. *Am J Nephrol,* 47**,** 275-282.

BOUBY, N., HUS-CITHAREL, A., MARCHETTI, J., BANKIR, L., CORVOL, P. & LLORENS-CORTES, C. 1997. Expression of type 1 angiotensin II receptor subtypes and angiotensin II-induced calcium mobilization along the rat nephron. *J Am Soc Nephrol,* 8**,** 1658-67.

BOURGEOIS, S., ROSSIGNOL, P., GRELAC, F., CHALUMEAU, C., KLEIN, C., LAGHMANI, K., CHAMBREY, R., BRUNEVAL, P., DUONG, J. P., POGGIOLI, J., HOUILLIER, P., PAILLARD, M., KELLERMANN, O. & FROISSART, M. 2003. Differentiated thick ascending limb (TAL) cultured cells derived from SV40 transgenic mice express functional apical NHE2 isoform: effect of nitric oxide. *Pflugers Arch,* 446**,** 672-83.

BRESALIER, R. S., SANDLER, R. S., QUAN, H., BOLOGNESE, J. A., OXENIUS, B., HORGAN, K., LINES, C., RIDDELL, R., MORTON, D., LANAS, A., KONSTAM, M. A. & BARON, J. A. 2005. Cardiovascular events associated with rofecoxib in a colorectal adenoma chemoprevention trial. *N Engl J Med,* 352**,** 1092-102.

BROWN, M. J. 2012. Platt versus Pickering: what molecular insight to primary hyperaldosteronism tells us about hypertension. *JRSM Cardiovasc Dis,* 1.

BRUNATI, M., PERUCCA, S., HAN, L., CATTANEO, A., CONSOLATO, F., ANDOLFO, A., SCHAEFFER, C., OLINGER, E., PENG, J., SANTAMBROGIO, S., PERRIER, R., LI, S., BOKHOVE, M., BACHI, A., HUMMLER, E., DEVUYST, O., WU, Q., JOVINE, L. & RAMPOLDI, L. 2015. The serine protease hepsin mediates urinary secretion and polymerisation of Zona Pellucida domain protein uromodulin. *Elife,* 4**,** e08887.

BRUNISHOLZ, M., GENITEAU-LEGENDRE, M., RONCO, P. M., MOULLIER, P., PONTILLON, F., RICHET, G. & VERROUST, P. J. 1986. Characterization of monoclonal antibodies specific for human Tamm-Horsfall protein. *Kidney Int,* 29**,** 971-6.

CAMARGO, L. L., HARVEY, A. P., RIOS, F. J., TSIROPOULOU, S., DA SILVA, R. N. O., CAO, Z., GRAHAM, D., MCMASTER, C., BURCHMORE, R. J., HARTLEY, R. C., BULLEID, N., MONTEZANO, A. C. & TOUYZ, R. M. 2018. Vascular Nox (NADPH Oxidase) Compartmentalization, Protein Hyperoxidation, and Endoplasmic Reticulum Stress Response in Hypertension. *Hypertension,* 72**,** 235-246.

CARNEVALE, D., PALLANTE, F., FARDELLA, V., FARDELLA, S., IACOBUCCI, R., FEDERICI, M., CIFELLI, G., DE LUCIA, M. & LEMBO, G. 2014. The angiogenic factor PlGF mediates a neuroimmune interaction in the spleen to allow the onset of hypertension. *Immunity,* 41**,** 737-52.

CARRARA, M., FERRARIO, M., BOLLEN PINTO, B. & HERPAIN, A. 2021. The autonomic nervous system in septic shock and its role as a future therapeutic target: a narrative review. *Ann Intensive Care,* 11**,** 80.

CARRISOZA-GAYTAN, R., KROLL, K. T., HIRATSUKA, K., GUPTA, N. R., MORIZANE, R., LEWIS, J. A. & SATLIN, L. M. 2023. Functional maturation of kidney organoid tubules: PIEZO1-mediated Ca(2+) signaling. *Am J Physiol Cell Physiol,* 324**,** C757-C768.

CARTY, D. M., SIWY, J., BRENNAND, J. E., ZÜRBIG, P., MULLEN, W., FRANKE, J., MCCULLOCH, J. W., ROBERTS, C. T., NORTH, R. A., CHAPPELL, L. C., MISCHAK, H., POSTON, L., DOMINICZAK, A. F. & DELLES, C. 2011. Urinary proteomics for prediction of preeclampsia. *Hypertension,* 57**,** 561-9.

CASTROP, H. & SCHIEßL, I. M. 2014. Physiology and pathophysiology of the renal Na-K-2Cl cotransporter (NKCC2). *Am J Physiol Renal Physiol,* 307**,** F991-f1002.

CASTROP, H. & SCHIESSL, I. M. 2014. Physiology and pathophysiology of the renal Na-K-2Cl cotransporter (NKCC2). *Am J Physiol Renal Physiol,* 307**,** F991-F1002.

CESARATTO, F., SASSET, L., MYERS, M. P., RE, A., PETRIS, G. & BURRONE, O. R. 2019. BiP/GRP78 Mediates ERAD Targeting of Proteins Produced by Membrane-Bound Ribosomes Stalled at the STOP-Codon. *J Mol Biol,* 431**,** 123-141.

CHABARDES-GARONNE, D., MEJEAN, A., AUDE, J. C., CHEVAL, L., DI STEFANO, A., GAILLARD, M. C., IMBERT-TEBOUL, M., WITTNER, M., BALIAN, C., ANTHOUARD, V., ROBERT, C., SEGURENS, B., WINCKER, P., WEISSENBACH, J., DOUCET, A. & ELALOUF, J. M. 2003. A panoramic view of gene expression in the human kidney. *Proc Natl Acad Sci U S A,* 100**,** 13710-5.

CHAN, C. T., SOBEY, C. G., LIEU, M., FERENS, D., KETT, M. M., DIEP, H., KIM, H. A., KRISHNAN, S. M., LEWIS, C. V., SALIMOVA, E., TIPPING, P., VINH, A., SAMUEL, C. S., PETER, K., GUZIK, T. J., KYAW, T. S., TOH, B. H., BOBIK, A. & DRUMMOND, G. R. 2015. Obligatory Role for B Cells in the Development of Angiotensin II-Dependent Hypertension. *Hypertension,* 66**,** 1023-33.

CHANG, C. J., CHI, C. Y. & YANG, H. Y. 2023. Heat exposure and chronic kidney disease: a temporal link in a Taiwanese agricultural county. *Int J Environ Health Res***,** 1-14.

CHANG, Y.-P. C., LIU, X., KIM, J. D. O., IKEDA, M. A., LAYTON, M. R., WEDER, A. B., COOPER, R. S., KARDIA, S. L. R., RAO, D. C., HUNT, S. C., LUKE, A., BOERWINKLE, E. & CHAKRAVARTI, A. 2007. Multiple Genes for Essential-Hypertension Susceptibility on Chromosome 1q. *The American Journal of Human Genetics,* 80**,** 253-264.

CHARKOUDIAN, N. & RABBITTS, J. A. 2009. Sympathetic neural mechanisms in human cardiovascular health and disease. *Mayo Clin Proc,* 84**,** 822-30.

CHAUDHRY, R., MIAO, J. H. & REHMAN, A. 2023. Physiology, Cardiovascular. *StatPearls.* Treasure Island (FL) ineligible companies. Disclosure: Julia Miao declares no relevant financial relationships with ineligible companies. Disclosure: Afzal Rehman declares no relevant financial relationships with ineligible companies.

CHIBA, T., ITOH, T., TABUCHI, M., NAKAZAWA, T. & SATOU, T. 2012. Interleukin-1β accelerates the onset of stroke in stroke-prone spontaneously hypertensive rats. *Mediators Inflamm,* 2012**,** 701976.

CHIPURUPALLI, S., SAMAVEDAM, U. & ROBINSON, N. 2021. Crosstalk Between ER Stress, Autophagy and Inflammation. *Front Med (Lausanne),* 8**,** 758311.

CHOI, H. K., ATKINSON, K., KARLSON, E. W. & CURHAN, G. 2005. Obesity, weight change, hypertension, diuretic use, and risk of gout in men: the health professionals follow-up study. *Arch Intern Med,* 165**,** 742-8.

CHURCHILL, P. C., CHURCHILL, M. C., GRIFFIN, K. A., PICKEN, M., WEBB, R. C., KURTZ, T. W. & BIDANI, A. K. 2002. Increased genetic susceptibility to renal damage in the stroke-prone spontaneously hypertensive rat. *Kidney Int,* 61**,** 1794-800.

CLARK, J. S., JEFFS, B., DAVIDSON, A. O., LEE, W. K., ANDERSON, N. H., BIHOREAU, M. T., BROSNAN, M. J., DEVLIN, A. M., KELMAN, A. W., LINDPAINTNER, K. & DOMINICZAK, A. F. 1996. Quantitative trait loci in genetically hypertensive rats. Possible sex specificity. *Hypertension,* 28**,** 898-906.

COLLETT, J. A., PAULOSE, J. K., CASSONE, V. M. & OSBORN, J. L. 2015. Kidney-Specific Reduction of Oxidative Phosphorylation Genes Derived from Spontaneously Hypertensive Rat. *PLoS One,* 10**,** e0136441.

COWLEY, A. W., JR. 2006. The genetic dissection of essential hypertension. *Nat Rev Genet,* 7**,** 829-40.

CRIVAT, G. & TARASKA, J. W. 2012. Imaging proteins inside cells with fluorescent tags. *Trends Biotechnol,* 30**,** 8-16.

CROWLEY, S. D., GURLEY, S. B., OLIVERIO, M. I., PAZMINO, A. K., GRIFFITHS, R., FLANNERY, P. J., SPURNEY, R. F., KIM, H. S., SMITHIES, O., LE, T. H. & COFFMAN, T. M. 2005. Distinct roles for the kidney and systemic tissues in blood pressure regulation by the renin-angiotensin system. *J Clin Invest,* 115**,** 1092-9.

CROWLEY, S. D. & JEFFS, A. D. 2016. Targeting cytokine signaling in salt-sensitive hypertension. *Am J Physiol Renal Physiol,* 311**,** F1153-F1158.

CURTSINGER, J. M. & MESCHER, M. F. 2010. Inflammatory cytokines as a third signal for T cell activation. *Curr Opin Immunol,* 22**,** 333-40.

DAHAN, K., DEVUYST, O., SMAERS, M., VERTOMMEN, D., LOUTE, G., POUX, J. M., VIRON, B., JACQUOT, C., GAGNADOUX, M. F., CHAUVEAU, D., BÜCHLER, M., COCHAT, P., COSYNS, J. P., MOUGENOT, B., RIDER, M. H., ANTIGNAC, C., VERELLEN-DUMOULIN, C. & PIRSON, Y. 2003. A cluster of mutations in the UMOD gene causes familial juvenile hyperuricemic nephropathy with abnormal expression of uromodulin. *J Am Soc Nephrol,* 14**,** 2883-93.

DAHLY, A. J., HOAGLAND, K. M., FLASCH, A. K., JHA, S., LEDBETTER, S. R. & ROMAN, R. J. 2002. Antihypertensive effects of chronic anti-TGF-beta antibody therapy in Dahl S rats. *Am J Physiol Regul Integr Comp Physiol,* 283**,** R757-67.

DALAL, R., BRUSS, Z. S. & SEHDEV, J. S. 2023. Physiology, Renal Blood Flow and Filtration. *StatPearls.* Treasure Island (FL) ineligible companies. Disclosure: Zachary Bruss declares no relevant financial relationships with ineligible companies. Disclosure: Jasjit Sehdev declares no relevant financial relationships with ineligible companies.

DANGE, R. B., AGARWAL, D., TERUYAMA, R. & FRANCIS, J. 2015. Toll-like receptor 4 inhibition within the paraventricular nucleus attenuates blood pressure and inflammatory response in a genetic model of hypertension. *J Neuroinflammation,* 12**,** 31.

DE ALMEIDA, L. F. & COIMBRA, T. M. 2019. When Less or More Isn't Enough: Renal Maldevelopment Arising From Disequilibrium in the Renin-Angiotensin System. *Front Pediatr,* 7**,** 296.

DE MIGUEL, C., RUDEMILLER, N. P., ABAIS, J. M. & MATTSON, D. L. 2015. Inflammation and hypertension: new understandings and potential therapeutic targets. *Curr Hypertens Rep,* 17**,** 507.

DE WARDENER, H. E. & HERXHEIMER, A. 1957. The effect of a high water intake on the kidney's ability to concentrate the urine in man. *J Physiol,* 139**,** 42-52.

DEGASPERI, A., BIRTWISTLE, M. R., VOLINSKY, N., RAUCH, J., KOLCH, W. & KHOLODENKO, B. N. 2014. Evaluating strategies to normalise biological replicates of Western blot data. *PLoS One,* 9**,** e87293.

DELGADO, G. E., KLEBER, M. E., SCHARNAGL, H., KRÄMER, B. K., MÄRZ, W. & SCHERBERICH, J. E. 2017. Serum Uromodulin and Mortality Risk in Patients Undergoing Coronary Angiography. *J Am Soc Nephrol,* 28**,** 2201-2210.

DENIC, A., GLASSOCK, R. J. & RULE, A. D. 2016. Structural and Functional Changes With the Aging Kidney. *Adv Chronic Kidney Dis,* 23**,** 19-28.

DEVUYST, O., OLINGER, E. & RAMPOLDI, L. 2017. Uromodulin: from physiology to rare and complex kidney disorders. *Nat Rev Nephrol,* 13**,** 525-544.

DEVUYST, O. & PATTARO, C. 2018. The UMOD Locus: Insights into the Pathogenesis and Prognosis of Kidney Disease. *J Am Soc Nephrol,* 29**,** 713-726.

DI CASTRO, S., SCARPINO, S., MARCHITTI, S., BIANCHI, F., STANZIONE, R., COTUGNO, M., SIRONI, L., GELOSA, P., DURANTI, E., RUCO, L., VOLPE, M. & RUBATTU, S. 2013. Differential modulation of uncoupling protein 2 in kidneys of stroke-prone spontaneously hypertensive rats under high-salt/low-potassium diet. *Hypertension,* 61**,** 534-41.

DIDION, S. P., KINZENBAW, D. A., SCHRADER, L. I., CHU, Y. & FARACI, F. M. 2009. Endogenous interleukin-10 inhibits angiotensin II-induced vascular dysfunction. *Hypertension,* 54**,** 619-24.

DIMKE, H., DESAI, P., BOROVAC, J., LAU, A., PAN, W. & ALEXANDER, R. T. 2013. Activation of the Ca(2+)-sensing receptor increases renal claudin-14 expression and urinary Ca(2+) excretion. *Am J Physiol Renal Physiol,* 304**,** F761-9.

DOGGRELL, S. A. & BROWN, L. 1998. Rat models of hypertension, cardiac hypertrophy and failure. *Cardiovasc Res,* 39**,** 89-105.

DONG, K., YAN, Q., LU, M., WAN, L., HU, H., GUO, J., BOULPAEP, E., WANG, W., GIEBISCH, G., HEBERT, S. C. & WANG, T. 2016. Romk1 Knockout Mice Do Not Produce Bartter Phenotype but Exhibit Impaired K Excretion. *J Biol Chem,* 291**,** 5259-69.

DOU, W., THOMPSON-JAEGER, S., LAULEDERKIND, S. J., BECKER, J. W., MONTGOMERY, J., RUIZ-BUSTOS, E., HASTY, D. L., BALLOU, L. R., EASTMAN, P. S., SRICHAI, B., BREYER, M. D. & RAGHOW, R. 2005. Defective expression of Tamm-Horsfall protein/uromodulin in COX-2-deficient mice increases their susceptibility to urinary tract infections. *Am J Physiol Renal Physiol,* 289**,** F49-60.

DU, M. F., YAO, S., ZOU, T., MU, J. J., ZHANG, X. Y., HU, G. L., CHU, C., JIA, H., LIAO, Y. Y., CHEN, C., WANG, D., MA, Q., YAN, Y., WANG, K. K., SUN, Y., NIU, Z. J., YAN, R. C., ZHANG, X., ZHOU, H. W., GAO, W. H., LI, H., LI, C. H., GAO, K., ZHANG, J., YANG, T. L. & WANG, Y. 2021. Associations of plasma uromodulin and genetic variants with blood pressure responses to dietary salt interventions. *J Clin Hypertens (Greenwich),* 23**,** 1897-1906.

DUŁAWA, J., KOKOT, F., KOKOT, M. & PANDER, H. 1998. Urinary excretion of Tamm-Horsfall protein in normotensive and hypertensive elderly patients. *J Hum Hypertens,* 12**,** 635-7.

DUŁAWA, J., KOKOT, M. & KOKOT, F. 1992. [Effects of furosemide, propranolol and nifedipine on urinary excretion of Tamm-Horsfall protein in patients with arterial hypertension]. *Pol Arch Med Wewn,* 88**,** 212-8.

DYCKNER, T. & WESTER, P. O. 1983. Effect of magnesium on blood pressure. *Br Med J (Clin Res Ed),* 286**,** 1847-9.

EATON, S. B. & EATON, S. B. 2003. An evolutionary perspective on human physical activity: implications for health. *Comp Biochem Physiol A Mol Integr Physiol,* 136**,** 153-9.

ECKARDT, K. U., ALPER, S. L., ANTIGNAC, C., BLEYER, A. J., CHAUVEAU, D., DAHAN, K., DELTAS, C., HOSKING, A., KMOCH, S., RAMPOLDI, L., WIESENER, M., WOLF, M. T. & DEVUYST, O. 2015. Autosomal dominant tubulointerstitial kidney disease: diagnosis, classification, and management--A KDIGO consensus report. *Kidney Int,* 88**,** 676-83.

EHRET, G. B. & CAULFIELD, M. J. 2013. Genes for blood pressure: an opportunity to understand hypertension. *Eur Heart J,* 34**,** 951-61.

EHRET, G. B., MUNROE, P. B., RICE, K. M., BOCHUD, M., JOHNSON, A. D., CHASMAN, D. I., SMITH, A. V., TOBIN, M. D., VERWOERT, G. C., HWANG, S.-J., PIHUR, V., VOLLENWEIDER, P., O'REILLY, P. F., AMIN, N., BRAGG-GRESHAM, J. L., TEUMER, A., GLAZER, N. L., LAUNER, L., HUA ZHAO, J., AULCHENKO, Y., HEATH, S., SÕBER, S., PARSA, A., LUAN, J. A., ARORA, P., DEHGHAN, A., ZHANG, F., LUCAS, G., HICKS, A. A., JACKSON, A. U., PEDEN, J. F., TANAKA, T., WILD, S. H., RUDAN, I., IGL, W., MILANESCHI, Y., PARKER, A. N., FAVA, C., CHAMBERS, J. C., FOX, E. R., KUMARI, M., JIN GO, M., VAN DER HARST, P., HONG LINDA KAO, W., SJÖGREN, M., VINAY, D. G., ALEXANDER, M., TABARA, Y., SHAW-HAWKINS, S., WHINCUP, P. H., LIU, Y., SHI, G., KUUSISTO, J., TAYO, B., SEIELSTAD, M., SIM, X., HOANG NGUYEN, K.-D., LEHTIMÄKI, T., MATULLO, G., WU, Y., GAUNT, T. R., CHARLOTTE ONLAND-MORET, N., COOPER, M. N., PLATOU, C. G. P., ORG, E., HARDY, R., DAHGAM, S., PALMEN, J., VITART, V., BRAUND, P. S., KUZNETSOVA, T., UITERWAAL, C. S. P. M., ADEYEMO, A., PALMAS, W., CAMPBELL, H., LUDWIG, B., TOMASZEWSKI, M., TZOULAKI, I., PALMER, N. D., ASPELUND, T., GARCIA, M., CHANG, Y.-P. C., O'CONNELL, J. R., STEINLE, N. I., GROBBEE, D. E., ARKING, D. E., KARDIA, S. L., MORRISON, A. C., HERNANDEZ, D., NAJJAR, S., MCARDLE, W. L., HADLEY, D., BROWN, M. J., CONNELL, J. M., HINGORANI, A. D., DAY, I. N. M., LAWLOR, D. A., BEILBY, J. P., LAWRENCE, R. W., CLARKE, R., et al. 2011. Genetic variants in novel pathways influence blood pressure and cardiovascular disease risk. *Nature,* 478**,** 103-109.

EHRET, G. B., O'CONNOR, A. A., WEDER, A., COOPER, R. S. & CHAKRAVARTI, A. 2009. Follow-up of a major linkage peak on chromosome 1 reveals suggestive QTLs associated with essential hypertension: GenNet study. *European Journal of Human Genetics,* 17**,** 1650-1657.

EL-ACHKAR, T. M., MCCRACKEN, R., LIU, Y., HEITMEIER, M. R., BOURGEOIS, S., RYERSE, J. & WU, X. R. 2013. Tamm-Horsfall protein translocates to the basolateral domain of thick ascending limbs, interstitium, and circulation during recovery from acute kidney injury. *Am J Physiol Renal Physiol,* 304**,** F1066-75.

EL KAROUI, K., VIAU, A., DELLIS, O., BAGATTIN, A., NGUYEN, C., BARON, W., BURTIN, M., BROUEILH, M., HEIDET, L., MOLLET, G., DRUILHE, A., ANTIGNAC, C., KNEBELMANN, B., FRIEDLANDER, G., BIENAIMÉ, F., GALLAZZINI, M. & TERZI, F. 2016. Endoplasmic reticulum stress drives proteinuria-induced kidney lesions via Lipocalin 2. *Nat Commun,* 7**,** 10330.

ELIJOVICH, F., WEINBERGER, M. H., ANDERSON, C. A., APPEL, L. J., BURSZTYN, M., COOK, N. R., DART, R. A., NEWTON-CHEH, C. H., SACKS, F. M. & LAFFER, C. L. 2016. Salt Sensitivity of Blood Pressure: A Scientific Statement From the American Heart Association. *Hypertension,* 68**,** e7-e46.

ELLGAARD, L. & HELENIUS, A. 2003. Quality control in the endoplasmic reticulum. *Nat Rev Mol Cell Biol,* 4**,** 181-91.

ERIKSSON, J. G., FORSÉN, T. J., KAJANTIE, E., OSMOND, C. & BARKER, D. J. 2007. Childhood growth and hypertension in later life. *Hypertension,* 49**,** 1415-21.

EVANS, A. L., BROWN, W., KENYON, C. J., MAXTED, K. J. & SMITH, D. C. 1994. Improved system for measuring systolic blood pressure in the conscious rat. *Med Biol Eng Comput,* 32**,** 101-2.

EWING, G. W. 2010. Mathematical modeling the neuroregulation of blood pressure using a cognitive top-down approach. *N Am J Med Sci,* 2**,** 341-52.

FAGUER, S., DECRAMER, S., DEVUYST, O., LENGELÉ, J. P., FOURNIÉ, G. J. & CHAUVEAU, D. 2012. Expression of renal cystic genes in patients with HNF1B mutations. *Nephron Clin Pract,* 120**,** c71-8.

FEHER, J. 2017. 7.2 - Functional Anatomy of the Kidneys and Overview of Kidney Function. *In:* FEHER, J. (ed.) *Quantitative Human Physiology (Second Edition).* Boston: Academic Press.

FERBER, U. M., KAGGWA, G. & JARVIS, S. P. 2011. Direct imaging of salt effects on lipid bilayer ordering at sub-molecular resolution. *Eur Biophys J,* 40**,** 329-38.

FERRERI, N. R., ESCALANTE, B. A., ZHAO, Y., AN, S. J. & MCGIFF, J. C. 1998. Angiotensin II induces TNF production by the thick ascending limb: functional implications. *Am J Physiol,* 274**,** F148-55.

FERRERI, N. R., HAO, S., PEDRAZA, P. L., ESCALANTE, B. & VIO, C. P. 2012. Eicosanoids and tumor necrosis factor-alpha in the kidney. *Prostaglandins Other Lipid Mediat,* 98**,** 101-6.

FLACK, J. M. & ADEKOLA, B. 2020. Blood pressure and the new ACC/AHA hypertension guidelines. *Trends Cardiovasc Med,* 30**,** 160-164.

FOUNTAIN, J. H., KAUR, J. & LAPPIN, S. L. 2023. Physiology, Renin Angiotensin System. *StatPearls.* Treasure Island (FL) ineligible companies. Disclosure: Jasleen Kaur declares no relevant financial relationships with ineligible companies. Disclosure: Sarah Lappin declares no relevant financial relationships with ineligible companies.

FRANCO, M., MARTÍNEZ, F., QUIROZ, Y., GALICIA, O., BAUTISTA, R., JOHNSON, R. J. & RODRÍGUEZ-ITURBE, B. 2007. Renal angiotensin II concentration and interstitial infiltration of immune cells are correlated with blood pressure levels in salt-sensitive hypertension. *Am J Physiol Regul Integr Comp Physiol,* 293**,** R251-6.

FRANCO, M., TAPIA, E., BAUTISTA, R., PACHECO, U., SANTAMARIA, J., QUIROZ, Y., JOHNSON, R. J. & RODRIGUEZ-ITURBE, B. 2013. Impaired pressure natriuresis resulting in salt-sensitive hypertension is caused by tubulointerstitial immune cell infiltration in the kidney. *Am J Physiol Renal Physiol,* 304**,** F982-90.

FREIS, E. D. 1992. The role of salt in hypertension. *Blood Press,* 1**,** 196-200.

GANGEL, M. J., SHANAHAN, L., KOLACZ, J., JANSSEN, J. A., BROWN, A., CALKINS, S. D., KEANE, S. P. & WIDEMAN, L. 2017. Vagal Regulation of Cardiac Function in Early Childhood and Cardiovascular Risk in Adolescence. *Psychosom Med,* 79**,** 614-621.

GARIMELLA, P. S., BIGGS, M. L., KATZ, R., IX, J. H., BENNETT, M. R., DEVARAJAN, P., KESTENBAUM, B. R., SISCOVICK, D. S., JENSEN, M. K., SHLIPAK, M. G., CHAVES, P. H. & SARNAK, M. J. 2015. Urinary uromodulin, kidney function, and cardiovascular disease in elderly adults. *Kidney Int,* 88**,** 1126-34.

GARIMELLA, P. S., LEE, A. K., AMBROSIUS, W. T., BHATT, U., CHEUNG, A. K., CHONCHOL, M., CRAVEN, T., HAWFIELD, A. T., JOTWANI, V., KILLEEN, A., PUNZI, H., SARNAK, M. J., WALL, B. M., IX, J. H. & SHLIPAK, M. G.

2019. Markers of kidney tubule function and risk of cardiovascular disease events and mortality in the SPRINT trial. *Eur Heart J,* 40**,** 3486-3493.

GARRETA, E., GONZALEZ, F. & MONTSERRAT, N. 2018. Studying Kidney Disease Using Tissue and Genome Engineering in Human Pluripotent Stem Cells. *Nephron,* 138**,** 48-59.

GARRETA, E., PRADO, P., TARANTINO, C., ORIA, R., FANLO, L., MARTI, E., ZALVIDEA, D., TREPAT, X., ROCA-CUSACHS, P., GAVALDA-NAVARRO, A., COZZUTO, L., CAMPISTOL, J. M., IZPISUA BELMONTE, J. C., HURTADO DEL POZO, C. & MONTSERRAT, N. 2019. Fine tuning the extracellular environment accelerates the derivation of kidney organoids from human pluripotent stem cells. *Nat Mater,* 18**,** 397-405.

GIGANTE, B., RUBATTU, S., STANZIONE, R., LOMBARDI, A., BALDI, A., BALDI, F. & VOLPE, M. 2003. Contribution of genetic factors to renal lesions in the stroke-prone spontaneously hypertensive rat. *Hypertension,* 42**,** 702-6.

GLAUDEMANS, B., TERRYN, S., GOLZ, N., BRUNATI, M., CATTANEO, A., BACHI, A., AL-QUSAIRI, L., ZIEGLER, U., STAUB, O., RAMPOLDI, L. & DEVUYST, O. 2014. A primary culture system of mouse thick ascending limb cells with preserved function and uromodulin processing. *Pflugers Arch,* 466**,** 343-56.

GLORIOSO, N., FILIGHEDDU, F., TROFFA, C., SORO, A., PARPAGLIA, P. P., TSIKOUDAKIS, A., MYERS, R. H., HERRERA, V. L. & RUIZ-OPAZO, N. 2001. Interaction of alpha(1)-Na,K-ATPase and Na,K,2Cl-cotransporter genes in human essential hypertension. *Hypertension,* 38**,** 204-9.

GONG, Y. & HOU, J. 2014. Claudin-14 underlies Ca^{++}-sensing receptor-mediated Ca^{++} metabolism via NFAT-microRNA-based mechanisms. *J Am Soc Nephrol,* 25**,** 745-60.

GONG, Y., RENIGUNTA, V., HIMMERKUS, N., ZHANG, J., RENIGUNTA, A., BLEICH, M. & HOU, J. 2012. Claudin-14 regulates renal Ca^{++} transport in response to CaSR signalling via a novel microRNA pathway. *Embo j,* 31**,** 1999-2012.

GONZALEZ-VICENTE, A., SAEZ, F., MONZON, C. M., ASIRWATHAM, J. & GARVIN, J. L. 2019. Thick Ascending Limb Sodium Transport in the Pathogenesis of Hypertension. *Physiol Rev,* 99**,** 235-309.

GORVIN, C. M. 2018. Insights into calcium-sensing receptor trafficking and biased signalling by studies of calcium homeostasis. *J Mol Endocrinol,* 61**,** R1-r12.

GRACA, J. A., SCHEPELMANN, M., BRENNAN, S. C., REENS, J., CHANG, W., YAN, P., TOKA, H., RICCARDI, D. & PRICE, S. A. 2016. Comparative expression of the extracellular calcium-sensing receptor in the mouse, rat, and human kidney. *Am J Physiol Renal Physiol,* 310**,** F518-33.

GRAHAM, D., MCBRIDE, M. W., GAASENBEEK, M., GILDAY, K., BEATTIE, E., MILLER, W. H., MCCLURE, J. D., POLKE, J. M., MONTEZANO, A., TOUYZ, R. M. & DOMINICZAK, A. F. 2007. Candidate genes that determine response to salt in the stroke-prone spontaneously hypertensive rat: congenic analysis. *Hypertension,* 50**,** 1134-41.

GRAHAM, L. A., AMAN, A., CAMPBELL, D. D., AUGLEY, J., GRAHAM, D., MCBRIDE, M. W., FRASER, N. J., FERRERI, N. R., DOMINICZAK, A. F. & PADMANABHAN, S. 2018. Salt stress in the renal tubules is linked to TAL-specific expression of uromodulin and an upregulation of heat shock genes. *Physiol Genomics,* 50**,** 964-972.

GRAHAM, L. A., DOMINICZAK, A. F. & FERRERI, N. R. 2017. Role of renal transporters and novel regulatory interactions in the TAL that control blood pressure. *Physiol Genomics,* 49**,** 261-276.

GRAHAM, L. A., PADMANABHAN, S., FRASER, N. J., KUMAR, S., BATES, J. M., RAFFI, H. S., WELSH, P., BEATTIE, W., HAO, S., LEH, S., HULTSTROM, M., FERRERI, N. R., DOMINICZAK, A. F., GRAHAM, D. & MCBRIDE, M. W. 2014. Validation of uromodulin as a candidate gene for human essential hypertension. *Hypertension,* 63**,** 551-8.

GRASSI, G., CATTANEO, B. M., SERAVALLE, G., LANFRANCHI, A. & MANCIA, G. 1998. Baroreflex control of sympathetic nerve activity in essential and secondary hypertension. *Hypertension,* 31**,** 68-72.

GRAUDAL, N. A., HUBECK-GRAUDAL, T. & JURGENS, G. 2011. Effects of low sodium diet versus high sodium diet on blood pressure, renin, aldosterone, catecholamines, cholesterol, and triglyceride. *Cochrane Database Syst Rev***,** Cd004022.

GRESH, L., FISCHER, E., REIMANN, A., TANGUY, M., GARBAY, S., SHAO, X., HIESBERGER, T., FIETTE, L., IGARASHI, P., YANIV, M. & PONTOGLIO, M. 2004. A transcriptional network in polycystic kidney disease. *Embo j,* 23**,** 1657-68.

GRIFFIN, K. A., CHURCHILL, P. C., PICKEN, M., WEBB, R. C., KURTZ, T. W. & BIDANI, A. K. 2001. Differential salt-sensitivity in the pathogenesis of renal damage in SHR and stroke prone SHR. *Am J Hypertens,* 14**,** 311-20.

GRILLO, A., SALVI, L., CORUZZI, P., SALVI, P. & PARATI, G. 2019. Sodium Intake and Hypertension. *Nutrients,* 11.

GRUNEWALD, R. W., OPPERMANN, M., SCHETTLER, V., FIEDLER, G. M., JEHLE, P. M. & SCHUETTERT, J. B. 2001. Polarized function of thick ascending limbs of Henle cells in osmoregulation. *Kidney Int,* 60**,** 2290-8.

GUDBJARTSSON, D. F., HOLM, H., INDRIDASON, O. S., THORLEIFSSON, G., EDVARDSSON, V., SULEM, P., DE VEGT, F., D'ANCONA, F. C., DEN HEIJER, M., WETZELS, J. F., FRANZSON, L., RAFNAR, T., KRISTJANSSON, K., BJORNSDOTTIR, U. S., EYJOLFSSON, G. I., KIEMENEY, L. A., KONG, A., PALSSON, R., THORSTEINSDOTTIR, U. & STEFANSSON, K. 2010. Association of variants at UMOD with chronic kidney disease and kidney stones-role of age and comorbid diseases. *PLoS Genet,* 6**,** e1001039.

GUERRERO-ROMERO, F., RODRÍGUEZ-MORÁN, M., HERNÁNDEZ-RONQUILLO, G., GÓMEZ-DÍAZ, R., PIZANO-ZARATE, M. L., WACHER, N. H., MONDRAGÓN-GONZÁLEZ, R. & SIMENTAL-MENDIA, L. E. 2016. Low Serum Magnesium Levels and Its Association with High Blood Pressure in Children. *J Pediatr,* 168**,** 93-98.e1.

GUIDI, E., GIGLIONI, A., COZZI, M. G. & MINETTI, E. E. 1998. Which urinary proteins are decreased after angiotensin converting--enzyme inhibition? *Ren Fail,* 20**,** 243-8.

GUO, X. Y., LIU, Y. S., GAO, X. D., KINOSHITA, T. & FUJITA, M. 2020. Calnexin mediates the maturation of GPI-anchors through ER retention. *J Biol Chem,* 295**,** 16393-16410.

GURDASANI, D., BARROSO, I., ZEGGINI, E. & SANDHU, M. S. 2019. Genomics of disease risk in globally diverse populations. *Nat Rev Genet,* 20**,** 520-535.

GUYTON, A. C., COLEMAN, T. G., COWLEY, A. V., JR., SCHEEL, K. W., MANNING, R. D., JR. & NORMAN, R. A., JR. 1972. Arterial pressure regulation. Overriding dominance of the kidneys in long-term regulation and in hypertension. *Am J Med,* 52**,** 584-94.

HALL, M. E., DO CARMO, J. M., DA SILVA, A. A., JUNCOS, L. A., WANG, Z. & HALL, J. E. 2014. Obesity, hypertension, and chronic kidney disease. *Int J Nephrol Renovasc Dis,* 7**,** 75-88.

HAO, C. M. & BREYER, M. D. 2008. Physiological regulation of prostaglandins in the kidney. *Annu Rev Physiol,* 70**,** 357-77.

HAO, S., BELLNER, L. & FERRERI, N. R. 2013. NKCC2A and NFAT5 regulate renal TNF production induced by hypertonic NaCl intake. *Am J Physiol Renal Physiol,* 304**,** F533-42.

HAQUE, M. Z., ARES, G. R., CACERES, P. S. & ORTIZ, P. A. 2011. High salt differentially regulates surface NKCC2 expression in thick ascending limbs of Dahl salt-sensitive and salt-resistant rats. *Am J Physiol Renal Physiol,* 300**,** F1096-104.

HARRIS, P. J., THOMAS, D. & MORGAN, T. O. 1987. Atrial natriuretic peptide inhibits angiotensin-stimulated proximal tubular sodium and water reabsorption. *Nature,* 326**,** 697-8.

HART, T. C., GORRY, M. C., HART, P. S., WOODARD, A. S., SHIHABI, Z., SANDHU, J., SHIRTS, B., XU, L., ZHU, H., BARMADA, M. M. & BLEYER, A. J. 2002. Mutations of the UMOD gene are responsible for medullary cystic kidney disease 2 and familial juvenile hyperuricaemic nephropathy. *J Med Genet,* 39**,** 882-92.

HARVEY, A. P., MONTEZANO, A. C., HOOD, K. Y., LOPES, R. A., RIOS, F., CERAVOLO, G., GRAHAM, D. & TOUYZ, R. M. 2017. Vascular dysfunction and fibrosis in stroke-prone spontaneously hypertensive rats: The aldosterone-mineralocorticoid receptor-Nox1 axis. *Life Sci,* 179**,** 110-119.

HASTY, A. H. & HARRISON, D. G. 2012. Endoplasmic reticulum stress and hypertension - a new paradigm? *J Clin Invest,* 122**,** 3859-61.

HATTON, D. C. & MCCARRON, D. A. 1994. Dietary calcium and blood pressure in experimental models of hypertension. A review. *Hypertension,* 23**,** 513-30.

HAVLIK, R. J., GARRISON, R. J., FEINLEIB, M., KANNEL, W. B., CASTELLI, W. P. & MCNAMARA, P. M. 1979. Blood pressure aggregation in families. *Am J Epidemiol,* 110**,** 304-12.

HE, F. J. & MACGREGOR, G. A. 2010. Reducing population salt intake worldwide: from evidence to implementation. *Prog Cardiovasc Dis,* 52**,** 363-82.

HE, F. J., TAN, M., MA, Y. & MACGREGOR, G. A. 2020. Salt Reduction to Prevent Hypertension and Cardiovascular Disease: JACC State-of-the-Art Review. *Journal of the American College of Cardiology,* 75**,** 632-647.

HE, J., OGDEN, L. G., VUPPUTURI, S., BAZZANO, L. A., LORIA, C. & WHELTON, P. K. 1999. Dietary sodium intake and subsequent risk of cardiovascular disease in overweight adults. *JAMA,* 282**,** 2027-34.

HEITMEIER, M., MCCRACKEN, R., MICANOVIC, R., KHAN, S. & EL-ACHKAR, T. M. 2014. The role of tumor necrosis factor alpha in regulating the expression of Tamm-Horsfall Protein (uromodulin) in thick ascending limbs during kidney injury. *Am J Nephrol,* 40**,** 458-67.

HERRERA, M., SILVA, G. B. & GARVIN, J. L. 2010. Angiotensin II stimulates thick ascending limb superoxide production via protein kinase C(α)-dependent NADPH oxidase activation. *J Biol Chem,* 285**,** 21323-8.

HIRSCHLER, V., GONZÁLEZ, C., MACCALLINI, G., MOLINARI, C. & CASTANO, L. 2017. Association between blood pressure and magnesium and uric acid levels in indigenous Argentinean children at high altitude. *Am J Hum Biol,* 29.

HOU, J., RENIGUNTA, A., GOMES, A. S., HOU, M., PAUL, D. L., WALDEGGER, S. & GOODENOUGH, D. A. 2009. Claudin-16 and claudin-19 interaction is required for their assembly into tight junctions and for renal reabsorption of magnesium. *Proc Natl Acad Sci U S A,* 106**,** 15350-5.

HOU, J., RENIGUNTA, A., KONRAD, M., GOMES, A. S., SCHNEEBERGER, E. E., PAUL, D. L., WALDEGGER, S. & GOODENOUGH, D. A. 2008. Claudin-16 and claudin-19 interact and form a cation-selective tight junction complex. *J Clin Invest,* 118**,** 619-28.

HOUSTON, M. 2011. Handbook of hypertension.

HUANG, C. L. 2007. Complex roles of PIP2 in the regulation of ion channels and transporters. *Am J Physiol Renal Physiol,* 293**,** F1761-5.

HUANG, W., WANG, W., ZHOU, M., CHEN, S., GAO, X., FAN, Q., DING, X. & ZHANG, X. 2013. Peripapillary choroidal thickness in healthy Chinese subjects. *BMC Ophthalmol,* 13**,** 23.

HYE KHAN, M. A., NECKAR, J., MANTHATI, V., ERRABELLI, R., PAVLOV, T. S., STARUSCHENKO, A., FALCK, J. R. & IMIG, J. D. 2013a. Orally active epoxyeicosatrienoic acid analog attenuates kidney injury in hypertensive Dahl salt-sensitive rat. *Hypertension,* 62**,** 905-13.

HYE KHAN, M. A., NECKÁR, J., MANTHATI, V., ERRABELLI, R., PAVLOV, T. S., STARUSCHENKO, A., FALCK, J. R. & IMIG, J. D. 2013b. Orally active epoxyeicosatrienoic acid analog attenuates kidney injury in hypertensive Dahl salt-sensitive rat. *Hypertension,* 62**,** 905-13.

ICHII, O., YABUKI, A., OJIMA, T., MATSUMOTO, M. & SUZUKI, S. 2006. Rodent renal structure differs among species. *J Vet Med Sci,* 68**,** 439-45.

IKARI, A., OKUDE, C., SAWADA, H., SASAKI, Y., YAMAZAKI, Y., SUGATANI, J., DEGAWA, M. & MIWA, M. 2008. Activation of a polyvalent cation-sensing receptor decreases magnesium transport via claudin-16. *Biochim Biophys Acta,* 1778**,** 283-90.

IMIG, J. D., ZHAO, X., CAPDEVILA, J. H., MORISSEAU, C. & HAMMOCK, B. D. 2002. Soluble epoxide hydrolase inhibition lowers arterial blood pressure in angiotensin II hypertension. *Hypertension,* 39**,** 690-4.

ISHIZAKA, N., AIZAWA, T., OHNO, M., USUI SI, S., MORI, I., TANG, S. S., INGELFINGER, J. R., KIMURA, S. & NAGAI, R. 2002. Regulation and localization of HSP70 and HSP25 in the kidney of rats undergoing long-term administration of angiotensin II. *Hypertension,* 39**,** 122-8.

JAMA, H. A., MURALITHARAN, R. R., XU, C., O'DONNELL, J. A., BERTAGNOLLI, M., BROUGHTON, B. R. S., HEAD, G. A. & MARQUES, F. Z. 2022. Rodent models of hypertension. *Br J Pharmacol,* 179**,** 918-937.

JANKOWSKI, J., FLOEGE, J., FLISER, D., BÖHM, M. & MARX, N. 2021. Cardiovascular Disease in Chronic Kidney Disease: Pathophysiological Insights and Therapeutic Options. *Circulation,* 143**,** 1157-1172.

JEFFS, B., NEGRIN, C. D., GRAHAM, D., CLARK, J. S., ANDERSON, N. H., GAUGUIER, D. & DOMINICZAK, A. F. 2000. Applicability of a "speed" congenic strategy to dissect blood pressure quantitative trait loci on rat chromosome 2. *Hypertension,* 35**,** 179-87.

JI, W., FOO, J. N., O'ROAK, B. J., ZHAO, H., LARSON, M. G., SIMON, D. B., NEWTON-CHEH, C., STATE, M. W., LEVY, D. & LIFTON, R. P. 2008. Rare independent mutations in renal salt handling genes contribute to blood pressure variation. *Nat Genet,* 40**,** 592-599.

JI, X., NAITO, Y., HIROKAWA, G., WENG, H., HIURA, Y., TAKAHASHI, R. & IWAI, N. 2012. P2X(7) receptor antagonism attenuates the hypertension and renal injury in Dahl salt-sensitive rats. *Hypertens Res,* 35**,** 173-9.

JIMÉNEZ-ALTAYÓ, F., BRIONES, A. M., GIRALDO, J., PLANAS, A. M., SALAICES, M. & VILA, E. 2006. Increased superoxide anion production by interleukin-1beta impairs nitric oxide-mediated relaxation in resistance arteries. *J Pharmacol Exp Ther,* 316**,** 42-52.

JUNG, J., BASILE, D. P. & PRATT, J. H. 2011. Sodium reabsorption in the thick ascending limb in relation to blood pressure: a clinical perspective. *Hypertension,* 57**,** 873-9.

KALRA, D., SIVASUBRAMANIAN, N. & MANN, D. L. 2002. Angiotensin II induces tumor necrosis factor biosynthesis in the adult mammalian heart through a protein kinase C-dependent pathway. *Circulation,* 105**,** 2198-205.

KAPALCZYNSKA, M., KOLENDA, T., PRZYBYLA, W., ZAJACZKOWSKA, M., TERESIAK, A., FILAS, V., IBBS, M., BLIZNIAK, R., LUCZEWSKI, L. & LAMPERSKA, K. 2018. 2D and 3D cell cultures - a comparison of different types of cancer cell cultures. *Arch Med Sci,* 14**,** 910-919.

KAUFMAN, D. P., BASIT, H. & KNOHL, S. J. 2023. Physiology, Glomerular Filtration Rate. *StatPearls.* Treasure Island (FL) ineligible companies. Disclosure: Hajira Basit declares no relevant financial relationships with ineligible companies. Disclosure: Stephen Knohl declares no relevant financial relationships with ineligible companies.

KEMTER, E., PRUECKL, P., SKLENAK, S., RATHKOLB, B., HABERMANN, F. A., HANS, W., GAILUS-DURNER, V., FUCHS, H., HRABE DE ANGELIS, M., WOLF, E., AIGNER, B. & WANKE, R. 2013. Type of uromodulin mutation and allelic status influence onset and severity of uromodulin-associated kidney disease in mice. *Hum Mol Genet,* 22**,** 4148-63.

KERR, S., BROSNAN, M. J., MCINTYRE, M., REID, J. L., DOMINICZAK, A. F. & HAMILTON, C. A. 1999. Superoxide anion production is increased in a model of genetic hypertension: role of the endothelium. *Hypertension,* 33**,** 1353-8.

KHADIVE, T., GHADIMI, D., HEMMATI, M. & GOLSHAHI, H. 2021. Impact of high salt diets on CHOP-mediated apoptosis and renal fibrosis in a rat model. *Mol Biol Rep,* 48**,** 6423-6433.

KHOSHDEL-RAD, N., AHMADI, A. & MOGHADASALI, R. 2022. Kidney organoids: current knowledge and future directions. *Cell Tissue Res,* 387**,** 207-224.

KIM, G. H., ECELBARGER, C., KNEPPER, M. A. & PACKER, R. K. 1999. Regulation of thick ascending limb ion transporter abundance in response to altered acid/base intake. *J Am Soc Nephrol,* 10**,** 935-42.

KIM, S., TOKUYAMA, M., HOSOI, M. & YAMAMOTO, K. 1992. Adrenal and circulating renin-angiotensin system in stroke-prone hypertensive rats. *Hypertension,* 20**,** 280-91.

KING, J. & LOWERY, D. R. 2023. Physiology, Cardiac Output. *StatPearls.* Treasure Island (FL) ineligible companies. Disclosure: David Lowery declares no relevant financial relationships with ineligible companies.

KIRABO, A., FONTANA, V., DE FARIA, A. P., LOPERENA, R., GALINDO, C. L., WU, J., BIKINEYEVA, A. T., DIKALOV, S., XIAO, L., CHEN, W., SALEH, M. A., TROTT, D. W., ITANI, H. A., VINH, A., AMARNATH, V., AMARNATH, K., GUZIK, T. J., BERNSTEIN, K. E., SHEN, X. Z., SHYR, Y., CHEN, S. C., MERNAUGH, R. L., LAFFER, C. L., ELIJOVICH, F., DAVIES, S. S., MORENO, H., MADHUR, M. S., ROBERTS, J., 2ND & HARRISON, D. G. 2014. DC isoketal-modified proteins activate T cells and promote hypertension. *J Clin Invest,* 124**,** 4642-56.

KIRCHNER, K. A. 1992. Increased loop chloride uptake precedes hypertension in Dahl salt-sensitive rats. *Am J Physiol,* 262**,** R263-8.

KIRCHNER, K. A., CROSBY, B. A., PATEL, A. R. & GRANGER, J. P. 1995. Segmental chloride transport in the Dahl-S rat kidney during L-arginine administration. *J Am Soc Nephrol,* 5**,** 1567-72.

KOBAYASHI, K. & FUKUOKA, S. 2001. Conditions for solubilization of Tamm-Horsfall protein/uromodulin in human urine and establishment of a sensitive and accurate enzyme-linked immunosorbent assay (ELISA) method. *Arch Biochem Biophys,* 388**,** 113-20.

KOMPATSCHER, A., DE BAAIJ, J. H. F., ABOUDEHEN, K., FARAHANI, S., VAN SON, L. H. J., MILATZ, S., HIMMERKUS, N., VEENSTRA, G. C., BINDELS, R. J. M. & HOENDEROP, J. G. J. 2018. Transcription factor HNF1β regulates expression of the calcium-sensing receptor in the thick ascending limb of the kidney. *Am J Physiol Renal Physiol,* 315**,** F27-f35.

KONONIKHIN, A. S., STARODUBTSEVA, N. L., BUGROVA, A. E., SHIROKOVA, V. A., CHAGOVETS, V. V., INDEYKINA, M. I., POPOV, I. A., KOSTYUKEVICH, Y. I., VAVINA, O. V., MUMINOVA, K. T., KHODZHAEVA, Z. S., KAN, N. E., FRANKEVICH, V. E., NIKOLAEV, E. N. & SUKHIKH, G. T. 2016. An untargeted approach for the analysis of the urine peptidome of women with preeclampsia. *J Proteomics,* 149**,** 38-43.

KÖTTGEN, A., GLAZER, N. L., DEHGHAN, A., HWANG, S. J., KATZ, R., LI, M., YANG, Q., GUDNASON, V., LAUNER, L. J., HARRIS, T. B., SMITH, A. V., ARKING, D. E., ASTOR, B. C., BOERWINKLE, E., EHRET, G. B., RUCZINSKI, I., SCHARPF, R. B., CHEN, Y. D., DE BOER, I. H., HARITUNIANS, T., LUMLEY, T., SARNAK, M., SISCOVICK, D., BENJAMIN, E. J., LEVY, D., UPADHYAY, A., AULCHENKO, Y. S., HOFMAN, A., RIVADENEIRA, F., UITTERLINDEN, A. G., VAN DUIJN, C. M., CHASMAN, D. I., PARÉ, G., RIDKER, P. M., KAO, W. H., WITTEMAN, J. C., CORESH, J., SHLIPAK, M. G. & FOX, C. S. 2009. Multiple loci associated with indices of renal function and chronic kidney disease. *Nat Genet,* 41**,** 712-7.

KÖTTGEN, A., HWANG, S. J., LARSON, M. G., VAN EYK, J. E., FU, Q., BENJAMIN, E. J., DEHGHAN, A., GLAZER, N. L., KAO, W. H., HARRIS, T. B., GUDNASON, V., SHLIPAK, M. G., YANG, Q., CORESH, J., LEVY, D. & FOX, C. S. 2010. Uromodulin levels associate with a common UMOD variant and risk for incident CKD. *J Am Soc Nephrol,* 21**,** 337-44.

KOUROUKLIS, A. P., WAHLSTEN, A., STRACUZZI, A., MARTYTS, A., PAGANELLA, L. G., LABOUESSE, C., AL-NUAIMI, D., GIAMPIETRO, C., EHRET, A. E., TIBBITT, M. W. & MAZZA, E. 2023. Control of hydrostatic pressure and osmotic stress in 3D cell culture for mechanobiological studies. *Biomater Adv,* 145**,** 213241.

KOZLOV, G. & GEHRING, K. 2020. Calnexin cycle - structural features of the ER chaperone system. *FEBS J,* 287**,** 4322-4340.

KROCHMAL, M., KONTOSTATHI, G., MAGALHAES, P., MAKRIDAKIS, M., KLEIN, J., HUSI, H., LEIERER, J., MAYER, G., BASCANDS, J. L., DENIS, C., ZOIDAKIS, J., ZURBIG, P., DELLES, C., SCHANSTRA, J. P., MISCHAK, H. & VLAHOU, A. 2017a. Urinary peptidomics analysis reveals proteases involved in diabetic nephropathy. *Sci Rep,* 7**,** 15160.

KROCHMAL, M., KONTOSTATHI, G., MAGALHÃES, P., MAKRIDAKIS, M., KLEIN, J., HUSI, H., LEIERER, J., MAYER, G., BASCANDS, J. L., DENIS, C., ZOIDAKIS, J., ZÜRBIG, P., DELLES, C., SCHANSTRA, J. P., MISCHAK, H. & VLAHOU, A. 2017b. Urinary peptidomics analysis reveals proteases involved in diabetic nephropathy. *Sci Rep,* 7**,** 15160.

KUHN, M. 2016. Molecular Physiology of Membrane Guanylyl Cyclase Receptors. *Physiol Rev,* 96**,** 751-804.

KUMAR, S. & MUCHMORE, A. 1990. Tamm-Horsfall protein--uromodulin (1950-1990). *Kidney Int,* 37**,** 1395-401.

KUNES, J. & ZICHA, J. 2006. Developmental windows and environment as important factors in the expression of genetic information: a cardiovascular physiologist's view. *Clin Sci (Lond),* 111**,** 295-305.

KUNES, J. & ZICHA, J. 2009. The interaction of genetic and environmental factors in the etiology of hypertension. *Physiol Res,* 58 Suppl 2**,** S33-s42.

KURT, B. & KURTZ, A. 2015. Plasticity of renal endocrine function. *Am J Physiol Regul Integr Comp Physiol,* 308**,** R455-66.

KYSELOVIC, J., KRENEK, P., WIBO, M. & GODFRAIND, T. 2001. Effects of amlodipine and lacidipine on cardiac remodelling and renin production in salt-loaded stroke-prone hypertensive rats. *Br J Pharmacol,* 134**,** 1516-22.

LAFAVERS, K. A., MACEDO, E., GARIMELLA, P. S., LIMA, C., KHAN, S., MYSLINSKI, J., MCCLINTICK, J., WITZMANN, F. A., WINFREE, S., PHILLIPS, C. L., HATO, T., DAGHER, P. C., WU, X. R., EL-ACHKAR, T. M. & MICANOVIC, R. 2019. Circulating uromodulin inhibits systemic oxidative stress by inactivating the TRPM2 channel. *Sci Transl Med,* 11.

LAFAVERS, K. A., MICANOVIC, R., SABO, A. R., MAGHAK, L. A. & EL-ACHKAR, T. M. 2022. Evolving Concepts in Uromodulin Biology, Physiology, and Its Role in Disease: a Tale of Two Forms. *Hypertension,* 79**,** 2409-2418.

LAZZERINI, P. E., HAMILTON, R. M. & BOUTJDIR, M. 2019. Editorial: Cardioimmunology: Inflammation and Immunity in Cardiovascular Disease. *Front Cardiovasc Med,* 6**,** 181.

LEE, J. W., CHOU, C. L. & KNEPPER, M. A. 2015. Deep Sequencing in Microdissected Renal Tubules Identifies Nephron Segment-Specific Transcriptomes. *J Am Soc Nephrol,* 26**,** 2669-77.

LEE, R. M., DICKHOUT, J. G. & SANDOW, S. L. 2017. Vascular structural and functional changes: their association with causality in hypertension: models, remodeling and relevance. *Hypertens Res,* 40**,** 311-323.

LEMAY, J., TEA, B. S., HAMET, P. & DEBLOIS, D. 2001. Regression of neointimal lesions in the carotid artery of nifedipine-treated SHR and WKY rats: possible role of apoptosis. *J Vasc Res,* 38**,** 462-70.

LEVICK, J. R. 2010. *An introduction to cardiovascular physiology / J. Rodney Levick,* London, Hodder Arnold.

LI, Y., CHENG, Y., CONSOLATO, F., SCHIANO, G., CHONG, M. R., PIETZNER, M., NGUYEN, N. Q. H., SCHERER, N., BIGGS, M. L., KLEBER, M. E., HAUG, S., GOCMEN, B., PIGEYRE, M., SEKULA, P., STEINBRENNER, I., SCHLOSSER, P., JOSEPH, C. B., BRODY, J. A., GRAMS, M. E., HAYWARD, C., SCHULTHEISS, U. T., KRAMER, B. K., KRONENBERG, F., PETERS, A., SEISSLER, J., STEUBL, D., THEN, C., WUTTKE, M., MARZ, W., ECKARDT, K. U., GIEGER, C., BOERWINKLE, E., PSATY, B. M., CORESH, J., OEFNER, P. J., PARE, G., LANGENBERG, C., SCHERBERICH, J. E., YU, B., AKILESH, S., DEVUYST, O., RAMPOLDI, L. & KOTTGEN, A. 2022. Genome-wide studies reveal factors associated with circulating uromodulin and its relationships to complex diseases. *JCI Insight,* 7.

LI, Y., XIA, W., ZHAO, F., WEN, Z., ZHANG, A., HUANG, S., JIA, Z. & ZHANG, Y. 2018. Prostaglandins in the pathogenesis of kidney diseases. *Oncotarget,* 9**,** 26586-26602.

LIFTON, R. P., GHARAVI, A. G. & GELLER, D. S. 2001. Molecular mechanisms of human hypertension. *Cell,* 104**,** 545-56.

LIN, H. Y., LEE, Y. T., CHAN, Y. W. & TSE, G. 2016. Animal models for the study of primary and secondary hypertension in humans. *Biomed Rep,* 5**,** 653-659.

LJUNGMAN, S., AURELL, M., HARTFORD, M., WIKSTRAND, J., WILHELMSEN, L. & BERGLUND, G. 1980. Blood pressure and renal function. *Acta Med Scand,* 208**,** 17-25.

LONG, A. N. & DAGOGO-JACK, S. 2011. Comorbidities of diabetes and hypertension: mechanisms and approach to target organ protection. *J Clin Hypertens (Greenwich),* 13**,** 244-51.

LOS, M., DRÖGE, W., STRICKER, K., BAEUERLE, P. A. & SCHULZE-OSTHOFF, K. 1995. Hydrogen peroxide as a potent activator of T lymphocyte functions. *Eur J Immunol,* 25**,** 159-65.

LOZIC, M., SARENAC, O., MURPHY, D. & JAPUNDZIC-ZIGON, N. 2018. Vasopressin, Central Autonomic Control and Blood Pressure Regulation. *Curr Hypertens Rep,* 20**,** 11.

LUYCKX, V. A., BERTRAM, J. F., BRENNER, B. M., FALL, C., HOY, W. E., OZANNE, S. E. & VIKSE, B. E. 2013. Effect of fetal and child health on kidney development and long-term risk of hypertension and kidney disease. *Lancet,* 382**,** 273-83.

LV, L., WANG, J., GAO, B., WU, L., WANG, F., CUI, Z., HE, K., ZHANG, L., CHEN, M. & ZHAO, M. H. 2018. Serum uromodulin and progression of kidney disease in patients with chronic kidney disease. *J Transl Med,* 16**,** 316.

LYNN, K. L., SHENKIN, A. & MARSHALL, R. D. 1982. Factors affecting excretion of human urinary Tamm-Horsfall glycoprotein. *Clin Sci (Lond),* 62**,** 21-6.

MA, K., GAO, W., XU, H., LIANG, W. & MA, G. 2022. Role and Mechanism of the Renin-Angiotensin-Aldosterone System in the Onset and Development of Cardiorenal Syndrome. *J Renin Angiotensin Aldosterone Syst,* 2022**,** 3239057.

MA, L., LIU, Y., EL-ACHKAR, T. M. & WU, X. R. 2012. Molecular and cellular effects of Tamm-Horsfall protein mutations and their rescue by chemical chaperones. *J Biol Chem,* 287**,** 1290-305.

MACGREGOR, G. A. 1985. Sodium is more important than calcium in essential hypertension. *Hypertension,* 7**,** 628-40.

MACHERET, F., HEUBLEIN, D., COSTELLO-BOERRIGTER, L. C., BOERRIGTER, G., MCKIE, P., BELLAVIA, D., MANGIAFICO, S., IKEDA, Y., BAILEY, K., SCOTT, C. G., SANDBERG, S., CHEN, H. H., MALATINO, L., REDFIELD, M. M., RODEHEFFER, R., BURNETT, J., JR. & CATALIOTTI, A. 2012. Human hypertension is characterized by a lack of activation of the antihypertensive cardiac hormones ANP and BNP. *J Am Coll Cardiol,* 60**,** 1558-65.

MACLELLAN, W. R., WANG, Y. & LUSIS, A. J. 2012. Systems-based approaches to cardiovascular disease. *Nat Rev Cardiol,* 9**,** 172-84.

MACRAE, C., MERCER, S. W., GUTHRIE, B. & HENDERSON, D. 2021. Comorbidity in chronic kidney disease: a large cross-sectional study of prevalence in Scottish primary care. *Br J Gen Pract,* 71**,** e243-e249.

MADSEN, K. M., VERLANDER, J. W. & TISHER, C. C. 1988. Relationship between structure and function in distal tubule and collecting duct. *J Electron Microsc Tech,* 9**,** 187-208.

MAILLARD, M. P., TEDJANI, A., PERREGAUX, C. & BURNIER, M. 2009. Calcium-sensing receptors modulate renin release in vivo and in vitro in the rat. *J Hypertens,* 27**,** 1980-7.

MARTINON, F. & TSCHOPP, J. 2004. Inflammatory caspases: linking an intracellular innate immune system to autoinflammatory diseases. *Cell,* 117**,** 561-74.

MARY, S., BODER, P., PADMANABHAN, S., MCBRIDE, M. W., GRAHAM, D., DELLES, C. & DOMINICZAK, A. F. 2022. Role of Uromodulin in Salt-Sensitive Hypertension. *Hypertension,* 79**,** 2419-2429.

MARY, S., BODER, P., ROSSITTO, G., GRAHAM, L., SCOTT, K., FLYNN, A., KIPGEN, D., GRAHAM, D. & DELLES, C. 2021. Salt loading decreases urinary excretion and increases intracellular accumulation of uromodulin in stroke-prone spontaneously hypertensive rats. *Clin Sci (Lond),* 135**,** 2749-2761.

MARY, S., SMALL, H. Y., SIWY, J., MULLEN, W., GIRI, A. & DELLES, C. 2017. Polymerization-Incompetent Uromodulin in the Pregnant Stroke-Prone Spontaneously Hypertensive Rat. *Hypertension,* 69**,** 910-918.

MASHIMO, T., VOIGT, B., KURAMOTO, T. & SERIKAWA, T. 2005. Rat Phenome Project: the untapped potential of existing rat strains. *J Appl Physiol (1985),* 98**,** 371-9.

MATAFORA, V., ZAGATO, L., FERRANDI, M., MOLINARI, I., ZERBINI, G., CASAMASSIMA, N., LANZANI, C., DELLI CARPINI, S., TREPICCIONE, F., MANUNTA, P., BACHI, A. & CAPASSO, G. 2014. Quantitative proteomics

reveals novel therapeutic and diagnostic markers in hypertension. *BBA Clin,* 2**,** 79-87.

MAYET, J. & HUGHES, A. 2003. Cardiac and vascular pathophysiology in hypertension. *Heart,* 89**,** 1104-9.

MENETON, P., JEUNEMAITRE, X., DE WARDENER, H. E. & MACGREGOR, G. A. 2005. Links between dietary salt intake, renal salt handling, blood pressure, and cardiovascular diseases. *Physiol Rev,* 85**,** 679-715.

MENTE, A., O'DONNELL, M. & YUSUF, S. 2021. Sodium Intake and Health: What Should We Recommend Based on the Current Evidence? *Nutrients,* 13.

MERKSAMER, P. I., TRUSINA, A. & PAPA, F. R. 2008. Real-time redox measurements during endoplasmic reticulum stress reveal interlinked protein folding functions. *Cell,* 135**,** 933-47.

MEUSSER, B., HIRSCH, C., JAROSCH, E. & SOMMER, T. 2005. ERAD: the long road to destruction. *Nat Cell Biol,* 7**,** 766-72.

MICANOVIC, R., LAFAVERS, K., GARIMELLA, P. S., WU, X. R. & EL-ACHKAR, T. M. 2020. Uromodulin (Tamm-Horsfall protein): guardian of urinary and systemic homeostasis. *Nephrol Dial Transplant,* 35**,** 33-43.

MISEREY-LENKEI, S., CHALANCON, G., BARDIN, S., FORMSTECHER, E., GOUD, B. & ECHARD, A. 2010. Rab and actomyosin-dependent fission of transport vesicles at the Golgi complex. *Nat Cell Biol,* 12**,** 645-54.

MIYATA, N., PARK, F., LI, X. F. & COWLEY, A. W., JR. 1999. Distribution of angiotensin AT1 and AT2 receptor subtypes in the rat kidney. *Am J Physiol,* 277**,** F437-46.

MO, L., HUANG, H. Y., ZHU, X. H., SHAPIRO, E., HASTY, D. L. & WU, X. R. 2004. Tamm-Horsfall protein is a critical renal defense factor protecting against calcium oxalate crystal formation. *Kidney Int,* 66**,** 1159-66.

MOMONIAT, T., ILYAS, D. & BHANDARI, S. 2019. ACE inhibitors and ARBs: Managing potassium and renal function. *Cleve Clin J Med,* 86**,** 601-607.

MONTEZANO, A. C. & TOUYZ, R. M. 2014. Reactive oxygen species, vascular Noxs, and hypertension: focus on translational and clinical research. *Antioxid Redox Signal,* 20**,** 164-82.

MOORE, A., MANGONI, A. A., LYONS, D. & JACKSON, S. H. 2003. The cardiovascular system. *Br J Clin Pharmacol,* 56**,** 254-60.

MORIGUCHI, T., URUSHIYAMA, S., HISAMOTO, N., IEMURA, S., UCHIDA, S., NATSUME, T., MATSUMOTO, K. & SHIBUYA, H. 2005. WNK1 regulates phosphorylation of cation-chloride-coupled cotransporters via the STE20-related kinases, SPAK and OSR1. *J Biol Chem,* 280**,** 42685-93.

MOUNT, D. B. 2014. Thick ascending limb of the loop of Henle. *Clin J Am Soc Nephrol,* 9**,** 1974-86.

MUNROE, P. B., WALLACE, C., XUE, M. Z., MARCANO, A. C., DOBSON, R. J., ONIPINLA, A. K., BURKE, B., GUNGADOO, J., NEWHOUSE, S. J., PEMBROKE, J., BROWN, M., DOMINICZAK, A. F., SAMANI, N. J., LATHROP, M., CONNELL, J., WEBSTER, J., CLAYTON, D., FARRALL, M., MEIN, C. A., CAULFIELD, M. & MEDICAL RESEARCH COUNCIL BRITISH GENETICS OF HYPERTENSION, S. 2006. Increased support for linkage of a novel locus on chromosome 5q13 for essential hypertension in the British Genetics of Hypertension Study. *Hypertension,* 48**,** 105-11.

MURPHY, S. R., DAHLY-VERNON, A. J., DUNN, K. M., CHEN, C. C., LEDBETTER, S. R., WILLIAMS, J. M. & ROMAN, R. J. 2012. Renoprotective effects of anti-TGF-β antibody and antihypertensive therapies in Dahl S rats. *Am J Physiol Regul Integr Comp Physiol,* 303**,** R57-69.

MUTIG, K., KAHL, T., SARITAS, T., GODES, M., PERSSON, P., BATES, J., RAFFI, H., RAMPOLDI, L., UCHIDA, S., HILLE, C., DOSCHE, C., KUMAR, S.,

CASTANEDA-BUENO, M., GAMBA, G. & BACHMANN, S. 2011a. Activation of the bumetanide-sensitive Na+,K+,2Cl- cotransporter (NKCC2) is facilitated by Tamm-Horsfall protein in a chloride-sensitive manner. *J Biol Chem,* 286**,** 30200-10.

MUTIG, K., KAHL, T., SARITAS, T., GODES, M., PERSSON, P., BATES, J., RAFFI, H., RAMPOLDI, L., UCHIDA, S., HILLE, C., DOSCHE, C., KUMAR, S., CASTAÑEDA-BUENO, M., GAMBA, G. & BACHMANN, S. 2011b. Activation of the bumetanide-sensitive Na+,K+,2Cl- cotransporter (NKCC2) is facilitated by Tamm-Horsfall protein in a chloride-sensitive manner. *J Biol Chem,* 286**,** 30200-10.

MYERS, J., PRAKASH, M., FROELICHER, V., DO, D., PARTINGTON, S. & ATWOOD, J. E. 2002. Exercise capacity and mortality among men referred for exercise testing. *N Engl J Med,* 346**,** 793-801.

NABIKA, T., OHARA, H., KATO, N. & ISOMURA, M. 2012. The stroke-prone spontaneously hypertensive rat: still a useful model for post-GWAS genetic studies? *Hypertens Res,* 35**,** 477-84.

NAGURA, J., HUI, C., YAMAMOTO, M., YASUDA, S., ABE, M., HACHISU, M. & KONNO, F. 1995. Effect of chronic treatment with ME3221 on blood pressure and mortality in aged stroke-prone spontaneously hypertensive rats. *Clin Exp Pharmacol Physiol Suppl,* 22**,** S363-5.

NATEKAR, A., OLDS, R. L., LAU, M. W., MIN, K., IMOTO, K. & SLAVIN, T. P. 2014. Elevated blood pressure: Our family's fault? The genetics of essential hypertension. *World J Cardiol,* 6**,** 327-37.

NAVAR, L. G. 2004. The intrarenal renin-angiotensin system in hypertension. *Kidney Int,* 65**,** 1522-32.

NAVAR, L. G., HARRISON-BERNARD, L. M., NISHIYAMA, A. & KOBORI, H. 2002. Regulation of intrarenal angiotensin II in hypertension. *Hypertension,* 39**,** 316-22.

NIE, M., BAL, M. S., LIU, J., YANG, Z., RIVERA, C., WU, X. R., HOENDEROP, J. G. J., BINDELS, R. J. M., MARCIANO, D. K. & WOLF, M. T. F. 2018. Uromodulin regulates renal magnesium homeostasis through the ion channel transient receptor potential melastatin 6 (TRPM6). *J Biol Chem,* 293**,** 16488-16502.

NIEDERER, S. A., LUMENS, J. & TRAYANOVA, N. A. 2019. Computational models in cardiology. *Nat Rev Cardiol,* 16**,** 100-111.

NIELSEN, S., MAUNSBACH, A. B., ECELBARGER, C. A. & KNEPPER, M. A. 1998. Ultrastructural localization of Na-K-2Cl cotransporter in thick ascending limb and macula densa of rat kidney. *Am J Physiol,* 275**,** F885-93.

NIIRANEN, T. J., MCCABE, E. L., LARSON, M. G., HENGLIN, M., LAKDAWALA, N. K., VASAN, R. S. & CHENG, S. 2017. Risk for hypertension crosses generations in the community: a multi-generational cohort study. *Eur Heart J,* 38**,** 2300-2308.

NIJENHUIS, T., HOENDEROP, J. G., VAN DER KEMP, A. W. & BINDELS, R. J. 2003. Localization and regulation of the epithelial Ca2+ channel TRPV6 in the kidney. *J Am Soc Nephrol,* 14**,** 2731-40.

NITO, M., SATO, H., HARA, T., KARASAWA, A., YAMADA, K. & OHTA, Y. 1995. Suppressive effects of benidipine on the development of hypertension and renal lesions in salt-loaded stroke-prone spontaneously hypertensive rats. *Clin Exp Pharmacol Physiol Suppl,* 22**,** S337-8.

NORDHEIM, E. & GEIR JENSSEN, T. 2021. Chronic kidney disease in patients with diabetes mellitus. *Endocr Connect,* 10**,** R151-r159.

NUNEZ-NESCOLARDE, A. B., NIKOLIC-PATERSON, D. J. & COMBES, A. N. 2022. Human Kidney Organoids and Tubuloids as Models of Complex Kidney Disease. *Am J Pathol,* 192**,** 738-749.

NYBERG, M., JENSEN, L. G., THANING, P., HELLSTEN, Y. & MORTENSEN, S. P. 2012. Role of nitric oxide and prostanoids in the regulation of leg blood flow and blood pressure in humans with essential hypertension: effect of high-intensity aerobic training. *J Physiol,* 590**,** 1481-94.

O'DONNELL, M., MENTE, A., ALDERMAN, M. H., BRADY, A. J. B., DIAZ, R., GUPTA, R., LOPEZ-JARAMILLO, P., LUFT, F. C., LUSCHER, T. F., MANCIA, G., MANN, J. F. E., MCCARRON, D., MCKEE, M., MESSERLI, F. H., MOORE, L. L., NARULA, J., OPARIL, S., PACKER, M., PRABHAKARAN, D., SCHUTTE, A., SLIWA, K., STAESSEN, J. A., YANCY, C. & YUSUF, S. 2020. Salt and cardiovascular disease: insufficient evidence to recommend low sodium intake. *Eur Heart J,* 41**,** 3363-3373.

O'DONNELL, M., MENTE, A., RANGARAJAN, S., MCQUEEN, M. J., WANG, X., LIU, L., YAN, H., LEE, S. F., MONY, P., DEVANATH, A., ROSENGREN, A., LOPEZ-JARAMILLO, P., DIAZ, R., AVEZUM, A., LANAS, F., YUSOFF, K., IQBAL, R., ILOW, R., MOHAMMADIFARD, N., GULEC, S., YUSUFALI, A. H., KRUGER, L., YUSUF, R., CHIFAMBA, J., KABALI, C., DAGENAIS, G., LEAR, S. A., TEO, K. & YUSUF, S. 2014a. Urinary sodium and potassium excretion, mortality, and cardiovascular events. *N Engl J Med,* 371**,** 612-23.

O'DONNELL, M., MENTE, A., RANGARAJAN, S., MCQUEEN, M. J., WANG, X., LIU, L., YAN, H., LEE, S. F., MONY, P., DEVANATH, A., ROSENGREN, A., LOPEZ-JARAMILLO, P., DIAZ, R., AVEZUM, A., LANAS, F., YUSOFF, K., IQBAL, R., ILOW, R., MOHAMMADIFARD, N., GULEC, S., YUSUFALI, A. H., KRUGER, L., YUSUF, R., CHIFAMBA, J., KABALI, C., DAGENAIS, G., LEAR, S. A., TEO, K., YUSUF, S. & INVESTIGATORS, P. 2014b. Urinary sodium and potassium excretion, mortality, and cardiovascular events. *N Engl J Med,* 371**,** 612-23.

O'SEAGHDHA, C. M., HWANG, S. J., LARSON, M. G., MEIGS, J. B., VASAN, R. S. & FOX, C. S. 2013. Analysis of a urinary biomarker panel for incident kidney disease and clinical outcomes. *J Am Soc Nephrol,* 24**,** 1880-8.

OBSERVATORY, T. S. P. H. 2022. *High Blood Pressure: key points* [Online]. The Scottish Public Health Observatory. Available: https://www.scotpho.org.uk/risk-factors/high-blood-pressure/key-points/#:~:text=In%202019%20around%20a%20quarter,years%20have%20high%20blood%20pressure [Accessed].

OGATA, H., RITZ, E., ODONI, G., AMANN, K. & ORTH, S. R. 2003. Beneficial effects of calcimimetics on progression of renal failure and cardiovascular risk factors. *J Am Soc Nephrol,* 14**,** 959-67.

OGOBUIRO, I. & TUMA, F. 2023. Physiology, Renal. *StatPearls.* Treasure Island (FL) with ineligible companies. Disclosure: Faiz Tuma declares no relevant financial relationships with ineligible companies.

OHSAKI, Y., O'CONNOR, P., MORI, T., RYAN, R. P., DICKINSON, B. C., CHANG, C. J., LU, Y., ITO, S. & COWLEY, A. W., JR. 2012. Increase of sodium delivery stimulates the mitochondrial respiratory chain H2O2 production in rat renal medullary thick ascending limb. *Am J Physiol Renal Physiol,* 302**,** F95-f102.

OKAMOTO, K., YAMAMOTO, K., MORITA, N., OHTA, Y., CHIKUGO, T., HIGASHIZAWA, T. & SUZUKI, T. 1986. Establishment and use of the M strain of stroke-prone spontaneously hypertensive rat. *J Hypertens Suppl,* 4**,** S21-4.

OLCZAK, K. J., TAYLOR-BATEMAN, V., NICHOLLS, H. L., TRAYLOR, M., CABRERA, C. P. & MUNROE, P. B. 2021. Hypertension genetics past, present and future applications. *Journal of Internal Medicine,* 290**,** 1130-1152.

OLDEN, M., CORRE, T., HAYWARD, C., TONIOLO, D., ULIVI, S., GASPARINI, P., PISTIS, G., HWANG, S. J., BERGMANN, S., CAMPBELL, H., COCCA, M., GANDIN, I., GIROTTO, G., GLAUDEMANS, B., HASTIE, N. D., LOFFING, J.,

POLASEK, O., RAMPOLDI, L., RUDAN, I., SALA, C., TRAGLIA, M., VOLLENWEIDER, P., VUCKOVIC, D., YOUHANNA, S., WEBER, J., WRIGHT, A. F., KUTALIK, Z., BOCHUD, M., FOX, C. S. & DEVUYST, O. 2014. Common variants in UMOD associate with urinary uromodulin levels: a meta-analysis. *J Am Soc Nephrol,* 25**,** 1869-82.

OLLIER-HARTMANN, M.-P., POUGET-ABADIE, C., BOUILLIE, J. & HARTMANN, L. 2008. Variations of Urinary Tamm-Horsfall Protein in Humans during the First Thirty Years of Life. *Nephron,* 38**,** 163-166.

OLINGER, E., HOUILLIER, P. & DEVUYST, O. 2018. Claudins: a tale of interactions in the thick ascending limb. *Kidney Int,* 93**,** 535-537.

OLINGER, E., LAKE, J., SHEEHAN, S., SCHIANO, G., TAKATA, T., TOKONAMI, N., DEBAIX, H., CONSOLATO, F., RAMPOLDI, L., KORSTANJE, R. & DEVUYST, O. 2019. Hepsin-mediated Processing of Uromodulin is Crucial for Salt-sensitivity and Thick Ascending Limb Homeostasis. *Sci Rep,* 9**,** 12287.

OTTERPOHL, K., BUSSELMAN, B., HART, R., SHAN, K., LIN, B., SURENDRAN, K. & CHANDRASEKAR, I. 2019. The apical membrane localization and trafficking of uromodulin (UMOD) is critically dependent on nonmuscle myosin II isoforms Myh9 and Myh10 in mouse thick ascending limb epithelial cells. *The FASEB Journal,* 33**,** 862.23-862.23.

PADMANABHAN, S., MELANDER, O., JOHNSON, T., DI BLASIO, A. M., LEE, W. K., GENTILINI, D., HASTIE, C. E., MENNI, C., MONTI, M. C., DELLES, C., LAING, S., CORSO, B., NAVIS, G., KWAKERNAAK, A. J., VAN DER HARST, P., BOCHUD, M., MAILLARD, M., BURNIER, M., HEDNER, T., KJELDSEN, S., WAHLSTRAND, B., SJÖGREN, M., FAVA, C., MONTAGNANA, M., DANESE, E., TORFFVIT, O., HEDBLAD, B., SNIEDER, H., CONNELL, J. M., BROWN, M., SAMANI, N. J., FARRALL, M., CESANA, G., MANCIA, G., SIGNORINI, S., GRASSI, G., EYHERAMENDY, S., WICHMANN, H. E., LAAN, M., STRACHAN, D. P., SEVER, P., SHIELDS, D. C., STANTON, A., VOLLENWEIDER, P., TEUMER, A., VÖLZKE, H., RETTIG, R., NEWTON-CHEH, C., ARORA, P., ZHANG, F., SORANZO, N., SPECTOR, T. D., LUCAS, G., KATHIRESAN, S., SISCOVICK, D. S., LUAN, J., LOOS, R. J., WAREHAM, N. J., PENNINX, B. W., NOLTE, I. M., MCBRIDE, M., MILLER, W. H., NICKLIN, S. A., BAKER, A. H., GRAHAM, D., MCDONALD, R. A., PELL, J. P., SATTAR, N., WELSH, P., MUNROE, P., CAULFIELD, M. J., ZANCHETTI, A. & DOMINICZAK, A. F. 2010. Genome-wide association study of blood pressure extremes identifies variant near UMOD associated with hypertension. *PLoS Genet,* 6**,** e1001177.

PANG, S., URQUHART, P. & HOOPER, N. M. 2004. N-glycans, not the GPI anchor, mediate the apical targeting of a naturally glycosylated, GPI-anchored protein in polarised epithelial cells. *J Cell Sci,* 117**,** 5079-86.

PARATI, G., CASTIGLIONI, P., FAINI, A., DI RIENZO, M., MANCIA, G., BARBIERI, R. & SAUL, J. P. 2019. Closed-Loop Cardiovascular Interactions and the Baroreflex Cardiac Arm: Modulations Over the 24 h and the Effect of Hypertension. *Front Physiol,* 10**,** 477.

PATTARO, C., TEUMER, A., GORSKI, M., CHU, A. Y., LI, M., MIJATOVIC, V., GARNAAS, M., TIN, A., SORICE, R., LI, Y., TALIUN, D., OLDEN, M., FOSTER, M., YANG, Q., CHEN, M. H., PERS, T. H., JOHNSON, A. D., KO, Y. A., FUCHSBERGER, C., TAYO, B., NALLS, M., FEITOSA, M. F., ISAACS, A., DEHGHAN, A., D'ADAMO, P., ADEYEMO, A., DIEFFENBACH, A. K., ZONDERMAN, A. B., NOLTE, I. M., VAN DER MOST, P. J., WRIGHT, A. F., SHULDINER, A. R., MORRISON, A. C., HOFMAN, A., SMITH, A. V., DREISBACH, A. W., FRANKE, A., UITTERLINDEN, A. G., METSPALU, A., TONJES, A., LUPO, A., ROBINO, A., JOHANSSON, Å., DEMIRKAN, A.,

KOLLERITS, B., FREEDMAN, B. I., PONTE, B., OOSTRA, B. A., PAULWEBER, B., KRÄMER, B. K., MITCHELL, B. D., BUCKLEY, B. M., PERALTA, C. A., HAYWARD, C., HELMER, C., ROTIMI, C. N., SHAFFER, C. M., MÜLLER, C., SALA, C., VAN DUIJN, C. M., SAINT-PIERRE, A., ACKERMANN, D., SHRINER, D., RUGGIERO, D., TONIOLO, D., LU, Y., CUSI, D., CZAMARA, D., ELLINGHAUS, D., SISCOVICK, D. S., RUDERFER, D., GIEGER, C., GRALLERT, H., ROCHTCHINA, E., ATKINSON, E. J., HOLLIDAY, E. G., BOERWINKLE, E., SALVI, E., BOTTINGER, E. P., MURGIA, F., RIVADENEIRA, F., ERNST, F., KRONENBERG, F., HU, F. B., NAVIS, G. J., CURHAN, G. C., EHRET, G. B., HOMUTH, G., COASSIN, S., THUN, G. A., PISTIS, G., GAMBARO, G., MALERBA, G., MONTGOMERY, G. W., EIRIKSDOTTIR, G., JACOBS, G., LI, G., WICHMANN, H. E., CAMPBELL, H., SCHMIDT, H., et al. 2016. Genetic associations at 53 loci highlight cell types and biological pathways relevant for kidney function. *Nat Commun,* 7**,** 10023.

PECK, R. N., SHEDAFA, R., KALLUVYA, S., DOWNS, J. A., TODD, J., SUTHANTHIRAN, M., FITZGERALD, D. W. & KATARAIHYA, J. B. 2014. Hypertension, kidney disease, HIV and antiretroviral therapy among Tanzanian adults: a cross-sectional study. *BMC Med,* 12**,** 125.

PEJCHINOVSKI, M., SIWY, J., MULLEN, W., MISCHAK, H., PETRI, M. A., BURKLY, L. C. & WEI, R. 2018. Urine peptidomic biomarkers for diagnosis of patients with systematic lupus erythematosus. *Lupus,* 27**,** 6-16.

PENNICA, D., KOHR, W. J., KUANG, W. J., GLAISTER, D., AGGARWAL, B. B., CHEN, E. Y. & GOEDDEL, D. V. 1987. Identification of human uromodulin as the Tamm-Horsfall urinary glycoprotein. *Science,* 236**,** 83-8.

PITTMAN, R. N. 2011. The Circulatory System and Oxygen Transport. *Regulation of Tissue Oxygenation.* San Rafael (CA).

POLLOCK, J. D., MURRAY, I. V., BORDES, S. J. & MAKARYUS, A. N. 2023. Physiology, Cardiovascular Hemodynamics. *StatPearls.* Treasure Island (FL) ineligible companies. Disclosure: Ian Murray declares no relevant financial relationships with ineligible companies. Disclosure: Stephen Bordes declares no relevant financial relationships with ineligible companies. Disclosure: Amgad Makaryus declares no relevant financial relationships with ineligible companies.

PONCE-CORIA, J., SAN-CRISTOBAL, P., KAHLE, K. T., VAZQUEZ, N., PACHECO-ALVAREZ, D., DE LOS HEROS, P., JUÁREZ, P., MUÑOZ, E., MICHEL, G., BOBADILLA, N. A., GIMENEZ, I., LIFTON, R. P., HEBERT, S. C. & GAMBA, G. 2008. Regulation of NKCC2 by a chloride-sensing mechanism involving the WNK3 and SPAK kinases. *Proc Natl Acad Sci U S A,* 105**,** 8458-63.

PONTE, B., PRUIJM, M., ACKERMANN, D., OLINGER, E., YOUHANNA, S., VOGT, B., BURNIER, M., PECHERE-BERTSCHI, A., BOCHUD, M. & DEVUYST, O. 2021. Uromodulin, Salt, and 24-Hour Blood Pressure in the General Population. *Clin J Am Soc Nephrol,* 16**,** 787-789.

POOK, M. A., JEREMIAH, S., SCHEINMAN, S. J., POVEY, S. & THAKKER, R. V. 1993. Localization of the Tamm-Horsfall glycoprotein (uromodulin) gene to chromosome 16p12.3-16p13.11. *Ann Hum Genet,* 57**,** 285-90.

PRABHAKAR, N. R., PENG, Y. J., KUMAR, G. K. & NANDURI, J. 2015. Peripheral chemoreception and arterial pressure responses to intermittent hypoxia. *Compr Physiol,* 5**,** 561-77.

PREUSS, H. G. 1993. Basics of renal anatomy and physiology. *Clin Lab Med,* 13**,** 1-11.

PRUIJM, M., PONTE, B., ACKERMANN, D., PACCAUD, F., GUESSOUS, I., EHRET, G., PECHERE-BERTSCHI, A., VOGT, B., MOHAUPT, M. G., MARTIN, P. Y., YOUHANNA, S. C., NAGELE, N., VOLLENWEIDER, P., WAEBER, G., BURNIER, M., DEVUYST, O. & BOCHUD, M. 2016a. Associations of Urinary

Uromodulin with Clinical Characteristics and Markers of Tubular Function in the General Population. *Clin J Am Soc Nephrol,* 11**,** 70-80.

PRUIJM, M., PONTE, B., ACKERMANN, D., PACCAUD, F., GUESSOUS, I., EHRET, G., PECHÈRE-BERTSCHI, A., VOGT, B., MOHAUPT, M. G., MARTIN, P. Y., YOUHANNA, S. C., NÄGELE, N., VOLLENWEIDER, P., WAEBER, G., BURNIER, M., DEVUYST, O. & BOCHUD, M. 2016b. Associations of Urinary Uromodulin with Clinical Characteristics and Markers of Tubular Function in the General Population. *Clin J Am Soc Nephrol,* 11**,** 70-80.

PUGH, D., GALLACHER, P. J. & DHAUN, N. 2019. Management of Hypertension in Chronic Kidney Disease. *Drugs,* 79**,** 365-379.

PYRAM, R., KANSARA, A., BANERJI, M. A. & LONEY-HUTCHINSON, L. 2012. Chronic kidney disease and diabetes. *Maturitas,* 71**,** 94-103.

RAFFI, H., BATES, J. M., LASZIK, Z. & KUMAR, S. 2006. Tamm-Horsfall protein knockout mice do not develop medullary cystic kidney disease. *Kidney Int,* 69**,** 1914-5.

RAINA, R., KRISHNAPPA, V., DAS, A., AMIN, H., RADHAKRISHNAN, Y., NAIR, N. R. & KUSUMI, K. 2019. Overview of Monogenic or Mendelian Forms of Hypertension. *Front Pediatr,* 7**,** 263.

RAJAGOPALAN, S., KURZ, S., MUNZEL, T., TARPEY, M., FREEMAN, B. A., GRIENDLING, K. K. & HARRISON, D. G. 1996. Angiotensin II-mediated hypertension in the rat increases vascular superoxide production via membrane NADH/NADPH oxidase activation. Contribution to alterations of vasomotor tone. *J Clin Invest,* 97**,** 1916-23.

RAKUSAN, K., CICUTTI, N., KAZDA, S. & TUREK, Z. 1994. Effect of nifedipine on coronary capillary geometry in normotensive and hypertensive rats. *Hypertension,* 24**,** 205-11.

RAMPOLDI, L., CARIDI, G., SANTON, D., BOARETTO, F., BERNASCONE, I., LAMORTE, G., TARDANICO, R., DAGNINO, M., COLUSSI, G., SCOLARI, F., GHIGGERI, G. M., AMOROSO, A. & CASARI, G. 2003. Allelism of MCKD, FJHN and GCKD caused by impairment of uromodulin export dynamics. *Hum Mol Genet,* 12**,** 3369-84.

RAMPOLDI, L., SCOLARI, F., AMOROSO, A., GHIGGERI, G. & DEVUYST, O. 2011. The rediscovery of uromodulin (Tamm-Horsfall protein): from tubulointerstitial nephropathy to chronic kidney disease. *Kidney Int,* 80**,** 338-47.

RAMSEYER, V. D. & GARVIN, J. L. 2013. Tumor necrosis factor-α: regulation of renal function and blood pressure. *Am J Physiol Renal Physiol,* 304**,** F1231-42.

RAMSEYER, V. D., ORTIZ, P. A., CARRETERO, O. A. & GARVIN, J. L. 2016. Angiotensin II-mediated hypertension impairs nitric oxide-induced NKCC2 inhibition in thick ascending limbs. *Am J Physiol Renal Physiol,* 310**,** F748-f754.

RENIGUNTA, A., RENIGUNTA, V., SARITAS, T., DECHER, N., MUTIG, K. & WALDEGGER, S. 2011. Tamm-Horsfall glycoprotein interacts with renal outer medullary potassium channel ROMK2 and regulates its function. *J Biol Chem,* 286**,** 2224-35.

RICCARDI, D., PARK, J., LEE, W. S., GAMBA, G., BROWN, E. M. & HEBERT, S. C. 1995. Cloning and functional expression of a rat kidney extracellular calcium/polyvalent cation-sensing receptor. *Proc Natl Acad Sci U S A,* 92**,** 131-5.

RICHARDSON, C. & ALESSI, D. R. 2008. The regulation of salt transport and blood pressure by the WNK-SPAK/OSR1 signalling pathway. *J Cell Sci,* 121**,** 3293-304.

RODRIGUEZ-ITURBE, B., PONS, H. & JOHNSON, R. J. 2017. Role of the Immune System in Hypertension. *Physiol Rev,* 97**,** 1127-1164.

RODRÍGUEZ-ITURBE, B., QUIROZ, Y., FERREBUZ, A., PARRA, G. & VAZIRI, N. D. 2004. Evolution of renal interstitial inflammation and NF-kappaB activation in spontaneously hypertensive rats. *Am J Nephrol,* 24**,** 587-94.

RODRÍGUEZ-ITURBE, B., QUIROZ, Y., NAVA, M., BONET, L., CHÁVEZ, M., HERRERA-ACOSTA, J., JOHNSON, R. J. & PONS, H. A. 2002. Reduction of renal immune cell infiltration results in blood pressure control in genetically hypertensive rats. *Am J Physiol Renal Physiol,* 282**,** F191-201.

RONDÓN, L. J., GROENESTEGE, W. M., RAYSSIGUIER, Y. & MAZUR, A. 2008. Relationship between low magnesium status and TRPM6 expression in the kidney and large intestine. *Am J Physiol Regul Integr Comp Physiol,* 294**,** R2001-7.

ROSSING, K., MISCHAK, H., PARVING, H. H., CHRISTENSEN, P. K., WALDEN, M., HILLMANN, M. & KAISER, T. 2005. Impact of diabetic nephropathy and angiotensin II receptor blockade on urinary polypeptide patterns. *Kidney Int,* 68**,** 193-205.

ROSSITTO, G., MAIOLINO, G., LERCO, S., CEOLOTTO, G., BLACKBURN, G., MARY, S., ANTONELLI, G., BERTON, C., BISOGNI, V., CESARI, M., SECCIA, T. M., LENZINI, L., PINATO, A., MONTEZANO, A., TOUYZ, R. M., PETRIE, M. C., DALY, R., WELSH, P., PLEBANI, M., ROSSI, G. P. & DELLES, C. 2021. High sodium intake, glomerular hyperfiltration, and protein catabolism in patients with essential hypertension. *Cardiovasc Res,* 117**,** 1372-1381.

RU, X. & YAO, X. 2014. TRPM2: a multifunctional ion channel for oxidative stress sensing. *Sheng Li Xue Bao,* 66**,** 7-15.

SACKS, F. M., SVETKEY, L. P., VOLLMER, W. M., APPEL, L. J., BRAY, G. A., HARSHA, D., OBARZANEK, E., CONLIN, P. R., MILLER, E. R., 3RD, SIMONS-MORTON, D. G., KARANJA, N. & LIN, P. H. 2001a. Effects on blood pressure of reduced dietary sodium and the Dietary Approaches to Stop Hypertension (DASH) diet. DASH-Sodium Collaborative Research Group. *N Engl J Med,* 344**,** 3-10.

SACKS, F. M., SVETKEY, L. P., VOLLMER, W. M., APPEL, L. J., BRAY, G. A., HARSHA, D., OBARZANEK, E., CONLIN, P. R., MILLER, E. R., 3RD, SIMONS-MORTON, D. G., KARANJA, N., LIN, P. H. & GROUP, D. A.-S. C. R. 2001b. Effects on blood pressure of reduced dietary sodium and the Dietary Approaches to Stop Hypertension (DASH) diet. DASH-Sodium Collaborative Research Group. *N Engl J Med,* 344**,** 3-10.

SALIDO, E. C., LAKSHMANAN, J., FISHER, D. A., SHAPIRO, L. J. & BARAJAS, L. 1991. Expression of epidermal growth factor in the rat kidney. An immunocytochemical and in situ hybridization study. *Histochemistry,* 96**,** 65-72.

SANDS, J. M. & LAYTON, H. E. 2009. The physiology of urinary concentration: an update. *Semin Nephrol,* 29**,** 178-95.

SCHAEFFER, C., MERELLA, S., PASQUALETTO, E., LAZAREVIC, D. & RAMPOLDI, L. 2017. Mutant uromodulin expression leads to altered homeostasis of the endoplasmic reticulum and activates the unfolded protein response. *PLoS One,* 12**,** e0175970.

SCHAEFFER, C., SANTAMBROGIO, S., PERUCCA, S., CASARI, G. & RAMPOLDI, L. 2009. Analysis of uromodulin polymerization provides new insights into the mechanisms regulating ZP domain-mediated protein assembly. *Mol Biol Cell,* 20**,** 589-99.

SCHERBERICH, J. E., GRUBER, R., NOCKHER, W. A., CHRISTENSEN, E. I., SCHMITT, H., HERBST, V., BLOCK, M., KADEN, J. & SCHLUMBERGER, W. 2018. Serum uromodulin-a marker of kidney function and renal parenchymal integrity. *Nephrol Dial Transplant,* 33**,** 284-295.

SCHIANO, G., GLAUDEMANS, B., OLINGER, E., GOELZ, N., MÜLLER, M., LOFFING-CUENI, D., DESCHENES, G., LOFFING, J. & DEVUYST, O. 2019. The Urinary Excretion of Uromodulin is Regulated by the Potassium Channel ROMK. *Sci Rep,* 9**,** 19517.

SCHRODER, K. & TSCHOPP, J. 2010. The inflammasomes. *Cell,* 140**,** 821-32.
SCHRÖTER, J., TIMMERMANS, G., SEYBERTH, H. W., GREVEN, J. & BACHMANN, S. 1993. Marked reduction of Tamm-Horsfall protein synthesis in hyperprostaglandin E-syndrome. *Kidney Int,* 44**,** 401-10.
SEDEEK, M., NASRALLAH, R., TOUYZ, R. M. & HEBERT, R. L. 2013. NADPH oxidases, reactive oxygen species, and the kidney: friend and foe. *J Am Soc Nephrol,* 24**,** 1512-8.
SEGAR, W. E. 1966. Chronic hyperosmolality. A condition resulting from absence of thirst, defective osmoregulation, and limited ability to concentrate urine. *Am J Dis Child,* 112**,** 318-27.
SELFA, I. L., GALLO, M., MONTSERRAT, N. & GARRETA, E. 2021. Directed Differentiation of Human Pluripotent Stem Cells for the Generation of High-Order Kidney Organoids. *Methods Mol Biol,* 2258**,** 171-192.
SERAFINI-CESSI, F., MALAGOLINI, N. & CAVALLONE, D. 2003. Tamm-Horsfall glycoprotein: biology and clinical relevance. *Am J Kidney Dis,* 42**,** 658-76.
SHANKAR, S. S. & BRATER, D. C. 2003. Loop diuretics: from the Na-K-2Cl transporter to clinical use. *Am J Physiol Renal Physiol,* 284**,** F11-21.
SHAO, J., NANGAKU, M., MIYATA, T., INAGI, R., YAMADA, K., KUROKAWA, K. & FUJITA, T. 2003. Imbalance of T-cell subsets in angiotensin II-infused hypertensive rats with kidney injury. *Hypertension,* 42**,** 31-8.
SHERBLOM, A. P., DECKER, J. M. & MUCHMORE, A. V. 1988. The lectin-like interaction between recombinant tumor necrosis factor and uromodulin. *J Biol Chem,* 263**,** 5418-24.
SHRIMANKER, I. & BHATTARAI, S. 2023. Electrolytes. *StatPearls.* Treasure Island (FL) ineligible companies. Disclosure: Sandeep Bhattarai declares no relevant financial relationships with ineligible companies.
SIMON, D. B., KARET, F. E., RODRIGUEZ-SORIANO, J., HAMDAN, J. H., DIPIETRO, A., TRACHTMAN, H., SANJAD, S. A. & LIFTON, R. P. 1996. Genetic heterogeneity of Bartter's syndrome revealed by mutations in the K+ channel, ROMK. *Nat Genet,* 14**,** 152-6.
SINGH, M. V., CHAPLEAU, M. W., HARWANI, S. C. & ABBOUD, F. M. 2014. The immune system and hypertension. *Immunol Res,* 59**,** 243-53.
SIRAGY, H. M. & CAREY, R. M. 2010. Role of the intrarenal renin-angiotensin-aldosterone system in chronic kidney disease. *Am J Nephrol,* 31**,** 541-50.
SIRONI, L., TREMOLI, E., MILLER, I., GUERRINI, U., CALVIO, A. M., EBERINI, I., GEMEINER, M., ASDENTE, M., PAOLETTI, R. & GIANAZZA, E. 2001. Acute-phase proteins before cerebral ischemia in stroke-prone rats: identification by proteomics. *Stroke,* 32**,** 753-60.
SLATER, M., PERRUCCIO, A. V. & BADLEY, E. M. 2011. Musculoskeletal comorbidities in cardiovascular disease, diabetes and respiratory disease: the impact on activity limitations; a representative population-based study. *BMC Public Health,* 11**,** 77.
SMALL, H. Y., MORGAN, H., BEATTIE, E., GRIFFIN, S., INDAHL, M., DELLES, C. & GRAHAM, D. 2016. Abnormal uterine artery remodelling in the stroke prone spontaneously hypertensive rat. *Placenta,* 37**,** 34-44.
SOBSEY, C. A., IBRAHIM, S., RICHARD, V. R., GASPAR, V., MITSA, G., LACASSE, V., ZAHEDI, R. P., BATIST, G. & BORCHERS, C. H. 2020. Targeted and Untargeted Proteomics Approaches in Biomarker Development. *Proteomics,* 20**,** e1900029.
SOLLINGER, D., EIßLER, R., LORENZ, S., STRAND, S., CHMIELEWSKI, S., AOQUI, C., SCHMADERER, C., BLUYSSEN, H., ZICHA, J., WITZKE, O., SCHERER, E., LUTZ, J., HEEMANN, U. & BAUMANN, M. 2014. Damage-

associated molecular pattern activated Toll-like receptor 4 signalling modulates blood pressure in L-NAME-induced hypertension. *Cardiovasc Res,* 101**,** 464-72.

SPARKS, M. A., CROWLEY, S. D., GURLEY, S. B., MIROTSOU, M. & COFFMAN, T. M. 2014. Classical Renin-Angiotensin system in kidney physiology. *Compr Physiol,* 4**,** 1201-28.

SRIRAMULA, S., HAQUE, M., MAJID, D. S. & FRANCIS, J. 2008. Involvement of tumor necrosis factor-alpha in angiotensin II-mediated effects on salt appetite, hypertension, and cardiac hypertrophy. *Hypertension,* 51**,** 1345-51.

SRIVASTAVA, R., MICANOVIC, R., EL-ACHKAR, T. M. & JANGA, S. C. 2014. An intricate network of conserved DNA upstream motifs and associated transcription factors regulate the expression of uromodulin gene. *J Urol,* 192**,** 981-9.

STANISICH, J. J., ZYLA, D. S., AFANASYEV, P., XU, J., KIPP, A., OLINGER, E., DEVUYST, O., PILHOFER, M., BOEHRINGER, D. & GLOCKSHUBER, R. 2020. The cryo-EM structure of the human uromodulin filament core reveals a unique assembly mechanism. *Elife,* 9.

STANTON, B. A. & KAISSLING, B. 1989. Regulation of renal ion transport and cell growth by sodium. *Am J Physiol,* 257**,** F1-10.

STAUFFER, W., SHENG, H. & LIM, H. N. 2018. EzColocalization: An ImageJ plugin for visualizing and measuring colocalization in cells and organisms. *Sci Rep,* 8**,** 15764.

STEUBL, D., BLOCK, M., HERBST, V., SCHLUMBERGER, W., NOCKHER, A., ANGERMANN, S., SCHMADERER, C., HEEMANN, U., RENDERS, L. & SCHERBERICH, J. 2017. Serum uromodulin predicts graft failure in renal transplant recipients. *Biomarkers,* 22**,** 171-177.

STEUBL, D., BUZKOVA, P., GARIMELLA, P. S., IX, J. H., DEVARAJAN, P., BENNETT, M. R., CHAVES, P. H. M., SHLIPAK, M. G., BANSAL, N. & SARNAK, M. J. 2020a. Association of serum uromodulin with mortality and cardiovascular disease in the elderly-the Cardiovascular Health Study. *Nephrol Dial Transplant,* 35**,** 1399-1405.

STEUBL, D., SCHNEIDER, M. P., MEISELBACH, H., NADAL, J., SCHMID, M. C., SARITAS, T., KRANE, V., SOMMERER, C., BAID-AGRAWAL, S., VOELKL, J., KOTSIS, F., KÖTTGEN, A., ECKARDT, K. U. & SCHERBERICH, J. E. 2020b. Association of Serum Uromodulin with Death, Cardiovascular Events, and Kidney Failure in CKD. *Clin J Am Soc Nephrol,* 15**,** 616-624.

STEUBL, D., SCHNEIDER, M. P., MEISELBACH, H., NADAL, J., SCHMID, M. C., SARITAS, T., KRANE, V., SOMMERER, C., BAID-AGRAWAL, S., VOELKL, J., KOTSIS, F., KOTTGEN, A., ECKARDT, K. U., SCHERBERICH, J. E. & INVESTIGATORS, G. S. 2020c. Association of Serum Uromodulin with Death, Cardiovascular Events, and Kidney Failure in CKD. *Clin J Am Soc Nephrol,* 15**,** 616-624.

STOLARZ-SKRZYPEK, K., KUZNETSOVA, T., THIJS, L., TIKHONOFF, V., SEIDLEROVÁ, J., RICHART, T., JIN, Y., OLSZANECKA, A., MALYUTINA, S., CASIGLIA, E., FILIPOVSKÝ, J., KAWECKA-JASZCZ, K., NIKITIN, Y. & STAESSEN, J. A. 2011. Fatal and nonfatal outcomes, incidence of hypertension, and blood pressure changes in relation to urinary sodium excretion. *Jama,* 305**,** 1777-85.

STSIAPANAVA, A., XU, C., BRUNATI, M., ZAMORA-CABALLERO, S., SCHAEFFER, C., BOKHOVE, M., HAN, L., HEBERT, H., CARRONI, M., YASUMASU, S., RAMPOLDI, L., WU, B. & JOVINE, L. 2020. Cryo-EM structure of native human uromodulin, a zona pellucida module polymer. *Embo j,* 39**,** e106807.

SUMITRA, K., PRAGASAM, V., SAKTHIVEL, R., KALAISELVI, P. & VARALAKSHMI, P. 2005. Beneficial effect of vitamin E supplementation on the

biochemical and kinetic properties of Tamm-Horsfall glycoprotein in hypertensive and hyperoxaluric patients. *Nephrol Dial Transplant,* 20**,** 1407-15.

SZABO, S. J., KIM, S. T., COSTA, G. L., ZHANG, X., FATHMAN, C. G. & GLIMCHER, L. H. 2000. A novel transcription factor, T-bet, directs Th1 lineage commitment. *Cell,* 100**,** 655-69.

TABET, F., SCHIFFRIN, E. L., CALLERA, G. E., HE, Y., YAO, G., OSTMAN, A., KAPPERT, K., TONKS, N. K. & TOUYZ, R. M. 2008. Redox-sensitive signaling by angiotensin II involves oxidative inactivation and blunted phosphorylation of protein tyrosine phosphatase SHP-2 in vascular smooth muscle cells from SHR. *Circ Res,* 103**,** 149-58.

TAMM, I. & HORSFALL, F. L., JR. 1950. Characterization and separation of an inhibitor of viral hemagglutination present in urine. *Proc Soc Exp Biol Med,* 74**,** 106-8.

TANG, K. W., TOH, Q. C. & TEO, B. W. 2015. Normalisation of urinary biomarkers to creatinine for clinical practice and research--when and why. *Singapore Med J,* 56**,** 7-10.

TINSLEY, J. H., SOUTH, S., CHIASSON, V. L. & MITCHELL, B. M. 2010. Interleukin-10 reduces inflammation, endothelial dysfunction, and blood pressure in hypertensive pregnant rats. *Am J Physiol Regul Integr Comp Physiol,* 298**,** R713-9.

TOKONAMI, N., OLINGER, E., DEBAIX, H., HOUILLIER, P. & DEVUYST, O. 2018a. The excretion of uromodulin is modulated by the calcium-sensing receptor. *Kidney Int,* 94**,** 882-886.

TOKONAMI, N., TAKATA, T., BEYELER, J., EHRBAR, I., YOSHIFUJI, A., CHRISTENSEN, E. I., LOFFING, J., DEVUYST, O. & OLINGER, E. G. 2018b. Uromodulin is expressed in the distal convoluted tubule, where it is critical for regulation of the sodium chloride cotransporter NCC. *Kidney Int,* 94**,** 701-715.

TOMIYAMA, H., KUSHIRO, T., ABETA, H., KURUMATANI, H., TAGUCHI, H., KUGA, N., SAITO, F., KOBAYASHI, F., OTSUKA, Y., KANMATSUSE, K. & ET AL. 1992. Blood pressure response to hyperinsulinemia in salt-sensitive and salt-resistant rats. *Hypertension,* 20**,** 596-600.

TORFFVIT, O., AGARDH, C. D. & THULIN, T. 1999. A study of Tamm-Horsfall protein excretion in hypertensive patients and type 1 diabetic patients. *Scand J Urol Nephrol,* 33**,** 187-91.

TORFFVIT, O., MELANDER, O. & HULTÉN, U. L. 2004. Urinary excretion rate of Tamm-Horsfall protein is related to salt intake in humans. *Nephron Physiol,* 97**,** p31-6.

TROYANOV, S., DELMAS-FRENETTE, C., BOLLÉE, G., YOUHANNA, S., BRUAT, V., AWADALLA, P., DEVUYST, O. & MADORE, F. 2016. Clinical, Genetic, and Urinary Factors Associated with Uromodulin Excretion. *Clin J Am Soc Nephrol,* 11**,** 62-9.

TRUDU, M., JANAS, S., LANZANI, C., DEBAIX, H., SCHAEFFER, C., IKEHATA, M., CITTERIO, L., DEMARETZ, S., TREVISANI, F., RISTAGNO, G., GLAUDEMANS, B., LAGHMANI, K., DELL'ANTONIO, G., LOFFING, J., RASTALDI, M. P., MANUNTA, P., DEVUYST, O. & RAMPOLDI, L. 2013a. Common noncoding UMOD gene variants induce salt-sensitive hypertension and kidney damage by increasing uromodulin expression. *Nat Med,* 19**,** 1655-60.

TRUDU, M., JANAS, S., LANZANI, C., DEBAIX, H., SCHAEFFER, C., IKEHATA, M., CITTERIO, L., DEMARETZ, S., TREVISANI, F., RISTAGNO, G., GLAUDEMANS, B., LAGHMANI, K., DELL'ANTONIO, G., TEAM, S., LOFFING, J., RASTALDI, M. P., MANUNTA, P., DEVUYST, O. & RAMPOLDI, L. 2013b. Common noncoding UMOD gene variants induce salt-sensitive hypertension and kidney damage by increasing uromodulin expression. *Nat Med,* 19**,** 1655-60.

TSAI, B., RODIGHIERO, C., LENCER, W. I. & RAPOPORT, T. A. 2001. Protein disulfide isomerase acts as a redox-dependent chaperone to unfold cholera toxin. *Cell,* 104**,** 937-48.

TU, B. P., HO-SCHLEYER, S. C., TRAVERS, K. J. & WEISSMAN, J. S. 2000. Biochemical basis of oxidative protein folding in the endoplasmic reticulum. *Science,* 290**,** 1571-4.

TUCKER, W. D., ARORA, Y. & MAHAJAN, K. 2023. Anatomy, Blood Vessels. *StatPearls.* Treasure Island (FL) ineligible companies. Disclosure: Yingyot Arora declares no relevant financial relationships with ineligible companies. Disclosure: Kunal Mahajan declares no relevant financial relationships with ineligible companies.

USHIO-FUKAI, M., ALEXANDER, R. W., AKERS, M. & GRIENDLING, K. K. 1998. p38 Mitogen-activated protein kinase is a critical component of the redox-sensitive signaling pathways activated by angiotensin II. Role in vascular smooth muscle cell hypertrophy. *J Biol Chem,* 273**,** 15022-9.

UTO, I., ISHIMATSU, T., HIRAYAMA, H., UEDA, S., TSURUTA, J. & KAMBARA, T. 1991. Determination of urinary Tamm-Horsfall protein by ELISA using a maleimide method for enzyme-antibody conjugation. *J Immunol Methods,* 138**,** 87-94.

VAN BEUSECUM, J. & INSCHO, E. W. 2015. Regulation of renal function and blood pressure control by P2 purinoceptors in the kidney. *Curr Opin Pharmacol,* 21**,** 82-8.

VAN, J. A. D., CLOTET-FREIXAS, S., ZHOU, J., BATRUCH, I., SUN, C., GLOGAUER, M., RAMPOLDI, L., ELIA, Y., MAHMUD, F. H., SOCHETT, E., DIAMANDIS, E. P., SCHOLEY, J. W. & KONVALINKA, A. 2020. Peptidomic Analysis of Urine from Youths with Early Type 1 Diabetes Reveals Novel Bioactivity of Uromodulin Peptides In Vitro. *Mol Cell Proteomics,* 19**,** 501-517.

VAN ROOIJEN, J. J., VOSKAMP, A. F., KAMERLING, J. P. & VLIEGENTHART, J. F. 1999. Glycosylation sites and site-specific glycosylation in human Tamm-Horsfall glycoprotein. *Glycobiology,* 9**,** 21-30.

VAN VLIET, B. N. & MONTANI, J. P. 2008. The time course of salt-induced hypertension, and why it matters. *Int J Obes (Lond),* 32 Suppl 6**,** S35-47.

VIDAL-PETIOT, E., METZGER, M., FAUCON, A. L., BOFFA, J. J., HAYMANN, J. P., THERVET, E., HOUILLIER, P., GERI, G., STENGEL, B., VRTOVSNIK, F. & FLAMANT, M. 2018. Extracellular Fluid Volume Is an Independent Determinant of Uncontrolled and Resistant Hypertension in Chronic Kidney Disease: A NephroTest Cohort Study. *J Am Heart Assoc,* 7**,** e010278.

VINH, A., CHEN, W., BLINDER, Y., WEISS, D., TAYLOR, W. R., GORONZY, J. J., WEYAND, C. M., HARRISON, D. G. & GUZIK, T. J. 2010. Inhibition and genetic ablation of the B7/CD28 T-cell costimulation axis prevents experimental hypertension. *Circulation,* 122**,** 2529-37.

VOETS, T., NILIUS, B., HOEFS, S., VAN DER KEMP, A. W., DROOGMANS, G., BINDELS, R. J. & HOENDEROP, J. G. 2004. TRPM6 forms the Mg2+ influx channel involved in intestinal and renal Mg2+ absorption. *J Biol Chem,* 279**,** 19-25.

VONEND, O., TURNER, C. M., CHAN, C. M., LOESCH, A., DELL'ANNA, G. C., SRAI, K. S., BURNSTOCK, G. & UNWIN, R. J. 2004. Glomerular expression of the ATP-sensitive P2X receptor in diabetic and hypertensive rat models. *Kidney Int,* 66**,** 157-66.

WADEI, H. M. & TEXTOR, S. C. 2012. The role of the kidney in regulating arterial blood pressure. *Nat Rev Nephrol,* 8**,** 602-9.

WALLACE, A. C. & NAIRN, R. C. 1971. Tamm-Horsfall protein in kidneys of human embyros and foreign species. *Pathology,* 3**,** 303-310.

WANG, T. 2012. Renal outer medullary potassium channel knockout models reveal thick ascending limb function and dysfunction. *Clin Exp Nephrol,* 16**,** 49-54.

WANG, D., WANG, Y., LIU, F. Q., YUAN, Z. Y. & MU, J. J. 2016. High Salt Diet Affects Renal Sodium Excretion and ERRα Expression. Int J Mol Sci, 17, 480.

WANG, Y., DU, M. F., YAO, S., ZOU, T., ZHANG, X. Y., HU, G. L., CHU, C., LIAO, Y. Y., CHEN, C., WANG, D., MA, Q., WANG, K. K., SUN, Y., NIU, Z. J., YAN, R. C., YAN, Y., ZHOU, H. W., JIA, H., GAO, W. H., LI, H., LI, C. H., CHEN, F. Y., GAO, K., ZHANG, J., SAFIRSTEIN, R., WANG, F., YANG, T. L. & MU, J. J. 2021. Associations of Serum Uromodulin and Its Genetic Variants With Blood Pressure and Hypertension in Chinese Adults. *Front Cardiovasc Med,* 8**,** 710023.

WANG, Z., DO CARMO, J. M., ABERDEIN, N., ZHOU, X., WILLIAMS, J. M., DA SILVA, A. A. & HALL, J. E. 2017. Synergistic Interaction of Hypertension and Diabetes in Promoting Kidney Injury and the Role of Endoplasmic Reticulum Stress. *Hypertension,* 69**,** 879-891.

WARD, H. H., ROMERO, E., WELFORD, A., PICKETT, G., BACALLAO, R., GATTONE, V. H., 2ND, NESS, S. A., WANDINGER-NESS, A. & ROITBAK, T. 2011. Adult human CD133/1(+) kidney cells isolated from papilla integrate into developing kidney tubules. *Biochim Biophys Acta,* 1812**,** 1344-57.

WEBSTER, A. C., NAGLER, E. V., MORTON, R. L. & MASSON, P. 2017. Chronic Kidney Disease. *Lancet,* 389**,** 1238-1252.

WEI, Y., BABILONIA, E., PEDRAZA, P. L., FERRERI, N. R. & WANG, W. H. 2003. Acute application of TNF stimulates apical 70-pS K+ channels in the thick ascending limb of rat kidney. *Am J Physiol Renal Physiol,* 285**,** F491-7.

WEISS, G. L., STANISICH, J. J., SAUER, M. M., LIN, C. W., ERAS, J., ZYLA, D. S., TRÜCK, J., DEVUYST, O., AEBI, M., PILHOFER, M. & GLOCKSHUBER, R. 2020. Architecture and function of human uromodulin filaments in urinary tract infections. *Science,* 369**,** 1005-1010.

WELLING, P. A. & HO, K. 2009. A comprehensive guide to the ROMK potassium channel: form and function in health and disease. *Am J Physiol Renal Physiol,* 297**,** F849-63.

WHELTON, P. K., APPEL, L. J., ESPELAND, M. A., APPLEGATE, W. B., ETTINGER, W. H., JR., KOSTIS, J. B., KUMANYIKA, S., LACY, C. R., JOHNSON, K. C., FOLMAR, S. & CUTLER, J. A. 1998. Sodium reduction and weight loss in the treatment of hypertension in older persons: a randomized controlled trial of nonpharmacologic interventions in the elderly (TONE). TONE Collaborative Research Group. *JAMA,* 279**,** 839-46.

WHELTON, P. K. & HE, J. 2014. Health effects of sodium and potassium in humans. *Curr Opin Lipidol,* 25**,** 75-9.

WIEDENMANN, J., OSWALD, F. & NIENHAUS, G. U. 2009. Fluorescent proteins for live cell imaging: opportunities, limitations, and challenges. *IUBMB Life,* 61**,** 1029-42.

WILLEBRAND, R. & KLEINEWIETFELD, M. 2018. The role of salt for immune cell function and disease. *Immunology,* 154**,** 346-353.

WILSON, F. H., KAHLE, K. T., SABATH, E., LALIOTI, M. D., RAPSON, A. K., HOOVER, R. S., HEBERT, S. C., GAMBA, G. & LIFTON, R. P. 2003. Molecular pathogenesis of inherited hypertension with hyperkalemia: the Na-Cl cotransporter is inhibited by wild-type but not mutant WNK4. *Proc Natl Acad Sci U S A,* 100**,** 680-4.

WIROMRAT, P., BJORNSTAD, P., RONCAL, C., CREE-GREEN, M., BAUMGARTNER, A., COE, G., REYES, Y. G., SCHAFER, M., TRUONG, U., PYLE, L., JOHNSON, R. J. & NADEAU, K. J. 2019a. Serum uromodulin inversely associates with aortic stiffness in youth with type 1 diabetes: A brief report from EMERALD study. *J Diabetes Complications,* 33**,** 434-436.

WIROMRAT, P., BJORNSTAD, P., RONCAL, C., CREE-GREEN, M., BAUMGARTNER, A., COE, G., REYES, Y. G., SCHÄFER, M., TRUONG, U., PYLE, L., JOHNSON, R. J. & NADEAU, K. J. 2019b. Serum uromodulin inversely associates with aortic stiffness in youth with type 1 diabetes: A brief report from EMERALD study. *J Diabetes Complications,* 33**,** 434-436.

WOLF, M. T., WU, X. R. & HUANG, C. L. 2013. Uromodulin upregulates TRPV5 by impairing caveolin-mediated endocytosis. *Kidney Int,* 84**,** 130-7.

WRIGHT, J. T., JR., WILLIAMSON, J. D., WHELTON, P. K., SNYDER, J. K., SINK, K. M., ROCCO, M. V., REBOUSSIN, D. M., RAHMAN, M., OPARIL, S., LEWIS, C. E., KIMMEL, P. L., JOHNSON, K. C., GOFF, D. C., JR., FINE, L. J., CUTLER, J. A., CUSHMAN, W. C., CHEUNG, A. K. & AMBROSIUS, W. T. 2015. A Randomized Trial of Intensive versus Standard Blood-Pressure Control. *N Engl J Med,* 373**,** 2103-16.

WU, C. H., LI, K. J., SIAO, S. C., CHEN, Y. H., WU, T. H., TSAI, C. Y. & YU, C. L. 2012a. The binding affinity and molecular basis of the structure-binding relationship between urinary Tamm-Horsfall glycoprotein and tumor necrosis factor-alpha. *Molecules,* 17**,** 11978-89.

WU, C. H., LI, K. J., SIAO, S. C., CHEN, Y. H., WU, T. H., TSAI, C. Y. & YU, C. L. 2012b. The binding affinity and molecular basis of the structure-binding relationship between urinary Tamm-Horsfall glycoprotein and tumor necrosis factor-α. *Molecules,* 17**,** 11978-89.

WU, J., WANG, N., WANG, J., XIE, Y., LI, Y., LIANG, T., WANG, J., YIN, Z., HE, K. & CHEN, X. 2010. Identification of a uromodulin fragment for diagnosis of IgA nephropathy. *Rapid Commun Mass Spectrom,* 24**,** 1971-8.

WU, P., WANG, M., LUAN, H., LI, L., WANG, L., WANG, W. H. & GU, R. 2013. Angiotensin II stimulates basolateral 10-pS Cl channels in the thick ascending limb. *Hypertension,* 61**,** 1211-7.

XIAO, L., KIRABO, A., WU, J., SALEH, M. A., ZHU, L., WANG, F., TAKAHASHI, T., LOPERENA, R., FOSS, J. D., MERNAUGH, R. L., CHEN, W., ROBERTS, J., 2ND, OSBORN, J. W., ITANI, H. A. & HARRISON, D. G. 2015. Renal Denervation Prevents Immune Cell Activation and Renal Inflammation in Angiotensin II-Induced Hypertension. *Circ Res,* 117**,** 547-57.

XU, C., DING, W., YANG, L., YANG, M., ZHANG, M. & GU, Y. 2014. Contributions of endoplasmic reticulum stress and reactive oxygen species to renal injury in aldosterone/salt-induced rats. *Nephron Exp Nephrol,* 126**,** 25-32.

XU, Z. C., YANG, Y. & HEBERT, S. C. 1996. Phosphorylation of the ATP-sensitive, inwardly rectifying K+ channel, ROMK, by cyclic AMP-dependent protein kinase. *J Biol Chem,* 271**,** 9313-9.

YAMASUE, K., TOCHIKUBO, O., KONO, E. & MAEDA, H. 2006. Self-monitoring of home blood pressure with estimation of daily salt intake using a new electrical device. *J Hum Hypertens,* 20**,** 593-8.

YAMORI, Y., HORIE, R., AKIGUCHI, I., NARA, Y., OHTAKA, M. & FUKASE, M. 1977. Pathogenic mechanisms and prevention of stroke in stroke-prone spontaneously hypertensive rats. *Prog Brain Res,* 47**,** 219-34.

YAMORI, Y., NARA, Y., KIHARA, M., HORIE, R. & OOSHIMA, A. Sodium and Other Dietary Factors in Experimental and Human Hypertension: The Japanese Experience. *In:* LARAGH, J. H., BÜHLER, F. R. & SELDIN, D. W., eds. Frontiers in Hypertension Research, 1981// 1981 New York, NY. Springer New York, 46-48.

YAMORI, Y., TOMIMOTO, K., OOSHIMA, A., HAZAMA, F. & OKAMOTO, K. 1974. Proceedings: Developmental course of hypertension in the SHR-substrains susceptible to hypertensive cerebrovascular lesions. *Jpn Heart J,* 15**,** 209-10.

YILMAZER, I., ABT, M. R., LIANG, Y., SEUNG, D., ZEEMAN, S. C. & SHARMA, M. 2023. Determining Protein-Protein Interaction with GFP-Trap Beads. *Methods Mol Biol,* 2564**,** 317-323.

YING, W. Z. & SANDERS, P. W. 1998. Dietary salt regulates expression of Tamm-Horsfall glycoprotein in rats. *Kidney Int,* 54**,** 1150-6.

YOO, D., FANG, L., MASON, A., KIM, B. Y. & WELLING, P. A. 2005. A phosphorylation-dependent export structure in ROMK (Kir 1.1) channel overrides an endoplasmic reticulum localization signal. *J Biol Chem,* 280**,** 35281-9.

YOUHANNA, S., WEBER, J., BEAUJEAN, V., GLAUDEMANS, B., SOBEK, J. & DEVUYST, O. 2014. Determination of uromodulin in human urine: influence of storage and processing. *Nephrol Dial Transplant,* 29**,** 136-45.

YOUNG, C. N. 2017. Endoplasmic reticulum stress in the pathogenesis of hypertension. *Exp Physiol,* 102**,** 869-884.

YUM, V., CARLISLE, R. E., LU, C., BRIMBLE, E., CHAHAL, J., UPAGUPTA, C., ASK, K. & DICKHOUT, J. G. 2017. Endoplasmic reticulum stress inhibition limits the progression of chronic kidney disease in the Dahl salt-sensitive rat. *Am J Physiol Renal Physiol,* 312**,** F230-f244.

ZACCHIA, M. & CAPASSO, G. 2015. The importance of uromodulin as regulator of salt reabsorption along the thick ascending limb. *Nephrol Dial Transplant,* 30**,** 158-60.

ZACCHIA, M., CAPOLONGO, G., RINALDI, L. & CAPASSO, G. 2018. The importance of the thick ascending limb of Henle's loop in renal physiology and pathophysiology. *Int J Nephrol Renovasc Dis,* 11**,** 81-92.

ZBROCH, E., MALYSZKO, J., MALYSZKO, J. S., KOC-ZORAWSKA, E. & MYSLIWIEC, M. 2012. Renalase, a novel enzyme involved in blood pressure regulation, is related to kidney function but not to blood pressure in hemodialysis patients. *Kidney Blood Press Res,* 35**,** 395-9.

ZENG, F., SINGH, A. B. & HARRIS, R. C. 2009. The role of the EGF family of ligands and receptors in renal development, physiology and pathophysiology. *Exp Cell Res,* 315**,** 602-10.

ZHANG, J., DING, E. L. & SONG, Y. 2006. Adverse effects of cyclooxygenase 2 inhibitors on renal and arrhythmia events: meta-analysis of randomized trials. *Jama,* 296**,** 1619-32.

ZHANG, J., PATEL, M. B., GRIFFITHS, R., MAO, A., SONG, Y. S., KARLOVICH, N. S., SPARKS, M. A., JIN, H., WU, M., LIN, E. E. & CROWLEY, S. D. 2014a. Tumor necrosis factor-alpha produced in the kidney contributes to angiotensin II-dependent hypertension. *Hypertension,* 64**,** 1275-81.

ZHANG, J. D., PATEL, M. B., GRIFFITHS, R., DOLBER, P. C., RUIZ, P., SPARKS, M. A., STEGBAUER, J., JIN, H., GOMEZ, J. A., BUCKLEY, A. F., LEFLER, W. S., CHEN, D. & CROWLEY, S. D. 2014b. Type 1 angiotensin receptors on macrophages ameliorate IL-1 receptor-mediated kidney fibrosis. *J Clin Invest,* 124**,** 2198-203.

ZHANG, W. R., CRAVEN, T. E., MALHOTRA, R., CHEUNG, A. K., CHONCHOL, M., DRAWZ, P., SARNAK, M. J., PARIKH, C. R., SHLIPAK, M. G. & IX, J. H. 2018. Kidney Damage Biomarkers and Incident Chronic Kidney Disease During Blood Pressure Reduction: A Case-Control Study. *Ann Intern Med,* 169**,** 610-618.

ZHANG, Y., HE, D., ZHANG, W., XING, Y., GUO, Y., WANG, F., JIA, J., YAN, T., LIU, Y. & LIN, S. 2020. ACE Inhibitor Benefit to Kidney and Cardiovascular Outcomes for Patients with Non-Dialysis Chronic Kidney Disease Stages 3-5: A Network Meta-Analysis of Randomised Clinical Trials. *Drugs,* 80**,** 797-811.

ZHOU, X., FUKUDA, N., MATSUDA, H., ENDO, M., WANG, X., SAITO, K., UENO, T., MATSUMOTO, T., MATSUMOTO, K., SOMA, M., KOBAYASHI, N. & NISHIYAMA, A. 2013. Complement 3 activates the renal renin-angiotensin system

by induction of epithelial-to-mesenchymal transition of the nephrotubulus in mice. *Am J Physiol Renal Physiol,* 305**,** F957-67.

ZHOU, Y. & GREKA, A. 2016. Calcium-permeable ion channels in the kidney. *Am J Physiol Renal Physiol,* 310**,** F1157-67.

ZOIS, N. E., BARTELS, E. D., HUNTER, I., KOUSHOLT, B. S., OLSEN, L. H. & GOETZE, J. P. 2014. Natriuretic peptides in cardiometabolic regulation and disease. *Nat Rev Cardiol,* 11**,** 403-12.